Memoria de Tesis Doctoral

Modelización regional del Campo Geomagnético en Europa para los últimos 8000 años y desarrollo de aplicaciones.

Francisco Javier Pavón - Carrasco

Directores: M.L. Osete y J.M. Torta

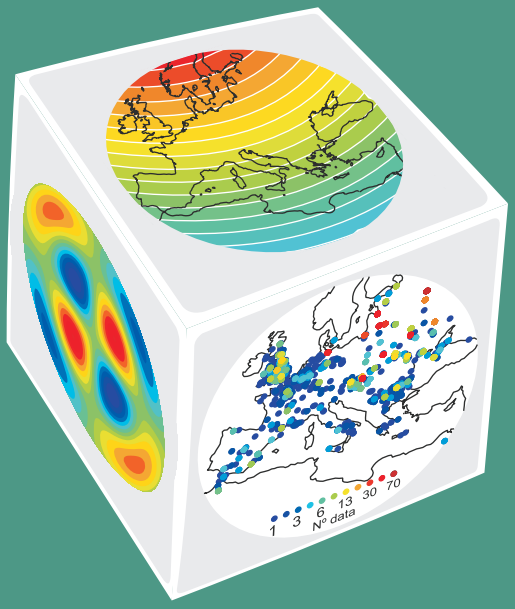

Departamento de Física de la Tierra, Astronomía y Astrofísica I
(Geofísica y Meteorología)

Facultad de Física. Universidad Complutense de Madrid

Madrid, 2010

UNIVERSIDAD COMPLUTENSE DE MADRID
FACULTAD DE CIENCIAS FÍSICAS

Departamento de Física de la Tierra, Astronomía y Astrofísica I
(Geofísica y Meteorología)

Modelización regional del Campo Geomagnético en Europa para los últimos 8000 años y desarrollo de aplicaciones.

MEMORIA PARA OPTAR AL GRADO DE DOCTOR
PRESENTADA POR

Francisco Javier Pavón – Carrasco

Bajo la dirección de los doctores

María Luisa Osete López
Joan Miquel Torta Margalef

Madrid, 2010

A mi familia

Agradecimientos

Llega el final de esta etapa de cinco años y toca pasar página. Escribir esto me está costando más que el resto de la Tesis, quizás por temor a que mi memoria me juegue una mala pasada y olvide nombrar a alguien. La lista de nombres seguro que es corta, pues harían falta muchas páginas para daros las gracias a todos.

A Marisa Osete y Miquel Torta, mis directores de Tesis, gracias. Con este trabajo cerramos el libro que ya empezasteis a escribir vosotros unos años atrás. A Marisa le debo todo lo relacionado a este trabajo, por ofrecerme la oportunidad de crecer, creer y disfrutar en la investigación que tantas satisfacciones me ha y nos ha dado. En este tiempo he conocido a mucha gente en muchos lugares del mundo y, Marisa, tú eres partícipe de ello. A Miquel Torta le quiero agradecer su esfuerzo y dedicación en mis continuas llamadas de ayuda. Siempre ha sido, y será, un referente en mi investigación. Espero y deseo que en el futuro próximo sigamos trabajando codo a codo con el campo magnético de la Tierra.

A Lluis Gaya, por sus grandes aportaciones y sus acertados comentarios, gracias!.

A mi grupo de Paleomagnetismo y demás paleomagnetas que he conocido a lo largo de estos años, con especial cariño a Carlos – Ali *et al. (2005, 2007, 2009)*, *mio fratello italiano* Gianluca – Benedetta *et al. (2007, 2009)*, Víctor (y Lucía), Gregg, Fátima, Esther y Sara. Y a todos los *Magiber@s*.

A mis compañeros y amigos del día a día en la facultad (*y noches*…) Teresa, Javi G., Irene P., Álvaro, Blanca, Marta, Elsa, Luis, Samu,... Y en especial a Ana y Belén.

A mis compañeros del despacho 213, los que estaban cuando llegué y los que llegaron cuando yo estaba, entre todos han hecho que las horas pasadas allí fueran amenas. En especial a Juan, *1/eps* gracias, por todo y por soportar mis *cánticos populares*. Y también, a mis compañeros geofísicos Tatiana, Juan-Luis, Diana, Társilo, Paco, Rafa, Bea, Ana G., Almu, Simone, Jacques, Dani, Javi M., María, Irene M., Bea S., Lidia, Lucía,…

Al departamento, y su director Michel Herraiz, por facilitarme la elaboración de este trabajo. Un agradecimiento cariñoso a nuestra querida Elvira. A Lucía y Salva, por su disponibilidad para todo. Y a Pedro, que facilita la burocracia doctoral.

Al servicio de Geomagnetismo del IGN y a los que me apoyaron en mis decisiones, en especial a Isabel Socias.

Au IPGP et aux départements de Géomagnétisme et Paléomagnétisme, je veux particulièrement remercier Erwan Thébault et Yves Gallet pour leur aide, merçi! J'ai beaucoup appris de vous ! Mon séjour à Paris a été enrichissant et agréable. Gracias a mis amigos del Collège d'Espagne, a mi *Petite Cousine*, Inma, Agustín, Blanca, Jovi, Luz, Awelo y Awela, Carlos, Dani J.,… y a los de *Jussieu*, Rocío, Leti, Carlos, Dani F. y al resto de la gran familia de la *Cité Universitaire*. A todos, gracias! Nos seguiremos viendo en nuestras quedadas anuales.

Al Dipartimento di Scienze della Terra della Universitá degli Studi di Torino. Un ringraziamento particolare a Roberto Lanza, a Elena Zanella e a Evdokia Tema... Evdokia, grazie a te la mia esperienza in Italia é stata assai fruttuosa, non solo in termini scintifici e professionali... Come dimenticare i gelati di Fiorio e di Grom?... E grazie anche ai tuoi amici che con la loro accoglienza mi hanno fatto trascorrere un piacevole periodo che non dimenticheró.

A mis amigos de *aquí, de Madrid*, Carlos M. y Cris, Carlos H., Sergio y Maria, ¡el piso Peñuelas!, Dani… y a la gran tropa de amigos de Bonares, gracias! En especial a la que me ha acompañado en muchos momentos, gracias Edu. Y a mis italianas preferidas Laura y Fede.

Y finalmente a los más importantes, a los que he dedicado esta Tesis Doctoral, mi familia, muchas gracias por todo, en especial a los que por mi lejanía no estoy disfrutando de ellos: mis sobrinos Juanma, Julio, Laura y Adán… aunque cuando estoy un día completo con ellos… añoro la lejanía de Madrid ;).

El presente trabajo ha sido financiado por el Ministerio de Ciencia e Innovación gracias al programa de Formación del Personal Investigador BES-2006-13488 asociado al proyecto de investigación CGL2005-00211. Además, este trabajo ha sido financiado por el proyecto europeo AARCH (HPRN-CT-2002-00219) y el proyecto de investigación nacional CGL2008-02203. Finalmente, el programa de ayudas complementarias para Estancias Breves en el extranjero ha permitido la realización de estancias en el IPG París (Francia) y la Universidad de Torino (Italia).

... Now must we consider separately the globe itself of the earth. Those experiments which have been proved by means of the terrella, how magnetick things conform themselves to the terrella, are all or at least the principal and most important of them, displayed by means of the earth's Body: And to the earth things magnetical are in all respects associate …

[*On the magnet, magnetick bodies also, and on the great magnet the earth; a new Physiology, demonstrated by many arguments & experiments* (*De magnete*). Book Sixth. Chapter 1: *On the Globe of the Earth, the great magnet*.
William Gilbert, London, **1600**]

Modelización Regional del Campo Geomagnético en Europa para los últimos 8000 años y desarrollo de aplicaciones.

Resumen

En esta tesis doctoral se proponen los primeros modelos regionales del campo geomagnético en la región europea basados en datos paleomagnéticos (datos arqueomagnéticos y datos de sedimentos lacustres). En conjunto, los modelos regionales obtenidos permiten analizar la variación paleosecular del campo geomagnético en los últimos 8000 años: desde el año 6000 a.C. hasta el 1900 d.C., conectando así con los modelos instrumentales, como el IGRF. Se han analizado numerosas estrategias para la inversión espacial de los datos paleomagnéticos mediante el uso de la técnica de modelado regional con armónicos en un casquete esférico SCHA y de su revisión R-SCHA2D. En el dominio temporal, todos los modelos se han obtenido mediante el uso de ventanas móviles solapadas dependientes de las características del dato paleomagnético.

El primer modelo, **SCHA.DI.00**, se ha obtenido mediante el uso de las curvas de variación paleosecular bayesianas de Europa. Se trata de un modelo direccional (declinación e inclinación) y proporciona los valores de los elementos del campo geomagnético para los últimos dos milenios. El segundo es una versión actualizada del primero, reescalándolo con los valores de intensidad de los últimos 2000 años. Este nuevo modelo, llamado **SCHA.DI.00-F**, permite analizar de forma completa los elementos de declinación, inclinación e intensidad de los últimos 2000 años y muestra que el campo geomagnético ha registrado 8 máximos de intensidad en la región europea entorno a 160, 320, 590, 820, 1070, 1310–1400, 1570 y 1770–1850 d.C. Con estos dos modelos iniciales se analiza la aplicación de la técnica SCHA en datos paleomagnéticos, obteniéndose resultados satisfactorios.

En un tercer paso, se ha desarrollado un nuevo modelo regional para Europa, norte de África y oeste de Asia. El modelo **SCHA.DIF.3K** ha sido desarrollado, también, mediante la aplicación de la técnica SCHA conjuntamente a los tres elementos del campo geomagnético y su período de validez cubre desde el año 1000 a.C. hasta el 1900 d.C. Los datos de entrada de este nuevo modelo son los datos paleomagnéticos *in situ*, por lo que se elimina el error de relocalización inherente en la creación de las Curvas de Variación Paleosecular, por lo que es más robusto y coherente que el previo SCHA.DI.00-F, aunque son estadísticamente indistinguibles. El modelo permite identificar al menos 5 *jerks* arqueomagnéticos o variaciones bruscas en los últimos 3000 años (AMJ-300, AMJ300, AMJ800, AMJ1350, AMJ1600) y un supuesto *jerk* entorno a 1800 d.C. (AMJ1800). Finalmente, el período de validez temporal del modelo anterior ha sido ampliado 5000 años más (desde el 6000 a.C. hasta el 1000 a.C) mediante la inclusión de datos sedimentarios y el uso de la versión revisada de la técnica SCHA (R-SCHA2D): el modelo **SCHA.DIF.8K**.

Finalmente, se ha visto cómo ambos modelos, SCHA.DIF.3K y .8K, pueden ser usados para analizar la variación paleosecular del campo geomagnético en Europa en los últimos 8000 años y sus características: aparición de jerks arqueomagnéticos, la posible (o causal) relación entre campo magnético de la Tierra y cambio climático, o la hipótesis del Dipolo Geocéntrico Axial (GAD). Además se ha demostrado con casos prácticos cómo pueden ser usados como herramienta de datación arqueológica.

Regional modelling of the Geomagnetic Field in Europe for the last 8000 years and applications.

Summary

In this thesis, the first regional models of the geomagnetic field in the European region based on palaeomagnetic data (archaeomagnetic data and lake sediment records) are proposed. Overall, the regional models allow us to analyze the paleosecular variation of the geomagnetic field for the last 8000 years: from 6000 BC to 1900 AD, connecting with the instrumental models, such as the IGRF. Several strategies have been developed for the inversion process of the palaeomagnetic data by applying, in the space, the spherical cap harmonic analysis SCHA and its revised version R-SCHA2D. In time, all models were obtained using the sliding overlapping windows method.

The first model, called **SCHA.DI.00**, was obtained using the European Bayesian palaeosecular variation curves. This directional model provides the values of the directional geomagnetic field elements (declination and inclination) for the last two millennia. This initial regional model was completed with the *in situ* archaeointensity data. The new **SCHA.DI.00-F** model provides a complete description (declination, inclination and intensity) of the geomagnetic field in Europe for the last 2000 years and suggests that the Earth's magnetic field strength reached 8 maxima in Europe at: 160, 320, 590, 820, 1070, 1310–1400, 1570 and 1770–1850 AD. Both initial regional models were used for testing the SCHA regional technique to palaeomagnetic data.

In a third step, a new regional model for Europe, Northern Africa and Western Asia was developed. The model, called **SCHA.DIF.3K**, was obtained using again the SCHA regional technique and is valid for the last 3000 years, from 1000 BC to 1900 AD. An algorithm was developed to jointly model the three archaeomagnetic elements declination, inclination, and intensity. In this sense, the new regional model is more robust and thus it replaces both initial models. The SCHA.DIF.3K model suggests that the Earth's magnetic field has experienced a minimum of 5 archaeomagnetic jerks in Europe for the last 3000 years (AMJ-300, AMJ300, AMJ800, AMJ1350, AMJ1600) and a suspected jerk (AMJ1800). Finally, the previous regional model was extended backwards in time by another model called **SCHA.DIF.8K**. This model was developed by applying the R-SCHA2D regional technique from 6000 BC to 1000 BC to archaeomagnetic data and lake sediment records.

Both models, SCHA.DIF.3K/8K, can be used for analyzing the behaviour of the palaeosecular variation of the geomagnetic field in Europe for the last 8000 years and related phenomena, such as the archaeomagnetic jerks, the possible (or causal) relationship between the Earth's magnetic field and the climate change, or the Geocentric Axial Dipole hypothesis (GAD). Moreover, it has been shown how they can be used as a tool for archaeological dating.

Índice

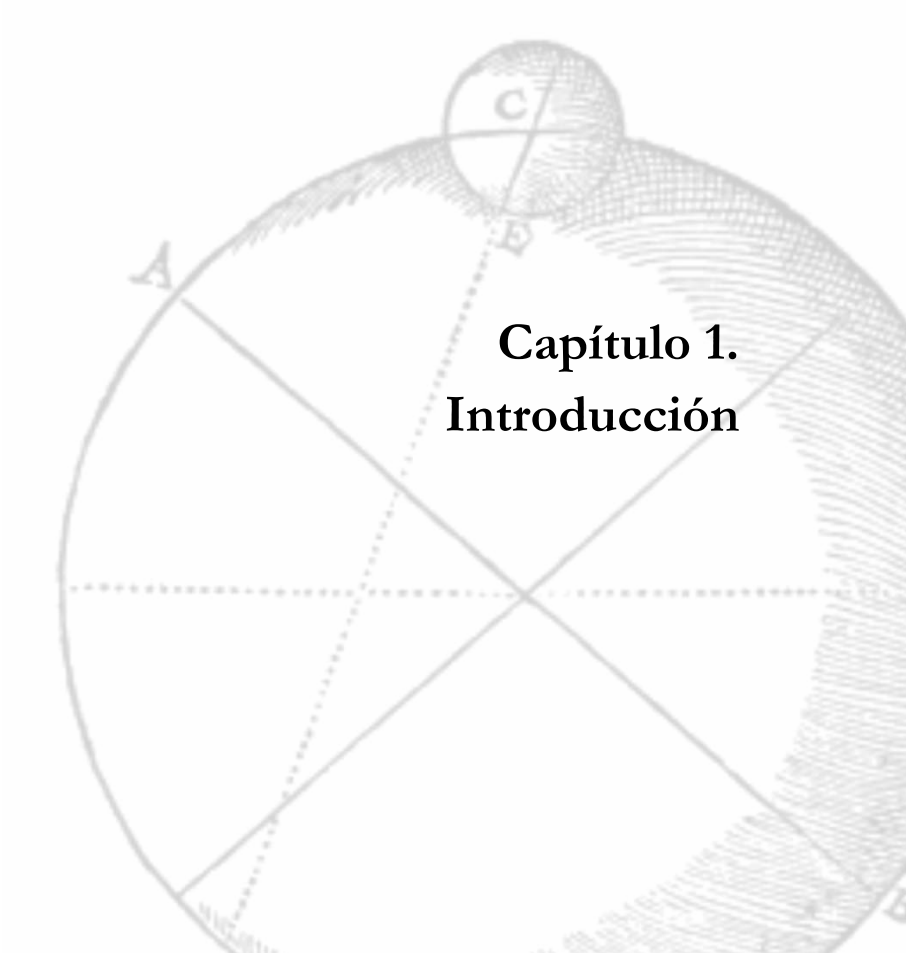

Capítulo 1.
Introducción

1.1. Motivación e hipótesis.

Observaciones directas del campo geomagnético en la superficie de la Tierra para los últimos 400 años muestran que la intensidad dipolar (o momento dipolar) está en continuo decrecimiento. Además, los valores de la declinación indican un movimiento del campo hacia el oeste, conocido como *Westward drift* en inglés (ver Merrill et al., 1996, para una revisión). Pero este registro instrumental (o histórico) sólo abarca los últimos 4 siglos y éste es un período de tiempo muy corto si se pretende analizar patrones de comportamiento en la variación de largo período del campo geomagnético: la llamada variación paleosecular (PSV, del inglés *Palaeosecular Variation*).

Para analizar épocas anteriores hay que hacer uso de la magnetización remanente característica de algunas rocas terrestres. Esta magnetización remanente se presenta en los materiales denominados ferromagnéticos (en *sensu lato*). Es decir, el campo geomagnético deja su *huella* en las rocas debido a que éstas contienen trazas de minerales ferromagnéticos. Estos minerales adquirieron un magnetismo remanente estable en presencia del campo geomagnético que actuó durante la formación del material o durante una serie de procesos fisicoquímicos a los que fue sometido posteriormente (calentamientos, transformaciones químicas,…).

Al estudio del campo geomagnético en el pasado a través del magnetismo remanente de las rocas se le denomina Paleomagnetismo. Esta disciplina permite conocer el pasado del campo geomagnético hasta edades muy antiguas, entorno a los 3500 millones de años (Usui et al., 2009 y referencias internas). En escalas geológicas el Paleomagnetismo juega un papel importante en el estudio de paleoreconstrucciones continentales y patrones magnetoestratigráficos, donde las inversiones del campo geomagnético quedan reflejadas. En este caso, se asume que el campo geomagnético es dipolar geocéntrico y axial (GAD, del inglés *Geocentrical Axial Dipole*) ya que la variación secular se promedia a partir de los 10.000 años (ver por ejemplo *Lectures in Paleomagnetism* de L. Tauxe, 2005). Para estudiar el campo geomagnético reciente, últimos 12000 años (el período del Holoceno), la hipótesis del GAD es demasiado simplista, y la variación secular del campo geomagnético no dipolar cobra gran importancia. En este período temporal los materiales que tienen más interés para el Paleomagnetismo son las lavas volcánicas, los sedimentos lacustres y los materiales arqueológicos.

Las coladas volcánicas tienen potencial como registradores del campo magnético terrestre en el pasado debido a su termorremanencia (remanencia de origen térmico). Pero en ocasiones la remanencia volcánica presenta una baja estabilidad magnética durante los experimentos de desimanación térmica realizados para determinar la dirección y/o la intensidad del campo geomagnético. Esta inestabilidad se traduce muchas veces en resultados difíciles de interpretar (especialmente en los estudios de intensidad) y en tasas de éxito a menudo muy bajas. Además, debe realizarse una revisión crítica de la edad asociada al evento volcánico, pues hay numerosos datos volcánicos sujetos a grandes discusiones (Lanza y Zanella, 2006 y referencias interiores).

Los sedimentos lacustres permiten, en general, un registro continuo del campo magnético terrestre pero, debido a la remanencia deposicional (o post-deposiciaonal) característica de estos materiales, se suavizan altamente las amplitudes de la variación paleosecular. Además, resulta todavía difícil establecer una escala temporal absoluta. Sin embargo, como veremos a lo largo de esta memoria, representan un potencial importante a tener en cuenta para poder conocer las características del campo geomagnético anteriores a los últimos 3000 años.

Finalmente, el material arqueológico que ha sufrido importantes calentamientos adquiere una remanencia térmica que presenta una gran estabilidad durante los experimentos de desimanación, lo que da lugar a resultados de fácil interpretación y a altos índices de éxito (a menudo más del 80% en estudios direccionales o de intensidad). Por esta razón, la información proporcionada por materiales arqueológicos calentados bien datados constituye el método más eficaz para analizar la variación paleosecular del campo magnético terrestre de los últimos milenios. En este caso, el Paleomagnetismo deriva en el Arqueomagnetismo.

La remanencia de los materiales arqueológicos de interés paleomagnético es debida, principalmente, al calentamiento al que fue sometido el material. Cuando éste se enfría por última vez por debajo de su temperatura de bloqueo (en general, durante el último uso de la estructura) se queda grabado el campo geomagnético existente en ese instante de tiempo. Los hornos, hogares, termas, suelos quemados,… son materiales arqueológicos de un estudio arqueomagnético. Tras someter a un material arqueológico a la técnica arqueomagnética, éste genera un dato arqueomagnético, caracterizado por una dirección (declinación e inclinación) y/o una intensidad del campo magnético terrestre asociados a su edad y a las coordenadas geográficas del mismo. Por tanto, si en una cierta región de la Tierra tenemos varios materiales arqueológicos de edades distintas y con potencial arqueomagnético, podemos determinar el comportamiento del campo geomagnético en dicha región en el período temporal que abarcan dichos materiales.

Los datos de lavas volcánicas y sedimentos lacustres bien datados pueden ser usados también como información adicional en el análisis de la variación paleosecular del campo geomagnético, ya que pueden aportar una mejor cobertura espaciotemporal que la que cubren los datos arqueomagnéticos.

En las últimas décadas se han desarrollado numerosas estrategias para analizar el campo geomagnético a partir de datos arqueomagnéticos. La primera, y quizás la más tradicional, se basa en la construcción de las curvas de variación paleosecular (PSVC, del inglés *palaeosecular variation curve*) características de una región o país. Para construir estas curvas, los datos arqueomagnéticos analizados deben ser corregidos para extrapolar sus valores desde el lugar del yacimiento arqueológico hasta el lugar de referencia donde se pretende elaborar la PSVC. Para realizar dicha transferencia se asume un campo geomagnético dipolar inclinado y por ello, la región de validez de dichas curvas no puede ser mayor a los 200.000 km^2 (Tarling, 1983).

Existen varios métodos matemáticos que pueden ser aplicados en la construcción de la PSVC a partir de los datos arqueomagnéticos, como son el clásico método de ventanas móviles (e.g. Sternberg and McGuire, 1990) o su modificación a partir de ventanas con tamaño adaptable (e.g. Le Goff et al., 2002). Recientemente se ha desarrollado el uso de la estadística bayesiana para la construcción de dichas curvas (ver Lanos et al., 2005 para una revisión). El problema asociado a las PSVCs es su restringida validez espacial, el error de relocalización producido por el traslado del dato arqueomagnético (Casas e Incoronato, 2007), y la posible incoherencia con otras PSVCs de regiones vecinas debido a las distintas bases de datos arqueomagnéticos usadas.

Otra forma de abordar el problema consiste en representar analíticamente el comportamiento espacial y temporal del campo geomagnético a partir de los datos paleomagnéticos, mediante el análisis armónico de Gauss de la misma forma que se aplica a datos instrumentales y/o históricos (Jackson et al., 2000). A escala global esta representación ha sido ampliamente ensayada durante la última década (Hongre et al., 1998, Korte y Constable, 2003 y 2005, Korte et al., 2009). Pero la resolución de los modelos y el grado de los coeficientes de Gauss dependen de la cantidad y calidad de los datos y de su distribución global. Los datos arqueomagnéticos no tienen la calidad de los instrumentales y además su distribución espaciotemporal es muy pobre (prácticamente no hay datos en el hemisferio sur) por lo que en los modelos globales deben introducirse fuertes parámetros de suavizado y, en muchos casos, deben incorporar datos de coladas volcánicas y registros sedimentarios. En la figura 1.1 se ha representado la actual localización de los datos arqueomagnéticos, de coladas volcánicas y de sedimentos lacustres para los últimos 7000 años (Korte et al., 2005 y Donadini et al., 2009). Para cubrir los vacíos de los datos arqueomagnéticos en el espacio y el

tiempo, los largos registros sedimentarios son una buena alternativa, pero implican un mayor grado de suavizado en la amplitud de la variación paleosecular (Korte y Constable, 2005, Korte et al., 2009).

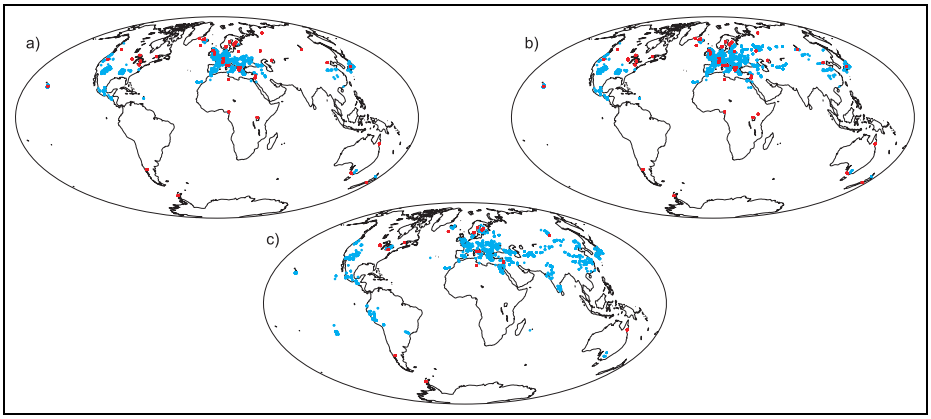

Figura 1.1. Localización global de los estudios arqueomagnéticos (puntos azules, incluyendo lavas) y sedimentos lacustres (puntos rojos) que permiten analizar el campo geomagnético de los últimos 7000 años. Bases de datos de Korte et al. (2005) y Donadini et al. (2009). a) Datos de declinación, b) de inclinación y c) de intensidad (intensidad relativa en el caso de sedimentos lacustres).

En resumen, las curvas de variación Paleosecular permiten un análisis del campo arqueomagnético muy restringido en el espacio. Por otra parte, el número de estudios arqueomagnéticos realizados hasta la actualidad es aún escaso para poder determinar un modelo global de gran precisión.

Europa es el continente donde la densidad de datos arqueomagnéticos es mayor que en cualquier otra parte del mundo (ver figura 1.1) y ésta ha aumentado considerablemente durante los últimos años, gracias al desarrollo del proyecto europeo AARCH (*Archaeomagnetic Applications for Rescue of Cultural Heritage*). Ante esta alta densidad de datos arqueomagnéticos en el continente Europeo y los problemas derivados del uso de PSVCs y modelos globales, nos planteamos las siguientes cuestiones:

• ¿Se puede aplicar un método de modelización regional en Europa para analizar el campo geomagnético?
• ¿Qué método regional es el más adecuado para la distribución de datos actual?
• ¿Permitirá un modelo regional solventar los problemas que presentan las PSVCs y los modelos globales?

La respuesta a la primera pregunta parece lógica. Si con la pobre distribución global de datos paleomagnéticos es posible la generación de modelos globales, restringir el modelo a la región mundial con mayor densidad de datos parece razonable y podría ser el mejor camino para analizar el campo geomagnético en

dicha región, ya que no se ve afectado por la escasez de datos del resto del mundo.

El método de modelización regional más adecuado debería ser aquel que analice el campo geomagnético como solución de la ecuación de Laplace, del mismo modo que ocurre para los modelos globales. En este sentido, el método del Análisis Armónico sobre un Casquete Esférico o SCHA (del inglés *Spherical Cap Harmonic Analysis*), introducido originalmente por Haines (1985a), es la mejor opción.

Los estudios regionales del campo geomagnético en época instrumental (últimos 100 años) indican que, en general, estos modelos regionales permiten determinar con mayor precisión las características del campo geomagnético que los modelos globales, ya que las longitudes de onda representadas son de menor longitud. En este contexto podemos encontrar ejemplos como los estudios del campo geomagnético de referencia de España (Torta et al. 1993), de la región Antártica (Gaya-Piqué, 2004) o más recientemente de la región francesa (Thébault et al., 2006b).

El primer análisis regional del campo geomagnético basado en datos paleomagnéticos fue llevado a cabo por Torta et al. (2000). Los autores emplearon la técnica SCHA para la modelización regional del campo en Europa para el intervalo temporal 0 - 500 años d.C. El modelo SCHA resultante mejoró en Europa al modelo global de Hongre et al (1998), pero distó de dar una precisa representación del campo. Para alcanzar resultados adecuados debe realizarse una revisión crítica de la base de datos paleomagnéticos y una adaptación del método regional SCHA aplicado a este tipo de datos.

1.2. Objetivos.

De acuerdo con las hipótesis planteadas en el apartado anterior, los principales objetivos de este trabajo son:

• Estudio del método SCHA y sus posteriores versiones revisadas (R-SCHA y R-SCHA2D).

En el capítulo 3 damos un amplio resumen del método regional de modelización SCHA introducido por Haines en 1985. Además, se incluyen las últimas revisiones llevadas a cabo por Thébault et al. (2006a) y Thébault (2008).

• Estudio y ampliación de la base de datos arqueomagnéticos.

La adquisición de nuevos datos en regiones ausentes de información. Aunque la región Europea sea la más altamente investigada (Korte et al., 2005 y

Donadini et al., 2009), existen numerosas áreas en las que los datos son escasos o no existen. Incluso en países con alta cultura arqueológica, como Italia, el número de datos arqueomagnéticos es pequeño (Tema et al., 2006). Uno de los primeros objetivos del presente trabajo ha sido ampliar y analizar de forma exhaustiva la base de datos paleomagnética de Europa, aportando un estudio arqueomagnético realizado en el Principado de Asturias (España), que constituye la primera fuente de datos arqueomagnéticos para la región centro-norte de la Península Ibérica. Dicho estudio se detalla en el capítulo 4 de la memoria.

Consideramos, además, que es necesario conocer el proceso de obtención de datos arqueomagnéticos para poder ser más conscientes del valor, las características y las limitaciones de los datos.

• Obtención de modelos regionales del campo geomagnético para los últimos dos milenios.

Al no existir estudios previos con resultados satisfactorios sobre la aplicación del método SCHA a los datos paleomagnéticos, debemos establecer estrategias para abordar el problema de la modelización regional a varios niveles. El primer paso ha consistido en analizar y probar la aplicación de la técnica SCHA. Para ello, generamos modelos iniciales del campo geomagnético en el período temporal con mayor número de datos arqueomagnéticos, i.e., los últimos 2000 años. Los modelos iniciales se han abordado en dos pasos: primero se ha obtenido un modelo direccional y, en una segunda etapa, un modelo que incluye la intensidad. El capítulo 5 de la memoria contiene el desarrollo de estos modelos iniciales.

• Desarrollo de un Modelo Arqueomagnético para Europa válido para los últimos 3000 años.

Una vez alcanzados los primeros objetivos y teniendo en cuenta los resultados satisfactorios obtenidos, se genera un modelo para el vector campo geomagnético (declinación, inclinación e intensidad) para Europa (capítulo 6 de la memoria). Este nuevo modelo regional es más robusto y coherente que los anteriores y tiene una validez temporal mayor, cubriendo los últimos 3000 años.

• Ampliación del modelo anterior en el tiempo 5000 años más, mediante la incorporación de datos sedimentarios.

Los modelos globales han demostrado que el uso de registros paleomagnéticos de sedimentos lacustres puede mejorar la cobertura espaciotemporal de los datos (Korte y Constable, 2003), aunque ello implica un suavizado en el registro de las amplitudes de la variación paleosecular. En el capítulo 7 se presenta un nuevo modelo del vector geomagnético generado

mediante la combinación de sedimentos lacustres y datos arqueomagnéticos en la región Europea ampliando el modelo anterior hasta los últimos 8000 años.

• Desarrollo de aplicaciones.

En el capítulo 8 se analizan algunas de las aplicaciones directas que se han desarrollado a partir de los modelos regionales obtenidos, como detectar y estudiar cambios bruscos en la variación paleosecular e investigar su posible relación con el clima. Además, el hecho de que la variación secular tenga una dependencia espaciotemporal, ésta puede ser usada para datar estructuras arqueológicas con potencial arqueomagnético cuya edad es desconocida (e.g. Le Goff et al., 2002). En el capítulo se presenta un software en lenguaje Matlab desarrollado para la datación arqueomagnética.

Capítulo 2.
El campo geomagnético y su modelización

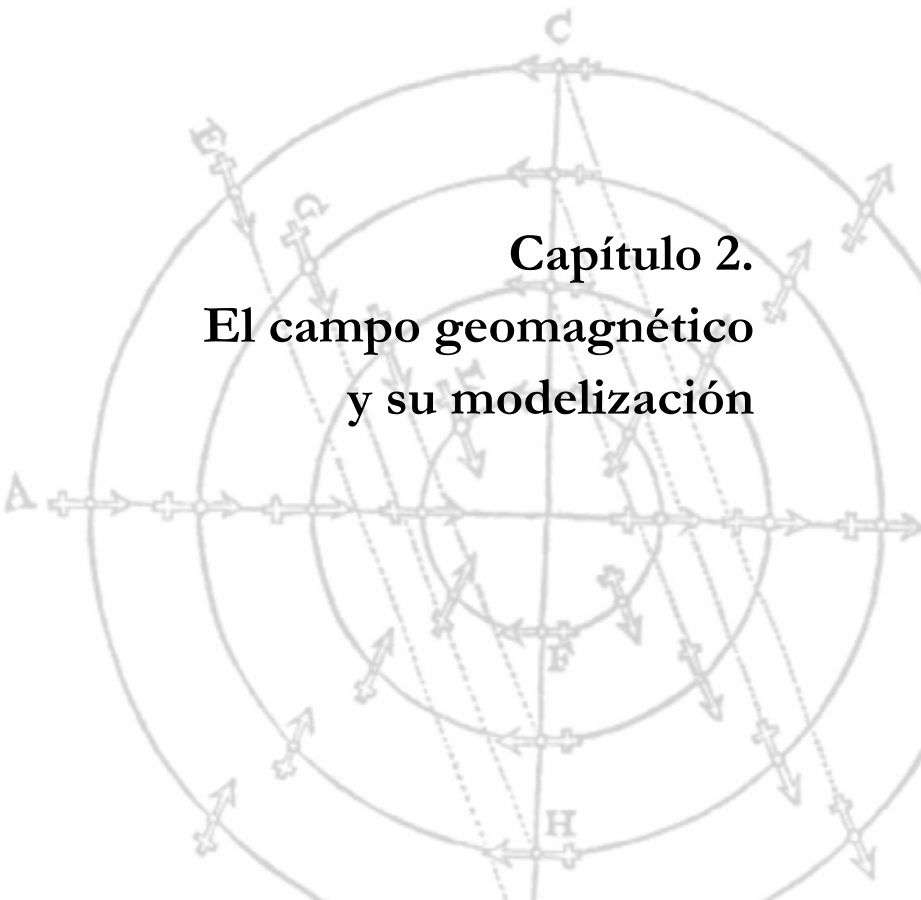

El magnetismo terrestre, como todo fenómeno electromagnético, se analiza a partir de las ecuaciones de Maxwell. Las ecuaciones relativas al vector inducción magnética **B** (e.g., Parkinson, *Introduction to Geomagnetism*, 1983) son:

$$\vec{\nabla}\mathbf{B} = 0 \qquad [2.1]$$

$$\vec{\nabla}\times\mathbf{B} = \mu\left(\mathbf{J} + \vec{\nabla}\times\mathbf{M} + \frac{\partial\mathbf{D}}{\partial t}\right) \qquad [2.2]$$

La primera ecuación [2.1] indica la imposibilidad de la existencia de cargas magnéticas aisladas (no se puede aislar un polo magnético) obligando a que las líneas de fuerza del campo magnético siempre sean cerradas. En el caso del campo geomagnético, al considerar la Tierra como un gran imán, las líneas de fuerza surgen desde las proximidades del polo sur geográfico (polo norte magnético) y penetran en la Tierra en la zona boreal (polo sur magnético).

La segunda expresión [2.2] relaciona el vector inducción con sus posibles fuentes de creación, como son una densidad de corriente **J**, una distribución de material imantado **M** y una corriente eléctrica de desplazamiento variable en el tiempo **D**. La magnetohidrodinámica y la electrodinámica son las disciplinas encargadas del análisis de estas expresiones, que junto con las ecuaciones de continuidad de los fluidos y de la transferencia de calor, gobiernan el origen del campo magnético de la Tierra.

La unidad de medida del vector inducción magnética **B** es el tesla (T). En nuestro caso el tesla es una unidad demasiado grande ya que, por ejemplo, el valor del módulo de **B** (intensidad) en la superficie de la Tierra en latitudes medias es del orden de $4\text{x}10^{-5}$ T. Por lo que será muy común expresarlo en μT (10^{-6} T) o nT (10^{-9} T).

2.1. Elementos del campo geomagnético

La mayor contribución al campo geomagnético es la generada por fuentes magnéticas situadas en el núcleo externo. A la resultante de los campos magnéticos originados en el núcleo externo se le denomina Campo Interno o Campo Principal, cuya naturaleza es aproximadamente dipolar. Oscila en la superficie de la Tierra con valores entre los 60000 nT en los polos norte y sur magnéticos y los 30000 nT en el ecuador magnético (Jacobs, *Geomagnetism*, 1987-1991). La variación temporal que sufre es muy lenta, apreciable a partir de decenas de años, por lo que es llamada Variación Secular. Pero no todas las

características del campo geomagnético se describen a partir del Campo Principal, ya que existen otros campos magnéticos de naturalezas distintas que se suman a este último.

Un segundo campo que contribuye al campo geomagnético es también de origen interno: el llamado campo cortical o campo de anomalías magnéticas. Dicho campo es el resultante de la magnetización de las rocas en la corteza terrestre. Esta magnetización tiene dos orígenes: la primera puede ser debida a los campos inducidos o viscosos en los materiales, cuyas variaciones temporales son análogas a las del Campo Principal bajo un cierto tiempo de retraso; y la segunda corresponde a los campos magnéticos remanentes de las rocas originados durante su formación geológica o producidos por otros fenómenos físico-químicos. La magnetización remanente es estable en la escala de tiempo geológico.

Contribuyen, además, al campo total, los campos de origen externo, generados en las regiones ionosféricas y magnetosféricas, cuyos períodos de variación van desde años (por el ciclo undecenal de la actividad solar) hasta segundos (pulsaciones magnéticas), pasando por variaciones anuales, estacionales y diarias, con sus correspondientes armónicos.

Por último, otra fuente importante son los campos inducidos en la corteza y en el manto terrestre, originados por las variaciones del campo externo, al ser todas esas corrientes externas variables en el tiempo.

Un resumen de todos los campos contribuyentes lo podemos ver en la siguiente Tabla 2.1.

Tabla 2.1. Campos contribuyentes al magnetismo terrestre (Adaptada de Parkinson, 1983).

Campo Magnético	Fuente del campo	Intensidad máxima	Carácter	Variación temporal
Principal	Núcleo externo	65000 nT	Dipolar más contribución no dipolar	Variación secular Inversiones
Cortical	Corteza	100 nT	Irregular	Escala Geológica
Ionosférico	Ionosfera	200 nT	Global	Variación Diurna Tormentas
Magnetosférico	Magnetosfera	100 nT	Global	Tormentas Pulsaciones
Inducidos	Corteza y manto superior	50 nT	Global con irregularidades de tipo local	Análoga a los ionosféricos y magnetosféricos

Para eliminar variaciones de corto período y poder así determinar el Campo Principal, se hace necesario promediar su valor en un rango temporal de un año y en una superficie no mayor de 10^6 km^2.

El campo total viene expresado por el vector inducción magnética **B**, que puede descomponerse en coordenadas polares o cartesianas:

$$\mathbf{B} = \mathbf{B}_r + \mathbf{B}_\theta + \mathbf{B}_\lambda \equiv \mathbf{X} + \mathbf{Y} + \mathbf{Z} \qquad [2.3]$$

Se definen así los elementos del campo geomagnético: la componente horizontal **H** está subdividida en componente norte $\mathbf{X} = -\mathbf{B}_\theta$ con sentido hacia el norte geográfico, componente este $\mathbf{Y} = \mathbf{B}_\lambda$ hacia el este geográfico, y la componente vertical: $\mathbf{Z} = -\mathbf{B}_r$, con sentido hacia el nadir en el hemisferio norte y al cenit en el hemisferio sur.

Otra forma de definirlo es a través de sus elementos angulares (la declinación *D*, la inclinación *I*) y el campo total **F** (que corresponde al módulo del vector). La relación que existe entre ellos se describe gráficamente en la figura 2.1.

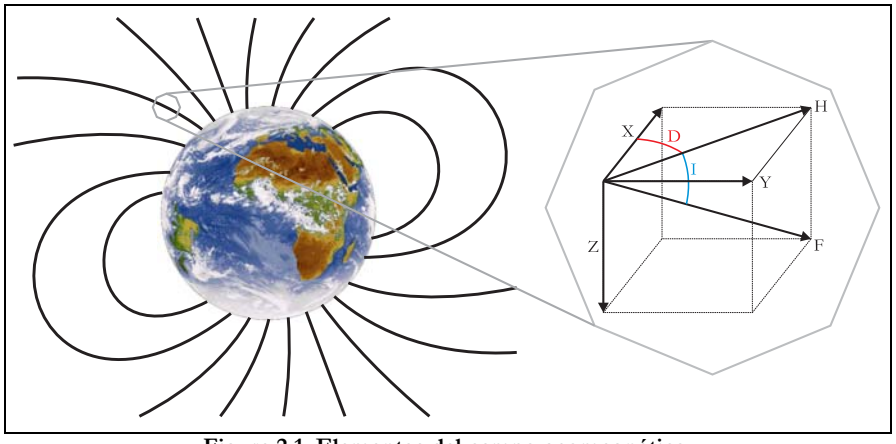

Figura 2.1. Elementos del campo geomagnético.

Acorde a la figura 2.1 podemos desarrollar expresiones trigonométricas que relacionan todos los elementos:

$$X = H\cos D = F\cos D\cos I \qquad [2.4]$$

$$Y = H\sin D = F\sin D\cos I \qquad [2.5]$$

$$Z = F\sin I \qquad [2.6]$$

Y por tanto podemos deducir:

$$F = B = \left(X^2 + Y^2 + Z^2\right)^{1/2} \qquad [2.7]$$

$$H = \left(X^2 + Y^2\right)^{1/2} \qquad [2.8]$$

$$tgI = \frac{Z}{H} \qquad [2.9]$$

$$tgD = \frac{Y}{X} \qquad [2.10]$$

En la figura 2.2 se muestran los valores de los elementos del campo en la superficie de la Tierra para la época 2010.0. Dichos valores se han generado a partir de la 11ª generación del IGRF (Internacional Geomagnetic Reference Field, IAGA, 2009).

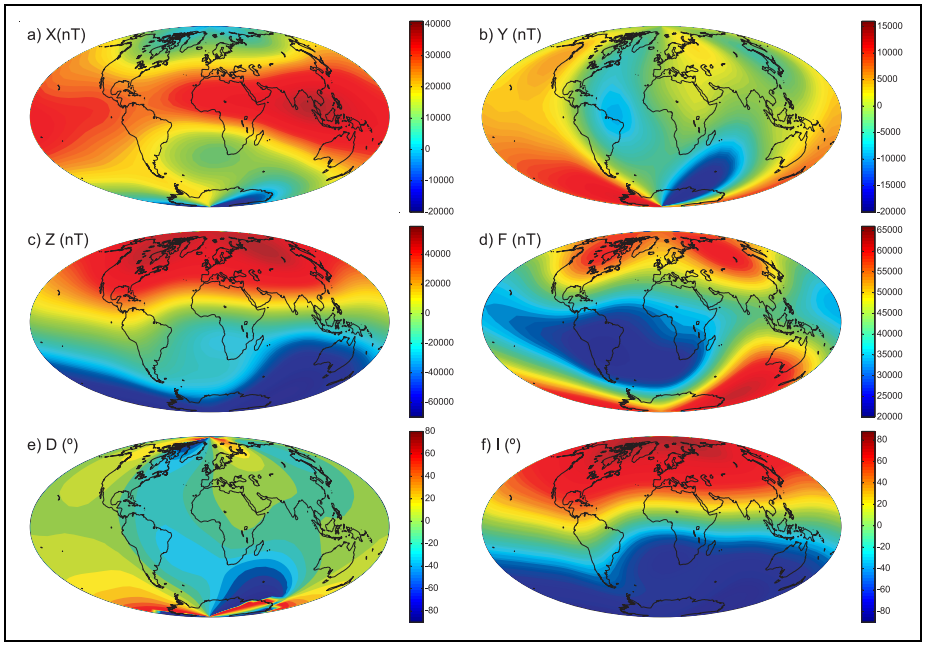

Figura 2.2. Mapas de la componente norte (a), este (b), vertical (c) y de la intensidad (d) en nT. Mapas de declinación (e) e inclinación (f) en grados. Undécima generación del IGRF para la época 2010.0 (IAGA, 2009).

2.2. Modelos de campo geomagnético.

Desde hace siglos se ha modelado el fenómeno geomagnético en la superficie terrestre desarrollando modelos matemáticos globales o regionales. Que podamos generar unos u otros depende de la distribución de datos disponible (ver Schott y Thébault, 2010, para una revisión).

El primer intento de modelar el campo geomagnético en la superficie terrestre fue descrito por William Gilbert en 1600 al considerar que la Tierra en sí misma se comporta como un gigantesco imán esférico cuyos polos magnéticos coincidían con los polos geográficos. Ello implica valores nulos de declinación magnética para cualquier punto de la superficie de la Tierra, consideración errónea, como se vio posteriormente. Años después, en 1610 se modela la inclinación. Para ello, Edward Wright, impuso dos condiciones: que fuese nula en el ecuador y máxima en el polo norte geográfico. En 1688 fue modelada la declinación por Henry Bond usando valores de los observatorios de Londres y ajustando su variación secular.

El primer modelo completo (por modelo completo se entiende aquel que se genera teniendo en cuenta las tres componentes ortogonales del campo geomagnético: **X**, **Y** y **Z,** o bien cualquier otra combinación de tres elementos independientes, como *D*, *I* y *F*) fue realizado en 1838 por C. F. Gauss mediante un desarrollo en armónicos esféricos. Basados en la misma técnica que Gauss, aunque perfeccionada a lo largo del tiempo, se han desarrollado la mayor parte de los modelos globales existentes hasta la actualidad. Cuando los datos de campo geomagnético están distribuidos en una región, la mejor opción es generar modelos regionales válidos sólo para la zona de estudio. En las próximas secciones desarrollamos los métodos de modelización tanto para el caso global como el regional.

2.2.1. Análisis armónico global.

La descripción matemática del Campo Principal se basa en las dos ecuaciones de Maxwell dadas anteriormente (ec. [2.1] y [2.2]). La aplicación tendrá lugar en una región libre de fuentes magnéticas y corrientes eléctricas. Esta región está limitada en su base inferior por la superficie de la Tierra y en la parte superior por la Ionosfera, a partir de unos 50 km de altura aproximadamente. Esto implica que los términos de la derecha de la expresión [2.2] son nulos:

$$\vec{\nabla}\mathbf{B} = 0 \qquad [2.11]$$

$$\vec{\nabla} \times \mathbf{B} = 0 \qquad [2.12]$$

Lo cual hace que la inducción magnética **B** se pueda derivar de un campo escalar, llamado potencial geomagnético V.

$$\mathbf{B} = -\vec{\nabla} V \qquad [2.13]$$

Teniendo en cuenta [2.13] y aplicando las ecuaciones [2.11] y [2.12] el potencial escalar verifica la ecuación de Laplace en la región indicada:

$$\nabla^2 V = 0 \qquad [2.14]$$

Que un potencial escalar verifique la ecuación de Laplace tiene importantes implicaciones. En primer lugar, dadas unas condiciones de contorno, el potencial existirá siempre (teorema de Dirichlet), será único (teorema de Stokes) y armónico (es una función analítica). Además Gauss, en 1839, demostró que dicho potencial puede ser descrito como una expansión en armónicos esféricos (SHA, Spherical Harmonic Analysis), ya que la geometría que nos exige el campo geomagnético es la esférica. Sin embargo otro tipo de representaciones analíticas del campo son posibles, y éstas serán discutidas más adelante en la sección dedicada a los métodos de modelización regional.

El desarrollo SHA del campo geomagnético consiste en la resolución del potencial magnético escalar, que satisface la expresión [2.14] bajo una serie de condiciones de contorno. El potencial magnético no es más que una expresión

matemática para la representación del campo a través de fuentes magnéticas "virtuales" situadas en el centro de la Tierra, y a pesar de alejarse de la realidad física, permite definir de forma analítica el comportamiento del campo en las regiones dadas.

Si definimos el potencial geomagnético en coordenadas esféricas $V(r,\theta,\lambda)$, el laplaciano del mismo viene expresado por:

$$\frac{1}{r^2}\frac{\partial}{\partial r}\left(r^2\frac{\partial V}{\partial r}\right)+\frac{1}{r^2\sin\theta}\frac{\partial}{\partial\theta}\left(\sin\theta\frac{\partial V}{\partial\theta}\right)+\frac{1}{r^2\sin^2\theta}\frac{\partial^2 V}{\partial\lambda^2}=0 \qquad [2.15]$$

Aplicando el método de separación de variables, se puede escribir el potencial como producto triple de tres funciones analíticas dependientes de la distancia radial, la colatitud y la longitud geográfica respectivamente:

$$V(r,\theta,\lambda)=f(r)\cdot g(\theta)\cdot h(\lambda) \qquad [2.16]$$

Del potencial derivan entonces tres ecuaciones diferenciales de autovalores, una para cada variable. Para la distancia radial:

$$\frac{1}{r^2}\frac{d^2 f(r)}{dr^2}+2r\frac{df(r)}{dr}-kf(r)=0 \qquad [2.17]$$

Para la colatitud:

$$\frac{d}{d\theta}\left(\sin\theta\frac{dg(\theta)}{d\theta}\right)+g(\theta)\left[n(n+1)\sin\theta-\frac{m^2}{\sin\theta}\right]=0 \qquad [2.18]$$

Y para la longitud:

$$\frac{d^2 h(\lambda)}{d\lambda^2}+m^2 h(\lambda)=0 \qquad [2.19]$$

La solución de las tres ecuaciones está determinada por las condiciones de contorno en la esfera (Tierra):

$$V(r,\theta,\lambda)=V(r,\theta,\lambda+2\pi);\ \frac{\partial V(r,\theta,\lambda)}{\partial\lambda}=\frac{\partial V(r,\theta,\lambda+2\pi)}{\partial\lambda} \qquad [2.20]$$

$$V(r,\theta_i,\lambda)=0,\ si\ m\neq 0;\ \frac{\partial V(r,\theta_i,\lambda)}{\partial\theta}=0,\ si\ m=0,\quad con\ \theta_i=0,\pi \qquad [2.21]$$

Las soluciones a las ecuaciones diferenciales [2.17], [2.18] y [2.19] teniendo en cuenta las condiciones de contorno son:

$$f(r)=Ar^n+Br^{-(n+1)} \qquad [2.22]$$

$$h(\lambda)=Ce^{im\lambda}+De^{-im\lambda} \qquad [2.23]$$

$$g(\theta)=P_n^m(\cos\theta) \qquad [2.24]$$

Donde $P_n^m(\cos\theta)$ son las funciones asociadas de Legendre de primera y segunda especie. Las de segunda especie poseen una singularidad en $\theta = 0$, por lo que no pueden ser consideradas como solución. Serán las de primera especie, también llamadas de Newman, la solución en colatitud.

Los autovalores *m* y *n(n+1)* son constantes enteras para la solución en la esfera, donde *n* indica el grado del polinomio y *m* el orden de la función, verificándose que $m \leq n$. La combinación de las funciones asociadas de Legendre y las soluciones en longitud nos proporciona los armónicos de superficie o armónicos esféricos. Dichas funciones son ortogonales en la esfera y están normalizadas (semi-normalización de Schmidt). Una mejor descripción de las funciones armónicas en la esfera se puede encontrar en *Spherical Functions of Mathematical Geosciences* (Freeden y Schreiner, 2009):

$$Y_n^m(\theta,\lambda) = P_n^m(\cos\theta)\cos m\lambda \qquad [2.25]$$

$$Z_n^m(\theta,\lambda) = P_n^m(\cos\theta)\sin m\lambda \qquad [2.26]$$

Si agrupamos las soluciones, tenemos dos tipos de ecuaciones para el potencial geomagnético dependiendo si $r > a$ ó $r < a$, siendo *a* el radio medio de la Tierra. Todas las posibles combinaciones de estas funciones darán una solución al potencial magnético escalar, el cual se podrá expresar a través de una contribución interna y otra externa:

$$V(r,\theta,\lambda) = V_{\text{int}}(r,\theta,\lambda) + V_{ext}(r,\theta,\lambda) \qquad [2.27]$$

$$V_{\text{int}}(r,\theta,\lambda) = a\sum_{n=0}^{\infty}\left(\frac{a}{r}\right)^{n+1}\sum_{m=0}^{n}P_n^m(\cos\theta)(g_{n,\text{int}}^m\cos m\lambda + h_{n,\text{int}}^m\sin m\lambda) \qquad [2.28]$$

$$V_{ext}(r,\theta,\lambda) = a\sum_{n=0}^{\infty}\left(\frac{r}{a}\right)^{n}\sum_{m=0}^{n}P_n^m(\cos\theta)(g_{n,ext}^m\cos m\lambda + h_{n,ext}^m\sin m\lambda) \qquad [2.29]$$

El potencial interno será aquel que describe fuentes situadas en el interior de la Tierra, mientras que el potencial externo indica fuentes magnéticas situadas a alturas superiores a los 100 km (Barraclough, 1978). A los coeficientes que aparecen en la expresión del potencial, *g* y *h*, se les denominan coeficientes de Gauss y sus dimensiones son las mismas que las del campo magnético. Los coeficientes h_n^0 son nulos, debido a la condición de contorno [2.21].

Algunas consideraciones: el sumatorio que define el potencial geomagnético no puede empezar con el grado $n = 0$. Para dicho orden nulo, el potencial interno [2.28] es inversamente proporcional a *r* dando lugar a una fuente magnética monopolar situada en el centro de la Tierra, lo cual violaría la ecuación [2.1]. Además, el potencial externo [2.29] es constante y de él no se deriva ningún campo magnético ($\vec{\nabla}V = \mathbf{0} = -\mathbf{B}$). Señalar también que el sumatorio no se extiende a infinito, si no a un grado máximo de $n = N_{máx}$.

Si queremos representar el campo geomagnético mediante el potencial geomagnético, hay que tener en cuenta que éste no es observable (no se puede medir), y por tanto necesitamos relacionarlo con magnitudes reales, como son las componentes del campo magnético *X*, *Y*, *Z*. Las relaciones entre estas magnitudes son:

$$X = \frac{1}{r}\frac{\partial V}{\partial \theta} \qquad [2.30]$$

$$Y = -\frac{1}{r\sin\theta}\frac{\partial V}{\partial \lambda} \qquad [2.31]$$

$$Z = \frac{\partial V}{\partial r} \qquad [2.32]$$

2.2.2. Coeficientes de Gauss.

Si se expresa el Campo Principal como un desarrollo en armónicos esféricos, cobran gran importancia los coeficientes de Gauss del potencial interno (coeficientes *g* y *h* en [2.28]). Para analizar e interpretar físicamente los coeficientes, vamos a sustituir en la expresión [2.28] los valores de los primeros armónicos esféricos hasta grado 1, orden 1 (e.g. Parkinson, *Introduction of the Geomagnetism*, 1983):

$$\begin{aligned} V(r,\theta,\lambda) &= \frac{a^3}{r^2}\left[g_1^0\ P_1^0(\cos\theta) + (g_1^1\cos\lambda + h_1^1\sin\lambda)\,P_1^1(\cos\theta)\right] = \\ &= \frac{a^3}{r^2}\left[g_1^0\ \cos\theta + (g_1^1\cos\lambda + h_1^1\sin\lambda)\sin\theta\right] \end{aligned} \qquad [2.33]$$

Por otro lado, el potencial de un dipolo magnético viene dado por la expresión:

$$V(r,\theta,\lambda) = K\cdot\frac{\mathbf{m}\cdot\hat{\mathbf{e}}_\mathbf{r}}{r^2} = \frac{K}{r^2}(m_x\cos\lambda\sin\theta + m_y\sin\lambda\sin\theta + m_z\cos\theta) \qquad [2.34]$$

Si comparamos esta expresión con los términos de [2.33] vemos que los primeros coeficientes de Gauss están relacionados con las componentes del momento dipolar **m**, la constante electrostática *K* y el radio medio de la Tierra:

$$g_1^0 = K\frac{m_z}{a^3},\ g_1^1 = K\frac{m_x}{a^3},\ h_1^1 = K\frac{m_y}{a^3} \qquad [2.35]$$

El módulo del momento dipolar será:

$$m = \frac{a^3}{K}\sqrt{(g_1^0)^2 + (g_1^1)^2 + (h_1^1)^2} = B_0 \qquad [2.36]$$

Siendo B_0 la constante geomagnética. La dirección del dipolo (θ_0, λ_0) se calculará a través de las componentes del momento dipolar:

$$tg\theta_0 = \frac{\sqrt{(g_1^1)^2 + (h_1^1)^2}}{g_1^0} \qquad [2.37]$$

$$tg\lambda_0 = \frac{h_1^1}{g_1^1} \qquad [2.38]$$

Este dipolo genera en la superficie de la Tierra el llamado campo dipolar, la diferencia con el campo real es el campo no dipolar. Si aumentamos el grado, para n = 2, éste representa un cuadrupolo, con n = 3 un octupolo y así continuamente aproximándose con mayor exactitud el campo real. A medida que aumentamos el grado de desarrollo la magnitud de los coeficientes disminuye, ya que la mayor contribución se debe a los coeficientes de menor grado. A continuación se muestra una gráfica donde se observa la caída exponencial de los coeficientes a medida que se aumenta el grado del desarrollo (coeficientes proporcionados también por la 11ª generación del IGRF para 2010.0, IAGA, 2009).

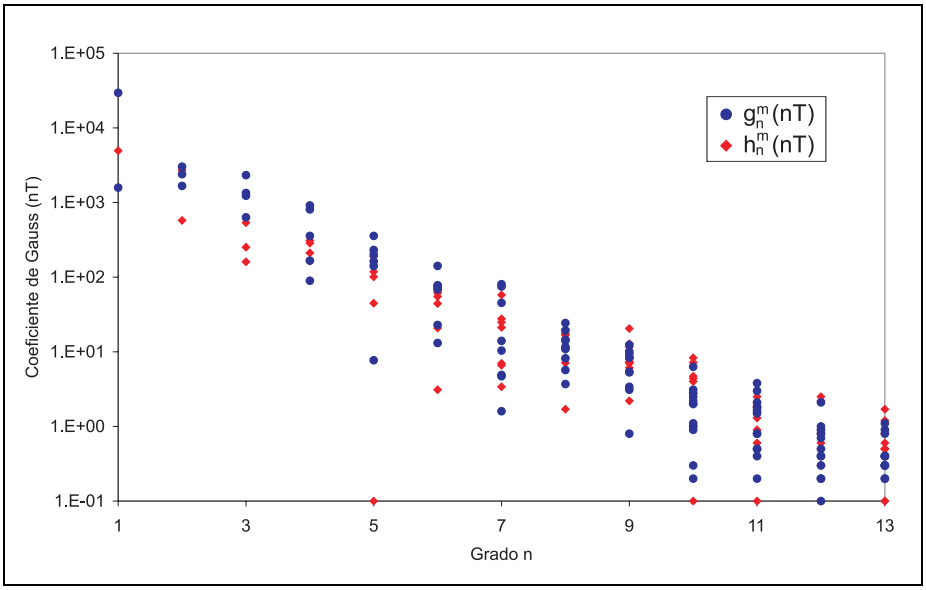

Figura 2.3. Valores absolutos de los coeficientes de Gauss para 2010.0 según IGRF undécima generación (IAGA, 2009) frente al grado del desarrollo en armónicos esféricos, *n*. Nota: el eje de ordenadas está en escala logarítmica.

El espectro de los coeficientes de Gauss presenta un cambio de pendiente significativo a partir del grado 13 o 14 (Langel y Estes, 1982; Cain et al., 1984), lo cual es interpretado como el paso de una contribución puramente nuclear a una contribución cortical. Los de menor grado dan lugar a variaciones espaciales del campo magnético de gran longitud de onda generadas en zonas del núcleo externo. A medida que n aumenta las longitudes de onda disminuyen.

La aproximación dipolar conseguida con el grado $n = 1$ define en un 90% el valor del Campo Principal, variando este porcentaje dependiendo de unas zonas u otras de la Tierra. El resto del desarrollo corresponde al campo no dipolar cuya variación espacio-temporal es diferente al dipolar.

2.2.3. Modelos globales IGRF/DGRF y *Comprehensive Models*.

Dentro los modelos de descripción del Campo Principal cabe destacar los que han sido (y siguen siendo) modelos de referencia. Éstos son los denominados "Modelos Internacionales de Referencia de Campo Geomagnético" (*Internacional Geomagnetic Reference Field*, IGRF). En 1969, la IAGA (*Internacional Association of Geomagnetism and Aeronomy*) inaugura la generación de estos modelos. El primero describe el Campo Principal (desarrollo en armónicos esféricos) y su variación secular. Fue referido al 1 de Enero de 1965 e incluía los valores de los coeficientes de Gauss y sus primeras derivadas temporales hasta un grado $n = 8$. Este modelo tuvo validez desde 1955 hasta 1975. La segunda generación IGRF es consecuencia de la evolución tecnológica, pues se introducen también datos obtenidos por satélites. Se aporta un nuevo modelo de campo geomagnético para 1975, y de su variación secular, válido de 1975 a 1980. Estos modelos previos han sido criticados y revisados y han dado origen a los modelos de referencia definitivos (*Definitive Geomagnetic Reference Field*, DGRF).

Generalmente cada cinco años han ido apareciendo diferentes modelos IGRF válidos para el año de publicación y pronóstico en los 5 años posteriores (por medio de la variación secular), modelos retrospectivos para la primera mitad del siglo XX y progresivamente los modelos definitivos DGRF. Estos son el fruto de la revisión que hace la IAGA a partir de diferentes propuestas de determinados grupos científicos dedicados al geomagnetismo. En la actualidad contamos con once generaciones de modelos de referencia IGRF. Estos describen el Campo Principal en épocas separadas por intervalos de cinco años desde 1900 hasta 2010; y el último da la predicción a través de la variación secular para el intervalo 2010 – 2015. También en intervalos de cinco años desde 1945 hasta el 2005 se dan los modelos definitivos (DGRF). Todos ellos se han generado considerando la forma semi – normalizada de Schmidt (Chapman y Bartels, 1940). La última revisión del IGRF corresponde a la undécima generación (IAGA, 2009), proporcionando un modelo para el 2010.0 con un total de 195 coeficientes, hasta el grado 13 y variación secular hasta grado 8. En la figura 2.2 de la sección 2.1 se muestran los valores de las componentes del campo geomagnético dados por la última generación del IGRF para 2010.0. Para más información: http://www.ngdc.noaa.gov/IAGA/vmod/igrf.html.

En los últimos años se han desarrollado modelos que intentan superar el problema de la unión de la variación espacio – temporal del campo geomagnético en la superficie terrestre y las observaciones en satélites (unión

entre campo de origen interno y externo). Aparecen así los Modelos Completos (*Comprehensive Models*, CM) del campo geomagnético, usando principalmente los datos proporcionados por los satélites Ørsted, CHAMP, Magsat y POGO y datos en tierra de los observatorios geomagnéticos. En el modelo CM3 (*Comprehensive model* 3, Sabaka et al., 2002) se hace un análisis de los datos del satélite Magsat y la serie POGO en el intervalo 1960 – 1985, y considera todas las fuentes posibles del campo geomagnético, desde el núcleo externo hasta la magnetosfera. Más recientemente se ha actualizado dicho modelo, apareciendo el CM4 (Sabaka et al., 2004), que utilizó datos de los satélites CHAMP y Øersted, y amplió el período de validez del CM3 hasta mediados de 2002. Para más información de estos modelos ver http://core2.gsfc.nasa.gov/CM/.

Actualmente la variación secular del Campo Principal se caracteriza por una disminución del campo dipolar y por una deriva hacia el oeste tanto del campo dipolar como del no-dipolar. El primer intento de modelar en armónicos esféricos la variación secular fue llevado a cabo por Carlheim-Gyllensköld (1896), generando una serie de modelos de Campo Principal para el período 1550 – 1900 y relacionándolos entre sí a través de la variación secular. Pero fue en 1925 cuando Julius Bartels genera el primer modelo de variación secular para el período 1902 – 1919, basado en datos de 14 observatorios y con un número máximo de coeficientes igual a 8. Barraclough (1976) hace un recopilatorio de los diferentes modelos de variación secular desarrollados a través de la técnica de armónicos esféricos. Estos modelos han permitido conocer la variación del campo geomagnético en los últimos cien años. Los modelos actuales del Campo Principal también describen la variación secular, como es el caso del IGRF.

2.2.4. Modelos generados con datos históricos y/o paleomagnéticos.

Uno de los objetivos principales del Geomagnetismo es conocer el comportamiento de la variación secular durante largos períodos de tiempo. Surgen así, en las últimas décadas, modelos globales basados en datos aportados por medidas históricas (Jackson et al., 2000) y datos paleomagnéticos (Hongre et al., 1998, Korte and Constable, 2003, 2005; y Korte et al., 2009). Estos últimos incluyen datos provenientes de yacimientos arqueológicos (arqueomagnetismo), de erupciones volcánicas históricas y de sedimentos lacustres.

i. Modelo global histórico (1590 – 1990).

Uno de los modelos globales más citado es el modelo GUFM1 (Jackson et al., 2000) que está basado en medidas históricas e instrumentales. Proporciona los valores del campo para los últimos cuatrocientos años (desde 1590 al 1990). Los datos utilizados del último siglo son aportados por los observatorios geomagnéticos, y los datos anteriores al siglo XIX (sólo direccionales: declinación e inclinación) han sido obtenidos a través de la información

proporcionada por los marineros de la época (mapas, cartas y apuntes). El hecho de que solo haya datos direccionales históricos se debe a que el instrumento de medida de intensidades absolutas fue desarrollado por Gauss en 1837, por lo que no hay valores de intensidad hasta esa fecha. En la figura 2.4 se muestran las localizaciones de los datos que estos autores usaron.

Al no disponer de valores de intensidad histórica en el período 1590 – 1840 d.C. Jackson et al. (2000) asumieron un valor estimado del primer coeficiente de Gauss g_1^0 para ese período. Dicha estimación la obtuvieron extrapolando linealmente el valor de g_1^0 de 1840 y asumiendo una variación temporal constante de 15 nT/año. Esta variación corresponde al valor medio de la derivada de g_1^0 en el período instrumental: 1850 – 1990 d.C. En la figura 2.5 se muestra el valor del coeficiente g_1^0 del modelo GUFM1 para los últimos 400 años, donde se observa el comportamiento lineal para edades anteriores a 1840 d.C.

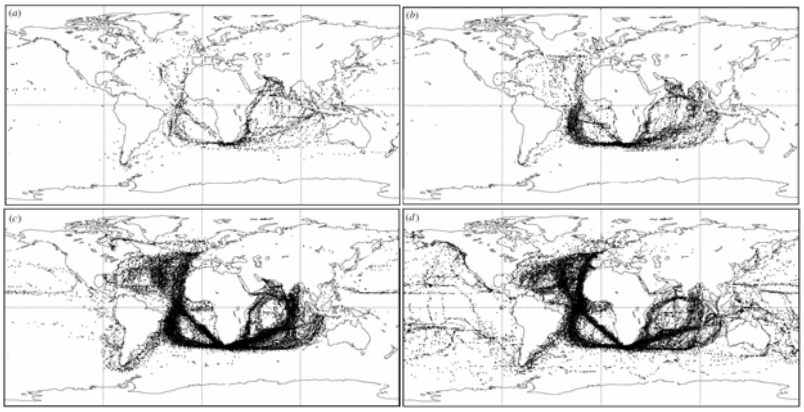

Figura 2.4. Localización espacial de los puntos de medidas de la declinación tomados de las rutas marítimas: a) período de 1600 a 1649; b) de 1650 a 1699; c) de 1700 a 1749 y c) de 1750 a 1799. De Jackson et al. (2000).

Jackson et al. (2000) aplicaron el análisis armónico global para desarrollar un modelo de Campo Principal hasta grado 14 (orden 14) y utilizaron esplines cúbicos para dar continuidad temporal a los coeficientes de Gauss obtenidos. Los datos de entrada obtenidos de las cartas marítimas tienen dos tipos de errores, el error en la determinación de la posición de los puntos de medida (especialmente importante) y el error de la propia medida. Para tratar esta información, los autores propusieron un modelo estocástico, estableciendo una dispersión aleatoria de los errores análoga al movimiento Browniano.

Para generar el modelo global introdujeron en el proceso de inversión de datos, métodos de regularización espacio-temporales para asegurar la convergencia y permitir obtener modelos más realistas. Aplicaron dos métodos de regulación (o normas): uno a la parte espacial y otro a la parte temporal. La expresión que regula la norma espacial se obtuvo a partir de la mínima disipación

óhmica en la frontera manto – núcleo externo (CMB del ingés *Core-Mantle Boundary*) y viene dada por (Gubbins, 1975):

$$\Psi = \frac{1}{t_e - t_s}\int_{t_s}^{t_e} f(B_r)dt \qquad [2.39]$$

donde [t_e , t_s] es el intervalo temporal donde se calcula la integral, B_r es la componente Vertical del campo y $f(B_r)$ es la norma cuadrática del campo geomagnético asociada con el mínimo calentamiento óhmico dado en función de los coeficientes de Gauss:

$$f(B_r) = 4\pi\sum_{n=1}^{N}\frac{(n+1)(2n+2)(2n+3)}{n}\left(\frac{a}{c}\right)^{2n+4}\sum_{m=0}^{n}[(g_n^m)^2 + (h_n^m)^2] \qquad [2.40]$$

siendo c el radio medio del CMB. La regulación en la parte temporal la obtuvieron minimizando la siguiente función en la superficie del CMB:

$$\Phi = \frac{1}{t_e - t_s}\int_{t_s}^{t_e}\oint(\partial_t^2 B_r)^2 d\Omega dt \qquad [2.41]$$

Ambas funciones (espacial y temporal) pueden ser transformadas matricialmente de la forma:

$$\Psi = \mathbf{m}^T\mathbf{S}^{-1}\mathbf{m} \qquad [2.42]$$

$$\Phi = \mathbf{m}^T\mathbf{T}^{-1}\mathbf{m} \qquad [2.43]$$

donde **m** es el vector que contiene los coeficientes de Gauss y **S** y **T** son las matrices dependientes de los parámetros del modelo para la norma espacial y temporal respectivamente. Ambas matrices, junto con sus respectivos parámetros de amortiguación o multiplicadores de Lagrange (λ_S y λ_T), conforman la matriz general de regularización que es usada en el proceso de inversión de datos:

$$\mathbf{M_R} = \lambda_S \cdot \mathbf{S} + \lambda_T \cdot \mathbf{T} \qquad [2.44]$$

Estos parámetros de amortiguamiento deben ser fijados teniendo en cuenta el mejor compromiso entre el modelo obtenido y los observables.

Posterior a la publicación del modelo GUFM1, se publicaron dos modificaciones del mismo que modifican la estimación del primer coeficiente de Gauss g_1^0. La primera, llevada a cabo por Gubbins et al. (2006), utilizó la base de datos de intensidad de Korte et al. (2005) en el período 1590 – 1840 d.C. para obtener un valor más realista del primer coeficiente de Gauss. Asumieron también un comportamiento lineal y propusieron una variación de 2.28 nT/año de acuerdo al ajuste proporcionado por los datos de intensidad. Y la última modificación ha sido llevada a cabo por Finlay (2008) que revisó el trabajo anterior de Gubbins et al. (2006) aplicando numerosos métodos estadísticos (estadística Bayesiana) para evaluar de nuevo el coeficiente g_1^0 en el período 1590

– 1840 d.C. El autor propuso que el primer coeficiente de Gauss era constante en todo el intervalo de tiempo. Estas propuestas y la dada originalmente por Jackson et al. (2000) son comparadas en la figura 2.5.

Con los nuevos valores de g_1^0 se pueden reescalar los valores de intensidad del modelo GUFM1 para el período 1590 – 1840 d.C. sin alterar la parte direccional del mismo (declinación e inclinación), ya que dichos elementos no dependen del valor numérico de g_1^0.

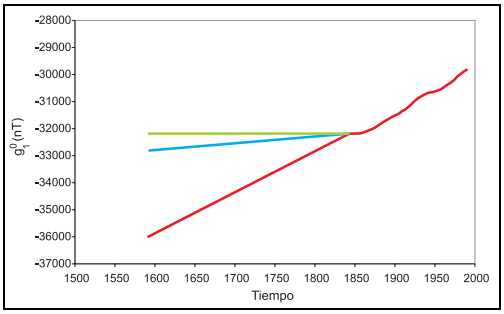

Figura 2.5. Coeficiente de Gauss g_1^0 según el modelo GUFM1 (Jackson et al., 2000), Gubbins et al. (2006) y Finlay (2008). Curvas roja, azul y verde respectivamente.

ii. Modelos globales basados en datos paleomagnéticos: La familia de modelos CALS.

Los primeros modelos basados en datos paleomagnéticos fueron publicados por Johnson y Constable (1997), Kelly y Gubbins (1997), Carlut y Courtillot (1998) y Hatekeyama y Kono (2002). Todos ellos analizan el comportamiento del Campo Principal de los últimos cinco millones de años mediante modelos promediados en el tiempo (modelos TAF, del inglés *Time-Average Field model*). Con los datos paleomagnéticos estimaron el valor del primer coeficiente de Gauss (g_1^0) que define al campo dipolar axial (GAD). Y mediante técnicas estadísticas cuantificaron la dispersión de los datos paleomagnéticos respecto al GAD proporcionando porcentajes de contribución del campo cuadrupolar y octupolar. Las bases de datos paleomagnéticos que fueron usadas en estos modelos fueron recopiladas por Quidelleur et al. (1994), Johnson y Constable (1997), y McElhinny y Lock (1996).

Basado en la recopilación de datos arqueomagnéticos realizada por Daly and Le Goff (1996), Hongre et al. (1988) generaron un modelo de Campo Principal desde el inicio de nuestra Era hasta el año 1700. Este modelo basado en armónicos esféricos considera solo los primeros armónicos: hasta grado 2 más el de grado 3 y orden 3. En este mismo año se publicó también un modelo pseudo-temporal, el ALS3K (Johnson y Constable, 1998). Tras una nueva recopilación de datos paleomagnéticos (arqueomagnéticos, lavas históricas y de sedimentos lacustres) de los últimos 3000 años efectuada por Lund y Constable

(PSVMOD1.0), Constable et al. (2000) elaboraron un modelo para los últimos 3000 años. Se trata de un modelo promediado por ventanas de cien años.

En 2003, Korte y Constable publicaron un modelo continuo en el tiempo para los últimos tres mil años: el modelo CALS3K.1. Con este modelo comienzó la familia de modelos CALS (*Continuous Archeomagnetic and Lake Sediment*) que se resumen en la Tabla 2.2. En la construcción del modelo CALS3K.1 solo hacen uso de los datos direccionales, agrupándolos por regiones y generando como datos de entrada varias curvas de variación paleosecular (12 curvas arqueomagnéticas y 12 de sedimentos lacustres). Como sustituto a los datos de intensidad prefijaron el primer coeficiente de Gauss g_1^0 asumiéndolo lineal por tramos dentro del período temporal 1000 a.C – 1800 d.C. En su generación usaron los armónicos esféricos globales (para la parte espacial), los esplines cúbicos (parte temporal) y la regularización del Campo Principal en el CMB descrita anteriormente para el modelo GUFM1. Debido a la gran ausencia de datos paleomagnéticos en el hemisferio sur incluyeron parámetros de suavizado muy altos en el proceso de inversión de datos. Ello da lugar a un modelo muy suavizado, incluso en zonas con alta densidad de datos paleomagnéticos, como es el caso de la región europea. Así, aunque el grado y el orden del desarrollo en armónicos esféricos usado es 10, la resolución no dista más allá de un modelo global de grado 4 (Korte y Constable, 2005).

Tras la revisión de datos paleomagnéticos del Holoceno (últimos 10000 años), Korte et al. (2005) publicaron una nueva base de datos paleomagnéticos, que incluye datos de lavas históricas, sedimentos lacustres y de yacimientos arqueológicos. Usando esta base de datos Korte y Constable (2005) generaron, siguiendo el mismo protocolo de su modelo previo, tres nuevos modelos globales basados en armónicos esféricos globales de grado 10. El modelo CALS3K.2 y los modelos CALS7K.1 y CALS7K.2. El primero corresponde a una versión actualizada del previo 3K.1 debido a la utilización de la nueva base de datos. Además, incrementa su período de validez de 1800 d.C. hasta 1950 d.C. Los últimos dos modelos fueron desarrollados usando todo el período temporal: desde el 5000 a.C. hasta el 1950 d.C. La diferencia entre los modelos 7K.1 y el 7K.2 radica en que el primero contiene una serie temporal de datos sedimentarios antárticos con incertidumbres posiblemente erróneas, por lo que los pesos asociados a estos datos no estaban bien estimados. El nuevo modelo 7K.2 solventa dicho error, pero aun así los autores prefieren mantener ambos modelos. Estos tres modelos se diferencian del previo 3K.1 en que los datos paleomagnéticos son usados *in situ* (sin relocalizarlos a regiones comunes) y usan los tres elementos del campo conjuntamente, incluida la intensidad. Además la incertidumbre del dato paleomagnético viene dada, no solo por la incertidumbre de la medida instrumental, sino también por la incertidumbre en la edad asociada. Ello hace que de dos datos de igual incertidumbre en la medida tenga más peso aquel con menor incertidumbre en la edad. De nuevo y debido a la

gran ausencia de datos en el hemisferio sur, los autores tuvieron que aumentar los parámetros de suavizado en el proceso de inversión, lo cual genera un modelo muy suave que equivale, nuevamente, a un desarrollo de grado 4 en armónicos esféricos.

Finalmente en 2009 y tras el aumento considerable de publicaciones de nuevos datos arqueomagnéticos en los últimos 5 años, Donadini et al. (2009) publicaron una nueva base de datos mundial para los últimos 4000 años basada en datos arqueomagnéticos y datos paleomagnéticos de lavas históricas y sedimentos lacustres. En base a esta nueva base de datos, Korte et al. (2009) proporcionan cinco nuevo modelos globales de Campo Principal válidos desde el año 1000 a.C. hasta 1990 d.C. Estos nuevos modelos son generados a partir de cinco bases de datos diferentes, dependiendo de la naturaleza del dato paleomagnético, aplicando la misma metodología que los modelos anteriores.

Pero aunque el número de datos arqueomagnéticos haya aumentado notablemente en los últimos 5 años, éstos han sido llevados a cabo principalmente en el continente Europeo; por lo que el vacío de datos paleomagnéticos en el hemisferio sur no ha sido solventado. En la figura 2.6 se muestra las localizaciones de los datos arqueomagnéticos para los últimos 4000 años (base de datos de Donadini et al., 2009). Los colores indican el número de datos para la misma localización en todo el período temporal. Más del 90% de los datos se encuentran en el Hemisferio Norte.

A partir de datos arqueomagnéticos y de coladas históricas, Korte et al. (2009) generan dos modelos: ARCH3K.1 y ARCH3K_cst.1. El primero usa todos los datos arqueomagnéticos, mientras que el segundo es generado seleccionando *a priori* los datos arqueomagnéticos que superan un cierto criterio de selección basado en las incertidumbres asociadas a cada dato. Usando todos los datos de sedimentos lacustres construyen un tercer modelo, llamado SED3K.1. Y, finalmente, haciendo uso de todos los tipos de datos, generan otros dos modelos: CALS3K.3 y CALS3K_cst.1. El primero de ellos generado con el total de datos paleomagnéticos y el segundo con los datos que han superado el criterio de selección considerado.

Aunque este nuevo conjunto de modelos han sido construidos siguiendo el mismo protocolo que los anteriores (Korte y Constable, 2005) se diferencian en algunos aspectos: (i) no modifican la incertidumbre del dato en función de la incertidumbre de la edad, sino que prefijan unos valores mínimos de incertidumbre para cada elemento geomagnético. (ii) En los últimos 400 años usan el modelo histórico GUFM1 para constreñir los resultados.

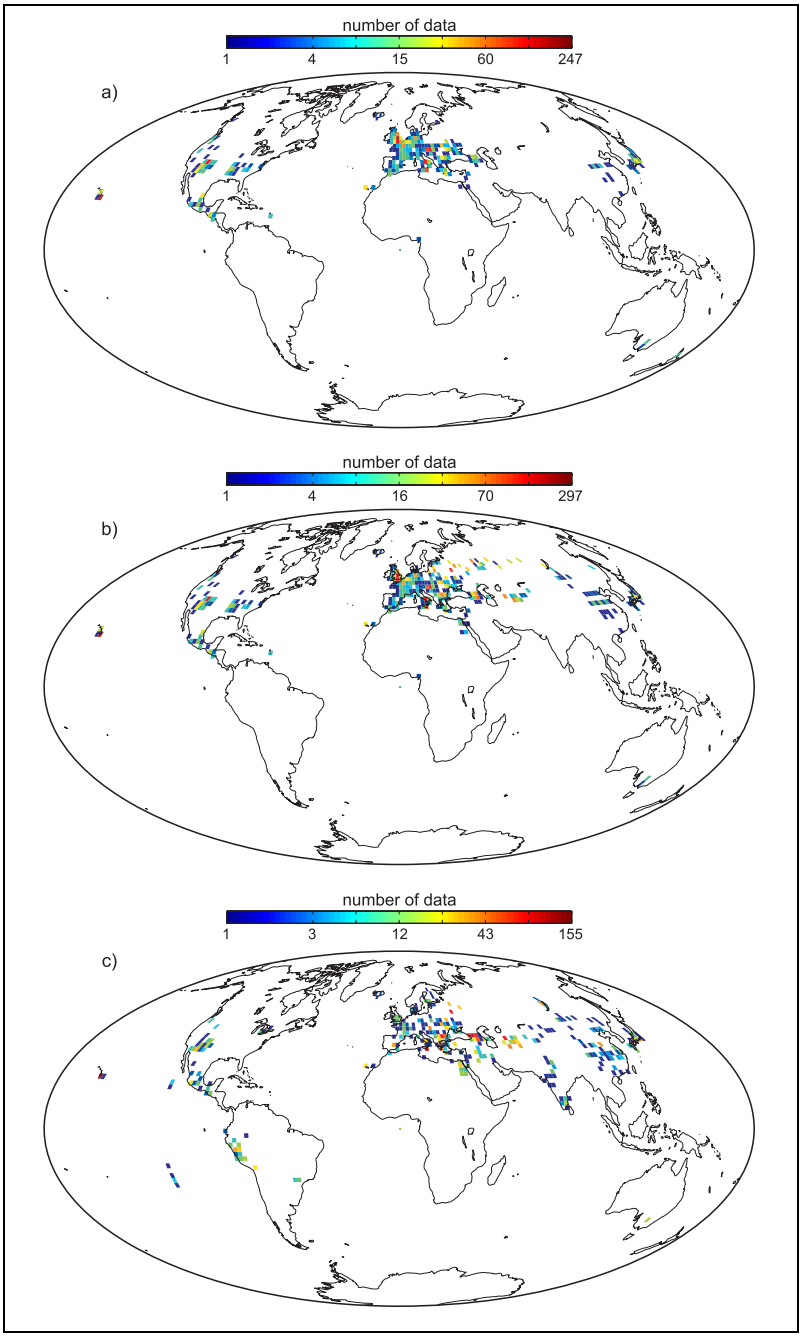

Figura 2.6. Localización global de los datos arqueomagnéticos para los últimos 4000 años para la (a) declinación, (b) inclinación e (c) intensidad. Datos de Donadini et al. (2009). Los datos han sido agrupados en una malla de 2º × 2º y los colores están relacionados con el número de datos dentro de la malla.

Como ejemplo comparativo, en la figura 2.7 mostramos los valores generados por todos los modelos de la familia CALS en dos puntos geográficos de longitud 0º y 45º N / 45º S de latitud respectivamente. Vemos como la mayor diferencia entre ellos corresponde a los valores del hemisferio sur. Recordemos que es en este hemisferio donde el número de datos es mucho menor y por tanto los modelos están peor definidos.

En la Tabla 2.2 resumimos todos los modelos de Campo Principal de la familia CALS, junto con el número de datos usados en su construcción y el período de validez.

Tabla 2.2. Familia de modelos globales CALS. Las columnas muestran por orden: Nombre del modelo. Tipo de dato (A: arqueomagnético, LH: lava histórica y LS: sedimento lacustre). Número de datos usados en la versión final del modelo global. Validez temporal.

Nombre del modelo	Tipo de dato Paleomagnético	Número de datos paleomagnéticos	Validez temporal
CALS3K.1	A, LH, LS	24 series**	1000 a.C. – 1800 d.C.
CALS3K.2	A, LH, LS	16683	1000 a.C. – 1950 d.C.
CALS7K.1	A, LH, LS	27080	5000 a.C. – 1950 d.C.
CALS7K.2	A, LH, LS	27080	5000 a.C. – 1950 d.C.
ARCH3K.1	A, LH	9483	1000 a.C. – 1990 d.C.
ARCH3K_cst.1	A*, LH*	6122	1000 a.C. – 1990 d.C.
SED3K.1	LS	20090	1000 a.C. – 1990 d.C.
CALS3K.3	A, LH, LS	29585	1000 a.C. – 1990 d.C.
CALS3K_cst.1	A*, LH*, LS*	19687	1000 a.C. – 1990 d.C.

* Datos que han superado un criterio de selección basado en sus incertidumbres.
** 24 series temporales: 12 arqueomagnéticas y 12 de sedimentos lacustres.

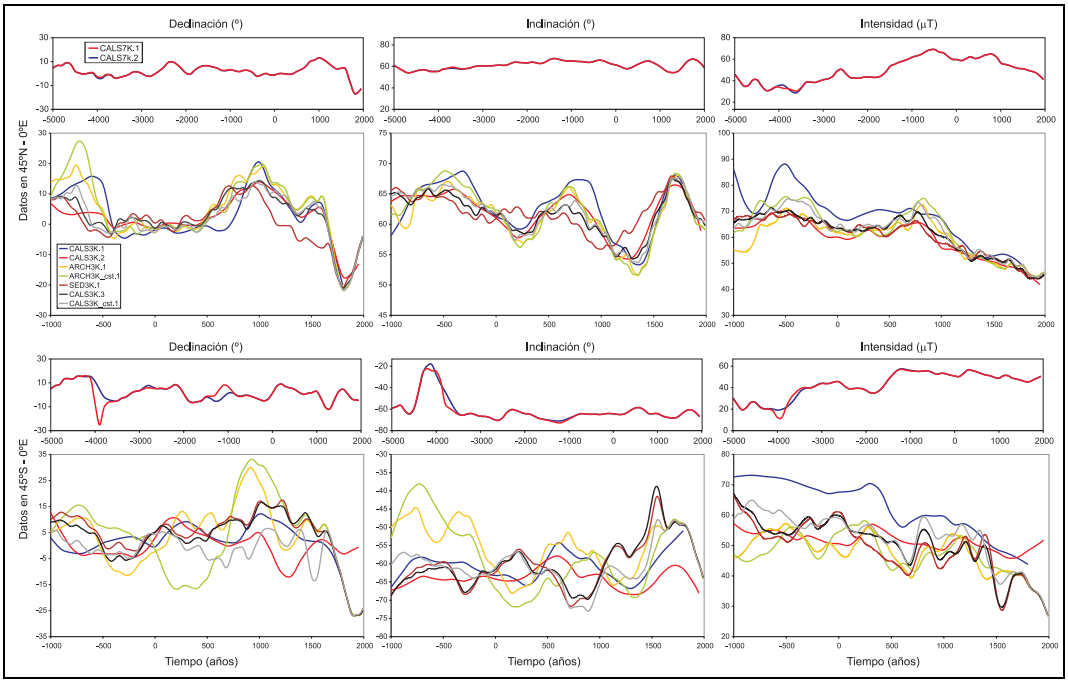

Figura 2.7. Curvas de variación Secular para las latitudes 45ºN y 45ºS (ambas con longitud 0º) dadas por la familia de modelos CALS (Korte y Constable, 2003, 2005; y Korte et al., 2009). Se han separado en las gráficas los modelos válidos para los últimos 7000 y 3000 años.

2.3. Modelos regionales

Cuando la densidad de datos se concentra en una determinada zona de la superficie de la Tierra, es más adecuado realizar representaciones regionales del campo geomagnético. Estos modelos regionales tienen validez solo en la región que encierra a los datos de entrada y es en esta región donde el modelo tendrá, en general, mayor resolución que cualquier modelo global, ya que con los modelos regionales es posible la representación de menores longitudes de onda (mayor resolución). Ver Schott y Thébault (2010) para una revisión de las técnicas regionales.

Las funciones que describen los modelos globales (ec. 2.28 y 2.29) no constituyen una base de funciones apropiadas para el ajuste regional. Por lo cual, hay que desarrollar nuevas técnicas para poder escoger las funciones base más apropiadas a los estudios regionales. Haines (1990a) proporciona una serie de métodos matemáticos para poder abordar el problema de la modelización del campo geomagnético y su variación secular en áreas regionales. Según él, podemos clasificar las diferentes técnicas de modelado regional en gráficas y analíticas.

Los modelos gráficos son los más antiguos. Inicialmente se obtenían representando las observaciones en un mapa y contorneándolas a mano. Actualmente las isolíneas se trazan con algoritmos de interpolación que permiten trazar las isolíneas. En este caso, los valores del campo entre dos isolíneas contiguas tienen que calcularse a través de interpolación sobre el mapa.

Las técnicas analíticas tienen mayor potencial ya que permiten obtener un modelo matemático que mejor ajusta a los datos observados. Existen varias técnicas analíticas de modelización regional. A continuación resumimos los diferentes tipos de técnicas así como sus principales características:

2.3.1. Ajuste polinomial.

Es un método sencillo de ajuste de las componentes del campo geomagnético a una distribución polinomial en función de los datos de observación. Se ha recurrido a esta técnica en numerosas ocasiones, por ejemplo en la península Ibérica (Ardizone y Herraiz, 2000; Marín y Pavón-Carrasco, 2006). Básicamente se basa en relacionar un observable del campo geomagnético (como pueden ser las componentes X, Y o Z, o los valores angulares de declinación e inclinación, e incluso la variación secular de cualquiera de ellos) con las coordenadas del punto de observación a través de una función polinomial. Si denotamos la componente del campo como E, ésta vendrá dada por (Barraclough y Clarke, 1988):

$$E = e_0 + e_1(\theta - \theta_C) + e_2(\lambda - \lambda_C) + e_3(\theta - \theta_C)^2 + e_4(\theta - \theta_C)(\lambda - \lambda_C)^2 + e_5(\lambda - \lambda_C)^2 + \ldots \quad [2.45]$$

Siendo θ la colatitud y λ la longitud del dato y θ_C y λ_C las coordenadas de un punto central de la distribución de datos (punto de referencia). Del mismo modo que las representaciones gráficas, esta técnica no contempla las altitudes de los datos de entrada. Por otra parte, las ecuaciones que se establecen para el modelo no satisfacen la ecuación de Laplace [2.14], pero ésta se puede imponer parcialmente estableciendo que la componente radial del rotacional del campo sea cero (Haines, 1968).

Esta técnica también se ha utilizado en la modelización de la variación secular del Campo Principal. Como ejemplo, en la siguiente figura se muestran los diferentes modelos polinomiales de variación secular de las componentes del campo (Norte, Este y Vertical) para la península Ibérica y Baleares en el año 2005.0 (Marín y Pavón-Carrasco, 2006).

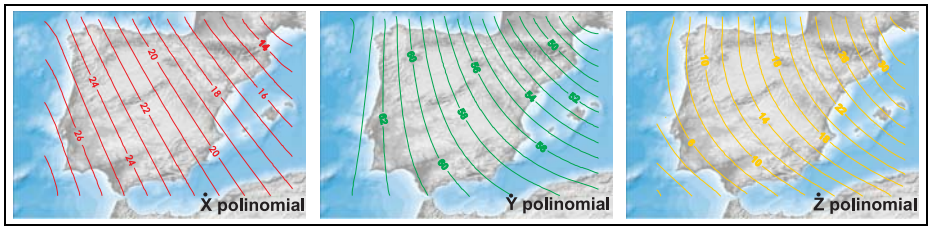

Figura 2.8. Mapas de los modelos polinomiales de la variación secular de las componentes geomagnéticas en la Península Ibérica y Baleares para el año 2005.0 (Marín y Pavón-Carrasco, 2006).

2.3.2. Ajuste mediante armónicos esféricos ordinarios.

Otra posibilidad de ajuste consiste en la aplicación del método clásico de armónicos esféricos globales (método de Gauss) en la región seleccionada. Pero ésto puede generar inestabilidades en el modelo, pues las funciones de Legendre no son ortogonales a escala regional. Esta inestabilidad puede ser corregida añadiendo datos sintéticos en una malla regular distribuida en el resto de la superficie terrestre. Otro inconveniente está relacionado con la longitud de onda, ya que al usarse armónicos ordinarios, estos modelos no tendrán longitudes de onda menores (mayor resolución) que los modelos globales.

2.3.3. Análisis armónico rectangular.

El hecho de que en una determinada región no se verifique la ortogonalidad de las funciones asociadas de Legendre o de las series de Fourier en longitud, hace que éstas se tengan que modificar para poder ser aplicadas a zonas restringidas de la Tierra. Una de estas modificaciones corresponde al análisis armónico rectangular (RHA, del inglés *Rectangular Harmonic Analysis*). Sus funciones base se obtienen tras aplicar la ecuación de Laplace [2.14] en coordenadas cartesianas al potencial geomagnético, pudiéndose expresar éste en función de las coordenadas cartesianas, los índices del desarrollo (n y m) y en función de los parámetros que definen la región de estudio ($K_X = 2/ L_X$ y $K_Y = 2/ L_Y$, donde L_X y L_Y son las dimensiones de la región rectangular):

$$\begin{aligned} V(x,y,z) = Ax + By + Cz + \sum_{m=1}^{M} (a_0^m \cos(mx) + b_0^m \sin(mx)) \cdot e^{-K_X m z} + \\ + \sum_{n=1}^{N} (a_n^0 \cos(ny) + c_n^0 \sin(ny)) \cdot e^{-K_Y n z} + \\ + \sum_{m=1}^{M} \sum_{n=1}^{N} (a_n^m \cos(mx)\cos(ny) + b_n^m \sin(mx)\cos(ny) + \\ + c_n^m \cos(mx)\sin(ny) + d_n^m \sin(mx)\sin(ny)) \cdot e^{-\sqrt{(K_X m)^2 + (K_Y n)^2} \cdot z} \end{aligned} \qquad [2.46]$$

El método, estudiado en detalle por Alldredge (1981) presenta algunos inconvenientes. En concreto la convergencia del método de inversión no se da

uniformemente dentro del intervalo de validez y sólo convergen en media (Haines, 1990b). Este hecho se debe a la no periodicidad de algunas de las funciones en la región de estudio, como es el caso de los términos en x, y o z de la expresión [2.46]. Además, estas funciones lineales hacen que no se cumpla la condición de contorno del potencial, ya que éste no tiende a cero cuando las coordenadas tienden a infinito. A destacar, también, su uso limitado a regiones muy pequeñas de la superficie de la Tierra, ya que solo en este caso se puede aproximar la geometría esférica a la rectangular.

2.3.4. Análisis armónico ajustado.

Este método, introducido por De Santis (1992), considera un casquete esférico de semiángulo θ_0 en una región lo suficientemente pequeña en la que se pueda verificar para las colatitudes que $\sin\theta \approx \theta$. Para ello, se escalan los armónicos esféricos globales a todo el casquete, es decir que la colatitud pasa de tomar cualquier valor entre los dos polos a tener valores entre 0º y el borde del casquete θ_0. Esta técnica, llamada también ASHA (del inglés *Adjusted Spherical Harmonic Análisis*), ha sido aplicada a datos geomagnéticos del sur de Italia por Chiappini et al. (1997).

2.3.5. Análisis armónico en un casquete esférico.

A partir de su publicación en 1985 por Haines (Haines, 1985a), muchos de los trabajos en modelización regional se han llevado a cabo usando este método de modelización: el análisis armónico en un casquete esférico. No solo el campo geomagnético ha sido analizado mediante esta técnica, sino también a sido empleada, por ejemplo, en Gravimetría. Con ella se pueden obtener modelos regionales del Campo Principal, de la variación secular, de las anomalías magnéticas, de las corrientes eléctricas de la ionosfera que generan la variación geomagnética diurna, etc. La técnica, denotada como SCHA (del inglés *Spherical Cap Harmonic Analysis*), permite una representación del campo geomagnético a escala regional mediante el desarrollo de funciones base en un casquete esférico. En el próximo capítulo se analiza en detalle dicha técnica regional, ya que ha sido la técnica elegida en este trabajo.

Capítulo 3.
Análisis armónico en un casquete esférico. Diferentes alternativas para la modelización de datos regionales

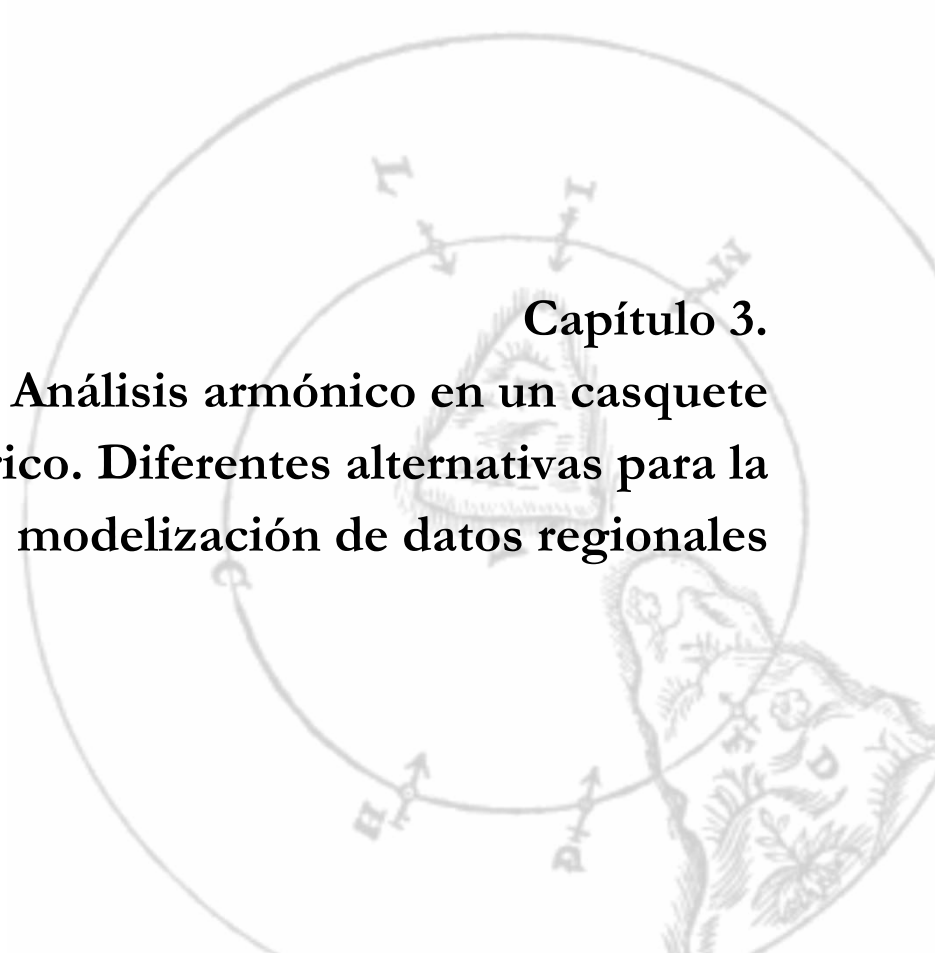

Dedicamos este capítulo al estudio de la resolución de la ecuación de Laplace (ec. 2.14) en un casquete esférico. Está dividido en cuatro secciones. En primer lugar se analiza la técnica clásica del análisis armónico en un casquete esférico (SCHA) para, a continuación, describir las nuevas técnicas desarrolladas recientemente de modelado regional: las técnicas revisadas R-SCHA y R-SCHA2D. En una tercera sección analizamos las funciones base que aparecen en el desarrollo del potencial geomagnético regional: las funciones asociadas de Legendre de grado real y las funciones cónicas de Mehler; además de definir la norma del Campo Geomagnético que puede ser usada en las técnicas de inversión. La siguiente sección está dedicada al tratamiento previo que hay que aplicar a los datos geomagnéticos (o paleomagnéticos) para poder ser utilizados en los métodos de modelización regional. En la última sección se analizan las técnicas de inversión empleadas en este trabajo.

3.1. El método clásico SCHA. Ecuaciones básicas.

La primera aplicación de la técnica clásica SCHA (Spherical Cap Harmonic Analysis) se realizó en la modelización de anomalías de la componente vertical del Campo Geomagnético (Haines, 1985b). Posteriormente fue aplicada al análisis del Campo Principal y a la contribución litosférica de larga longitud de onda en Europa (De Santis et al., 1989; Rotanova and Odintsov, 1999) y en regiones subcontinentales como Italia (De Santis et al., 1990), España (Torta, 1992), China (An et al., 1992) o Polonia (Rotanova et al., 2000).

En lo que respecta específicamente a la variación secular, el primer modelo generado por la técnica SCHA fue el propuesto por Haines en 1985 (1985c). Utilizó datos de observatorios y estaciones seculares a lo largo de 20 años en América del Norte. Basada en la misma técnica, Korte and Haak (2000) modelaron la variación secular en Europa durante la segunda mitad del siglo XX. Torta et al. (2002) representaron la variación secular en la Antártida para el período 1960 – 1998 mediante esta técnica. Y en cuanto a modelos conjuntos (Campo Principal más variación secular) fueron Haines y Newitt (1986) los que desarrollaron el primer modelo para Canadá. De forma análoga fue aplicado a España por Torta et al. (1993) usando datos de satélites, observatorios y estaciones seculares.

En 1997 se produce una mejora del método SCHA para la modelización de la variación secular. Haines y Newitt (1997) introdujeron el método de diferencias del Campo Principal en el análisis regional y reevaluaron el campo en Canadá. Esta nueva mejora fue adoptada por Torta et al. (2002) y De Santis et al. (2002) quienes obtuvieron el primer modelo regional de variación secular y de referencia para la Antártida, respectivamente.

Como vimos en el Capítulo 2, existe la posibilidad de representar el campo de origen externo a través del desarrollo del potencial geomagnético en armónicos (ec. 2.29), por lo que se puede emplear la técnica SCHA para modelar las corrientes externas e inducidas en el interior de la Tierra a partir de las variaciones magnéticas generadas por esas corrientes. Haines y Torta (1994) presentaron la formulación necesaria para evaluar las corrientes ionosféricas e inducidas, a partir de la modelización de los cambios en el campo geomagnético. Posteriormente, Torta et al. (1997) usaron la técnica para analizar el comportamiento de las corrientes ionosféricas que originan la variación diurna del campo geomagnético sobre Europa. También se ha aplicado la técnica SCHA para el modelado de otros campos potenciales, como el gravitatorio. En esta línea hay que destacar el trabajo de De Santis y Torta (1997) que desarrollaron la técnica para obtener modelos locales de gravedad. En la Tabla 2 de Torta et al. (2006) se muestra un resumen de las publicaciones de todos los estudios llevados a cabo por la aplicación de la técnica regional SCHA en diferentes áreas de interés. A continuación indicamos las principales características de la técnica clásica SCHA.

La ecuación de Laplace (ec. 2.14) en un casquete esférico se resuelve de forma análoga al caso global esférico (Capítulo 2.2.2) obteniéndose, mediante el método de separación de variables, tres ecuaciones diferenciales correspondientes a cada una de las coordenadas geográficas: distancia radial, colatitud y longitud.

$$V(r,\theta,\lambda) = R(r)\cdot G(\theta)\cdot H(\lambda) \qquad [3.1]$$

La diferencia con el caso esférico radica en las condiciones de contorno que se imponen en los límites del casquete esférico. Estos límites vienen dados por las distancias radiales *a* y *b*, y el semiángulo θ_0 (ver figura 3.1). En el caso de la componente radial *r*, las condiciones son las mismas que el caso esférico, imponiendo que el potencial tenga un valor finito para $r = 0$ y un valor nulo cuando $r \to \infty$, por lo que se anula el primer término de la función radial *R(r)*, que viene dada por:

$$R(r) = A\left(\frac{r}{a}\right)^n + B\left(\frac{a}{r}\right)^{n+1} \qquad [3.2]$$

Para la longitud λ las condiciones de contorno son las mismas que en el caso de la esfera (condiciones de contorno 2.20), donde la función $H(\lambda)$ y su derivada deben ser continuas en $\lambda + 2\pi$. Esto implica que el orden m sigue siendo un número natural (incluyendo el 0) y obtenemos también la expresión, análoga al caso de la esfera:

$$H(\lambda) = A\cos m\lambda + B\sin m\lambda \qquad [3.3]$$

Para la colatitud θ las condiciones de contorno serían las mismas que en el caso de la esfera (condiciones de contorno 2.21) si $\theta_i = 0$. Pero cuando la colatitud θ_i es igual a θ_0, el potencial y su derivada tienen que cumplir:

$$V(r,\theta_0,\lambda) = f(r,\lambda) \qquad [3.4]$$

$$\frac{\partial V(r,\theta_0,\lambda)}{\partial \theta} = g(r,\lambda) \qquad [3.5]$$

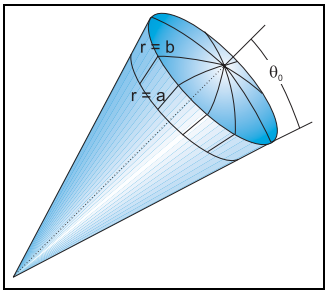

Figura 3.1. Casquete esférico de semiángulo θ_0. La región entre $r = a$ y $r = b$, junto con la delimitación de θ_0, definen el área a analizar (Figura modificada de Haines, 1985a).

Siendo las funciones f y g arbitrarias y sujetas a las mismas condiciones de contorno que la componente radial y la longitud geográfica. Se puede demostrar que, tomando unos ciertos valores del grado n, las funciones f y g pueden ser nulas (Haines, 1985a), verificándose que para una serie de valores de n:

$$V(r,\theta_0,\lambda) = 0 \qquad [3.6]$$

Y para otros ciertos valores del grado n :

$$\frac{\partial V(r,\theta_0,\lambda)}{\partial \theta} = 0 \qquad [3.7]$$

La solución del potencial con condiciones de contorno dadas en las expresiones 3.6 y 3.7 son también las funciones asociadas de Legendre de primera especie, $G(\theta) = P_n^m(\cos\theta)$, pero el grado n ya no tiene, en general, valor entero y pasa a ser un número real. Como los diferentes valores de m dependen del valor real de n, para su representación vamos a hacer uso de un nuevo índice entero, k, que será escogido para ordenar de forma creciente las diferentes raíces n dado un valor de m (además, k empieza por el valor de m, de manera análoga al

caso de *n* entero). Esto da lugar a que los valores de *n* vengan descritos a través de *m* y *k* de forma unívoca: $n_k(m)$. Así los valores de $n_k(m)$ para los que $k - m$ es *impar* corresponden a las raíces de 3.6 y aquellos para los que $k - m$ sea *par* a las raíces de 3.7, cuando estas ecuaciones son consideradas como funciones de $n_k(m)$. Es decir, que los posibles grados de las funciones asociadas de Legendre se determinan a partir de los ceros de las propias funciones de Legendre y su derivada en colatitud en la frontera del casquete, θ_0:

$$\frac{dP^m_{n_k(m)}(\cos\theta_0)}{d\theta} = 0, \quad para\ k - m = par \qquad [3.8]$$

$$P^m_{n_k(m)}(\cos\theta_0) = 0, \qquad para\ k - m = impar \qquad [3.9]$$

Se puede observar como el método SCHA es un *reajuste* del método ordinario esférico SHA pasando de un casquete de 90º (hemisferio) a un casquete de semiángulo θ_0. En la figura 3.2 se da un ejemplo gráfico, comparando las funciones de Legendre de grado entero y las de grado real. Se observa como las condiciones de contorno descritas en 3.8 y 3.9 para el casquete esférico hace que en la frontera, el comportamiento de los dos grupos de funciones de Legendre sea análogo a lo que ocurre en el borde del hemisferio de 90º para el caso SHA. En la sección 3.3 analizaremos las funciones de Legendre de grado real en mayor detalle.

Finalmente, la expresión del potencial geomagnético dentro del casquete esférico es análogo al caso de la esfera (ec. 2.28 y 2.29) pero cambiando la notación de los índices:

$$V(r,\theta,\lambda) = a\sum_{k=0}^{K_{int}}\sum_{m=0}^{k}\left(\frac{a}{r}\right)^{n_k(m)+1} P^m_{n_k(m)}(\cos\theta)\cdot\left(g^{i,m}_{n_k(m)}\cos m\lambda + h^{i,m}_{n_k(m)}\sin m\lambda\right) +$$
$$+a\sum_{k=1}^{K_{ext}}\sum_{m=0}^{k}\left(\frac{r}{a}\right)^{n_k(m)} P^m_{n_k(m)}(\cos\theta)\cdot\left(g^{e,m}_{n_k(m)}\cos m\lambda + h^{e,m}_{n_k(m)}\sin m\lambda\right) \qquad [3.10]$$

El parámetro K_{int} / K_{ext} indica el grado máximo del desarrollo de las fuentes internas/externas. En este caso, una expansión completa espacial e interna del potencial dará lugar a $(K_{int}+1)^2$ coeficientes y la externa a $(K_{ext}+1)^2 - 1$ coeficientes. Para distinguirlos de los coeficientes de Gauss (notación reservada para el caso esférico) los coeficientes regionales pueden ser llamados pseudo-coeficientes de Gauss o coeficientes SCH.

En la expresión del potencial aparecen los armónicos como producto entre las funciones asociadas de Legendre de grado real y las series de cosenos y senos en longitud. Por tanto, tenemos dos bases de funciones armónicas en el casquete esférico: aquellos definidos por la condición de contorno 3.8 y las definidas por la condición 3.9. Dentro de la misma base, los armónicos sobre el casquete esférico son ortogonales, pero las de una base no son ortogonales con respecto a

las de otra base (Haines, 1985a). De esta forma, los coeficientes de la expansión no pueden expresarse algebraicamente en términos de la integral del producto entre las observaciones y la correspondiente función base, como en el caso de una expansión ortogonal. Aunque este hecho supone un impedimento analítico no representa un gran inconveniente práctico, puesto que en la realidad se cuenta con un número discreto de observaciones y los coeficientes se determinan por procedimientos numéricos. Conviene indicar, también, que dichos armónicos no están completamente normalizados, si no que son calculados bajo la semi – normalización de Schmidt. Esta parte se explica más en detalle en el Capítulo 3.3.

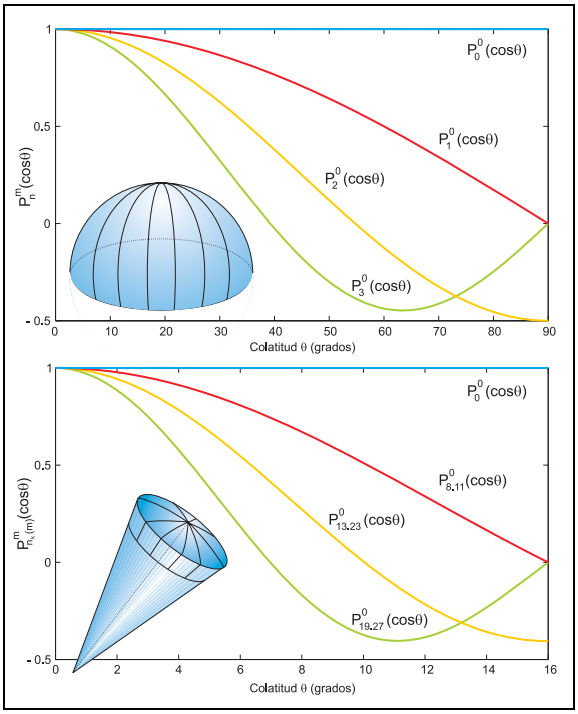

Figura 3.2. Funciones asociadas de Legendre (con *m* = 0). Arriba, para el caso del hemisferio. Abajo, para un casquete esférico de semiángulo 16º. Para *n – m = par* (línea amarilla) las funciones han de tener sus derivadas iguales a cero en la frontera. Para *n – m = impar* (línea roja y verde) las funciones son nulas en la frontera. El índice *k* reemplaza a *n*. Modificada de De Santis (1991).

La longitud de onda que proporciona un modelo regional SCHA viene dada por la expresión de Bullard (1967), análoga al caso ordinario (esfera), pero con el grado real $n_k(m)$:

$$\omega = \frac{2\pi a}{n_k(m)} \qquad [3.11]$$

El método SCHA proporciona longitudes de onda más pequeñas (mayor resolución) con un número igual de coeficientes SCH que el caso SHA. Esto se

debe a que los grados $n_k(m)$ reales son siempre mayores que los grados n enteros del caso global (ver figura 3.2). Además esta longitud de onda será más pequeña a medida que se disminuya el tamaño del casquete. Teniendo en cuenta la longitud de onda mínima que el modelo SCHA puede reproducir, podemos obtener el valor máximo del índice k asociado. Usando la expresión 3.11, cuyo numerador se aproxima a 40000 km, el valor máximo de k viene dado por (Haines, 1988):

$$K_{máx} = \frac{\theta_0}{90^o}\left(\frac{40000}{\omega_{mín}} + \frac{1}{2}\right) - \frac{1}{2} \qquad [3.12]$$

Finalmente, si tenemos en cuenta el potencial en el casquete esférico (ec. 3.10) y las expresiones que lo relacionan con las componentes del Campo Geomagnético (ec. 2.30, 2.31 y 2.32), éstas tienen las siguientes expresiones:

$$X = \sum_{k=1}^{K_{int}} \sum_{m=0}^{k} \left(\frac{a}{r}\right)^{n_k(m)+2} \frac{dP^m_{n_k(m)}(\cos\theta)}{d\theta} (g^{i,m}_{n_k(m)} \cos m\lambda + h^{i,m}_{n_k(m)} \sin m\lambda) + \\ + \sum_{k=1}^{K_{ext}} \sum_{m=0}^{k} \left(\frac{r}{a}\right)^{n_k(m)-1} \frac{dP^m_{n_k(m)}(\cos\theta)}{d\theta} (g^{e,m}_{n_k(m)} \cos m\lambda + h^{e,m}_{n_k(m)} \sin m\lambda) \qquad [3.13]$$

$$Y = \sum_{k=1}^{K_{int}} \sum_{m=1}^{k} \left(\frac{a}{r}\right)^{n_k(m)+2} \frac{m \cdot P^m_{n_k(m)}(\cos\theta)}{\sin\theta} (g^{i,m}_{n_k(m)} \sin m\lambda - h^{i,m}_{n_k(m)} \cos m\lambda) + \\ + \sum_{k=1}^{K_{ext}} \sum_{m=1}^{k} \left(\frac{r}{a}\right)^{n_k(m)-1} \frac{m \cdot P^m_{n_k(m)}(\cos\theta)}{\sin\theta} (g^{e,m}_{n_k(m)} \sin m\lambda - h^{e,m}_{n_k(m)} \cos m\lambda) \qquad [3.14]$$

$$Z = -\sum_{k=1}^{K_{int}} \sum_{m=0}^{k} (n_k(m)+1) \left(\frac{a}{r}\right)^{n_k(m)+2} P^m_{n_k(m)}(\cos\theta) (g^{i,m}_{n_k(m)} \cos m\lambda + h^{i,m}_{n_k(m)} \sin m\lambda) + \\ + \sum_{k=1}^{K_{ext}} \sum_{m=0}^{k} n_k(m) \left(\frac{r}{a}\right)^{n_k(m)-1} P^m_{n_k(m)}(\cos\theta) (g^{e,m}_{n_k(m)} \cos m\lambda + h^{e,m}_{n_k(m)} \sin m\lambda) \qquad [3.15]$$

Estas expresiones son la herramienta matemática usada en este trabajo para la construcción de un modelo regional de campo geomagnético mediante la técnica clásica SCHA (modelos SCHA.DI.00 y SCHA.DIF.3K).

Pero la técnica SCHA tiene limitaciones. La principal es la pérdida del significado físico de los coeficientes SCH. Además, la base de funciones que se utiliza es incompleta (ver Thébault y Gaya-Piqué, 2008). Las dos bases de funciones de Legendre que se proponen para la técnica SCHA no son suficientes para poder representar de forma precisa el campo geomagnético dentro del casquete (Thébault et al., 2006a).

Métodos empíricos han demostrado que para estabilizar la técnica SCHA el primer coeficiente g_0^0, que no tiene su homólogo en el caso SHA, debe tener bajas amplitudes. Ello se consigue restando a los datos geomagnéticos un campo

de referencia antes de aplicar la técnica SCHA. Por otra parte, los problemas asociados a las funciones base son reducidos considerablemente al aumentar artificialmente el tamaño del casquete (Torta et al., 1992).

Otra limitación radica en que los modelos SCHA se deterioran con al altura o distancia radial (Haines, 1985), por lo que existe una gran limitación a la hora de modelar el campo geomagnético a diferentes alturas, por ejemplo con datos de superficie y de satélites. Esta limitación también se reduce para casquetes grandes, donde el grado real SCH tiende al grado entero SH y θ_0 a π.

Finalmente, indicar que mediante la técnica SCHA no se pueden realizar prolongaciones descendentes para analizar el campo geomagnético en el límite núcleo externo – manto (CMB). Hecho que si es posible mediante la técnica SHA (modelos globales).

3.2. Revisión del método: R-SCHA y R-SCHA2D. Ecuaciones básicas.

Como hemos visto, uno de los límites de la técnica clásica SCHA es su aplicación a datos que se encuentren a diferentes altitudes (Thébault y Gaya – Piqué, 2008). Problema que es de relevancia si se desean utilizar, por ejemplo, datos de satélites, pero que no es tan importante cuando se utilizan datos paleomagnéticos. No obstante, analizaremos las nuevas técnicas propuestas recientemente porque resuelven más rigurosamente la ecuación de Laplace. De hecho, la fuente del problema de la técnica SCHA radica en que en la solución de la ecuación de Laplace (ec. 2.14) para un casquete esférico no se tienen en cuenta todas las condiciones de contorno posibles, en particular las relativas a la distancia radial.

La técnica fue revisada por Thébault et al. (2004, 2006a) quienes propusieron una nueva solución a la que llamanon R-SCHA (Revised Spherical Harmonic Analysis) en la cual se resuelve de nuevo la ecuación de Laplace con todas las posibles condiciones de contorno. De este modo el campo geomagnético, encerrado dentro del cono que define el casquete esférico (Figura 3.1), está definido por una familia completa de nuevas funciones base. Hasta la actualidad dicho método ha sido aplicado para analizar el campo geomagnético sobre Francia (Thébault et al., 2006b) y Alemania (Korte y Thébault, 2007) y mediante el uso de numerosos casquetes se han analizado las anomalías magnéticas de toda la corteza terrestre (Thébault, 2006). En esta sección vamos a analizar las principales características de la técnica R-SCHA y de un caso particular de la misma: la R-SCHA2D (Thébault, 2008).

Las nuevas condiciones de contorno que se ven involucradas en la revisión de la técnica regional están en relación con la distancia radial *r* en los límites del casquete esférico. Para resolver de nuevo la ecuación de Laplace vamos a separar el potencial en dos: V_1 y V_2, de tal forma que el potencial geomagnético es suma de ambos: $V = V_1 + V_2$.

Resolución del potencial V_1.

El primer potencial V_1 corresponde al potencial geomagnético obtenido aplicando la técnica clásica SCHA (Haines, 1985a) y que ya ha sido resuelto en la sección anterior. Pero hay una diferencia, y es que en el nuevo potencial V_1 solo aparecen las funciones de Legendre obtenidas para valores $k - m$ par, debido a que sólo V_1 satisface la ecuación de contorno 3.8. El otro conjunto de funciones de Legendre que cumplían la condición de contorno 3.9 (los de valores $k - m$ impar) será reemplazado por las nuevas funciones obtenidas con el potencial V_2.

Resolución del potencial V_2.

El nuevo potencial V_2, además de satisfacer la ecuación de Laplace, debe de cumplir las siguientes condiciones en el borde del casquete esférico:

$$V_2(r,\theta_0,\lambda) = f(r,\lambda) \qquad [3.16]$$

$$\frac{\partial V_2(a,\theta,\lambda)}{\partial r} = 0 \qquad [3.17]$$

$$\frac{\partial V_2(b,\theta,\lambda)}{\partial r} = 0 \qquad [3.18]$$

Resolviendo de nuevo la ecuación de Laplace mediante el método de separación de variables, ya visto en la sección anterior, obtenemos 3 ecuaciones diferenciales dependientes de la distancia radial $R(r)$, la longitud $H(\lambda)$ y la colatitud $G(\theta)$.

La función radial $R(r)$ es análoga a la dada en [2.17], pero su autovalor cambia de signo:

$$\frac{d^2R(t)}{dt^2} + \frac{dR(t)}{dt} - \nu R(t) = 0 \qquad [3.19]$$

Donde *t* surge con el cambio de variable $r = a\,e^t$, siendo *a* el radio medio de la Tierra. La solución de esta expresión depende del valor de su discriminante $\Delta = 1 - 4\nu$.

Si $\Delta \neq 0$ entonces la solución para la componente radial *r* es análoga a la expresión 2.22 con $\nu = n(n+1)$:

$$R(r) = A\left(\frac{r}{a}\right)^n + B\left(\frac{a}{r}\right)^{n+1} \qquad [3.20]$$

Si $\Delta = 0$ el autovalor ν toma el valor ¼ y la solución de la ec. 3.19 viene dada por:

$$R(r) = \sqrt{\frac{a}{r}}\left[A\log\left(\frac{r}{a}\right) + B \right] \qquad [3.21]$$

El primer caso ($\Delta \neq 0$) es análogo al del potencial V_1, pero las condiciones de contorno 3.17 y 3.18 del potencial V_2 en los bordes del casquete esférico obligan a que los valores reales del grado n pasen a valer 0/-1 o sean complejos. Si $n = 0, n = -1$ la solución es trivial y la función radial correspondiente es una constante que obviamente satisface las ecuaciones de contorno: $R_0(r) = R_0$. Y si el grado n es complejo toma la forma:

$$n = -\frac{1}{2} + i\frac{p\pi}{\log(b/a)} \qquad [3.22]$$

Siendo p un número natural no nulo. Si usamos la fórmula trigonométrica de Euler con S = log(b/a), aplicando las condiciones de contorno 3.17 y 3.18 y normalizamos las funciones radiales de tal forma que su norma sea igual al radio medio de la tierra a, ambas funciones radiales vienen dadas por:

$$R_0(r) = \frac{1}{\sqrt{e^S - 1}}, \; para\; n = 0, n = -1 \qquad [3.23]$$

$$R_p(r) = \frac{(2S)^{-1/2}}{\sqrt{\left(\frac{2\pi P}{S}\right)^2 + 1}}\sqrt{\frac{a}{r}}\left[\frac{2\pi p}{S}\cos\left[\frac{p\pi}{S}\log\left(\frac{r}{a}\right)\right] + \sin\left[\frac{p\pi}{S}\log\left(\frac{r}{a}\right)\right]\right], \; para\; n\; complejo \qquad [3.24]$$

El segundo caso implica un discriminante igual a cero ($\Delta = 0$), con lo cual ν = ¼, y aplicando las condiciones de contorno 3.17 y 3.18 el grado n toma el valor - ½. Además obliga a que las distancias radiales del cono esférico sean iguales: $a = b$ (Figura 3.1), por lo que se trata de un caso particular: cuando los datos geomagnéticos están a una misma altura. Este caso es de especial interés para nosotros, pues los datos paleomagnéticos están situados aproximadamente a la misma distancia radial. Aquí la técnica R-SCHA pasa a llamarse R-SCHA2D (Thébault, 2008) indicando que sólo puede ser aplicada a datos situados a la misma altura. En este caso la función radial normalizada toma la forma:

$$R_{-1/2}(r) = \sqrt{\frac{a}{r}}\left[\log\left(\frac{r}{a}\right) + 2 \right] \qquad [3.25]$$

La solución de la ecuación diferencial $H(\lambda)$ no difiere del caso clásico SCHA (y del caso global SHA) y viene dada por la ec. 3.3.

Por último, la función en colatitud $G(\theta)$ depende del grado n y de los posibles valores que tome éste : n complejo (caso A), $n = 0$ / $n = -1$ (caso B) ó $n = -½$

(caso C). En los tres casos, las funciones que se generan son las funciones cónicas de Mehler $K_n^m(\cos\theta)$. Estas funciones cónicas son ortogonales entre sí en el casquete esférico, al igual que las funciones asociadas de Legendre con $k - m$ par y además son funciones cónicas fuertemente normalizadas. Todas estas características las analizaremos en el Capítulo 3.3.

Usando la técnica R-SCHA, además de la longitud de onda en la superficie de la Tierra (longitud de onda horizontal, ec. 3.11) podemos hablar de longitud de onda radial (l_r), que vendrá dada por los parámetros que definen a la función radial:

$$l_r = a \cdot S \frac{1+e^S}{p} \qquad [3.26]$$

De la misma forma que obteníamos un valor de $K_{máx}$ en ec. 3.12, ahora podemos obtener el valor máximo del índice p para un casquete esférico en concreto:

$$P_{\max} \approx \frac{a+b}{2l_r} \log\left(\frac{a}{b}\right) \qquad [3.27]$$

Finalmente y como resumen de esta sección, el potencial V_2 en el método R-SCHA (caso A + caso B) viene dado por la expresión:

$$\begin{aligned} V_2(r,\theta,\lambda) &= a\sum_{p\geq 1}\sum_{m>0} \mathrm{R}_p(r)\cdot K_p^m(\theta)\cdot(G_p^m\cos m\lambda + H_p^m \sin m\lambda) + \\ &+ a\sum_{k=1}^{K_{est}} \mathrm{R}_0\cdot K_0^m(\theta)\cdot(G_0^m\cos m\lambda + H_0^m \sin m\lambda) \end{aligned} \qquad [3.28]$$

Y para el caso C (método R-SCHA2D) el potencial es:

$$V_2(r,\theta,\lambda) = a\sum_{p\geq 1}\sum_{m>0} \mathrm{R}_{-1/2}(r)\cdot K_{-1/2}^m(\theta)\cdot(G_{-1/2}^m\cos m\lambda + H_{-1/2}^m \sin m\lambda) \qquad [3.29]$$

Al sumar al potencial clásico V_1 (ec. 3.10), con $k - m$ par, el potencial obtenido V_2 (ec. 3.28 y 3.29), obtenemos el potencial geomagnético dentro del casquete esférico para las técnicas R-SCHA y R-SCHA2D respectivamente. Las componentes del campo geomagnético (X, Y y Z) son obtenidas del mismo modo que en las ec. 3.13, 3.14 y 3.15 derivando el potencial $V = V_1 + V_2$ respecto de las coordenadas esféricas.

Aunque la técnica R-SCHA solventa los problemas presentados en la técnica clásica SCHA, también presenta algunas limitaciones (ver Thébault y Gaya – Piqué, 2008). Quizás la más significativa es la convergencia del método, ya que las series de Fourier del potencial convergen de forma lenta. Esta limitación

desaparece si tenemos un número suficiente datos geomagnéticos. Por otra parte, al igual que su previa técnica SCHA, la técnica R-SCHA no permite la prolongación descendente para analizar el comportamiento del campo geomagnético en el límite núcleo externo – manto (CMB).

3.3. Funciones asociadas de Legendre de grado real y funciones cónicas de Mehler.

En la expresión del potencial geomagnético en un casquete esférico (ec. 3.10) cobran gran importancia las funciones asociadas de Legendre de grado real, por lo que en esta sección analizamos cómo se calculan y sus características principales. Además, en el potencial geomagnético definido en la técnica R-SCHA (ec. 3.28) y R-SCHA2D (ec. 3.29) aparecen, junto con las funciones asociadas de Legendre, las funciones cónicas de Mehler, las cuales son también analizadas en detalle a continuación.

3.3.1 Funciones asociadas de Legendre de grado real y armónicos en un casquete esférico.

Las funciones asociadas de Legendre, $P^{m}_{n_k(m)}(\cos\theta)$, que forman parte de los armónicos en el casquete esférico, no son ordinarias ya que, como hemos visto en la sección anterior, poseen grado real. Estas funciones vienen expresadas en función del grado *n*, el orden *m*, el índice de orden *k* y la colatitud (Haines, 1985a) de la siguiente forma:

$$P^{k}_{n}(\cos\theta) = K^{m}_{n} \sin^{m}\theta \cdot F\left(m-n, n+m+1, 1+m; \frac{1-\cos\theta}{2}\right) \qquad [3.30]$$

Siendo F una serie hipergeométrica o serie de Gauss y el parámetro K^{m}_{n} es una constante de normalización, cuyos valores en la forma semi–normalizada de Schmidt vienen dadas por:

$$K^{m}_{n} = 1 \quad , si \quad m = 0 \qquad [3.31]$$

$$K^{m}_{n} = \frac{2^{-m}}{(m\pi)^{1/2}} \left(\frac{n+m}{n-m}\right)^{\frac{n}{2}+\frac{1}{4}} p^{\frac{m}{2}} e^{e_1+e_2} \qquad [3.32]$$

donde:

$$p = \left(\frac{n}{m}\right)^{2} - 1 \qquad [3.33]$$

$$e_1 = -\frac{1}{12m}\left(1+\frac{1}{p}\right) \qquad [3.34]$$

$$e_2 = \frac{1}{360m^3}(1+\frac{3}{p^2}+\frac{4}{p^3}) \qquad [3.35]$$

La ec. 3.30 puede resolverse mediante recurrencia (recurrencia de Clenshaw), dando lugar a una expresión general para las funciones asociadas de Legendre con grado *n* real:

$$P_n^m(\cos\theta) = \sum_{k=0}^{\infty} A_k(m,n)\sin^{2k}(\theta/2) \qquad [3.36]$$

Los términos A_k son definidos como:

$$A_0(m,n) = K_n^m \sin^m\theta \qquad [3.37]$$

$$A_k(m,n) = \frac{(k+m-1)(k+m)-n(n+1)}{k(k+m)} A_{k-1}(m,n) \qquad [3.38]$$

Se puede demostrar que si *n* es entero, la serie (ec. 3.36) se podría truncar en un valor finito de *k*, obteniéndose la correspondiente función de Legendre ordinaria. Pero se debe truncar la expresión en el termino donde se proporcionen tantas cifras significativas como previamente se decida aceptar (De Santis, 1991).

Por otra parte se necesita determinar la derivada de las nuevas funciones de Legendre con respecto a la colatitud ya que ésta viene dada en la expresión de la componente norte (ec. 3.13):

$$\frac{dP_n^m(\cos\theta)}{d\theta} = \frac{\sin\theta}{2}\sum_{k=1}^{\infty} k\cdot A_k(m,n)\sin^{2(k-1)}(\theta/2), \quad si \quad m=0 \qquad [3.39]$$

$$\frac{dP_n^m(\cos\theta)}{d\theta} = \frac{m\cos\theta}{\sin\theta}P_n^m(\cos\theta) + \frac{\sin\theta}{2}\sum_{k=1}^{\infty} k\cdot A_k(m,n)\sin^{2(k-1)}(\theta/2), \; si \quad m\neq 0 \; [3.40]$$

Para poder obtener los valores de las funciones asociadas de Legendre de grado real tenemos que conocer *a priori* cuales son los valores del grado $n_k(m)$. Los valores de $n_k(m)$ son los ceros de las dos familias de funciones en el borde del casquete esférico y son obtenidos al resolver las ec. 3.8 y 3.9. Los ceros de la ec. 3.9 dan los valores de $n_k(m)$ con $k - m$ impar y los ceros de la ec. 3.8 los de $k - m$ par. Estos últimos ceros pueden ser analizados también con los máximos y mínimos de 3.9, ya que su derivada da los ceros de 3.8. En la figura 3.3 mostramos un ejemplo gráfico, calculando una función asociada de Legendre en función de $n_k(m)$ e indicando los ceros de la misma y de su derivada, que proporcionan los distintos valores de $n_k(m)$ ordenados mediante el índice *k*.

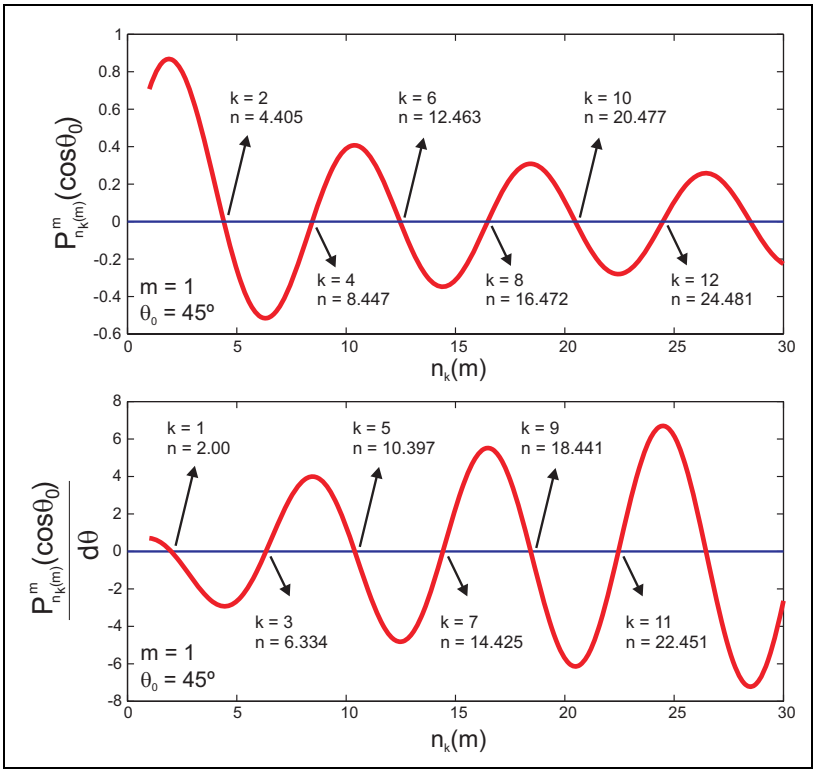

Figura 3.3. Función asociada de Legendre de grado real en función del grado $n_k(m)$ (arriba) y su derivada en función de θ (abajo). El orden m es igual a 1 y el tamaño del casquete esférico es θ_0 = 45º. Se indican las diferentes raíces que corresponden con los valores de $n_k(m)$ ordenados por el índice k.

Para el cálculo de dichas funciones y sus raíces $n_k(m)$, Haines (1988) desarrolló una rutina informática en lenguaje Fortran, pero el cálculo se hace complicado cuando el valor de la colatitud aumenta o cuando se precisa alcanzar valores altos de $n_k(m)$. En estos casos las rutinas de Haines fallan, es decir, que para un cierto valor de $n_k(m)$ o de colatitud θ, la función se hace inconsistente y diverge (ver figura 3.4, parte superior). Thébault et al. (2002), desarrolló una herramienta matemática para calcular las funciones asociadas de Legendre de grado no entero aplicando el algoritmo de Olver y Smith (1983), que consiste en un aumento del rango de precisión en el cálculo de las funciones. Con esta nueva herramienta se mejora sustancialmente la técnica SCHA, ya que con esta nueva rutina es posible evaluar con mayor precisión los valores de $n_k(m)$ eliminando la divergencia de las funciones para altos grados o para altas colatitudes (ver figura 3.4, parte inferior).

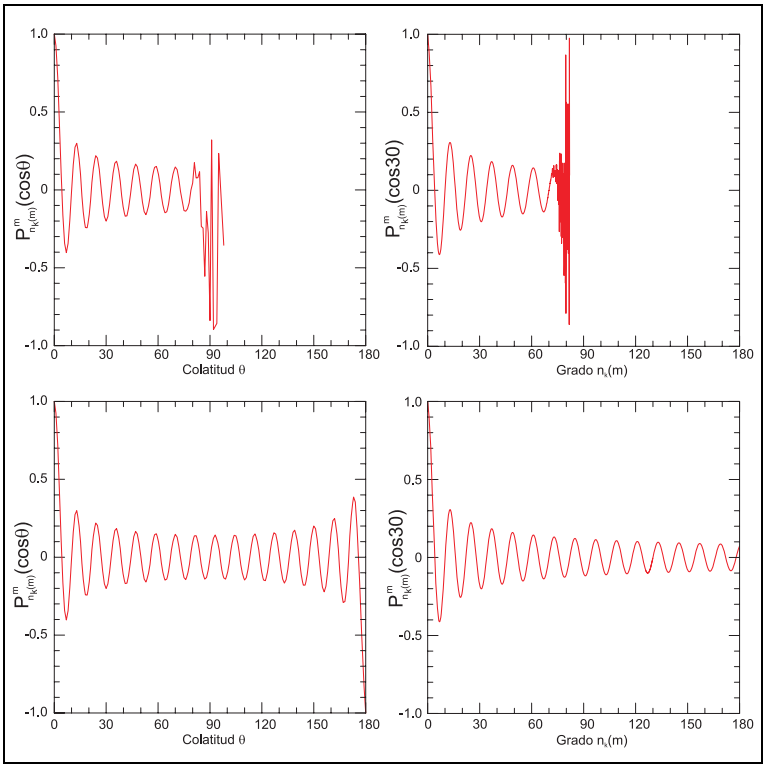

Figura 3.4. Arriba: función asociada de Legendre obtenida por el método desarrollado por Haines en 1988 (izquierda, para un grado *n* y orden *m* fijos; derecha, para un θ_0 fijo). Abajo: mismo análisis, pero con la nueva técnica de Thébault et al. (2002). Figura de Gaya-Piqué (2004).

El número de ceros en la colatitud dependerá de los valores de *m* y *k*. Veamos los posibles casos:

Caso 1. Para $m = 0$, la función tiene $\frac{k+\delta}{2}$ ceros.

Caso 2. Para $0 < m < k$, la función tiene $\frac{k-m+\delta}{2}+1$ ceros. En este caso como en el anterior $\delta = 0$ si $k - m$ es par y $\delta = 1$ si $k - m$ es impar.

Caso 3. Para $m = k > 0$, la función tiene un solo cero en $\theta = 0^o$.

A continuación mostramos (Figura 3.5) algunas funciones asociadas de Legendre de grado real obtenidas para un casquete esférico de tamaño 25º y diferentes valores del índice *k* y del orden *m*.

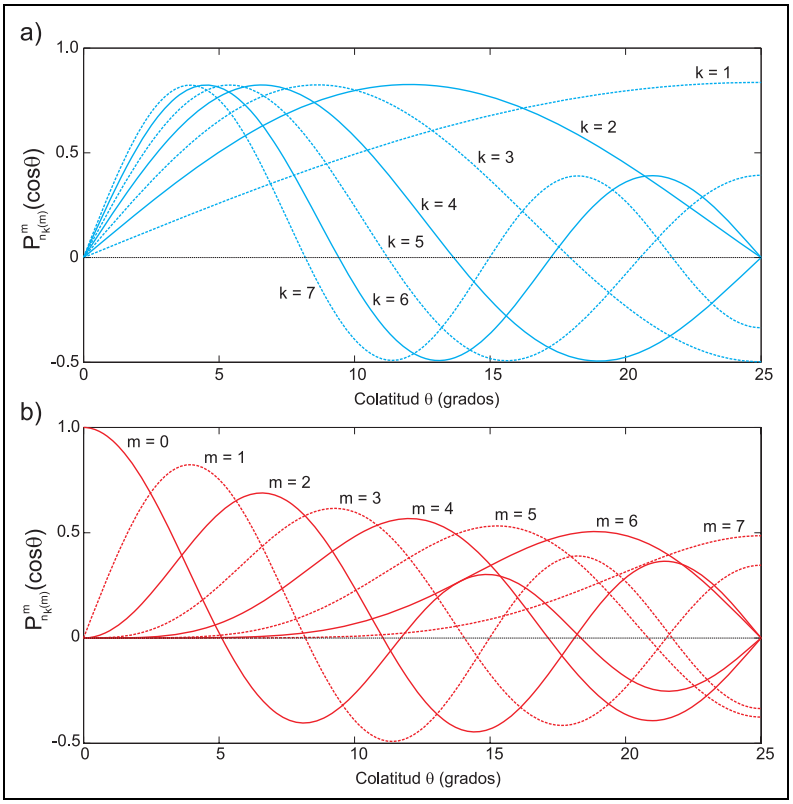

Figura 3.5. a) Funciones de Legendre con orden fijo m = 1 y k = 1,2,3,…,7. b) Funciones de Legendre con índice fijo k = 7 y m = 0,1,2,3,…,7. Las curvas discontinuas muestran las funciones con $k - m$ par (derivada nula en θ_0) y las continuas $k - m$ impar (función nula en θ_0). El semiángulo que define el casquete esférico tiene un valor de θ_0 = 25º.

Al igual que en el caso de la esfera, en la expresión del potencial geomagnético (ec. 3.10) en el casquete esférico, las funciones asociadas de Legendre son multiplicadas por las funciones en longitud (cos $m\lambda$ y sin $m\lambda$). El producto de ambas da lugar a los armónicos en el casquete esférico:

$$Y_k^m = P_{n_k(m)}^m(\cos\theta)\cdot\cos m\lambda \qquad [3.41]$$

$$Z_k^m = P_{n_k(m)}^m(\cos\theta)\cdot\sin m\lambda \qquad [3.42]$$

Estos armónicos, representados en la superficie del casquete esférico, hacen que aparezcan zonas de valores máximos, mínimos o nulos, que dependerán del índice k y del orden m. En colatitud ya hemos visto cuantos ceros tienen las funciones de Legendre y para la longitud las funciones cos $m\lambda$ y sin $m\lambda$ tienen $2m$ ceros. Además los armónicos Y_k^m y Z_k^m para los mismos valores de k y m son iguales, pero están girados uno respecto al otro. El ángulo de giro viene dado por $\pi/2m$. En la figura 3.6 se muestran algunos ejemplos gráficos.

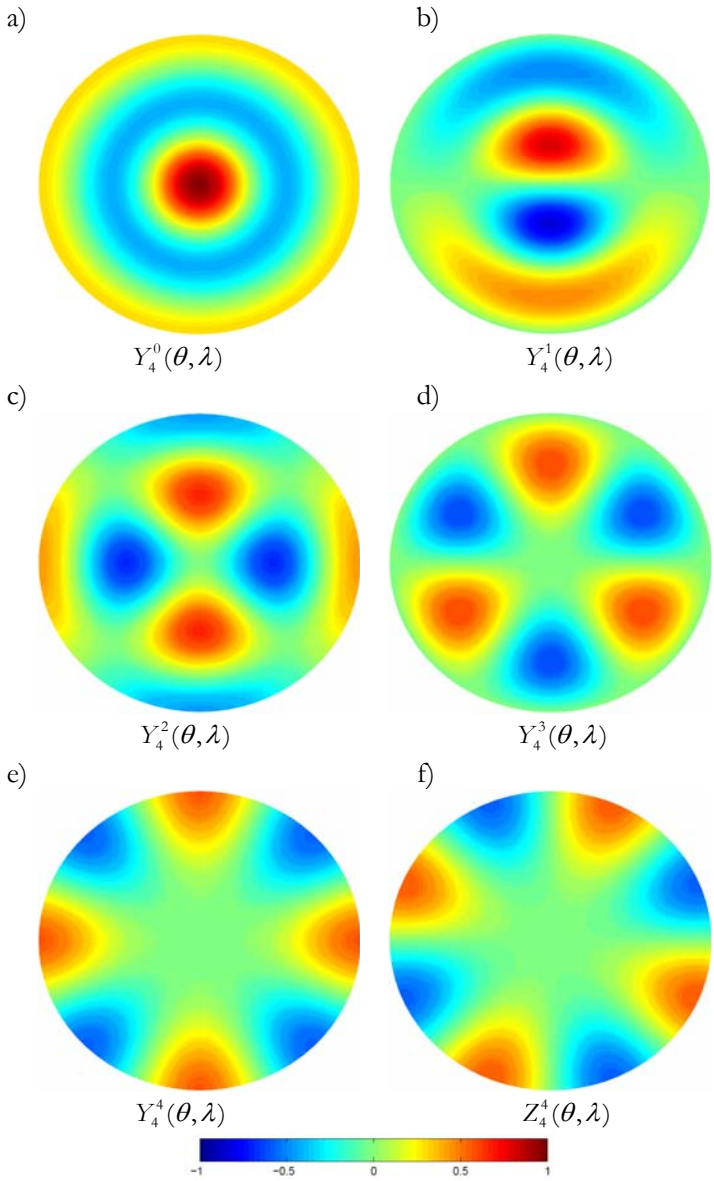

Figura 3.6. De a) a e) Armónicos $Y_k^m(\theta,\lambda)$ con índice k = 4 y m = 0,1,2,3,4. f) Armónico $Z_4^4(\theta,\lambda)$ donde se observa el giro de $\pi/2m$ (para este caso 22.5º) respecto al armónico $Y_4^4(\theta,\lambda)$. El semiángulo que define el casquete esférico tiene un valor de θ_0= 25º.

3.3.2 Las funciones cónicas de Mehler.

Las funciones cónicas o funciones de Mehler aparecen al resolver la ecuación diferencial en colatitud $G(\theta)$ en coordenadas esféricas para unos valores concretos del grado n. En la sección 3.2 vimos los tres valores posibles de n, y dependiendo de éstos, obtendremos una función de Mehler distinta. A continuación veremos en detalle cada caso:

Caso A. Grado n complejo: $n = -\frac{1}{2} + i\frac{p\pi}{S}$, con p natural no nulo y $S = log(b/a)$.

Las funciones de Mehler se obtienen a partir de la misma serie hipergeométrica que la dada para las funciones asociadas de Legendre de grado real (ec. 3.30), pero al ser n complejo, toma la forma:

$$K^m_{-\frac{1}{2}+i\frac{p\pi}{S}}(\cos\theta) = \frac{(-1)^m}{2^m m!} N^m_p \sin^m\theta \cdot F\left(m+\frac{1}{2}-i\frac{p\pi}{S}, m+\frac{1}{2}+i\frac{p\pi}{S}, 1+m; \frac{1-\cos\theta}{2}\right) \quad [3.43]$$

donde:

$$N^m_p = 1 \ , si \quad m = 0 \quad [3.44]$$

$$N^m_p = \frac{\Gamma(1/2+m+ip\pi/S)}{\Gamma(1/2-m+ip\pi/S)} = (-1)^m \prod_{j=1}^{m}\left(\left(\frac{p\pi}{S}\right)^2 + \left(\frac{2j-1}{2}\right)^2\right) \quad [3.45]$$

Por comodidad, este tipo de funciones cónicas de Mehler son denotadas como $K^m_p(\cos\theta)$. Aunque sean funciones con argumentos complejos, sus valores son reales, siendo un caso particular de las funciones de Legendre. Si resolvemos la serie hipergeométrica mediante el método de recurrencia de Clenshaw, podemos expresar la función de Mehler como una serie infinita:

$$K^m_p(\cos\theta) = \frac{(-1)^m}{2^m m!} N^m_p \sin^m\theta \cdot \sum_{j=0}^{\infty} A_j \sin^{2j}\frac{\theta}{2} \quad [3.46]$$

donde los términos A_j son definidos como:

$$A_0 = 0 \quad [3.47]$$

$$A_{j+1} = \frac{(m+1/2+j)^2 + (p\pi/S)^2}{(j+m+1)(j+1)} A_j \quad [3.48]$$

Caso B. Grado n igual a 0 ó -1: $n = 0, -1$.

De nuevo la expresión de las funciones cónicas de Mehler con grado nulo o -1 viene dada en función de la serie hipergeométrica de las funciones asociadas de Legendre mediante la siguiente expresión:

$$K^m_n(\cos\theta) = \frac{(-1)^m}{m!} N^m_p \tan^m\frac{\theta}{2} \cdot F\left(-n, n+1, m; \frac{1-\cos\theta}{2}\right) \quad [3.49]$$

con:

$$N_p^m = 1 \ , si \quad m = 0 \tag{3.50}$$

$$N_p^m = \frac{\Gamma(n+m+1)}{\Gamma(n-m+1)} \tag{3.51}$$

Al sustituir el grado *n* por 0 (o -1) y mediante el uso de la técnica de recurrencia de Clenshow, la función viene dada por:

$$K_0^m(\cos\theta) = K_{-1}^m(\cos\theta) = \Gamma(m)\tan^m\frac{\theta}{2} \tag{3.52}$$

siendo

$$K_0^0(\cos\theta) = 1 \tag{3.53}$$

Caso C. Grado *n* igual a -1/2: $n = -1/2$.

Estamos ante un caso especial del Caso A, donde el índice *p* vale 0 y *n* pasa a ser real con valor – ½. Por tanto, si sustituimos el valor del grado *n* = -1/2 en la ec. 3.43 obtenemos las funciones de Mehler con grado -1/2:

$$K_{-\frac{1}{2}}^m(\cos\theta) = \frac{(-1)^m}{2^m m!} N_{-1/2}^m \sin^m\theta \cdot F\left(m+\frac{1}{2}, m+\frac{1}{2}, 1+m; \frac{1-\cos\theta}{2}\right) \tag{3.54}$$

con:

$$N_{-1/2}^m = 1 \ , si \quad m = 0 \tag{3.55}$$

$$N_{-1/2}^m = \frac{\Gamma(1/2+m)}{\Gamma(1/2-m)} = (-1)^m \prod_{j=1}^{m}\left(\frac{2j-1}{2}\right)^2 \tag{3.56}$$

Y mediante recurrencia, obtenemos la expresión:

$$K_{-1/2}^m(\cos\theta) = \frac{(-1)^m}{2^m m!} N_{-1/2}^m \sin^m\theta \cdot \sum_{j=0}^{\infty} A_j \sin^{2j}\frac{\theta}{2} \tag{3.57}$$

donde:

$$A_0 = 0 \tag{3.58}$$

$$A_{j+1} = \frac{(m+1/2+j)^2}{(j+m+1)(j+1)} A_j \tag{3.59}$$

La figura 3.7 muestra las funciones cónicas de Mehler para los tres casos (A, B y C) y para distintos valores del orden *m* y del índice *p*. Los valores de las funciones de Mehler han sido obtenidos haciendo uso de las rutinas desarrolladas por E. Thébault (comunicación personal, 2008) en lenguaje Fortran y que permiten ser llamadas desde Matlab ®. En este caso, en lugar de usar el

índice p, vamos a reemplazarlo por el índice τ, que corresponde al argumento de la parte imaginaria del grado n: $\tau = p \cdot \pi / S$ que está relacionado directamente con la altura $h = b - a$, pues $S = \log(b/a) = \log(1+h/a)$.

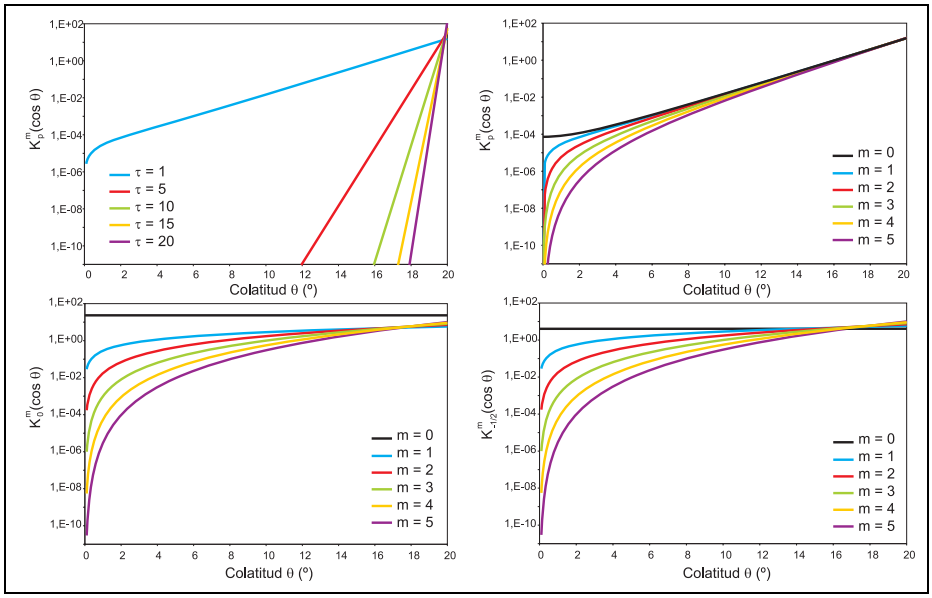

Figura 3.7. a) Funciones cónicas de Mehler de grado complejo para un orden fijo $m = 1$ y $\tau = 1,5,10,15,20$ y b) para un orden $m = 0,1,2,\ldots,5$ y un valor fijo de $\tau = 1$. c) Funciones cónicas de Mehler de grado nulo (o $n = -1$) para $m = 0,1,2,\ldots,5$, y d) funciones cónicas de Mehler de grado -1/2 para $m = 0,1,2,\ldots,5$. Todas las funciones están fuertemente normalizadas dentro del casquete esférico de tamaño $\theta_0 = 20^o$. Las funciones de Mehler de a), b) y c) son usadas en la técnica R-SCHA y las de d) en la R-SCHA2D.

La expresión de los coeficientes que definen las funciones cónicas de Mehler hace que éstas sean estrictamente positivas en el intervalo $[0, \theta_0]$. En la expresión del potencial R-SCHA (o R-SCHA2D) aparecen las funciones de Mehler multiplicadas por las funciones en longitud (cos $m\lambda$ y sin $m\lambda$). Por tanto el producto de estas funciones no son rigurosamente armónicos esféricos. Nos hemos tomado la libertar de denominarlos "armónicos de Mehler". En la figura 3.8 mostramos los valores de dicho producto para algunos casos en concreto:

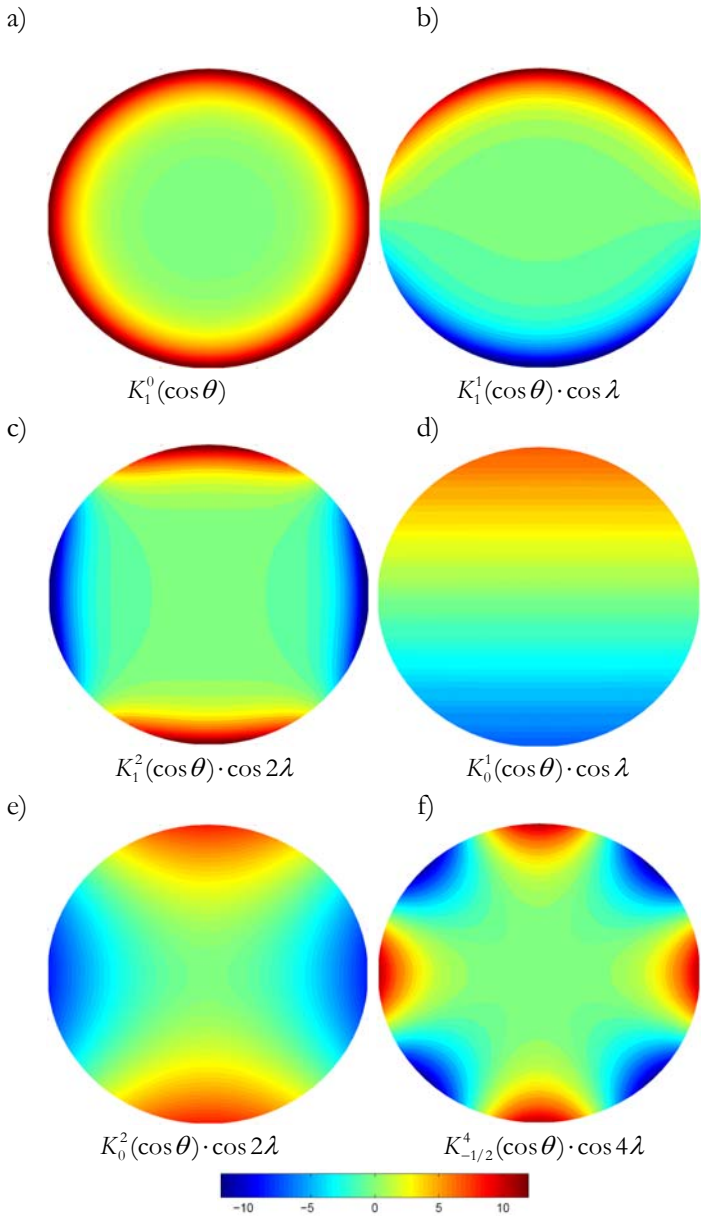

Figura 3.8. De a) a c) "armónicos de Mehler" de grado complejo para un índice $\tau = 1$ y m = 0,1,2; d) y e) "armónicos de Mehler" de grado nulo (o n = -1) para m = 1,2; y f) "armónico de Mehler" de grado -1/2 para $m = 4$.

En nuestro caso (independientemente del grado n) vamos a usar las funciones cónicas de Mehler fuertemente normalizadas por lo que los valores de los coeficientes serán modificados para ajustarlos a dicha normal. En la próxima

sección veremos dicha normalización junto con la de las funciones asociadas de Legendre de grado real.

3.3.3 Ortogonalidad y normalización de las funciones de Legendre y de las funciones de Mehler. Norma del Campo Geomagnético.

i. Ortogonalidad y norma de las funciones de Legendre de grado real.

Las funciones de Legendre de grado real son calculadas mediante la semi-normalización de Schmidt al igual que las funciones de grado entero (caso esférico). Esta semi-normalización hace que la integral del cuadrado de la función dentro del casquete esférico no sea igual a la unidad y tenga el siguiente valor (Haines, 1985a):

$$\left\| P_{n_k}^m \right\|^2 = \int_0^{\theta_0} \left[P_{n_k}^m(\cos\theta) \right]^2 \sin\theta d\theta = -\frac{\sin\theta_0}{2n_k+1} P_{n_k}^m(\cos\theta_0) \frac{\partial}{\partial n_k} \frac{dP_{n_k}^m(\cos\theta_0)}{d\theta}, \; para\ k-m\ par \quad [3.60]$$

$$\left\| P_{n_k}^m \right\|^2 = \int_0^{\theta_0} \left[P_{n_k}^m(\cos\theta) \right]^2 \sin\theta d\theta = \frac{\sin\theta_0}{2n_k+1} \frac{dP_{n_k}^m(\cos\theta_0)}{d\theta} \frac{\partial}{\partial n_k} P_{n_k}^m(\cos\theta_0), \; para\ k-m\ impar \quad [3.61]$$

En ambas familias de funciones, las generadas con $k-m$ par y las de $k-m$ impar, se cumple la ortogonalidad, es decir:

$$\left\langle P_{n_k}^m, P_{n_{k'}}^{m'} \right\rangle = \int_0^{\theta_0} P_{n_k}^m(\cos\theta) P_{n_{k'}}^{m'}(\cos\theta) \sin\theta d\theta = 0, \; para\ k-m\ y\ k'-m'\ par\ (o\ impar) \quad [3.62]$$

Sin embargo, funciones de distinta familia no son ortogonales y el producto entre ellas es no nulo:

$$\left\langle P_{n_k}^m, P_{n_{k'}}^{m'} \right\rangle = \int_0^{\theta_0} P_{n_k}^m(\cos\theta) P_{n_{k'}}^{m'}(\cos\theta) \sin\theta d\theta = -\frac{\sin\theta_0}{(n_k-n_{k'})(n_k+n_{k'}+1)} P_{n_k}^m(\cos\theta_0) \frac{dP_{n_{k'}}^{m'}(\cos\theta_0)}{d\theta}, \quad [3.63]$$

$$para\ k-m\ par(impar)\ y\ k'-m'\ impar(par)$$

ii. Ortogonalidad y norma de las funciones cónicas de Mehler.

En el caso de las funciones cónicas de Mehler se verifica que, independientemente del valor del grado n (complejo, nulo (ó – 1) ó -1/2), todas ellas están fuertemente normalizadas verificándose:

$$\left\| K_p^m \right\|^2 = \int_0^{\theta_0} \left[K_p^m(\cos\theta) \right]^2 \sin\theta d\theta = 1 \quad [3.64]$$

$$\left\| K_{0,-1}^m \right\|^2 = \int_0^{\theta_0} \left[K_{0,-1}^m(\cos\theta) \right]^2 \sin\theta d\theta = 1 \quad [3.65]$$

$$\left\| K_{-1/2}^m \right\|^2 = \int_0^{\theta_0} \left[K_{-1/2}^m(\cos\theta) \right]^2 \sin\theta d\theta = 1 \quad [3.66]$$

Las funciones cónicas de Mehler son ortogonales entre sí, por lo que en el dominio del casquete esférico el producto entre ellas, cuando los parámetros son diferentes, es nulo:

$$\left\langle K_p^m, K_{p'}^{m'} \right\rangle = \int_0^{\theta_0} K_p^m(\cos\theta) K_{p'}^{m'}(\cos\theta) \sin\theta d\theta = 0 \qquad [3.67]$$

Además se verifica que las funciones de Legendre de grado real y las de Mehler involucradas en el método R-SCHA son ortogonales entre sí, es decir, que la integral de su producto dentro del casquete esférico es nula. Sin embargo, para el caso de la técnica R-SCHA2D no se da dicha ortogonalidad y el producto de las funciones de Mehler con $n = -1/2$ y las funciones de Legendre con $k - m$ par es no nulo (ver Thébault, 2008) y toma el valor:

$$\left\langle P_{n_k}^m, K_{-1/2}^m \right\rangle = \int_0^{\theta_0} P_{n_k}^m(\cos\theta) K_{-1/2}^m(\cos\theta) \sin\theta d\theta =$$
$$= \frac{\sin\theta_0}{n_k(n_k+1)+1/4} \left[P_{n_k}^m(\cos\theta) \frac{dK_{-1/2}^m(\cos\theta)}{d\theta} - K_{-1/2}^m(\cos\theta) \frac{dP_{n_k}^m(\cos\theta)}{d\theta} \right]_0^{\theta_0}, \; si \; k-m \; es \; par \qquad [3.68]$$

iii. Norma del Campo Geomagnético y matriz de regularización.

La ortogonalidad de las funciones base (funciones de Legendre de grado real y de Mehler) que definen el potencial geomagnético cobra importancia en el proceso de inversión para determinar los coeficientes SCH. En ocasiones la norma del Campo Geomagnético $\|\mathbf{B}\|^2$ puede ser usada como información extra o *a priori* en el proceso de inversión y es de utilidad cuando trabajamos con datos mal distribuidos espacio – temporalmente o cuando la dispersión de su incertidumbre es alta, como es el caso de los datos paleomagnéticos. Como el Campo Geomagnético deriva directamente del potencial (ec. 2.13), su norma dependerá de la norma del gradiente del mismo:

$$\|\mathbf{B}\|^2 = \left\|B_r^2 + B_\theta^2 + B_\lambda^2\right\| = \left\|-\nabla V\right\|^2 = \left\|\nabla V \cdot \nabla V\right\| = \int_0^{\theta_0} \int_0^{2\pi} \nabla V \cdot \nabla V a^2 \sin\theta d\theta d\lambda \qquad [3.69]$$

Con ayuda de las expresiones anteriores (ortogonalidad y normalización de las funciones base) podremos obtener la norma del Campo Geomagnético dentro del casquete esférico para los tres diferentes tipos de técnicas de modelización: el método clásico SCHA, el R-SCHA y el R-SCHA2D. Dicha norma puede ser transformada en elementos de una matriz que se introduce en el proceso de inversión de datos. A la matriz se le denomina matriz de regularización $\boldsymbol{M_r}$ y tomará mayor o menor relevancia en la inversión dependiendo del valor escalar α por el que es multiplicada (siendo α un multiplicador de Lagrange). El valor óptimo de α será aquel en el que el compromiso entre el ajuste de los datos y el modelo obtenido sea el mejor posible.

iii.a. Caso A: norma del campo geomagnético aplicando la técnica SCHA.

En este caso, hay que tener en cuenta que funciones con $k - m$ par y $k - m$ impar no son ortogonales, por lo que aparecerán productos cruzados entre los coeficientes SCH, lo que implica que la matriz de regularización generada a partir de la norma no es diagonal. La expresión de la norma del campo geomagnético de origen interno es (según Korte y Holme, 2000):

$$\|\mathbf{B}\|^2 = \sum_{n_k}\sum_{n_{k'}}\sum_{m}\sum_{m'}\pi a^2\left(\frac{a}{r}\right)^{n_k+n_{k'}+4}\left(A_1+A_2+A_3\right)\left(g_{n_k}^{m}g_{n_{k'}}^{m'}+h_{n_k}^{m}h_{n_{k'}}^{m'}\right) \qquad [3.70]$$

donde:

$$A_1 = (1+\delta_{m=m',0})(n_k+1)(n_{k'}+1)\left\langle P_{n_k}^{m}, P_{n_{k'}}^{m'}\right\rangle \qquad [3.71]$$

$$A_2 = (1+\delta_{m,0})(1+\delta_{m',0})\frac{\sin\theta_0}{2}\left[P_{n_{k'}}^{m'}(\cos\theta_0)\frac{dP_{n_k}^{m}(\cos\theta_0)}{d\theta}+P_{n_k}^{m}(\cos\theta_0)\frac{dP_{n_{k'}}^{m'}(\cos\theta_0)}{d\theta}\right] \qquad [3.72]$$

$$A_3 = (1+\delta_{m,0})(1+\delta_{m',0})\frac{n_k(n_k+1)+n_{k'}(n_{k'}+1)}{2}\left\langle P_{n_k}^{m}, P_{n_{k'}}^{m'}\right\rangle \qquad [3.73]$$

iii.b. Caso B: norma del campo geomagnético aplicando la técnica R-SCHA.

En este caso todas las funciones son ortogonales por lo que la matriz generada a partir de la norma es diagonal. Thébault et al. (2006a) proporcionaron el valor de la norma para el campo geomagnético en función de los parámetros de la técnica R-SCHA:

$$\|\mathbf{B}\|^2 = \sum_{m}(1+\delta_{m,0})\pi a^2\left(B_1+B_2+B_3+B_4\right) \qquad [3.74]$$

donde:

$$B_1 = \sin\theta_0\sum_{p}(G_p^{2m}+H_p^{2m})K_p^{m}(\cos\theta_0)\frac{dK_p^{m}(\cos\theta_0)}{d\theta}\left\|R_p\right\|^2 \qquad [3.75]$$

$$B_2 = \sin\theta_0(G_0^{2m}+H_0^{2m})K_0^{2m}(\cos\theta_0)\frac{dK_0^{2m}(\cos\theta_0)}{d\theta}\left\|R_0\right\|^2 \qquad [3.76]$$

$$B_3 = a^3\sum_{k}(n_k+1)\left(1-\left(\frac{a}{b}\right)^{2n_k+1}\right)\left(g_{n_k}^{2i,m}+h_{n_k}^{2i,m}\right)\left\|P_{n_k}^{m}\right\|^2 \qquad [3.77]$$

$$B_4 = a^3\sum_{k}n_k\left(\left(\frac{a}{b}\right)^{2n+1}-1\right)\left(g_{n_k}^{2e,m}+h_{n_k}^{2e,m}\right)\left\|P_{n_k}^{m}\right\|^2 \qquad [3.78]$$

donde $\|R_0\|^2$ y $\|R_p\|^2$ se obtienen a partir de las ec. [2.23] y [2.24] respectivamente.

iii.c. Caso C: norma del campo geomagnético aplicando la técnica R-SCHA2D.

Teniendo en cuenta el potencial de la técnica R-SCHA2D (ec. 3.29) podemos obtener el valor de la norma del campo geomagnético como (ver Thébault, 2008):

$$\|B\|^2 = \sum_m (1+\delta_{m,0})\pi a^2 \left(C_1 + C_2 + 2\cdot C_3\right) \qquad [3.79]$$

donde:

$$C_1 = \sum_k [(2n_k^2 + 3n_k + 1)(g^{2i,m}_{n_k} + g^{2e,m}_{n_k}) + (2n_k^2 + n_k)(h^{2i,m}_{n_k} + h^{2e,m}_{n_k})] \left\| P^m_{n_k} \right\|^2 \qquad [3.80]$$

$$C_2 = \left[K^m_{-1/2}(\cos\theta_0) \left. \frac{dK^m_{-1/2}(\cos\theta)}{d\theta} \right|_{\theta_0} \sin\theta_0 - \frac{1}{4} \left\| K^m_{-1/2} \right\|^2 \right] (G^{2m}_{-1/2} + H^{2m}_{-1/2}) \qquad [3.81]$$

$$C_3 = \sum_k \left[P^m_{n_k}(\cos\theta_0) \left. \frac{dK^m_{-1/2}(\cos\theta)}{d\theta} \right|_{\theta_0} \sin\theta_0 - \frac{1}{4} \left\langle P^m_{n_k}, K^m_{-1/2} \right\rangle \right] \cdot \left[G^{2m}_{-1/2}(g^{2i,m}_{n_k} + g^{2e,m}_{n_k}) + H^{2m}_{-1/2}(h^{2i,m}_{n_k} + h^{2e,m}_{n_k}) \right] \qquad [3.82]$$

3.4. Conversión de las coordenadas y de los datos geomagnéticos (y/o paleomagnéticos).

El hecho de que la Tierra no sea esférica hace que tanto las coordenadas como las componentes del campo geomagnético en la superficie terrestre vengan expresadas en coordenadas geodésicas, las cuales tendremos que transformar a geocéntricas. Además, las coordenadas y componentes geocéntricas deben estar referidas al polo del casquete esférico y no al polo norte geográfico, por lo que es necesario realizar un giro de coordenadas y componentes para referirlas al nuevo sistema de referencia. Una vez obtenidas las coordenadas y componentes del campo geomagnético en el nuevo sistema de referencia del casquete esférico, podemos aplicar los métodos de modelización regional vistos anteriormente para obtener los coeficientes SCH que optimicen la relación entre ellos.

Los datos geomagnéticos y/o paleomagnéticos son tomados en la superficie terrestre y vienen expresados en coordenadas geodésicas (coordenadas sobre el geoide de referencia). Debemos de aplicar un giro en el plano que contiene las

componentes norte y vertical para pasar a coordenadas y componentes geocéntricas. Tanto la longitud como la componente este son invariantes a dicho giro. En la figura 3.9 representamos un esquema de los parámetros a transformar (GDlat, GDalt, X e Y) y los transformados (GClat, R, BN, BV).

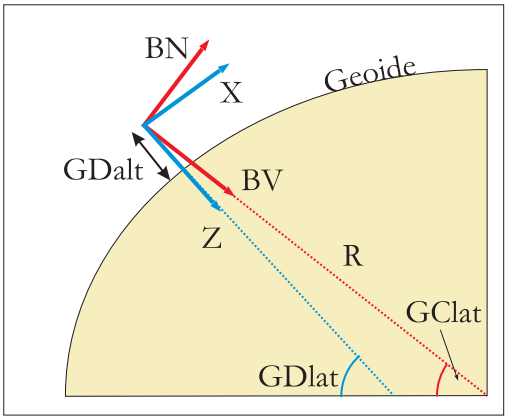

Figura 3.9. Conversión de coordenadas geodésicas a geocéntricas. GDlat/GDalt y GClat/R son la latitud/altitud geodésicas y la latitud geocéntrica/distancia radial respectivamente. X y Z corresponden a las componentes geodésicas norte y vertical y sus análogas BN y BV en geocéntricas

Una vez expresadas las componentes en el sistema de referencia geocéntrico, debemos girarlas de nuevo para referirlas al sistema de referencia del casquete esférico. En este caso la distancia radial y la componente vertical permanecen invariantes. Las ecuaciones del giro vienen dadas en De Santis et al. (1989):

$$\cos\theta' = \cos\theta_0 \cos\theta + \sin\theta_0 \sin\theta \cos(\lambda - \lambda_0) \qquad [3.83]$$

$$tg(\pi - \lambda') = \frac{\sin\theta \sin(\lambda - \lambda_0)}{\sin\theta_0 \cos\theta - \cos\theta_0 \sin\theta \cos(\lambda - \lambda_0)} \qquad [3.84]$$

donde θ' y λ' son las coordenadas en el nuevo sistema de referencia, mientras que θ y λ son las coordenadas en el sistema de referencia geocéntrico. θ_0 y λ_0 son las coordenadas del polo del casquete en el sistema de referencia previo. La siguiente figura 3.10 muestra un esquema aclaratorio de los diferentes sistemas de referencia.

El ángulo α determina el giro y con él podemos pasar de un sistema de referencia geocéntrico centrado en el polo a otro centrado en el polo del casquete. La relación entre las componentes horizontales del campo X y Y, y las nuevas componentes giradas X' y Y' viene dada por:

$$\begin{pmatrix} X' \\ Y' \end{pmatrix} = \begin{pmatrix} \cos\alpha & \sin\alpha \\ -\sin\alpha & \cos\alpha \end{pmatrix} \begin{pmatrix} X \\ Y \end{pmatrix} \qquad [3.85]$$

donde,

$$\cos\alpha = \frac{\cos\theta_0 - \cos\theta\cos\theta'}{\sin\theta\sin\theta'} \qquad [3.86]$$

Hay que tener en cuenta que el signo de alfa depende de si el polo del casquete esférico está al este u oeste del punto de estudio. En De Santis y Kerridge (1989) y Torta (1992) la ec. [3.85] aparece con errores tipográficos.

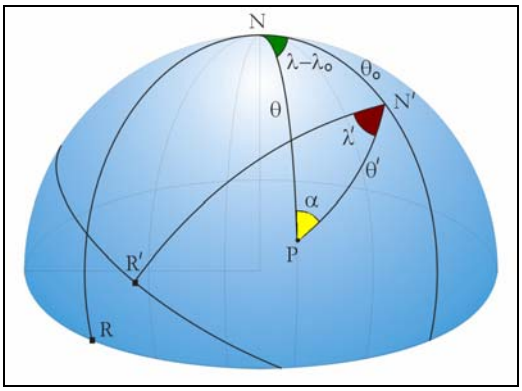

Figura 3.10. Cambio de sistema de referencia, del polo norte geográfico al nuevo polo del casquete.

3.5. Métodos de inversión.

En estos dos últimos capítulos hemos visto como el campo geomagnético puede ser expresado (tanto en el caso esférico como en el dominio de un casquete esférico) a través de una serie de productos entre las funciones base y los coeficientes de Gauss (o los coeficientes SCH). Esta sección la dedicamos a la obtención de los coeficientes SCH que mejor ajusten a una serie de observaciones, esto es, resolver el problema inverso y generar modelos regionales de campo geomagnético.

El potencial geomagnético no es un observable, por tanto, lo que se puede conocer son sus componentes norte (X), este (Y) y vertical (Z) o sus elementos angulares declinación (D) e inclinación (I) y la intensidad (F); que forman, junto con las coordenadas geográficas, el dato geomagnético. La primera terna de observables (X,Y,Z) se pueden expresar directamente de forma lineal con los coeficientes SCH como hemos visto en las ec. 3.13 – 3.15, sin embargo, en el caso de los elementos D, I y F, no se da dicha linealidad (ver las ec. 2.7 – 2.10). Veremos a continuación diferentes casos de aproximación al problema dependiendo del tipo de dato geomagnético y/o paleomagnético del que se dispone.

Caso 1. Se dispone de tres elementos independientes.

Se trata del caso más óptimo, pues independientemente de si son directamente las tres componentes ortogonales o cualquier terna de elementos independientes, siempre podemos obtener las tres componentes del campo X, Y y Z aplicando las ec. 2.7 a 2.10. En este caso, los coeficientes SCH se pueden obtener aplicando, por ejemplo, el método matricial de mínimos cuadrados. En este caso tendremos n observaciones de X, de Y y de Z que dan lugar a un vector de datos **D** de dimensión $3n \times 1$. La matriz de parámetros **A** tendrá una dimensión de $3n \times r$, siendo r el número de coeficientes SCH involucrados en el problema inverso y que depende del orden máximo del desarrollo: $K_{máx}$. Matricialmente tenemos:

$$\mathbf{D} = \mathbf{A} \cdot \mathbf{g} \qquad [3.87]$$

donde **g** es el vector de coeficientes SCH no conocidos. Si aplicamos un ajuste mediante mínimos cuadrados, los coeficientes se calculan como:

$$\mathbf{g} = \left(\mathbf{A}^T \cdot \mathbf{A}\right)^{-1} \mathbf{A}^T \mathbf{D} \qquad [3.88]$$

En este caso, hemos considerado que todos los observables tienen la misma incertidumbre (o peso), pero si queremos tener en cuenta la incertidumbre del dato, debemos añadir en la ec. 3.88 la matriz de covarianza **C** de pesos de los datos geomagnéticos. La ec. 3.88 se transforma en:

$$\mathbf{g} = \left(\mathbf{A}^T \cdot \mathbf{C} \cdot \mathbf{A}\right)^{-1} \mathbf{A}^T \cdot \mathbf{C} \cdot \mathbf{D} \qquad [3.89]$$

Se puede dar el caso de que algunos datos geomagnéticos y/o paleomagnéticos dispongan solo de dos componentes: XY, XZ o YZ. El procedimiento que se sigue es el mismo que en el caso anterior, pero las dimensiones del vector de observaciones **D** y de la matriz de parámetros **A** son diferentes, ya que, si tenemos n observaciones de X y p de Y (o p de Z) las dimensiones de **D** y **A** son, respectivamente, $(n+p) \times 1$ y $(n+p) \times r$.

Este método permite modelar de forma separada las componentes horizontales XY de la componente vertical Z. En general esto reduce el error cuadrático medio al comparar el modelo con los observables (García et al., 1991), sin embargo, creemos que trabajar con las tres componentes XYZ es más adecuado, ya que los coeficientes SCH son los mismos para las tres componentes y por tanto derivan de un mismo potencial.

Caso 2. Se dispone solo de la declinación D o de información direccional.

Un caso muy común en Paleomagnetismo es disponer solo del par declinación e inclinación para cada coordenada geográfica sin información de intensidad. En este caso debemos modificar la técnica SCHA. La modificación

que proponemos en este trabajo está basada en el método de Bauer (Barraclough, 1974) y se desarrolla en detalle en el Anexo 1. Este método relaciona los coeficientes SCH con los valores de declinación e inclinación y los elementos de la matriz de parámetros de la forma:

$$\mathbf{D} = \begin{pmatrix} 0 \\ \gamma_0 \cos D \cos I \\ \gamma_0 \sin D \cos I \end{pmatrix} \qquad [3.90]$$

$$\mathbf{A} = \begin{pmatrix} \alpha_j \cdot \sin D - \beta_j \cdot \cos D \\ \alpha_j \cdot \sin I - \gamma_j \cdot \cos D \cos I \\ \beta_j \cdot \sin I - \gamma_j \cdot \sin D \cos I \end{pmatrix} \qquad [3.91]$$

Siendo α, β y γ los elementos de la matriz de parámetros del **Caso 1**. De nuevo, los coeficientes SCH se obtienen aplicando la ec. 3.89. Hay que tener en cuenta que en este caso, los coeficientes SCH están normalizados respecto al primer coeficiente SCH g_0^0 (ver Anexo 1).

Caso 3. No se dispone de todos los elementos angulares y/o de intensidad: D, I, F, DI, DF y/o IF.

Cuando el dato geomagnético viene definido sólo por dos o un elemento angular y/o la intensidad es necesario recurrir a métodos de aproximación ya que no existe una relación lineal entre los coeficientes SCH y los observables. En este caso, tenemos dos caminos a seguir. El primero consiste en aplicar el método iterativo de Newton – Raphson (ver por ejemplo Jackson et al., 2000) y el segundo en el desarrollo de Taylor de los elementos angulares y la intensidad. Aunque en el caso de que solo tengamos valores de D o el par D-I podríamos tratarlos según lo explicado en el caso anterior: Caso 2.

El método iterativo de Newton – Raphson.

En este caso la ecuación a resolver no es lineal, pues tanto los elementos angulares D e I como la intensidad no son combinación lineal de los coeficientes SCH. En este caso debemos aplicar un proceso iterativo donde, partiendo de un modelo base $\mathbf{B_0}$, llegamos al modelo final. El método de Newton – Raphson es muy adecuado debido a la estabilidad que presenta el proceso iterativo. Los coeficientes SCH después de cada iteración, $\mathbf{g}_{i+1}$, vienen dados por la siguiente expresión:

$$\mathbf{g}_{i+1} = \mathbf{g}_i + \left(\mathbf{A}_i^T \cdot \mathbf{C} \cdot \mathbf{A}_i\right)^{-1} \mathbf{A}_i^T \cdot \mathbf{C} \cdot (\mathbf{D} - \hat{f}(\mathbf{g}_i)) \qquad [3.92]$$

Siendo $\mathbf{A}_i$ la matriz de Frechet de derivadas parciales entre los observables y los coeficientes SCH cuyos elementos vienen dados por: $A_{i,j} = \partial f_i / \partial g_j$. **D** es el

vector de los observables y $\hat{f}(\mathbf{g}_i)$ el vector de datos modelados obtenidos en la iteración anterior. **C** es la matriz de pesos. El número de iteraciones dependerá del error mínimo que se quiera alcanzar entre los observables y el modelo.

Desarrollo de Taylor de la declinación, inclinación e intensidad.

Otra opción a la hora de abordar el problema de no linealidad de los elementos angulares e intensidad es el desarrollo de los mismos en serie de Taylor. Al truncar el desarrollo de Taylor hasta orden primero los elementos vendrán dados por:

$$\mathbf{D} = \mathbf{D}_0 + \mathbf{A} \cdot \delta\mathbf{g} \qquad [3.93]$$

Siendo **D** la matriz de elementos (declinación, inclinación o intensidad), $\mathbf{A} = \partial\mathbf{D}/\partial\mathbf{g}$ la matriz de Frechet de derivadas y $\delta\mathbf{g}$ el vector de coeficientes SCH. De nuevo es necesario partir de un modelo de campo geomagnético inicial expresado en este caso por $\mathbf{D}_0$. Ahora la ecuación a resolver pasa a ser lineal pudiéndose aplicar el método matricial de mínimos cuadrados dados en la ec. 3.89. En el Anexo 2 damos las expresiones de las matrices de Frechet relativas a la declinación, inclinación e intensidad necesarias en cualquiera de los dos casos descritos.

Uso de la matriz de regularización.

Finalmente veremos como proceder en el caso de que decidamos incluir la matriz de regularización $\mathbf{M}_r$ en el proceso de inversión. En el capítulo 3.3.3 vimos la expresión de la matriz de regularización para el caso de la norma del campo geomagnético. La matriz será diagonal para el método R-SCHA y tiene elementos no – diagonales en el caso clásico SCHA y en el R-SCHA2D. En cualquier caso, las expresiones matriciales del método de inversión vienen dadas para el caso lineal (ec. 3.89) por:

$$\mathbf{g} = \left(\mathbf{A}^T \cdot \mathbf{C} \cdot \mathbf{A} + \alpha\mathbf{M}_r\right)^{-1} \mathbf{A}^T \cdot \mathbf{C} \cdot \mathbf{D} \qquad [3.94]$$

Y si usamos el método de iteración de Newton – Raphson (p.e. Jackson et al., 2000):

$$\mathbf{g}_{i+1} = \mathbf{g}_i + \left(\mathbf{A}_i^T \cdot \mathbf{C} \cdot \mathbf{A}_i + \alpha\mathbf{M}_r\right)^{-1} \left[\mathbf{A}_i^T \cdot \mathbf{C} \cdot (\mathbf{D} - \hat{f}(\mathbf{g}_i)) - \alpha\mathbf{M}_r\mathbf{g}_i\right] \qquad [3.95]$$

El escalar α es un multiplicador de Lagrange que se fija teniendo en cuenta el mejor compromiso entre el modelo obtenido y los observables.

Capítulo 4.
Datos Arqueomagnéticos

Para poder analizar el comportamiento del campo geomagnético en el pasado tenemos que usar los registros que éste ha dejado en las rocas, materiales arqueológicos, etc. En nuestro caso estamos interesados en registros paleomagnéticos en estructuras arqueológicas (estructuras con potencial arqueomagnético) y los registros en sedimentos lacustres.

En primer lugar debemos hacer referencia a dos textos muy útiles en el análisis paleomagnético: *Paleomagnetism* (Butler, 1992) y *Lectures in Paleomagnetism*, (L. Tauxe, 2005). En ambos libros se desarrollan en profundidad todos los fundamentos físicos en los que se basa dicha disciplina y se describen tanto las técnicas de laboratorio, como los análisis estadísticos que se llevan a cabo en la obtención de datos. En este capítulo, se desarrollará sólo algunos de los aspectos fundamentales necesarios para la compresión del mismo y de los futuros capítulos que conforman esta Memoria.

Los materiales de interés paleomagnético tienen una imanación remanente natural (NRM, *Natural Remanent Magnetisation*), que es suma (suma vectorial, ya que la imanación es un vector) de todas las posibles imanaciones que ha podido adquirir el material a lo largo de su historia. Esta imanación es suma de una posible magnetización primaria más otras secundarias. Se denomina magnetización primaria a la adquirida por la roca en su formación y magnetizaciones secundarias a las relacionadas con procesos físico-químicos posteriores.

Entre los posibles mecanismos de adquisición de la remanencia magnética, vamos a analizar la que en mayor medida afecta a los materiales arqueológicos: la remanencia térmica o termorremanencia (TRM, *Termal Remanent Magnetisation*). El caso de la remanencia deposicional o post-deposicional característica de los registros sedimentarios será discutido en el capítulo 7.

Cuando un material está sometido a altas temperaturas, por encima de la temperatura de bloqueo, los minerales ferromagnéticos contenidos en el material cambian su estado magnético, pasando a ser superparamagnéticos. En este estado, un campo magnético pequeño (como lo es el campo geomagnético, cuya intensidad máxima no alcanza las 60 μT a latitudes medias) es capaz de orientar los momentos magnéticos atómicos de los minerales. Cuando el material se enfría por debajo de la temperatura de bloqueo (que depende del tamaño de grano) la imanación inducida se bloquea, adquiriendo el material una

magnetización remanente térmica o termorremanencia. Esta remanencia es muy estable y solo desaparece cuando calentamos de nuevo al material a temperaturas mayores de la de bloqueo o aplicando un campo magnético particularmente intenso.

El arqueomagnetismo se centra en el análisis paleomagnético de materiales de origen arqueológico. El primer estudio relacionado con el arqueomagnétismo fue publicado en Italia por Gheradi en 1862: "Sul magnetismo polare de palazzi ed altri edifizi in Torino". Posteriormente Folgerhaiter, en 1899, analizó la remanencia en ladrillos y cerámicas, dando las primeras pinceladas de lo que son hoy las bases del arqueomagnetismo. Posteriormente, en Francia, Thellier desarrolló las técnicas arqueomagnéticas analizando la variación secular en Francia en los últimos dos milenios (Thellier, 1937, 1938, 1981; Thellier y Thellier 1952, 1959). Estudios que siguieron Cook y Belshé, en 1958, en el Reino Unido.

En los yacimientos arqueológicos podemos encontrar estructuras que han sido calentadas en su uso, como son termas, hornos, hogares, tumbas incendiarias, etc. O bien, calentadas accidentalmente como incendios. En estos casos los materiales adquieren una magnetización termorremanente o TRM. El calentamiento de la estructura actúa sobre los minerales ferromagnéticos que contiene y cuando ésta se enfría, la imanación de los minerales ferromagnéticos se orienta en la dirección del campo geomagnético local. Si queremos hacer un estudio de la dirección arqueomagnética almacenada en la estructura arqueológica, es necesario que desde el tiempo de adquisición de la magnetización hasta su muestreo la estructuras haya permanecido *in situ*, ya que un basculamiento de la misma puede producir cambios importantes en la orientación del momento magnético remanente. No ocurre lo mismo si pretendemos hacer análisis de la intensidad, ya que la posición de la estructura en este caso no es importante.

Si en una región, no mayor de 10^6 km^2 (Tarling, 1983), hay un suficiente número de datos arqueomagnéticos de edades diferentes, podemos conocer como ha evolucionado la dirección del campo geomagnético a lo largo de la Historia en dicha región. Así es posible la construcción de una curva de referencia que describa la variación temporal de los elementos angulares (declinación e inclinación) y de intensidad del campo geomagnético. A la curva se le denomina Curva de Variación Paleosecular (PSVC, del inglés Palaeosecular Variation Curve) y será característica de la región de estudio, no pudiendo ser extrapolada fuera de ella debido a las características del campo geomagnético y su carácter no dipolar. Aparecen así las PSVCs características de cada región. Curvas que existen ya en varios países de Europa y que en el capítulo siguiente serán usadas en la generación del primer modelo regional direccional de campo geomagnético para Europa para los últimos 2000 años.

En España el arqueomagnetismo se ha desarrollado mucho más tardíamente (última década) que en países como Francia o el Reino Unido (que tienen sus correspondientes PSVCs desde hace 50 años). El grupo de Paleomagnetismo de la UCM ha iniciado estos estudios en España (Núñez, 2005; Gómez-Paccard, 2006). Pero, a pesar del retraso inicial, Iberia cuenta ya con una PSVC (Gómez-Paccard et al., 2006b).

El hecho de tener una PSVC bien definida en el tiempo permite también actuar de forma inversa, es decir, que si conocemos la dirección (declinación e inclinación) y/o intensidad de una estructura arqueológica pero no su edad, con la curva de referencia podríamos evaluar la fecha de su último enfriamiento (es decir, de su último uso). Se trata, por tanto, de una técnica de datación arqueológica, ya que se comparan los valores direccionales y/o de intensidad con los de la curva de referencia. Pero para ello es necesario que las curvas estén bien definidas y ello solo es posible con aportaciones de declinación, inclinación e intensidad de yacimientos bien datados cronológicamente.

Para la selección de un yacimiento arqueológico es necesario recurrir al carácter multidisciplinar que presenta el arqueomagnetismo, ya que son los arqueólogos los que determinan esta primera fase de selección. Buscamos una distribución espacio – temporal de yacimientos lo más amplia posible estableciendo dos tipos de requisitos, unos *a priori*, relativos a las características que deben cumplir las estructuras arqueológicas para su muestreo; y otros *a posteriori*, que definen los requisitos que deben satisfacer los resultados teniendo en cuenta sus valores estadísticos.

En cuanto al primer tipo de selección, las principales características que deben de verificar las estructuras arqueológicas para poder ser investigadas paleomagnéticamente son (Núñez, 2005):
- Que hayan sido calentados hasta temperaturas del orden de 600ºC o superiores; es decir, hornos, termas, hogares, edificaciones incendiadas, etc. Aunque calentamientos menores (de hasta 200 – 300 ºC) también pueden ser investigados.
- Que no hayan sufrido calentamientos posteriores.
- Que los materiales calentados hayan permanecido *in situ*, es decir, que no hayan sufrido movimientos importantes (derrumbes, basculamientos, etc.) desde el último calentamiento. Esto es importante para el análisis direccional.
- Que la estructura esté bien datada (por criterios arqueológicos y/o por otras técnicas).

Tras el muestreo es necesario un tratamiento específico (preparado de muestras y trabajo de laboratorio) para obtener los valores de declinación, inclinación y/o de intensidad que han quedado *grabados* en la estructura. Ello da lugar al **dato arqueomagnético**. Si queremos usar este dato arqueomagnético en

la construcción de una curva de variación paleosecular, es necesario realizar el traslado de los elementos del campo arqueomagnético desde el lugar de muestreo hasta el punto donde se vaya a referir la curva, es lo que se llama corrección geográfica o relocalización. Se considera aceptable aplicar este traslado si los puntos de muestreo no distan más allá de 600 – 700 km del punto central o punto de referencia (Tarling, 1983).

Para trasladar los datos direccionales se hace uso del método de Conversión Vía Polo propuesto por Noël y Batt (1990). Para ello se asume un campo geomagnético dipolar y a través de los datos de declinación e inclinación *in situ*, se calcula el polo magnético virtual que generaría esa dirección geomagnética. Después de calcular el polo virtual, se calcula en las coordenadas de referencia los valores de declinación e inclinación que proporcionan el dipolo (ver figura 4.1).

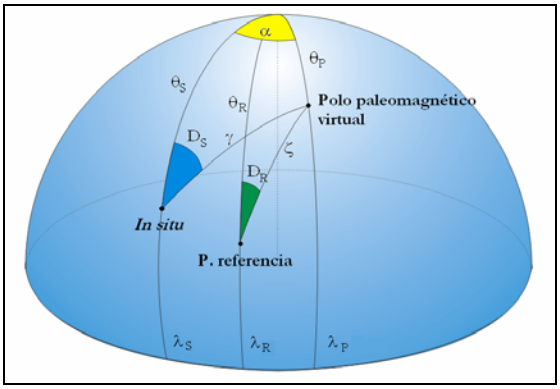

Figura 4.1. Esquema del método de conversión vía polo.

Teniendo en cuenta la notación usada en la figura 4.1, podemos calcular las coordenadas del polo magnético virtual usando razones trigonométricas esféricas:

$$\theta_P = a\cos(\cos\theta_S\cos\gamma + \sin\theta_S\sin\gamma\cdot\cos D_S) \qquad [4.1]$$

$$\lambda_P = \begin{cases} \lambda_S + \alpha & si, \quad \cos(\gamma) \geq \cos\theta_S\cos\theta_P \\ \lambda_S + \pi - \alpha & si, \quad \cos(\gamma) < \cos\theta_S\cos\theta_P \end{cases} \qquad [4.2]$$

Siendo γ la colatitud *in situ* referida al polo magnético virtual que se obtiene asumiendo la hipótesis del campo dipolar y α la diferencia entre longitudes:

$$tg\gamma = \frac{2}{tgI_S} \qquad [4.3]$$

$$\sin\alpha = \frac{\sin\gamma\cdot\sin D_S}{\sin\theta_P} \qquad [4.4]$$

A partir de las coordenadas del polo, obtenemos los valores de declinación e inclinación en el lugar de referencia:

$$I_R = atg(\frac{2}{tg\zeta}) \quad [4.5]$$

$$D_R = a\cos(\frac{\cos\theta_P - \cos\varsigma \cdot \cos\theta_R}{\sin\varsigma \cdot \sin\theta_R}) \quad [4.6]$$

Siendo ζ la colatitud del punto de referencia respecto del polo paleomagnético virtual:

$$\zeta = a\cos(\cos\theta_R \cos\theta_P + \sin\theta_R \sin\theta_P \cdot \cos(\lambda_P - \lambda_R)) \quad [4.7]$$

Para trasladar el dato de intensidad podemos optar por dos métodos (ver Merrill et al., 1996). El primero consiste en una traslación mediante el momento virtual dipolar axial (VADM, del inglés Virtual Axial Dipole Moment) en el que se considera un campo magnético dipolar axial (GAD, del inglés *Geocentric Axial Dipole*). En este caso sólo las colatitudes entran en juego y la nueva intensidad en el punto de referencia viene dada por:

$$F_R = F_S \sqrt{\frac{1+3\cos^2\theta_R}{1+3\cos^2\theta_S}} \quad [4.8]$$

Sin embargo, si se dispone de datos de inclinación, podemos usar la colatitud geomagnética en lugar de la geográfica, asumiendo en este caso un campo dipolar inclinado similar al que se asume en la Conversión Vía Polo. En este caso la traslación se hace a través del momento virtual dipolar (VDM, del inglés Virtual Dipole Moment) y su expresión es análoga a la dada en [4.8], pero cambiando la colatitud geográfica por la magnética. La colatitud magnética se obtiene a partir de la inclinación teniendo en cuenta la expresión [4.3]:

$$F_R = F_S \sqrt{\frac{1+3\cos^2\zeta}{1+3\cos^2\gamma}} \quad [4.9]$$

El error direccional que se comete al efectuar la traslación vía polo, es decir, al asumir un campo únicamente dipolar, es de unos 7º/1700 km (Casas e Incoronato, 2007). Para la intensidad el error cometido con la corrección VADM/VDM es de unas 4 μT/1000 km (Gómez-Paccard et al., 2008). Todo ello asumiendo que las características y magnitud del campo no dipolar se han mantenido constantes e iguales a las actuales.

Después de obtener el dato arqueomagnético, este tendrá potencial para definir las características del campo geomagnético si cumple un serie de requisitos *a posteriori*. Existen diferentes criterios de fiabilidad o de clasificación de la "bondad" del dato arqueomagnético. Un ejemplo de estos criterios viene dado en Tarling y Dobson (1995) donde se clasifican los resultados en categorías

de 0 a 5 dependiendo de los parámetros estadísticos asociados al cálculo del dato arqueomagnético. En el capítulo siguiente se describe en mayor detalle la obtención de un dato direccional arqueomagnético en una estructura arqueológica. En Gómez-Paccard et al. (2008) se puede encontrar los pasos a seguir en la obtención de datos de paleointensidad en materiales arqueológicos.

4.1 Primeros datos arqueomagnéticos del norte de Iberia.

Resumen.

En este trabajo se ha realizado un estudio arqueomagnético en ocho estructuras arqueológicas situadas en Asturias (norte de España): dos hornos, cuatro hogares y dos termas. Se han obtenido así las primeras direcciones arqueomagnéticas en el norte de la península Ibérica. El objetivo principal de este estudio es mejorar la inhomogénea distribución de datos arqueomagnéticos existente en Iberia (Gómez – Paccard et al., 2006a, 2006b) usados en la construcción de la Curva de Variación Paleosecular de Iberia. La litología de los materiales utilizados en las estructuras arqueológicas de esta zona (cuarzos y pizarras) difiere a la del resto de investigaciones arqueomagnéticas de la península. Las muestras han sido desimanadas térmicamente y por campos alternos decrecientes. Se han realizado, además, estudios de magnetismo de rocas orientados a identificar los portadores de la magnetización y evaluar su estado magnético. En general las muestras se han caracterizado por una baja coercitividad y moderadas temperaturas de desbloqueo indicando que la magnetita y/o la maghemita son los portadores más probables de la remanencia arqueomagnética. Se han obtenido las direcciones medias características siguiendo el método jerárquico y aplicando test estadísticos de distribución Fisheriana. Los resultados han sido comparados entre ellos mismos y con el resto de datos del período Romano de la base de datos de Iberia. También han sido comparados con la curva de variación paleosecular de Iberia generada a partir del método Bayesiano (Gómez-Paccard et al., 2006b). Este trabajo ha servido para confirmar la datación de las estructuras, pues hay un buen acuerdo entre las dataciones arqueomagnéticas, las dadas por métodos de radiocarbono y la información arqueológica. Las incertidumbres en las edades arqueomagnéticas son relativamente altas debido a que la curva de referencia de Iberia no sufre variaciones en declinación en el período romano. Por lo que son necesarios datos arqueomagnéticos de alta calidad para reducir dicho error temporal, sobre todo para la época que va desde el año 0 al 500 d.D.

Available online at www.sciencedirect.com
ScienceDirect
Physics and Chemistry of the Earth 33 (2008) 566–577
PHYSICS and CHEMISTRY of the EARTH
www.elsevier.com/locate/pce

First archaeomagnetic data from northern Iberia

V.C. Ruiz-Martínez *, F.J. Pavón-Carrasco, G. Catanzariti

Departamento de Física de la Tierra I: Geofísica y Meteorología, Facultad de C.C. Físicas, Universidad Complutense de Madrid, 28040 Madrid, Spain

Available online 19 February 2008

Abstract

An archaeomagnetic study has been conducted on eight archaeological structures (two kilns, four fireplaces and two saunas) from two different areas in Asturias (northern Spain). The results provide the first archaeomagnetic directions from the northern Iberian Peninsula. The main goal of this paper is to improve on the non-uniform site distribution used to construct the first archaeomagnetic Secular Variation Curve for Iberia ("SVC-I") by studying new sites from northern Spain, an area currently not represented. The lithologies of some of the studied archaeological structures from this zone (slates, quartzites) differ from those of the rest of the peninsula. Laboratory analysis includes both thermal and alternating field stepwise demagnetization and rock-magnetic studies. A low coercivity, moderate unblocking temperature (T_{ub}) phase, such as magnetite/maghemite, seems to be the carrier of the archaeomagnetic signal. This sometimes overlaps partially with a (geological) high coercivity/high T_{ub} phase. Site-mean characteristic directions have been calculated following a hierarchical approach and applying Fisherian distribution tests. Archaeomagnetic results have been compared, applying Fisherian distribution tests, among themselves and with Roman age entries of the Spanish archaeomagnetic database. They have also been compared with the reference "SVC-I" using Bayesian methods. These analyses have served to validate the archaeological dating of the structures. There is a good agreement between the results of archaeomagnetic dating and radiocarbon dating, both of which are consistent with archaeological constraints. The uncertainties in the archaeomagnetic ages are relatively large mainly because the reference curve hardly varies in declination during Roman times. This highlights the need of more high quality archaeomagnetic data (from very well-dated structures) in order to reduce the errors associated with the reference "SVC-I" and the archaeomagnetic dating technique, particularly between 0 and 500 AD.

Keywords: Archaeomagnetism; Spanish archaeomagnetic catalogue; Dating; Secular variation; Northern Iberia

1. Introduction

The Earth's magnetic field varies in direction and intensity over historical time scales, a feature that is thought to be generated by the non-dipole field components of the geodynamo. This secular variation (SV) can be used for dating purposes by comparing archaeomagnetic determinations from archaeological structures of unknown ages with a well-dated reference SV curve from the same region.

Archaeomagnetic SV curves have been established for different regions around the world, mainly focused on directional data. The reliability and precision of these curves depends on several parameters, such as the number of data and their distribution in time and space, the precision of the individual archaeomagnetic directions and archaeointensities, the dating precision of the studied archaeological structures, etc. In recent years, great effort has been made in Europe in order to fill temporal gaps and to increase the number of data available in published SV, as well as to determine reference SV curves in new regions (e.g. Gómez-Paccard et al., 2006b and references therein).

Recently, a catalogue of Spanish archaeomagnetic directions was published (Gómez-Paccard et al., 2006a) and a first archaeomagnetic SV curve for Iberia has been proposed (Gómez-Paccard et al., 2006b), hereafter referred to as "SVC-I". "SVC-I" includes 63 directions from Spain, with ages ranging between the 2nd century BC and the 20th

* Corresponding author. Tel.: +34 913945007; fax: +34 913944398.
E-mail addresses: vcarlos@fis.ucm.es (V.C. Ruiz-Martínez), fjpavon@fis.ucm.es (F.J. Pavón-Carrasco), gcatanza@fis.ucm.es (G. Catanzariti).

1474-7065/$ - see front matter © 2008 Elsevier Ltd. All rights reserved.
doi:10.1016/j.pce.2008.02.023

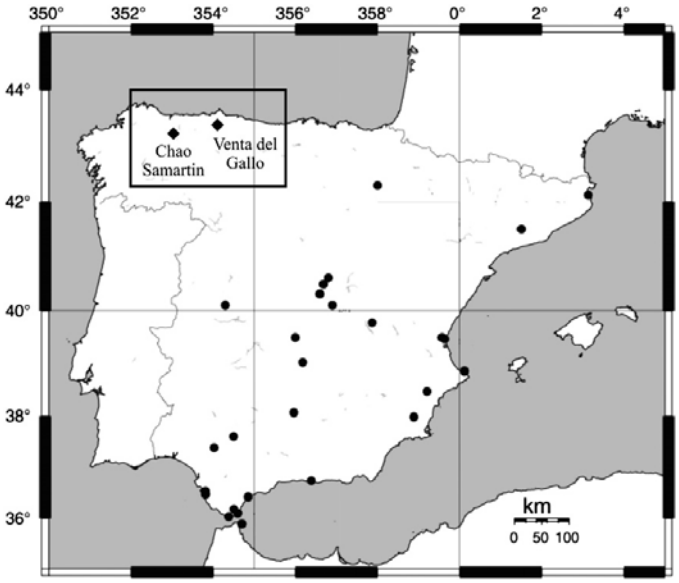

Fig. 1. Location of the seven archaeological structures from the hill-fort "Chao Samartín" and the kiln from "La Venta del Gallo" included in this study (black diamonds, one of them corresponding to seven sites); together with the 63 Spanish archaeomagnetic site-directions (black dots, some of them also corresponding to several structures) included in the construction of the "SVC-I" (modified from Gómez-Paccard et al., 2006a).

century AD, with several archaeomagnetic directions per century for Roman, Medieval and Modern times. One of the main problems with the Spanish data is the non-uniform geographical site distribution, with most of the sites located in central and southern Spain (Fig. 1).

The main goal of this paper is to improve on the distribution of sites used to construct "SVC-I" by studying new sites from northern Spain, an area currently devoid of data.

In addition, the lithologies studied in the Spanish catalogue mainly consist of baked clays, whereas many archaeological structures from northern Spain are built using native rocks, such as Palaeozoic slates and quartzites from the Iberian Variscan Belt. Another key objective of this study is to test the ability of native rocks to preserve an archaeomagnetic signal.

Finally, the precision of the archaeomagnetic dating technique using the present "SVC-I" will be evaluated during Roman times.

2. Archaeological setting and sampling

Two areas in Asturias, northern Spain (Fig. 1), have been studied. The archaeological conditions were favourable to archaeomagnetic investigation: in situ well-heated structures with archaeological and radiometric age constraints. A total of eight archaeological structures (60 samples, 68 specimens) have been studied.

The hill-fort "Chao Samartín" (43.2°N, 6.9°W) is a fortified settlement located in the West Asturian-Leonese Zone of the western European Variscan Belt, at the westernmost end of the Asturias Principality (Grandas de Salime Council). Based on radiocarbon and archaeological considerations (Villa Valdés and Cabo Pérez, 2003; Villa Valdés, 2005) its origin dates back to the 8th century BC, but the archaeological structures sampled in this study are mostly associated with the later Roman presence. This period spans the first decades of the 1st century AD to the second half of the 2nd century AD, when the hill-fort inhabitants suddenly left the settlement. The next occupational stage took place in High-Medieval times (8th to 10th centuries AD).

Seven different structures have been sampled at the hill-fort "Chao Samartín": a domestic stone built (quartzites and slates) kiln ("C18"); two flat, horizontal, stone built fireplaces ("C4B" and "C10B"); a brick built fireplace ("C15B"); a mixed stone-brick built fireplace ("C22B") and a stone built sauna, which was sampled at two different sites ("TFE" and "T").

For the age of the abandonment of these sites, archaeologists have proposed an age around the third quarter of the 2nd century AD, the relatively precise chronology constrained by a coin minted in 161 AD that predates the last use of the structures (i.e., when their remanences were acquired).

Exceptions are the fireplace structure "C22B", which is probably associated with deposits related to earlier times, and one of the studied sauna sites ("TFE"). For the sauna (Fig. 2), two sites were sampled since two different periods of use have been recognized. The older site ("TFE") corresponds to a wall located at one end of the sauna associated with the beginning of the second Iron Age (4th to 2nd

Fig. 2. One of the stone built structures from "Chao Samartín" (sauna, left); and kiln from "La Venta del Gallo" (right).

century BC). This wall was sealed with a new one in the structural alterations which were subsequently introduced during the Roman presence. Radiocarbon dating (C.S.I.C.-1776) of organic material recovered from the original structure gives a calibrated date between 62 BC and 84 AD at the 95% confidence level. After the Roman alterations, the sauna "T" is supposed to have been in use until the third quarter of the 2nd century AD (as with the other kiln and fireplaces).

In addition, three in situ native rocks from outside the hill-fort "Chao Samartín" were sampled in order to compare the archaeomagnetic remanences with the geological ones, in the same lithologies.

The kiln from "La Venta del Gallo" (Requejo Pagés, 2007a,b; Fig. 2) is located a few km north of Oviedo (43.4°N, 5.8°W; Cayés, Llanera council) and was discovered in 1999 during the archaeological reconnaissance of the roadwork between Oviedo and Gijón. It forms part of a Roman pottery complex, exclusively dedicated to the production of construction materials. Radiocarbon dating (Beta 141715) gives a temporal framework of 45 BC to 235 AD at the 95% confidence level (2σ) that it is reduced in age to 30–135 AD at the 68% confidence level (1σ).

Ten drilled samples were obtained from different clay-covered bricks belonging to the heating chamber of the kiln.

Samples were cored (2.54 cm in diameter) with a portable gasoline-powered drill and oriented using an inclinometer and a magnetic compass. Declination was later corrected, taking into account the IGRF declination value at each locality and sampling time. In the laboratory, cores were cut into standard specimens (2.2 cm length) for palaeomagnetic measurements. For most of the structures, samples yielded twin specimens. Core chips and pieces were used in rock-magnetic experiments.

3. Magnetic hysteresis and IRM acquisition curves

In order to characterize the magnetic minerals carrying the characteristic remanent magnetization (ChRM) related to the archaeomagnetic direction, magnetic hysteresis and IRM acquisition curves were measured in the Palaeomagnetism Laboratory of the Complutense University of Madrid, in 10 samples representative of all the studied structures and lithologies. Magnetic hysteresis was measured using a coercivity meter (Jasonov et al., 1998) with a maximum applied field of 500 mT. This instrument also generated stepwise acquisition and back-field acquisition of isothermal remanence (IRM). The results are summarized in Table 1 and show a strong dependence on lithology (bricks/baked clays, slates and quartzites).

Bricks and baked clays give the highest Mrs and Ms values and show a low paramagnetic contribution, which implies that their concentration of ferromagnetic minerals is higher than in the other cases. IRM acquisition curves are not completely saturated at 500 mT. The values of the coercivity of remanence (Hcr) lie between 58.3 and 89.5 mT (Fig. 3A). These values, associated with unsaturated IRM curves, can be considered typical of coexisting low and high coercivity magnetic phases (i.e. magnetite/maghemite and hematite) with a great contribution of the low coercivity phase. Hysteresis curves measured on the same samples give broad loops that are not completely saturated. A representative example is shown in Fig. 3B. Mrs/Ms' ratios (after paramagnetic contribution correction) are around 0.5 except for sample C22B.08 that gives a value of about 0.1.

Slate and quartzite samples produce different results whether considering the remanent or the induced curves. IRM curves are in general more noisy due to their lower intensities (~three orders of magnitude less than the bricks/baked clay). As before, the curves are not completely saturated and show differing contributions of high coercivity magnetic phases (such as hematite). Hcr values are also quite high in this case, varying up to 86.5 mT (Fig. 3C). The induced magnetization curves show an important contribution of paramagnetic phases, which dominate the hysteresis curves (e.g. Fig. 3D). After correcting for the paramagnetic contribution, Ms' has values that generally range between 10^{-3} and 10^{-5} A m^2/kg, markedly lower than in the bricks/baked clay. Clay minerals such as chlorite, typically contained in slates rocks, could be

Table 1
Representative hysteresis parameters of the different lithologies (S = quartzites and slates; B = bricks and baked clays)/structures sampled in this study, without and with (when a comma is added) correction for the paramagnetic contribution

Samples	Lithologies	Mrs (A m^2/kg)	Ms (A m^2/kg)	Ms' (A m^2/kg)	Hc (mT)	Hc′ (mT)	Hcr (mT)	Hcr/Hc′	Mrs/Ms'
C10B.08	S	3.7×10^{-5}	4.5×10^{-2}	2.4×10^{-3}	1.0	6.5	86.5	13.3	1.5×10^{-2}
C18B.02	S	4.4×10^{-5}	3.4×10^{-3}	4.2×10^{-4}	3.2	41.1	75.6	1.8	0.1
C4B.01	S	5.1×10^{-5}	4.7×10^{-2}	1.4×10^{-3}	1.4	13.1	74.1	5.7	1.0×10^{-3}
C18B.05	S	6.4×10^{-5}	4.9×10^{-2}	1.5×10^{-3}	1.9	23.0	45.2	2.0	1.3×10^{-3}
TFE.01	S	7.0×10^{-5}	3.8×10^{-2}	1.0×10^{-5}	2.1	4.3	44.6	10.5	7.0
T.02	S	7.2×10^{-5}	5.9×10^{-2}	1.4×10^{-3}	1.4	12.4	28.1	2.3	5.1×10^{-2}
C22B.08	B	2.6×10^{-3}	6.4×10^{-2}	3.4×10^{-2}	2.9	3.3	73.8	22.6	0.1
VG.00	B	7.1×10^{-2}	2.0×10^{-1}	1.5×10^{-1}	42.8	45.5	89.5	2.0	0.5
VG.07	B	8.4×10^{-2}	2.3×10^{-1}	1.7×10^{-1}	43.9	46.3	77.9	1.7	0.5
C15B.03	B	1.1×10^{-1}	2.8×10^{-1}	2.4×10^{-1}	31.3	31.4	58.3	1.9	0.5

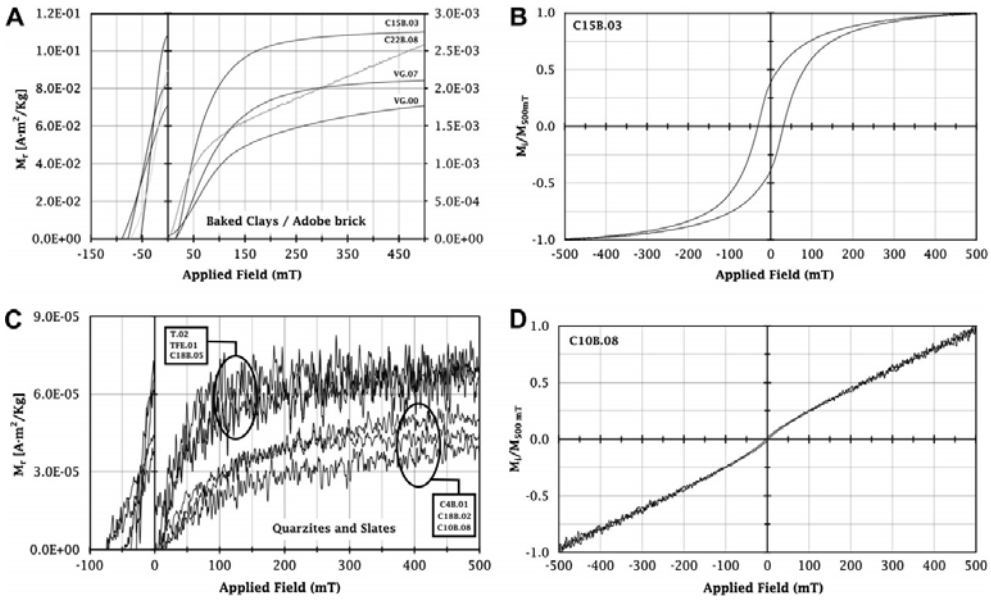

Fig. 3. Representative isothermal remanent magnetization and backfield curves (A,C) and hysteresis curves without paramagnetic correction (B,D) from baked clay-brick built (A,B) and stone built (C,D) structures.

responsible for the paramagnetic fraction observed in the hysteresis loops.

Summarizing, a low coercivity phase, such as magnetite/maghemite, with subordinate high coercivity phases such as hematite, seem to be the carriers of the magnetic signal in the case of the baked clays/adobe bricks. In contrast, slates and quartzites are dominated by a high coercivity phase (such as hematite), whilst the low coercivity fraction is less important. This explains the significantly lower values of Ms and Mrs.

4. NRM demagnetization procedures and behaviours

The NRM and its stability to stepwise thermal (Th) or alternating field (AF) demagnetization were measured using a JR5-A spinner magnetometer in the Palaeomagnetism Laboratory of the Complutense University of Madrid and 2G discrete sample Cryogenic magnetometers in the ''Investigation Support Centre" of Physics of the Complutense University, Madrid, and in the Palaeomagnetism Laboratory of Burgos University, Spain.

Thermal (Th)/alternating field (AF) demagnetization was carried out using TSD-1 Schonsted/2G Cryogenic magnetometers AF demagnetizers, respectively. The initial bulk magnetic susceptibility and its variation upon thermal treatment were measured on a Kappabridge (KLY-3) susceptibility meter instrument.

The initial NRM intensity and bulk magnetic susceptibility (χ) are shown in Fig. 4a. A wide range of NRM intensities (between 1.6×10^{-4} and 11.1 A m^{-1}) and χ (between

2.4×10^{-6} and 2.3×10^{-2} SI) is observed, depending both on the lithologies considered and how much they have been heated. The Koenigsberger value, Q_n (Stacey, 1967), which quantifies the ratio between the remanent and induced magnetization ($Q_n = \mathrm{NRM}/\chi H$, where $H = 39.8\ \mathrm{A\ m^{-1}}$ is the present, local geomagnetic field strength), is also shown. Q_n values depend on the lithologies and their degree of heating; they are generally consistent with an NRM that is a thermoremanent overprint, but they also point out those specimens not heated enough ($Q_n < 0.1$, Fig. 4a).

The one-piece built, rectangular fireplaces "C4B" and "C10B" were sampled along a profile with increasing distance from the hearth (i.e. heat source). This allowed the detection of a heating gradient. In both cases, Q_n decreased with distance from heat source (Fig. 4b), mainly due to the exponential decrease of NRM intensity. The χ values also show a similar trend (open symbols, Fig. 4a), which is interpreted in terms of magnetite production due to the gradual exposure to heat.

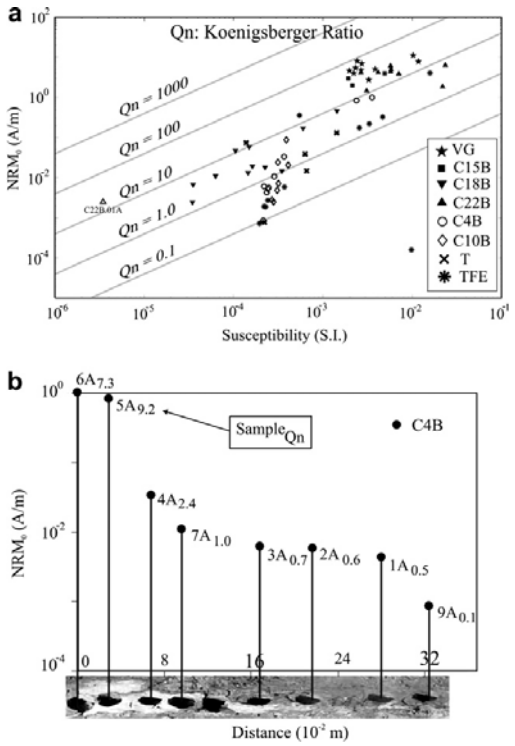

Fig. 4. (a) Initial NRM intensities vs. initial bulk magnetic susceptibility (χ) for all the studied specimens, together with Koenigsberger ratio (Q_n) isolines. Solid symbols: baked clays and bricks. Open symbols, crosses and asterisks: quartzites and slates. (b) Sampling detail (following the heating gradient) of the fireplace "C4B", and initial NRM intensities and Q_n values of its samples vs. distance. "C4B" and "C10B" specimens display a positive trend (increasing both NRM intensities and initial χ values), with increasing Q_n values as they are closer to the source of heat (a, open symbols).

Detailed thermal and AF demagnetization have been applied to twin pilot specimens from the same representative sample for each structure, allowing the choice of optimum demagnetization method for the remaining specimens from each structure (Fig. 5). The following 16 steps were used for thermal demagnetization of the pilot specimens: 40 °C steps from 80 up to 380 °C, 50 °C steps up to 580 °C, 600 °C and 640 °C. For pilot AF studies, around 20 steps were used, in intervals ranging from 3 mT to 20 mT, up to 170 mT.

Thermal demagnetization was chosen for all of the structures from the hill-fort "Chao Samartín". This was because of the evidence of partial thermoremanences in some of their structures, and with the ultimate aim of comparing the ChRMs (archaeomagnetic directions) in terms of their corresponding unblocking temperature spectra. Bulk magnetic susceptibility (χ) was monitored after each heating step to control possible thermally induced mineralogical changes. It remained practically constant in all structures/lithologies during thermal demagnetization (Fig. 6).

In contrast, brick specimens from "La Venta del Gallo" ("VG") exhibited only one magnetic component. Thermal demagnetization of the "B" specimen (less heated than the "A" specimen, from the part of the sample closer to the heat source) revealed a single component, with a maximum unblocking temperature spectra (T_{ub}) around 630 °C. AF demagnetization of the "A" specimen also yielded a single component, with the same ChRM direction as the "B" specimen. Therefore, AF demagnetization was chosen for routine demagnetization of the remaining specimens.

NRM demagnetization behaviour (Fig. 5) was interpreted using orthogonal projections onto horizontal and vertical planes and onto Lambert equal-area plots; and considering simultaneously the corresponding unblocking temperature (T_{ub})/coercivity spectra reflected in the absolute (and sum of difference vectors) intensity decay plots.

Archaeomagnetic directions (ChRMs) are revealed usually after removing a low T_{ub} viscous component. They are sometimes expressed as a single, stable component associated with a single magnetic phase or two phases with distinct T_{ub}'s. Occasionally, a high T_{ub}/high coercivity directional component is also present, and sometimes overlaps with the ChRM. This high T_{ub}/high coercivity has also been detected in the in situ native rock specimens of the same lithology that were sampled outside the hill-fort "Chao Samartín". These native rocks exhibit (after a viscous component due to the actual geomagnetic field that is removed around 100 °C) a geological, high coercivity magnetic remanence with a maximum T_{ub} of 660 °C. Its directions and maximum T_{ub} have no similarity at all with those corresponding to the archaeomagnetic remanences achieved in the same lithologies.

Specimens from "C4B", "C10B" and "C18B" structures reveal a ChRM generally isolated between 180 and 530 °C.

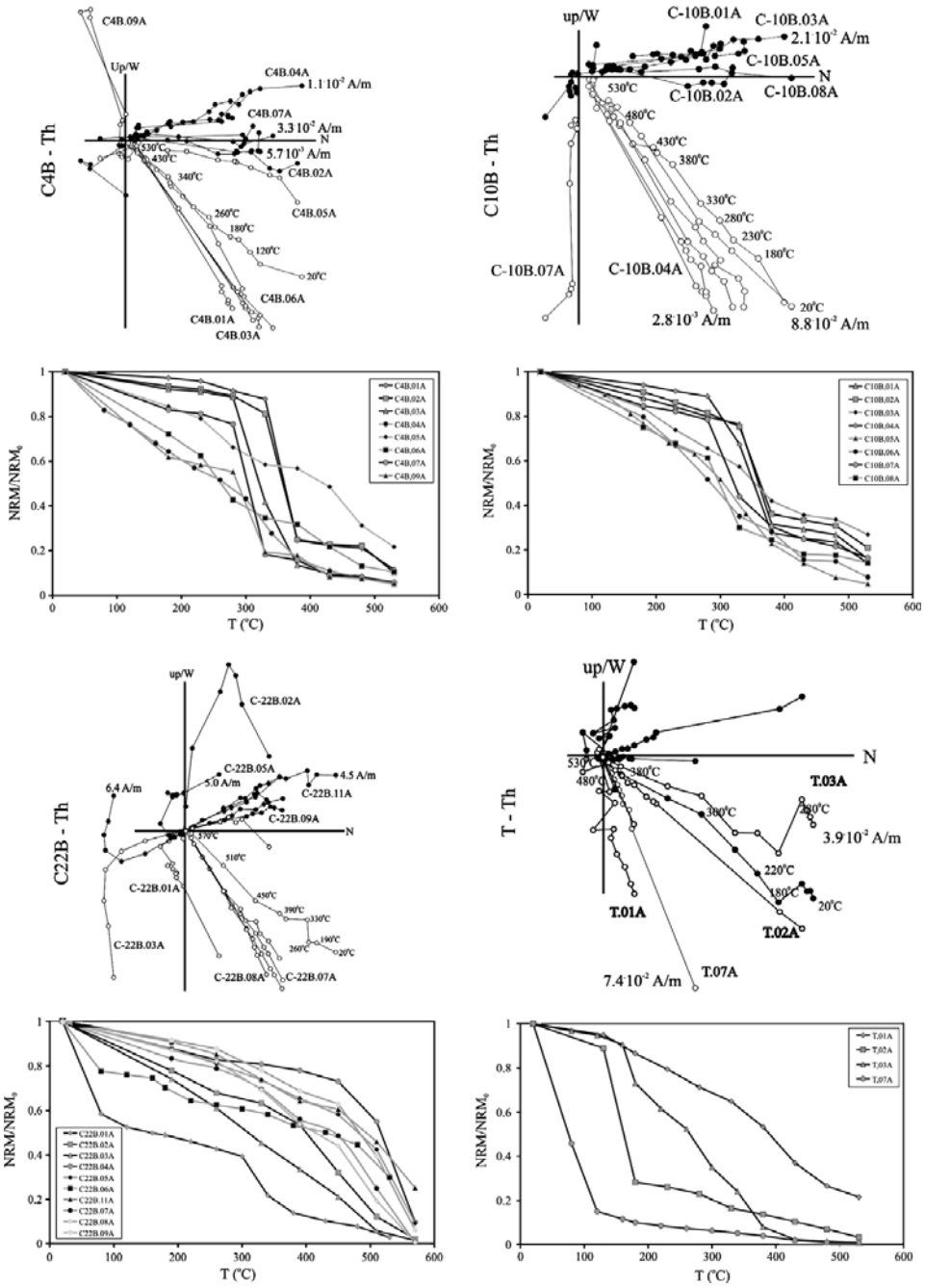

Fig. 5. Inset for each structure: (up) orthogonal projection of the remanence vector end point during demagnetization of its specimens (representative initial NRM intensities are also indicated, since axis scale is not equal for all of them); and (down) their respective intensity decay plots (normalized sum of difference vectors). Solid/open circles: projections onto the horizontal (W/N)/vertical (up/N) plane. Th/AF: thermal/alternating field demagnetization.

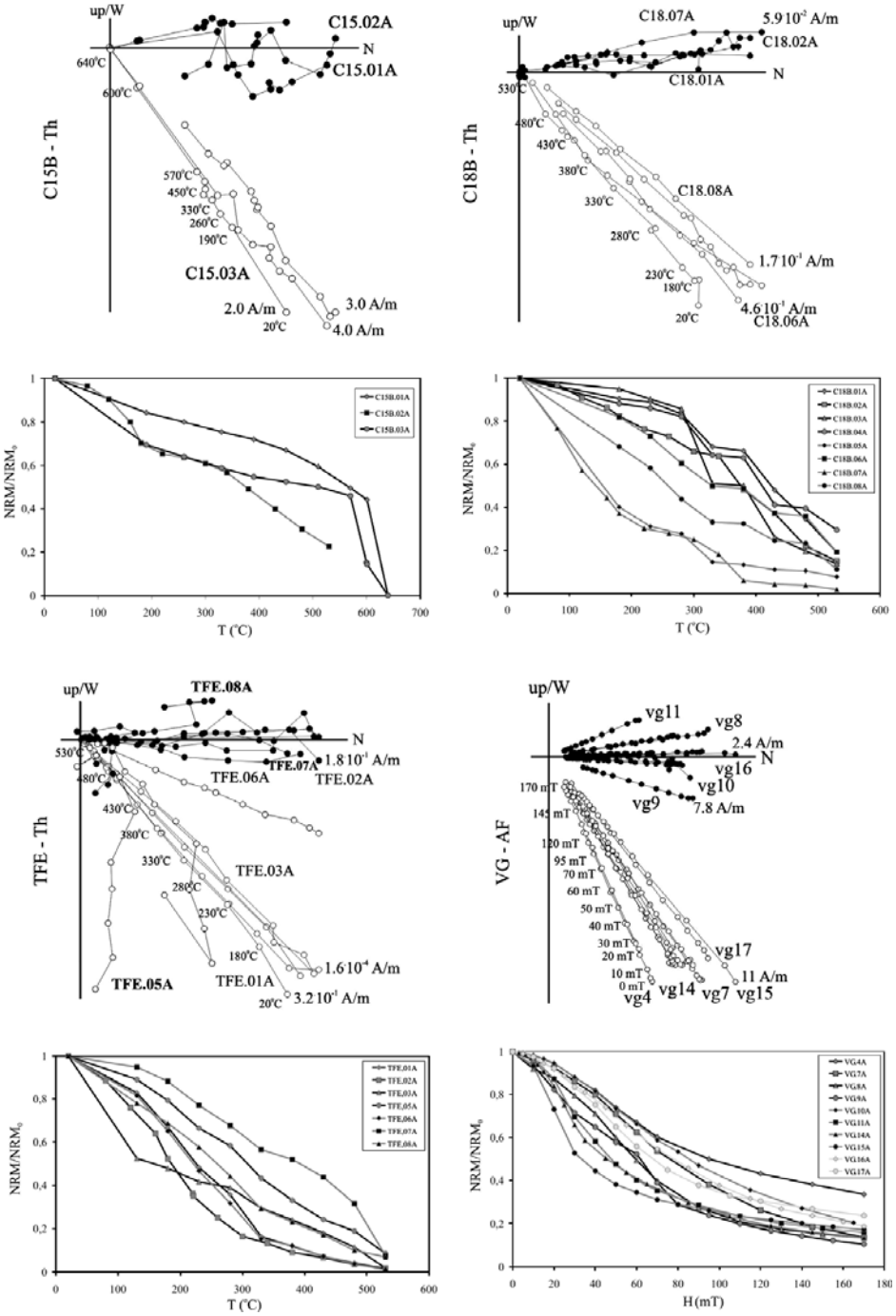

Fig. 5 (*continued*)

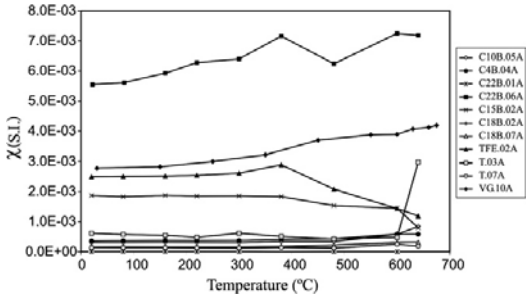

Fig. 6. Bulk magnetic susceptibility (χ) monitoring after each thermal demagnetization step, in specimens representative of all the sampled structures/lithologies.

A higher T_{ub} directional component is more visible in the less heated specimens. Specimens from the sauna "T" were not heated enough and thermal demagnetization reveals a ChRM highly overlapped with a higher T_{ub} directional component. This last behaviour was also observed in some specimens from "TFE", "C15B" and "C22B", whereas in their more heated ones, a ChRM could be isolated between 130–200 °C and 570–600 °C.

AF demagnetization (up to 170 mT) did not succeed in isolating any archaeomagnetic direction in specimens from "C4B", "C10B", "C18B" and "T", although it removed about 40–65% of their initial NRM intensities. This is interpreted as an overlapping during demagnetization of two different coercivity spectra components. On the contrary, AF demagnetization removed between 70% and 85% of the initial NRM of specimens from "TFE" and "C22B", and showed a single stable component with directional results similar to those obtained in thermally demagnetized twin specimens.

5. New archaeomagnetic directions from northern Iberia

Archaeomagnetic remanence directions were calculated using Principal Component Analysis (PCA, Kirchvink, 1980) in those specimens that displayed well-defined, linear trajectories. A minimum of five demagnetization steps were taken into account in the linear regression fits, without forcing the regression through the origin.

When archaeomagnetic remanence directions were overlapped with higher T_{ub} magnetic components, great circle analysis of remagnetization circles (RC) was used to calculate the site-mean direction (the common direction at which RC converge); on occasion in combination with PCA (McFadden and McElhinny, 1988).

A hierarchical approach (specimen, then independently oriented sample, then structure) has been followed in the calculations of all site-mean directions. For "C22B", 10 samples were drilled from six different bricks/stones. Here, each brick has been considered as an independent sample in order to prevent a bias due to post-cooling sample movement (or lithological control).

For each structure, the sample directions have been tested to see if their distributions are Fisherian (Fisher, 1953) in both declination and inclination. Deviation from a Fisher distribution has been interpreted in terms of undetected sampling orientation errors, or post-cooling movements, or to incomplete isolation of the archaeomagnetic directions (for example, due to insufficient heated samples). This provides an objective criterion for rejecting samples when computing the mean-site direction, by discarding that direction most distant from the mean and then repeating the test. It also permits the application of other statistical tests, performed in between site-mean directions, based on Fisher statistics (McFadden and Lowes, 1981; McFadden and McElhinny, 1990). Proceeding in this way, six samples in five structures ("C4B-5A", "C4B-9A", "C10B-7A", "C22B-2-3", "T-3" and "TFE-4", Fig. 5) have been rejected.

For each archaeological structure, the archaeomagnetic methodology, Fisherian site-mean ChRM directions and Fisher (1953) statistical parameters are summarized in Table 2. Site-mean archaeomagnetic directions are also projected onto Lambert equal-area projections together with their 95% cone of confidence (Fig. 7).

6. Comparison of the northern Iberia results with archaeological, radiocarbon, Spanish archaeomagnetic data and the "SVC-I

The archaeomagnetic site-mean directions of all of the archaeological structures from northern Iberia have been compared in order to test for a contemporaneously last cooling event.

For this, the McFadden and McElhinny (1990) test is applied to evaluate critically the hypothesis that two Fisherian distributions of individual directions share a common mean direction at a 95% confidence level (assuming that they share the same precision parameter k). The test works by evaluating both the angle between the two mean directions (γ_0) and the critical angle at which the hypothesis of common mean directions for the distribution would be rejected (γ_c). If $\gamma_0 > \gamma_c$, the test (negative) is that of McFadden and Lowes (1981) for discrimination of mean directions. In this case the null hypothesis of a common mean direction may be rejected at the 95% confidence level. If $\gamma_0 < \gamma_c$, the test (positive) is classified by McFadden and McElhinny (1990) in terms of the critical angle γ_c in descending order of quality ("Ra" if $\gamma_c \leqslant 5°$, "Rb" if $5° < \gamma_c \leqslant 10°$, "Rc" if $10° < \gamma_c \leqslant 20°$ and "indeterminate" if $\gamma_c > 20°$).

The statistical results are summarized in Table 3. Of 28 possible combinations, 13 led to positive "Rb" and 3 to positive "Rc" results, whereas 12 gave negative results. The structures "TFE", "T" and "C22B" do not share a common mean direction with the others.

When the two populations do not have a common precision parameter (see Table 3, where "T" and "TFE" display the maximum and minimum k values, respectively),

Table 2
Archaeomagnetic site-mean directions from Asturias, northern Iberia

Name	n/N	D_s	I_s	D_m	I_m	k	α_{95}	r	Treatment	ChRM	Site	Structure	Latitude (°N)	Longitude (°E)	Sample
C4B	8/6	354.4	52.1	355.3	48.7	73.8	7.9	5.932	Th, H	PCA	CS	Fireplace	43.20	−6.93	Drill
C10B	8/7	357.9	52.5	358.6	49.4	95.0	6.2	6.937	Th, H	PCA	CS	Fireplace	43.20	−6.93	Drill
C15B	3/3	1.3	54.0	1.8	51.1	500.0	6.4	2.997	Th, H	GCA + PCA(2)	CS	Fireplace	43.20	−6.93	Drill
C18B	8/8	351.1	47.0	352.3	43.1	89.5	5.9	7.922	Th, H	PCA	CS	Kiln	43.20	−6.93	Drill
C22B	6/(10/8)/5	345.0	55.3	346.0	51.9	272.7	5.1	4.989	Th, H	GCA + PCA(3)	CS	Fireplace	43.20	−6.93	Drill
T	5/4	357.8	61.0	358.0	58.5	1000.0	6.0	3.999	Th, H	GCA	CS	Sauna	43.20	−6.93	Drill
TFE	8/7	358.7	43.0	359.8	39.2	54.1	8.3	6.889	Th, H	PCA	CS	Sauna	43.20	−6.93	Drill
VG	10/10	358.0	57.4	358.3	54.5	128.9	4.3	9.930	AF, H	PCA	VG	Kiln	43.37	−5.83	Drill

Columns from left to right: Name, name of the structure; n/N, number of independently oriented samples taken from the site/samples taken into account in the calculation of the Fisherian site-mean ChRM direction (central bracket: specimens analysed/taken into account in the hierarchical calculation of the mean sample directions); D_s, I_s/D_m, I_m, declination and inclination in situ/reduced to Madrid; k, α_{95}, and r, precision parameter, 95% cone of confidence and length of the resultant vector for Fisher statistics (Fisher, 1953); Treatment, laboratory treatment (*AF*/*Th*: alternating field/thermal demagnetization, *H*: hysteresis and IRM measurements); ChRM, determination of ChRM (GCA: great circle analysis, PCA: principal component analysis – with number of samples when mixed with GCA); Site, site name (CS: Chao Samartín, *VG*: Venta del Gallo); Structure, kind of structure; Latitude/Longitude, site latitude/longitude; Sample, type of samples (drill: drilled samples).

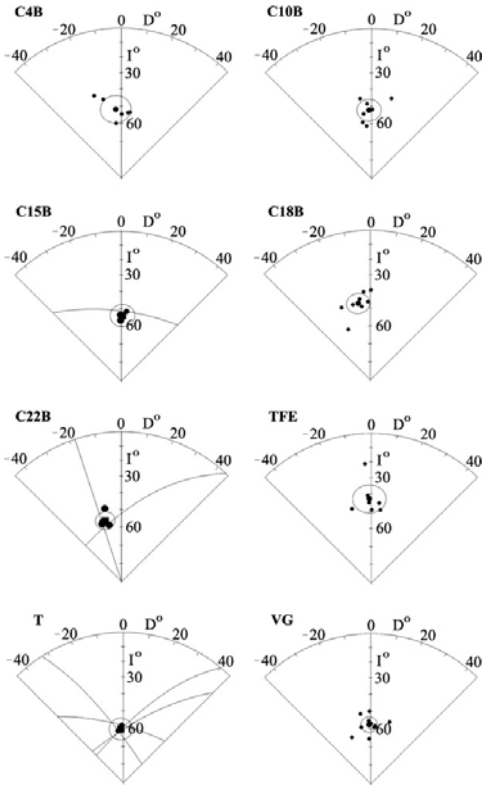

Fig. 7. Lambert equal-area projections of the Fisherian site-mean ChRM directions and the corresponding 95% cone of confidence (Fisher, 1953) for each structure. Linear directions (calculated by PCA; Kirchvink, 1980) and the great circle demagnetization paths with their final directional solutions (calculated by great circle analysis, sometimes combined with PCA; McFadden and McElhinny, 1988) of the individual samples are also shown.

the statistical test results must be considered approximate (even inadequate) and the decision should be deferred when the significance is marginal. Another possible explanation for these results is that the ChRMs of these structures consist of a mixture of partial thermoremanences (in "TFE" and "T" structures) with different archaeomagnetic directions. Alternatively, the archaeomagnetic direction corresponds to a different age to those from the rest of the structures (as archaeological considerations suggest in "C22B").

The McFadden and McElhinny (1990) test has also been applied to the best archaeomagnetic result obtained in this study (corresponding to "VG" structure) and the individual archaeomagnetic directions from the Spanish archaeomagnetic catalogue (Gómez-Paccard et al., 2006a) that could overlap in age with the "VG" age. "VG" was chosen because of its single, stable component, its low α_{95} (4.3°, the lowest of all of the structures), and because of its independent radiocarbon dating. "VG" site-mean direction was tested sequentially against the Spanish catalogue directions between 100 BC and 405 AD (entries 1 to 25 of the Spanish catalogue) and between 1025 and 1050 AD (entries 26 and 27) (Gómez-Paccard et al., 2006a). The tests are positive ($\gamma_0 < \gamma_c$), with "Ra" and "Rb" classifications, only when comparing "VG" direction with those of the Spanish catalogue ranging in mean age from 8 BC to 405 AD. These results give γc values ranging from 3.5° to 8.9°, without any grouping of the better quality ("Ra") results in any specific century. Tests were applied after reducing the directions to the same reference location, Madrid (the reference location for the "SVC-I", 40.4°N, 3.7°W), via the virtual geomagnetic pole (Noël and Batt, 1990), where a dipole field model is assumed over "small" regions. As was to be expected, performing the tests sequentially on the data without reducing to Madrid gives rise to both positive and negative results, which show no particular systematic behaviour.

Table 3
Tests of a common site-mean direction in Fisherian distributions (assuming they share the same precision parameter k), at the 95% confidence level, between the studied structures: γ_0 = angle between the two site-mean directions, γ_c = critical angle at which the hypothesis of common mean directions for the distribution would be rejected

	C22B	C4B	C10B	C 15B	C18B	T	TFE	VG
C22B		Rb	NEGATIVE	NEGATIVE	NEGATIVE	NEGATIVE	NEGATIVE	NEGATIVE
C4B	γo=6.4 < γc=8.7		Rb	Rc	Rb	Rb	Rc	Rb
C10B	*γo=8.1 > γc=7.7*	γo=2.2 < γc=9.2		Rb	Rb	NEGATIVE	Rb	Rb
C15B	*γo=9.5 > γc=5.6*	γo=4.6 < γc=11.2	γo=2.5 < γc=9.7		Rb	NEGATIVE	Rc	Rb
C18B	*γo=9.1 > γc=7.7*	γo=5.5 < γc=9.0	γo=7.0 < γc=8.1	γo=9.5 < γc=9.8		NEGATIVE	Rb	NEGATIVE
T	*γo=8.8 > γc=4.4*	γo=9.1 < γc=9.3	*γo=8.5 > γc=8.1*	*γo=7.2 > γc=3.5*	*γo=14.5 > γc=8.3*		NEGATIVE	Rb
TFE	*γo=15.2 > γc=9.8*	γo=9.5 < γc=10.8	γo=9.5 < γc=9.7	γo=11.1 < γc=12.8	γo=6.7 < γc=9.4	*γo=18.0 > γc=10.7*		NEGATIVE
VG	*γo=7.5 > γc=6.4*	γo=5.7 < γc=7.6	γo=4.9 < γc=6.9	γo=3.9 < γc=8.1	*γo=11.2 > γc=6.7*	γo=3.6 < γc=6.8	*γo=14.4 > γc=8.0*	

If $\gamma_0 > \gamma_c$ (results in italics), the test (McFadden and Lowes, 1981) is negative (the null hypothesis of a common mean direction may be rejected). If $\gamma_0 < \gamma_c$, the test (McFadden and McElhinny, 1990) is positive "Ra" ($\gamma_c \leqslant 5°$), "Rb" ($5° < \gamma_c \leqslant 10°$) or "Rc" ($10° < \gamma_c \leqslant 20°$).

As a reliability test for the ChRM determinations obtained in this study, they are compared with the available archaeological information, radiocarbon data and the archaeomagnetic dating. The Secular Variation Curve for the Iberian Peninsula ("SVC-I", Gómez-Paccard et al., 2006b) has been employed for the latter. To construct the curve "SVC-I", French and Moroccan archaeomagnetic directions obtained from sites less than 900 km from Madrid are also included, together with the sites from the Spanish archaeomagnetic data catalogue (Gómez-Paccard et al., 2006a).

In order to date the northern Iberia structures (this study) using the reference "SVC-I", the archaeomagnetic ChRM directions must first be reduced to Madrid, the reference location for "SVC-I". This has been done (Dm, Im, in Table 2) via the virtual geomagnetic pole (Noël and Batt, 1990). The maximum error due to relocating virtual geomagnetic poles from any point inside a reference area of 900 km distant from Madrid (≈3°) is considered included in the error inherent to the archaeomagnetic data, because it is lower than the uncertainties (≈5°) in declination and inclination obtained for the Bayesian reference "SVC-I"

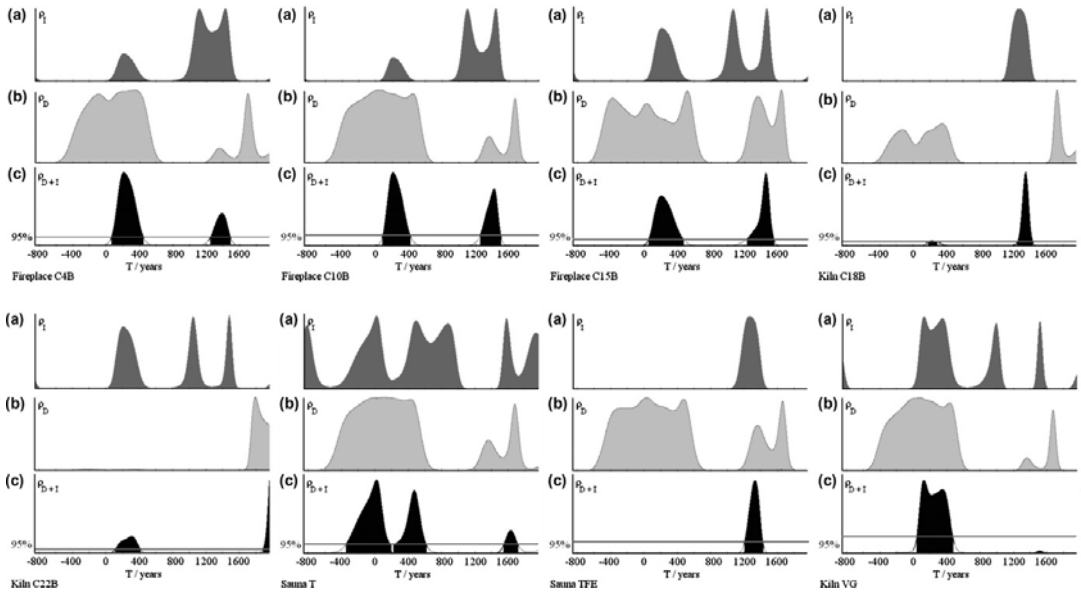

Fig. 8. Archaeomagnetic dating, at the 95% confidence level, of the site-mean ChRM directions obtained from northern Iberian structures (this study), using the reference "SVC-I" (Gómez-Paccard et al., 2006b) and the "RENDATE" program (available on http://www.meteo.be/CPG/aarch.net/index.html; Lanos, 2004, Lanos et al., 2005). From top to bottom (in each structure), probability density functions (PDFs) for (a) declination, (b) inclination and (c) combined declination and inclination (black coloured), are also shown.

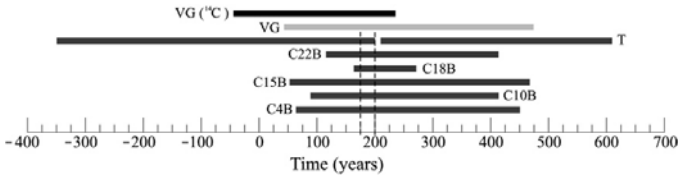

Fig. 9. Archaeomagnetic dating summary (time intervals at which cumulative PDFs are significant at the 95% confidence level, see Fig. 8) vs. archaeological constraints (age between the two vertical lines for the structures from Chao Samartín, and radiocarbon age for the kiln from Venta del Gallo).

(Gómez-Paccard et al., 2006b). A hierarchical Bayesian statistical method has also been adopted to calculate the archaeomagnetic date (Lanos, 2004), using the RENDATE software of Lanos et al. (2005). Probability density functions (PDFs) for each structure are generated for both the declination and inclination values, which are then combined to give the cumulative PDF (Fig. 8).

The overall PDF of most structures from the hill-fort "Chao Samartín" exhibit two peaks at the 95% confidence level, but archaeological considerations allow us to discard the youngest one (between the 13th and 20th centuries). In contrast, the older peak agrees with the archaeological dating (third quarter of the 2nd century AD). An exception is structure "TFE", which only exhibits the younger PDF peak (between the 13th and 20th centuries AD). The inclination value of "TFE" does not match with second Iron Age or any Roman period age inclinations (as declination do). Although no remanence anisotropy experiments have been carried out, we suggest this as an anisotropy of remanence effect. The stone bricks of the sauna wall are strongly foliated on a millimetric scale, with the foliation planes parallel to the floor, which may give rise to an inclination shallowing effect.

The time intervals at which the older overall PDFs from the rest of the hill-fort "Chao Samartín" structures are significant at the 95% probability level are (see Figs. 8 and 9): [63–450 AD] ("C4B"); [88–413 AD] ("C10B"); [53–468 AD] ("C15B"); [181–289 AD] ("C18"); [116–414 AD] ("C22B"); [350 BC – 200 AD] and [210–610 AD] ("T").

In the kiln from "Venta del Gallo" it is possible to compare, at the same confidence level (95%), the archaeomagnetic dating [43–474 AD] (see Fig. 9) and the radiocarbon dating [45 BC to 235 AD] results. Both intervals overlap, reducing the uncertainty estimation of its age ([43–235 AD]), which agrees with the PDF maximum of the archaeomagnetic dating, located at the beginning of the 2nd century AD.

Probably due to the present errors associated with both the reference "SVC-I" and this technique, the archaeomagnetic dating of "T" and "C22B" structures (Fig. 9) is not statistically different to those from most of the rest of the structures (excluding "TFE"), when Fisherian tests of a common site-mean direction are applied (Table 3).

There is a good agreement between the results of archaeomagnetic dating and radiocarbon dating, both of which are consistent with archaeological constraints. The uncertainties in the archaeomagnetic ages are relative large especially because the reference curve hardly varies in declination between 0 and 500 AD.

This highlights the need of more high quality archaeomagnetic data (from very well-dated structures) in order to reduce the errors associated with the reference "SVC-I" and the archaeomagnetic dating technique, particularly during Roman times. During this time, the directional changes of the geomagnetic field are only due to an inclination swinging, as declination hardly varies (Gómez-Paccard et al., 2006b).

7. Conclusions

Eight different structures have been analyzed in two different archaeological locations from Asturias, northern Spain. Except for two sites ("TFE" and "C22B"), their ages are calculated by archaeological estimations and radiocarbon data between the 1st and 2nd centuries AD.

Rock magnetic experiments and unblocking temperature spectra inspections reveal in the baked clay/brick samples a low coercivity and moderate T_{ub} phase, such as magnetite/maghemite, that seem to be the carriers of the archaeomagnetic signal. In the stone built structures a high coercivity/high T_{ub} phase (which is also seen in samples of the same lithology not used in construction of the archaeological structures), sometimes overlaps with the archaeomagnetic signal. The direction of the thermal gradients in fireplaces has been detected, suggesting (partial) thermoremanences as the origin of remanent magnetization, which is consistent with Q_n values. Detailed, full demagnetization of the archaeomagnetic remanences led to site-mean Fisherian directions that have been calculated following the hierarchical approach. These new data improve on the distribution of sites used to construct "SVC-I" by contributing new archaeomagnetic sites from northern Spain, an area currently not represented.

Archaeomagnetic results have been compared, applying Fisherian distribution tests, among themselves and with Roman age entries of the Spanish archaeomagnetic database. They have also been compared with the reference "SVC-I" using Bayesian methods. This has served to validate the archaeological dating of the structures, with the

exception of one of the stone-built sauna walls (“TFE”), possibly because of its highly foliated lithology.

The archaeomagnetic dating precision during Roman times is problematic because of the geomagnetic field behaviour in these times, where the segment of “SVC-I” related with the 1st and 2nd centuries AD overlaps with that one corresponding to the 3rd, 4th and 5th centuries (Gómez-Paccard et al., 2006b). More high quality archaeomagnetic data (from very well-dated structures) are needed in order to reduce the errors associated with the reference “SVC-I” and the archaeomagnetic dating technique, particularly between 0 and 500 AD.

Acknowledgements

The authors are especially grateful to Ángel Villa Valdés, archaeologist responsible for the hill-fort “Chao Samartín” and director of the “Navia Basin Archaeological Plan” (Historical and Cultural Patrimony Service, Council of Culture of the Asturias Principality) and to Otilia Requejo Pagés (Archaeological Department, S.L.), archaeologist responsible for the Roman kiln from “La Venta del Gallo”, without whose advising and facilities this work could not have been carried out. They appreciate very much the help during fieldwork at the hill-fort “Chao Samartín” of archaeologist Rubén Montes López, and his detailed archaeological explanations of the sampled structures, which have been included in the corresponding archaeological setting. They also acknowledge Gregg McIntosh for helpful discussions concerning the contents of the manuscript. This study has been developed in the framework of the European Network AARCH “Archaeomagnetic Applications for the Rescue of Cultural Heritage” (HPRN-CT-2002-00219) and the Spanish “MCyT” Project CGL2005-00211/BTE.

References

Fisher, R.A., 1953. Dispersion on a sphere. Proc. Roy. Soc. London A 271, 295–305.

Gómez-Paccard, M., Catanzariti, G., Ruiz-Martínez, V.C., McIntosh, G., Núñez, J.I., Osete, M.L., Lanos, Ph., Chauvin, A., Tarling, D.H., Bernal-Casasola, D., Thiriot, J.Archaeological Working Group, 2006a. A catalogue of Spanish archaeomagnetic data. Geophys. J. Int. 166, 1125–1143.

Gómez-Paccard, M., Chauvin, A., Lanos, Ph., McIntosh, G., Osete, M.L., Catanzariti, G., Ruiz-Martínez, V.C., Núñez, J.I., 2006b. First archaeomagnetic secular variation curve for the Iberian Peninsula: comparison with other data from western Europe and with global geomagnetic field models. Geochem. Geophys. Geosyst. 7, Q12001. doi:10.1029/2006GC001476.

Jasonov, P.G., Nurgaliev, D.K., Burov, D.V., Heller, F., 1998. A modernized coercivity spectrometer. Geol. Carpathica 49 (3), 224–225.

Kirchvink, J.L., 1980. The least-square line and plane and the analysis of palaeomagnetic data. Geophys. J. Roy. Astron. Soc. 62, 699–718.

Lanos, Ph., 2004. Bayesian inference of calibration curves, application to archaeomagnetism. In: Buck, C., Millard, A. (Eds.), . In: Tools for Constructing Chronologies, Crossing Disciplinary Boundaries, Series: Lecture Notes in Statistics, vol. 177. Springer-Verlag, London, pp. 43–82 (Chapter 3).

Lanos, P., Le Goff, M., Kovacheva, M., Schnepp, E., 2005. Hierarchical modelling of archaeomagnetic data and curve estimation by moving average technique. Geophys. J. Int. 160, 440–476.

McFadden, P.L., Lowes, F.J., 1981. The discrimination of mean directions drawn from Fisher distributions. Geophys. J. Roy. Astron. Soc. 67, 19–33.

McFadden, P.L., McElhinny, M.W., 1988. The combined analysis of remagnetization circles and direct observations in palaeomagnetism. Earth Planet. Sci. Lett. 87, 161–172.

McFadden, P.L., McElhinny, M.W., 1990. Classification of the reversal test in palaeomagnetism. Geophys. J. Int. 103, 725–729.

Noël, M., Batt, C.M., 1990. A method for correcting geographically separated remanence directions for the purpose of archaeomagnetic dating. Geophys. J. Int. 102, 753–756.

Requejo Pagés, O., 2007a. Noticia sobre el descubrimiento de los Hornos Romanos de la Venta del Gallo (Cayés, LLanera, Principado de Asturias). In: Excavaciones Arqueológicas en Asturias, 5, 1999–2002. Consejería de Educación, Cultura y Deportes del Principado de Asturias, Oviedo.

Requejo Pagés, O., 2007b. Hallazgos romanos en la zona central de Asturias: necrópolis de Paredes y hornos de Cayés (Llanera). In: Ciclo de Conferencias sobre Prehistoria tardía y romanización: Astures y Romanos, Real Instituto de Estudios Asturianos. Oviedo.

Stacey, F.D., 1967. The Koenigsberger ratio and the nature of thermoremanence in igneous rocks. Earth Planet. Sci. Lett. 2, 67–68.

Villa Valdés, A., 2005. El Castro Chao Samartín (Grandas de Salime, Asturias). Guía para su interpretación y visita, Grandas de Salime. Ediciones de la Conserjería de Cultura, Principado de Asturias, 136 pp.

Villa Valdés, A., Cabo Pérez, L., 2003. Depósito funerario y recinto fortificado de la Edad del Bronce en el castro del Chao Samartín: argumentos para su datación. Trabajos de Prehistoria 60 (2), 143–151.

4.2 Base europea de datos arqueomagnéticos.

La base de datos arqueomagnéticos de Europa tiene un antes y un después entorno al año 2000 gracias al proyecto europeo AARCH (*Archaeomagnetic Applications for the Rescue of Cultural Heritage*, HPRN-CT-2002-00219). En dicho proyecto participaba una red de 12 laboratorios de Paleomagnetismo y Arqueomagnetismo repartidos por toda Europa, incluyendo el grupo de Paleomagnetismo de la Universidad Complutense de Madrid. Promover el arqueomagnetismo en Europa era el principal objetivo del proyecto y éste se ha cumplido, pues en los años de ejecución del mismo, el número de estudios arqueomagnéticos creció enormemente en países con escasa tradición arqueomagnética. Como consecuencia la antigua base de datos europea se enriqueció con nuevos datos arqueomagnéticos provenientes de un gran número de países europeos. Así pues, estamos actualmente en las mejores condiciones para usar estos datos arqueomagnéticos y analizar el comportamiento del campo geomagnético en Europa en los últimos milenios, objetivo principal de este trabajo.

En los últimos diez años se han realizado numerosos esfuerzos en la generación de bases de datos arqueomagnéticos. Cada país o región ha ido agrupando y dejando a disposición de los interesados sus datos arqueomagnéticos mediante numerosas publicaciones. En este sentido podemos destacar las bases de datos arqueomagnéticos de Iberia (Gómez-Paccard et al., 2006a), de Alemania (Schnepp et al., 2003, 2004; Schnepp y Lanos, 2005), Reino Unido (Zananiri et al., 2007 y referencias interiores), Francia (Bucur, 1994; Gallet et al., 2002), Hungría (Marton, 2003, 2009; y Marton et al., 2006), Italia (Tema et al., 2006), Grecia (Evans, 2006, De Marco et al., 2008a, 2008b) y la reciente actualización de la base de datos búlgara (Kovacheva et al., 2009). Estas bases de datos están en continuo crecimiento y cada cierto tiempo se incluyen nuevos datos arqueomagnéticos.

Para facilitar a la comunidad científica el acceso a los datos arqueomagnéticos se han publicado también numerosas bases de datos globales donde mediante criterios de selección geográfica y/o temporal se puedan extraer los datos de interés. En este sentido tenemos que agradecer el esfuerzo de Korte et al. (2005), Genevey et al. (2008) y Donadini et al. (2009); que en los últimos años han compilado todos los datos arqueomagnéticos disponibles.

La actual base europea de datos arqueomagnéticos (Donadini et al., 2009) está caracterizada por un alto número de datos direccionales en comparación con los datos de intensidad. La figura 4.2 muestra la distribución espacio – temporal de datos arqueomagnéticos en la zona europea para los últimos 2000 años (período temporal con mayor densidad de datos). En los próximos dos capítulos (Capítulos 5 y 6) se analizará en profundidad las características de los datos

arqueomagnéticos de los últimos 2000 y 3000 años, respectivamente. En el Capítulo 7 se analizan los datos arqueomagnéticos más antiguos, los que tienen edades comprendidas entre el año 6000 a.C. y el 1000 a.C.

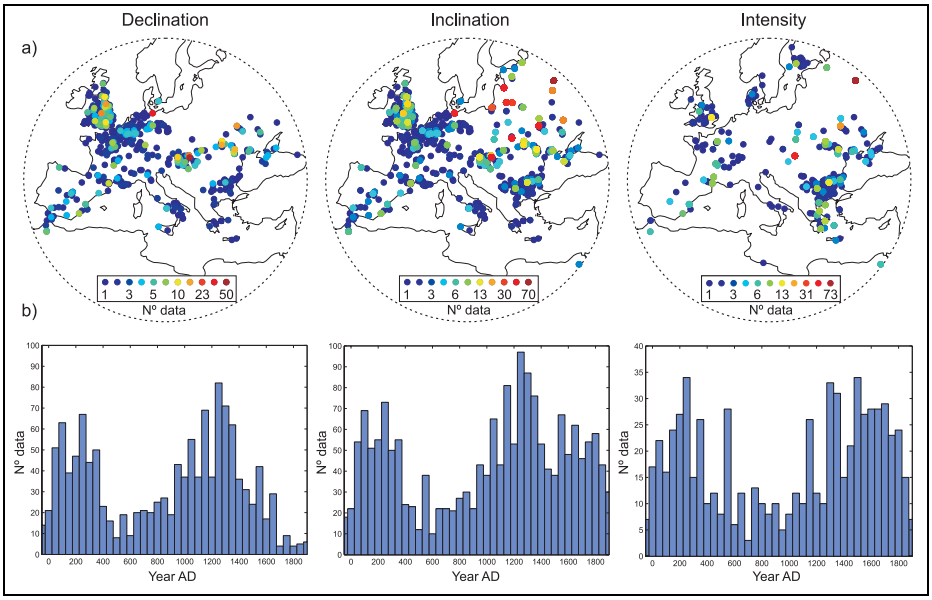

Figura 4.2. Distribución espacio – temporal de datos arqueomagnéticos en Europa y áreas vecinas. a) Distribución espacial de la declinación (izquierda), inclinación (centro) e intensidad (derecha). La escala de colores denota el número de datos localizados en las mismas coordenadas geográficas. b) Histogramas mostrando la distribución temporal de los datos arqueomagnéticos. Los datos han sido extraídos de la base de datos de Donadini et al. (2009) para el período comprendido entre el año 0 y el año 1900 d.D.

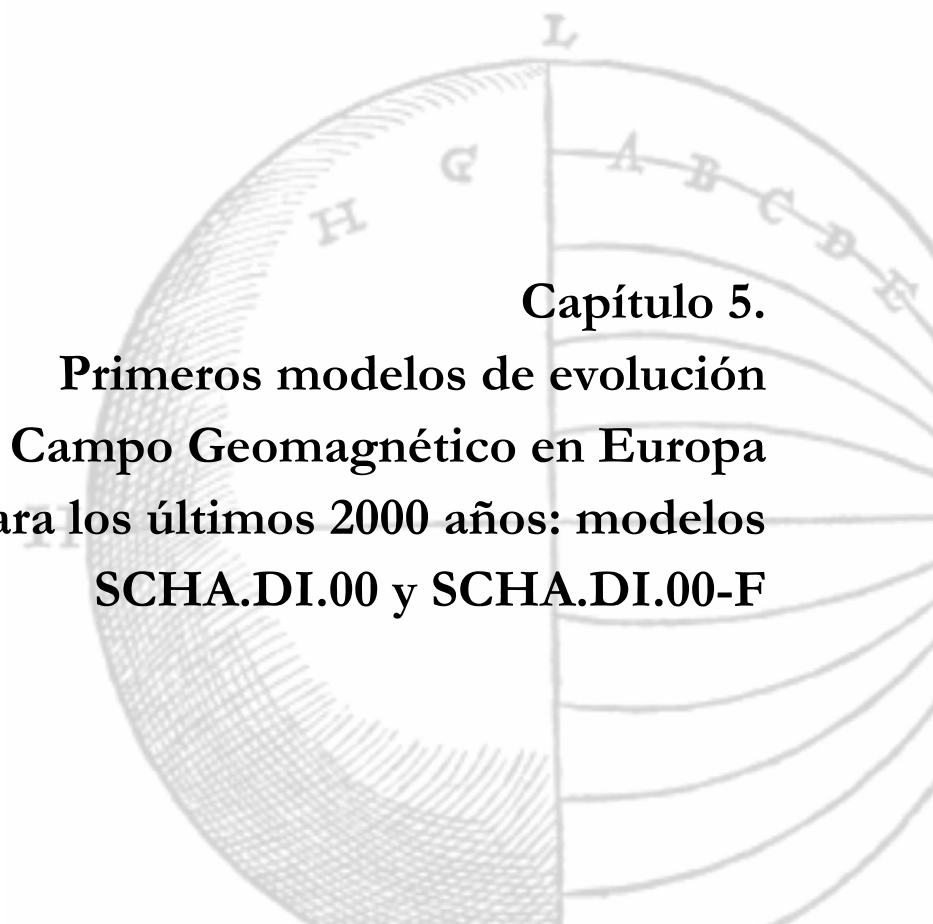

Capítulo 5.
Primeros modelos de evolución del Campo Geomagnético en Europa para los últimos 2000 años: modelos SCHA.DI.00 y SCHA.DI.00-F

El período de mayor densidad de datos arqueomagnéticos en la región europea y áreas adyacentes es el de los últimos 2000 años. Nuestra pregunta a la posibilidad de modelar el campo geomagnético a escala regional en este período de tiempo tiene respuesta en este capítulo. El contenido del mismo está dividido en dos secciones. En una primera parte se presenta el primer modelo direccional regional en el continente Europeo válido para los últimos 2000 años: el **modelo SCHA.DI.00**, y en la segunda sección veremos como dicho modelo direccional se completa con la adición de la intensidad arqueomagnética: el modelo **SCHA.DI.00-F**.

El modelo direccional **SCHA.DI.00** es el primer intento de aplicar la técnica clásica SCHA a los datos arqueomagnéticos. Hasta entonces la técnica clásica SCHA sólo había sido aplicada a datos geomagnéticos instrumentales, generando modelos regionales de campo para las últimas decenas de años (ver Torta et al., 2006 y referencias interiores). Por tanto, al no disponer de información previa que mostrara una aplicación satisfactoria de la técnica SCHA a los datos paleomagnéticos, hemos tenido que desarrollar una serie de estrategias para ir abordando el problema a diferentes niveles. El modelo **SCHA.DI.00** es el resultado obtenido una vez alcanzado el primer nivel. En este primer paso no se han usado los datos arqueomagnéticos tal y como son proporcionados en las bases de datos, sino que hemos acudido a las curvas de variación paleosecular. Curvas que describen de forma continua y suave las variaciones del campo geomagnético, como de si un observatorio geomagnético actual se tratara, y que permiten eliminar la incoherencia característica existente entre los datos arqueomagnéticos para un mismo intervalo de tiempo y región geográfica. Pero cuando se abordó este problema no existían curvas de variación paleosecular para la intensidad, por ello modificamos la técnica clásica SCHA para usar solo datos direccionales de declinación e inclinación (ver Anexo I para más detalle).

Posteriormente, avanzamos en nuestro estudio de modelización incluyendo la intensidad arqueomagnética al modelo anterior, generando el modelo completo regional **SCHA.DI.00-F**. Para ello aplicamos el teorema de Hulot et al., (1997) al modelo direccional previo. Dicho teorema indica que un factor escalar permite pasar de un modelo direccional a un modelo completo de campo geomagnético y dicho factor no es más que el primer coeficiente SCH del desarrollo del potencial geomagnético.

Ambos modelos **SCHA.DI.00** y **SCHA.DI.00-F** están disponibles en la dirección web: http://pc213fis.fis.ucm.es/scha_model.html.

5.1 Curvas de variación secular y el primer modelo geomagnético direccional SCHA.DI.00 para los últimos 2000 años en Europa.

Resumen.

Las Curvas de Variación Paleosecular (PSVCs) generadas mediante la estadística bayesiana y basadas en datos arqueomagnéticos han sido usadas para obtener el primer modelo regional de campo geomagnético de los últimos 2000 años en Europa. La técnica de modelización usada ha sido la del análisis armónico en un casquete esférico (método clásico SCHA). El modelo obtenido, llamado SCHA.DI.00, es solo direccional (declinación e inclinación) por lo que no puede dar información sobre la intensidad del campo geomagnético. Para eliminar la necesidad de información en intensidad se han normalizado los coeficientes que definen la expresión del potencial geomagnético interno respecto del primer coeficiente g_0^0. La expansión en armónicos de un casquete esférico se extiende hasta grado $K_{int} = 2$, que teniendo en cuenta el tamaño del casquete elegido y la distribución espacial de los datos arqueomagnéticos, equivalen en términos de longitud de onda, a un orden 5 en el desarrollo global en armónicos esféricos (SHA). El modelo SCHA.DI.00 se ajusta en buena medida a la presente base de datos arqueomagnética de Europa mejor que los modelos globales. Aunque debemos considerar que ambos modelos, regional y global, no han usado la misma base de datos. También hemos comparado las curvas de variación paleosecular generadas por el modelo SCHA.DI.00 con datos paleomagnéticos de Bulgaria (Sofía), Italia (Etna) y Austria (Radstadt), no usados en el desarrollo del modelo. El modelo SCHA.DI.00 también se ajusta mejor a estos datos que el modelo global CALS7K.2 (Korte y Constable, 2005). Es especialmente relevante el caso de los datos italianos.

Available online at www.sciencedirect.com
ScienceDirect
Physics and Chemistry of the Earth 33 (2008) 596–608
PHYSICS and CHEMISTRY of the EARTH
www.elsevier.com/locate/pce

Initial SCHA.DI.00 regional archaeomagnetic model for Europe for the last 2000 years

Fco. Javier Pavón-Carrasco [a,*], Maria Luisa Osete [a], J. Miquel Torta [b], Luis R. Gaya-Piqué [c], Ph. Lanos [d,1]

[a] Dpto de Geofísica y Meteorología, Universidad Complutense de Madrid, 28040 Madrid, Spain
[b] Observatori de l'Ebre, CSIC – Universitat Ramon Llull, Horta Alta 38, 43520 Roquetes, Spain
[c] Equipe de Géomagnétisme, Institut de Physique du Globe de Paris, CNRS; Tour 14, 2 place Jussieu, 75005 Paris, France
[d] Centre de Recherche en Physique Appliquée à l'Archéologie, CNRS, UMR5060-IRAMAT and UMR 6118, Géosciences-Rennes, France

Available online 19 February 2008

Abstract

The available Bayesian European Palaeosecular Variation Curves (PSVC) based on archaeomagnetic data have been used to derive an initial regional model for the geomagnetic field in Europe for the last 2000 years by using the Spherical Cap Harmonic Analysis (SCHA) technique. The resulting SCHA.DI.00 model provides the directional behaviour of the Earth's magnetic field, but no information about intensity is supplied because input data are only directional. The first spherical cap harmonic coefficient, g_0^0, has been used to normalise the rest of the coefficients. The spherical expansion extends up to $K_{\text{int}} = 2$ which, given the size of the spherical cap used and the maximum data resolution, is equivalent, in terms of spatial wavelength, to a maximum degree of approximately 5 in the ordinary Spherical Harmonic Analysis (SHA). The SCHA.DI.00 model fits the present archaeomagnetic database for Europe more accurately than global models, although it is necessary to consider that regional SCHA model and global models did not use the same database. Palaeosecular variation curves given by SCHA.DI.00 are compared with available archaeomagnetic data from Bulgaria (Sofia), Italy (Etna) and Austria (Radstadt), not used in the development of the model. The SCHA.DI.00 model improves the fit to these palaeomagnetic data with respect to the CALS7K.2 [Korte, M., Constable, C.G., 2005. Continuous geomagnetic field models for the past 7 millennia: 2. CALS7K. Geochem. Geophys. Geosyst. 6, Q02H16. doi:10.1029/2004GC000801] global model, especially for Italy.

IDT: 1503; 1522; 1532

Keywords: Archaeomagnetism; Geomagnetic secular variation; Regional models; Europe

1. Introduction

Detailed knowledge of the secular variation (SV) of the Earth's magnetic field is of crucial importance for understanding the dynamics of the Earth's core. Direct observatory measurements of the geomagnetic field and its variations have been carried out for the last two centuries. Measurements of declination (mostly) and inclination from shipboard and navigational purposes are available for the last four centuries (e.g. Jackson et al., 2000; Jonkers et al., 2003). To extend the knowledge of the geomagnetic field variations into the past, palaeomagnetic studies are needed. In addition to the geodynamic applications, a good description of the geomagnetic field provides the basis for the archaeomagnetic dating technique.

To investigate the dynamics of the Earth's core, a worldwide well-distributed palaeomagnetic data set is required to obtain global models based on spherical harmonic analyses. Palaeomagnetic global models have been obtained

* Corresponding author. Tel.: +34 91 3945190; fax: +34 91 3944398.
E-mail addresses: fjpavon@ fis.ucm.es (F.J. Pavón-Carrasco), mlosete@ fis.ucm.es (M.L. Osete), jmtorta@obsebre.es (J.M. Torta), gaya@ipgp.jussieu.fr (L.R. Gaya-Piqué), Philippe.lanos@univ-rennes1.fr (Ph. Lanos).
[1] Address: Université de Rennes 1, Géosciences-Rennes, Campus de Beaulieu, 35042, Rennes Cedex, France.

1474-7065/$ - see front matter © 2008 Elsevier Ltd. All rights reserved.
doi:10.1016/j.pce.2008.02.024

during the last decade (e.g. Ohno and Hamano, 1993; Hongre et al., 1998), and more recently by Korte and Constable (2003, 2005). But the number of palaeomagnetic data is still too small, and its distribution around the globe is still too inhomogeneous, to determine a global model accurate enough to describe the detailed variations for a given region and therefore to be used for archaeomagnetic dating.

The classical approach of palaeomagnetists to define the palaeosecular variation (PSV) in a region is to calculate a reference curve (PSVC) from palaeomagnetic directions. A high density of palaeomagnetic data, well-distributed in time, from a small region (usually less than 600–900 km radius) is needed. This can be obtained from heated archaeological structures, which are well-dated and not disturbed (archaeomagnetic curves), and from well-dated volcanic materials. Usually archaeological material is preferred for several reasons: (1) the stability and origin of its remanence, commonly a thermo-remanence (TRM) or a partial thermo-remanence (pTRM), (2) the absence of delays in the remanence acquisition mechanism, (3) the stability of the carriers of the remanence, and (4) the facility of some archaeological material to be accurately dated.

To build a PSVC, archaeomagnetic data are transferred from the sampling place to a reference point by the Conversion Via Pole (CVP) method (Noel and Batt, 1990). This relocation process introduces an error, which can be evaluated for the present time through the International Geomagnetic Reference Model (IGRF). For example, for an area of 900 km radius centred at Madrid, inclination errors are less than 2° and declination errors less than 3°. These errors are commonly within the uncertainty of palaeomagnetic directions. Consequently, if the harmonic content of the geomagnetic field was similar in the past, similar errors to the present are expected, which should be included in the palaeomagnetic uncertainty.

When a PSVC is determined for a region, this can be used for archaeomagnetic dating by using, for example, the method described by Lanos (2004). The limitation of this application is the distance from the dating point to the location of the reference curve (the relocation error). Therefore a high density of PSVC is needed.

In contrast, when a global model is determined, data from an area of 10^7 km^2 (the surface of Europe) are sometimes relocated to a common point (Hongre et al., 1998; Korte and Constable, 2003). The relocation error for the present geomagnetic field increases linearly with the relocation distance (a maximum of 7° for a 1700 km radius; Casas and Incoronato, 2007). Consequently global models constructed in this way can not be used for archaeomagnetic dating. The global model provided by Korte and Constable (2005) does not present this problem, but, as it will be discussed later, the model is too smoothed to adequately represent archaeomagnetic variations.

An intermediate approach between global models and PSVC is the determination of regional models. Up to now there is no regional model to describe the palaeomagnetic field at continental scales. During the last 10 years a considerable effort has been made in Europe to determine PSVC for several countries. Consequently, at present there is a high density of new archaeomagnetic data in this region to approach a regional modelling. The objective of this study is to provide an initial regional model of the Secular Variation for Europe for the last 2000 years by using Spherical Cap Harmonic Analysis (SCHA, Haines, 1985a).

2. SCHA method

Spherical Cap Harmonic Analysis was originally presented by Haines (1985a). Although it has been widely described and applied in many different studies (e.g. Haines, 1985b; De Santis et al., 1990; Korte and Haak, 2000; Gaya-Piqué et al., 2006; Torta et al., 2006), Thébault (2003) presented strong evidence that SCHA is, as many other regional techniques, a mathematical approximation that is unable to take into account all the natural properties of potential fields. Thébault et al. (2006) recently presented a new technique called Revised Spherical Cap Harmonic Analysis (R-SCHA) for which a complete boundary value problem is solved. This method represents the magnetic field in a closed conical domain by a complete family of functions; therefore R-SCHA is an exact mathematical method. Being designed to work within a volume, the R-SCHA technique however presents numerical problems which are difficult to solve when dealing with a single surface and very large caps (Thébault, personal communication). Consequently, and taking into account that only ground data will be considered, we decided to follow the classical approach by Haines (1985a), accepting the limitations of SCHA and the fact that the model cannot be extrapolated outside the limits of the cap. Other techniques like polynomial or spline modelling may be powerful enough for the purpose of developing regional or global models, but the broad use of SCHA in geomagnetism in the last two decades, and the fact that it satisfies (as the global Spherical Harmonic Analysis) Laplace's equation, made our choice for this regional technique.

The general solution that satisfies the conditions imposed by Laplace's equation is expressed for a spherical cap like an expansion in terms of spherical harmonics. The internal geomagnetic potential is

$$V(r,\theta,\lambda) = a\sum_{k=0}^{K_{\mathrm{int}}}\sum_{m=0}^{k}\left(\frac{a}{r}\right)^{n_k+1} P_{n_k}^{m}(\cos\theta)\cdot\left(g_{n_k}^{m}\cos m\lambda + h_{n_k}^{m}\sin m\lambda\right) \quad (2.1)$$

where $P_{n_k}^{m}(\cos\theta)$ are the colatitudinal Legendre functions, $\left(\frac{a}{r}\right)^{n_k+1}$ is the radial dependence (with r the radial distance and a the mean radius of the Earth) and $\cos m\lambda$, $\sin m\lambda$ the longitudinal Fourier functions.

The boundary conditions on the border of the cap involve the use of associated Legendre functions with real degree n. As the different real values of n depend on the order m, we use a new parameter k (an integer increasing

index for a given m) for its representation. The K_{int} parameter is the maximum degree of the expansion. The spatial expansion of the potential will give $(K_{\text{int}}+1)^2$ SCH coefficients if all solved coefficients are considered. The method applied in this paper, following Haines (1988), is based on a regression by least squares. The original Fortran code (Haines, 1988) includes a statistic parameter to define the degree of significance for each coefficient and so include it or not in the model (Draper and Smith, 1981). But in our case, we did not use this rejection criterion in order to have the same number of SCH coefficients for each individual model obtained through the entire time interval.

The minimum wavelength that can be represented by the model is given by Bullard (1967). Changing the integer degree n to the real degree n_k:

$$\lambda_{\min} = \frac{2\pi a}{n_k} \tag{2.2}$$

where $\lambda_{\min}$ is the minimum wavelength that the SCHA model can reproduce. The SCHA method models shorter wavelengths (i.e. represents higher resolution) than the global SHA for an equal expansion index. This wavelength gets smaller as the size of the cap decreases.

3. SCHA.DI

The classical SCHA modelling uses as input data the three Cartesian geomagnetic components X, Y and Z. However, in archaeomagnetic studies, the elements usually determined for a given site are the declination and inclination. Without intensity data a complete description of the geomagnetic field by SHA or SCHA techniques is not possible. Whether or not a model reconstructed from only directional data can predict (within a single global scaling factor) the intensity elsewhere, is a topic that has been widely discussed in the literature (Hulot et al., 1997, and references therein). For our practical purposes, i.e. the analytical representation of the regional behaviour of declination and inclination, we adapted the SCHA algorithms of Haines (1988) by using a classical method, known as Bauer's method (Barraclough, 1974), that relates the components X, Y and Z to the declination and inclination values.

From the trigonometric relations between the geomagnetic elements, we have:

$$\begin{aligned} X\sin D &= Y\cos D \\ X\sin I &= Z\cos D\cos I \\ Y\sin I &= Z\sin D\cos I \end{aligned} \tag{3.1}$$

Expanding X, Y and Z in the spherical cap harmonic series:

$$\begin{aligned} \sum_{k,m}\alpha_{k,m}\cdot g_{k,m}\cdot\sin D &= \sum_{k,m}\beta_{k,m}\cdot g_{k,m}\cdot\cos D \\ \sum_{k,m}\alpha_{k,m}\cdot g_{k,m}\cdot\sin I &= \sum_{k,m}\gamma_{k,m}\cdot g_{k,m}\cdot\cos D\cdot\cos I \\ \sum_{k,m}\beta_{k,m}\cdot g_{k,m}\cdot\sin I &= \sum_{k,m}\gamma_{k,m}\cdot g_{k,m}\cdot\sin D\cdot\cos I \end{aligned} \tag{3.2}$$

where $\alpha_{k,m}$, $\beta_{k,m}$, $\gamma_{k,m}$ include the radial power, the colatitudinal Legendre, and longitudinal Fourier dependences; and $g_{k,m}$ represents the spherical cap harmonic coefficients g_k^m and h_k^m. To produce a directional model (without intensity information) we divided all the expressions by the first coefficient $g_{0,0}$ (i.e., the g_0^0 SCH coefficient) and denoted $G_{k,m}=g_{k,m}/g_{0,0}$, obtaining a system of equations that depend on the declination and inclination data:

$$\begin{aligned} \sum_{k,m}G_{k,m}(\alpha_{k,m}\cdot\sin D-\beta_{k,m}\cdot\cos D) &= 0 \\ \sum_{k,m}G_{k,m}(\alpha_{k,m}\cdot\sin I-\gamma_{k,m}\cdot\cos D\cos I) &= \gamma_{0,0}\cos D\cos I \\ \sum_{k,m}G_{k,m}(\beta_{k,m}\cdot\sin I-\gamma_{k,m}\cdot\sin D\cos I) &= \gamma_{0,0}\sin D\cos I \end{aligned} \tag{3.3}$$

This new system of equations can be introduced in the SCHA routines of Haines (1988). For this new system, the input data (declination and inclination) must be transformed from geodetic to geocentric values and rotated to the cap's centre (Haines, 1988).

This method is thus applied under the assumption that the SCH coefficients are normalised to the value of the first coefficient of the expression. This is possible because declination and inclination values do not depend on the numerical value of this SCH coefficient. Consequently, we can obtain any element of the geomagnetic field, being Z, H and F, but they are standardized to the value of $g_{0,0}$.

4. Input data

For this initial archaeomagnetic European model we have considered as input data the best determined PSVC for different countries (or regions) of Europe. These curves allow a smooth and continuous evolution in time to facilitate the stability in the inversion process that will be used. All of them were determined by application of hierarchical Bayesian modelling based on roughness penalty (Lanos, 2004).

The number of PSVC used was five, and their locations are given in Fig. 1. They correspond to the regions of France, with its reference point located in Paris (Gallet et al., 2002); Germany, in Göttingen (Schnepp and Lanos, 2005); Hungary, in Budapest (Marton and Ferencz, 2006); Iberia, in Madrid (Gómez-Paccard et al., 2006b); and United Kingdom, in Meriden (Zananiri et al., 2007). In the same figure, the corresponding PSVC are shown. The PSVC of Bulgaria (Kovacheva et al., 1998) was not included as input data because it was not constructed under the same statistical approach as the rest of European curves. But the database from Bulgaria (Kovacheva et al., 1998, and references therein) will be used later to test our model.

5. Model parameterisation and results

The best compromise between the residual mean square (rms) error (the square root of the sum of the squared dif-

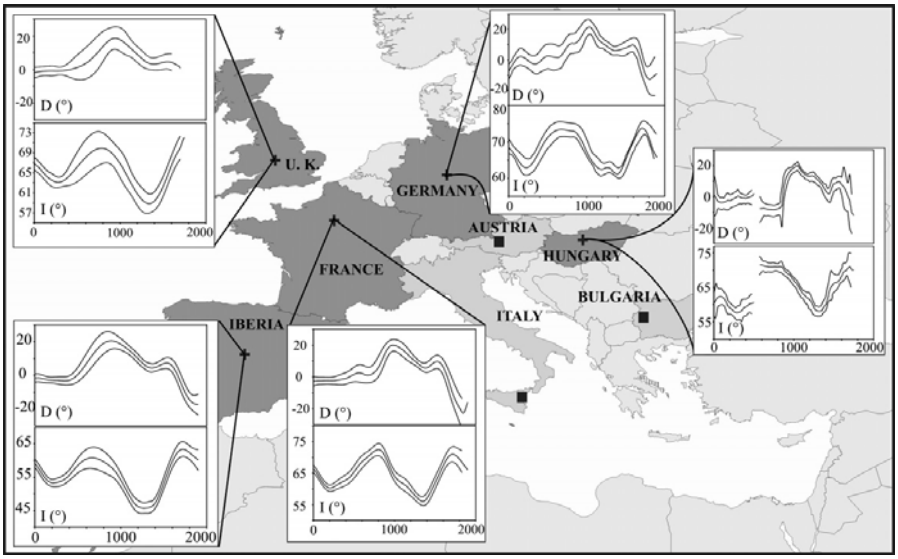

Fig. 1. Map showing locations of input data. Black crosses: location of the European PSVC. Black squares: location of other studies. The input PSVC for every location appears superimposed on the map. Pairs of curves: up, Declination curve; down, inclination curve vs. time (AD years).

ferences) and the minimum wavelength that we want to reproduce led us to choose the following parameters of the SCHA: a cap size of $\theta_0 = 40°$ and a maximum degree of the harmonic expansion $K_{\text{int}} = 2$. Input data (PSVC) have been discretised at intervals of 5 years. After this discretisation a method of sliding windows, analogous to that employed in the bivariant method of Le Goff (1990) and Daly and Le Goff (1996), has been used. The size of the window was 20 years (enough to reproduce the general smooth behaviour of the PSVC) and the step-window was 5 years. Five data sets were sampled for each window, corresponding to the central epoch and to laterals of the time interval.

A SCHA model was developed for each window by polynomial temporal expansion for the SCH coefficients, obtaining a set of coefficients valid for the particular temporal interval. By moving the window in steps of 5 years from 0 to 1900 AD, we obtain 381 sets of SCH coefficients (Fig. 2a).

To regularise the model for every window, we used an iterative approach. First we used a series of spherical cap harmonics only up to $k = m = 1$, and with the obtained SCH coefficients we synthesised contour values at the edge of the cap. In a second step we increased the indexes up to $k = 2$ and $m = 0$, and we used as input data the PSVC plus the peripheral data weighted one hundred times less than the real PSVC. And so on for successive steps with $k = 2$ and $m = 1$, and $k = m = 2$. For this last step we obtained the definitive SCH coefficients for the particular window. The total rms error decreases after increasing the number of SCH coefficients. Table 1 shows the declination, inclination, and overall rms errors for each step of the iterative process.

From the model coefficients obtained every 5 years, declination and inclination values for any point located in the spherical cap within the temporal validity of the models can be generated. The technique also allows evaluation of the errors in each coefficient (see Fig. 2b) and, consequently, the errors associated with the synthesis of declination and inclination elements (at 95% of confidence) from them.

From 600 to 900 AD and at about 1450 AD the SCH coefficients errors reach the highest values. The first time period corresponds to the so called "Dark Ages", from where few archaeomagnetic data are available and probably the input data (PSVC) may contain some internal discrepancies. Therefore the geomagnetic models derived from them are less well constrained. The second period (around 1450 AD) corresponds to a sharp change in the declination values of Hungary not observed in other curves (see Fig. 1). The rest of relative maximum errors correspond to other sharp variations of the input curves.

Fig. 3 shows the declination and inclination maps for Europe every 100 years from 0 to 1900 AD given by the SCHA.DI.00 model.

Values predicted by the model have been compared with input data. The spatial rms error for declination, inclination and both declination and inclination are given in Fig. 4. The inclination values are better fitted than the declination values, this is reasonable since declination input curves are more irregular than inclination variations. The rms error is higher for the "Dark Ages" due to the already

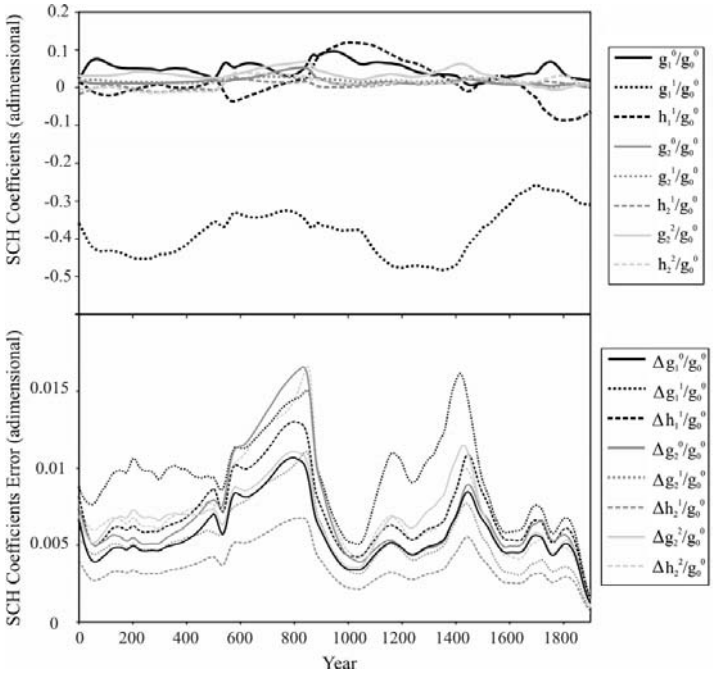

Fig. 2. SCH coefficients (up) and their errors (down). All values are normalized to the first SCH coefficient g_0^0. The SCH coefficient errors are at 95% of confidence.

Table 1
Different iterations to obtain the SCHA model and the declination, inclination and both declination and inclination rms errors

Step	SCH indexes	Declination RMS (°)	Inclination RMS (°)	Declination and inclination RMS (°)
1°	$K_{int} = 1$, $m = 1$	2.9	1.6	2.5
2°	$K_{int} = 2$, $m = 0$	2.7	1.3	2.3
3°	$K_{int} = 2$, $m = 1$	2.7	1.2	2.2
4°	$K_{int} = 2$, $m = 2$	1.6	1.0	1.4

mentioned lack of archaeomagnetic data. For the rest of the time span considered the model fits the input data reasonably well.

The SCHA.DI.00 model obtained is available from the web site: http://www.ucm.es/info/Geofis/grupos.html (palaeomagnetism group).

6. Discussion

6.1. Geomagnetic models and PSVC for Iberia, UK, France, Germany and Hungary

The SCHA.DI.00 model has been compared with each PSVC used as input data and with the predictions of global models – CALS7K.2 Korte and Constable, 2005 (valid from 5000 BC to 1950 AD); GUFM Jackson et al., 2000 (from 1590 to 1990 AD) and Hongre et al., 1998 (from 0 to 1700 AD) – at the considered five localities: Madrid (Iberia), Meriden (UK), Paris (France), Göttingen (Germany) and Budapest (Hungary). This comparison is shown in Fig. 5.

Archaeomagnetists commonly use angular errors to measure differences between expected and observed directions. The angular error (α) used in this work has been estimated from:

$$\cos\alpha = \cos I \cos I' \cos(D - D') + \sin I \sin I' \quad (6.1)$$

where D and I define the expected direction given by the SCHA.DI.00 model and D' and I' are the observed declination and inclination obtained from the Palaeosecular Variation Curves. These data are shown in Fig. 6a. In Fig. 6b angular global errors (the mean of the errors for all localities at a given time using quadratic error) are represented for different global models (CALS7K.2: Korte and Constable, 2005; GUFM: Jackson et al., 2000; Hongre et al., 1998).

Synthetic PSVC obtained for Iberia from SCHA.DI.00 model fit the Bayesian curve, as shown in Fig. 5. The SCHA.DI.00 synthetic curve lies within the 95% confidence level of the Bayesian curve. Other models describe the general behaviour of the Iberian PSVC, but expected values differ from observations more than SCHA.DI.00 predictions. Curves synthesised from CASL7K.2 model are much

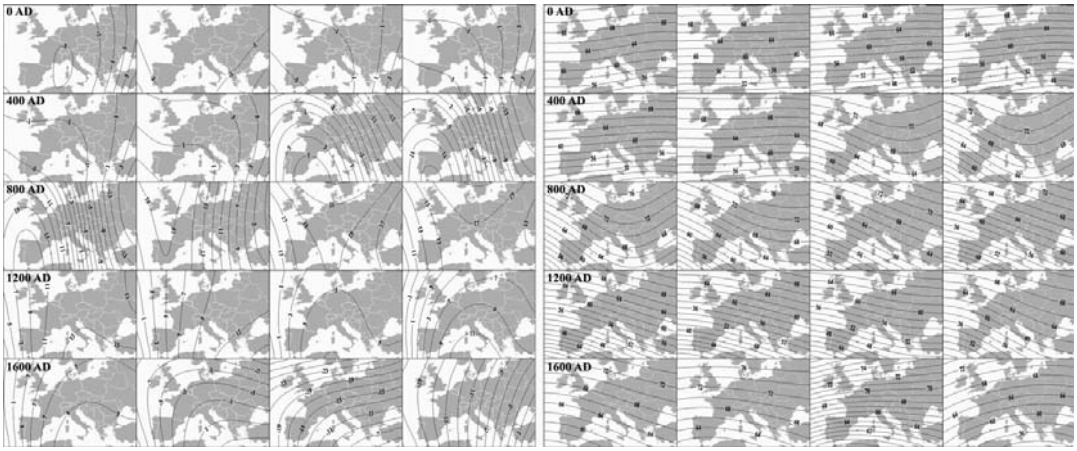

Fig. 3. From left to right and from top to bottom, declination (left) and inclination (right) maps from year 0 to 1900 AD at 100 years interval obtained from SCHA.DI.00 model.

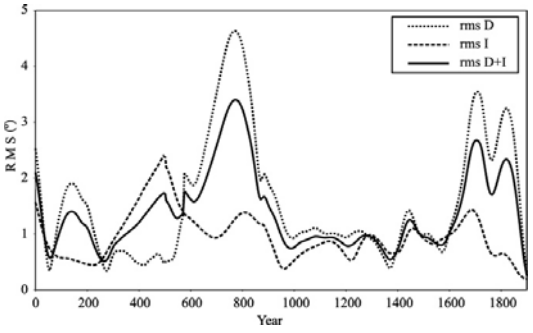

Fig. 4. Declination, inclination and overall declination and inclination rms errors for the complete time span of the SCHA.DI.00 model.

smoother. In contrast, synthetic inclination curves generated from Hongre et al. (1998) model exhibit higher variability than Bayesian curves. This is expected since the values of the smoothing parameters used to construct the Bayesian curves (Lanos, 2004) are probably higher than those used by Hongre et al. (1998). The inclination values synthesised from GUFM model seem to be higher than the Bayesian curve for the 1590–1800 AD period.

For Iberia the angular error of the SCHA.DI.00 model is very small (Fig. 6a). The maximum (about 1°) is achieved around 800 AD. For this period only 2 archaeomagnetic data are available for the Spanish archaeomagnetic curve (Gómez-Paccard et al., 2006b). Therefore, the Bayesian curve is poorly defined for this period. However, SCHA.DI.00 model predicts reasonably well the original archaeomagnetic data. Both predicted and observed archaeomagnetic directions are statistically indistinguishable.

It is important to remark that the Iberian archaeomagnetic data have only been available since 2006 (Gómez-Paccard et al., 2006a,b). Consequently, the only model under consideration in this paper that used Iberian data as input data is the SCHA.DI.00 model.

SCHA.DI.00 synthetic data for UK reproduce the input PSVC (Zananiri et al., 2007) well. Synthetic curves are within the 95% level of confidence of the Bayesian curves for the 0–1600 AD period. The maximum angular difference between expected and observed values is 3° (1700 AD). The other models fit also reasonably well the UK curve. The curve generated from Hongre et al. (1998) model differs in inclination for the 500–750 AD interval. GUFM model seems to fit very well instrumental observations for the 1700–1900 AD period, but differs significantly in inclination during the 1580–1650 AD interval.

Most models fit the French PSVC reasonably well. This is expected since this curve and French data have been used in all models as a reference dataset. Palaeosecular Variation Curve generated by SCHA.DI.00 is within the 95% of error of the Bayesian curve except for the 650–800 AD interval, when it differs slightly in declination, and during the 750–850 AD period where a small difference in inclination is observed. However when considering the 95% error in the SCHA.DI.00 curve as well, both curves are statistically indistinguishable. Maximum angular difference is about 3.5°, achieved around 800 AD.

Higher differences are observed between the French Bayesian PSVC and CALS7K.2 model. Especially for the 650–950 AD period, due to the strong smoothing of the CALS7K.2 model. Hongre et al. (1998) model reproduces the French Bayesian curve well except around 1300 AD, where expected inclination values seem to be lower than predicted by Bayesian PSVC. GUFM model also reproduces well the most recent part of the French curve (except inclination values around 1600 AD).

The best synthetic curve for Germany is the one generated by SCHA.DI.00 model. The PSVC for Germany is

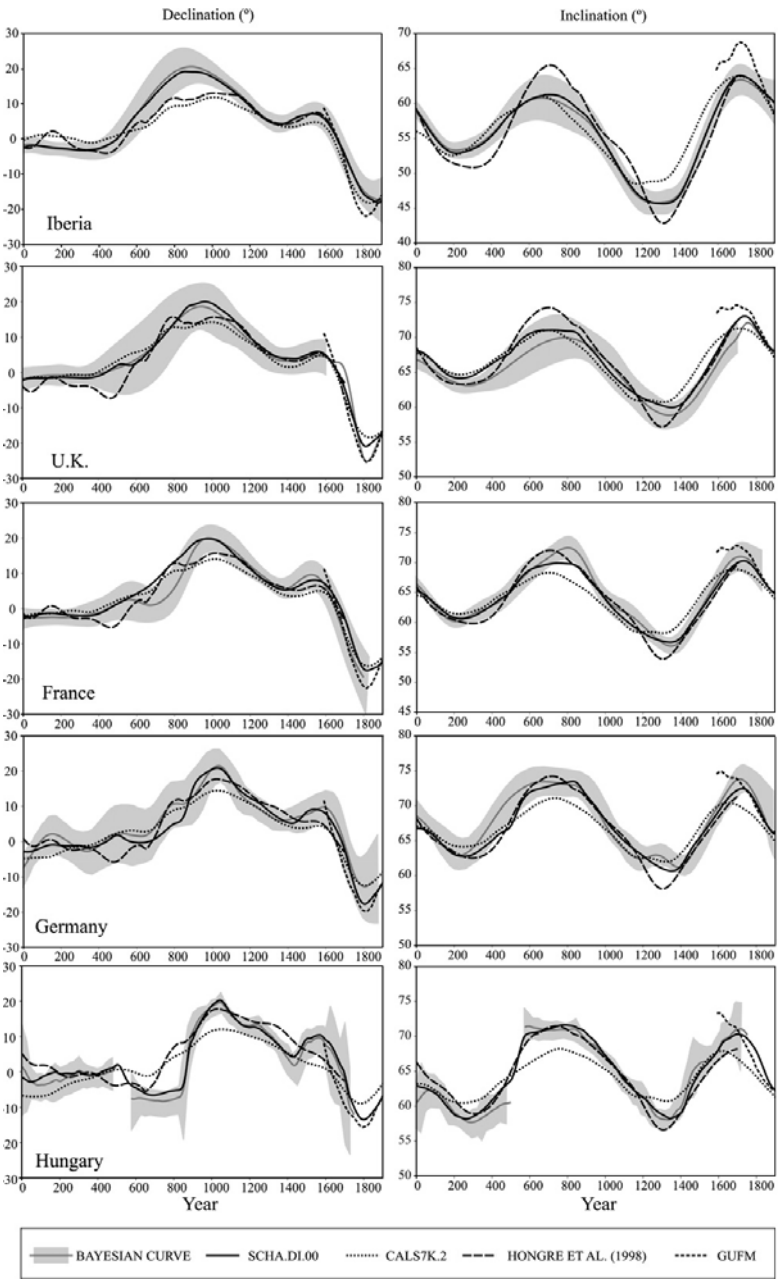

Fig. 5. Declination (left) and inclination (right) curves from SCHA.DI.00 model, the Bayesian PSV input curves, CALS7K.2 model (Korte and Constable, 2005), Hongre et al. (1998) model and GUFM model (Jackson et al., 2000). Gray band indicates the 95% confidence limit of input curves.

very similar to the French curve. Consequently, comparison between other synthetic curves and the Bayesian curve gives similar results: CALS7K.2 model seems too smoothed and Hongre et al. (1998) model predicts lower inclination than observed around 1300 AD. The highest angular deviation between SCHA.DI.00 model and PSVC is about 4° at 500 AD, probably due to the influence of the nearby Hungarian curve in the SCHA.DI.00 model.

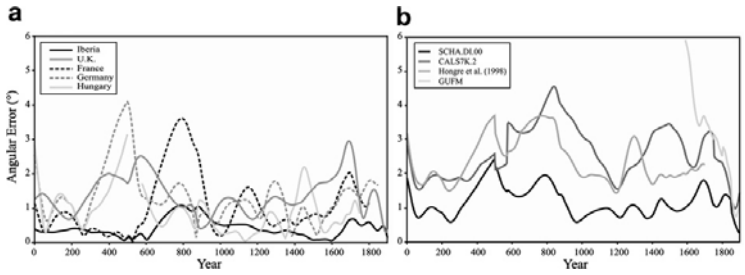

Fig. 6. (a) Angular errors of SCHA.DI.00 model for Iberia, UK, France, Germany and Hungary. (b) Overall angular errors for different geomagnetic models: SCHA.DI.00 (this study), CALS7K.2 (Korte and Constable, 2005), Hongre et al. (1998) and GUFM (Jackson et al., 2000).

PSVC for Hungary was also obtained by Bayesian statistics, but the method used to generate the curve differs from the other curves (Marton and Ferencz, 2006). That is why the Hungarian curve seems to be more irregular. However the synthetic curve from SCHA.DI.00 model lies within the 95% level of uncertainty of the input curve. Hongre et al. (1998) model reproduces the inclination curve well, but a discrepancy is observed in declination around 650–900 AD. In this case it is even more evident that CALS7K.2 model is too smoothed to reproduce the PSVC. GUFM model reproduces declination data well, but a small discrepancy in inclination is observed around 1600 AD.

The overall angular deviations between synthetic curves generated by different models and Bayesian PSVC of Fig. 6b show that the lowest error corresponds to the synthetic curves generated by the SCHA.DI.00 model. The maximum error is obtained in the 400–900 AD period, the "Dark Ages", when fewer archaeomagnetic data are available and, consequently, more discrepancies in the input data could be expected.

The global angular error of the model proposed by Hongre et al. (1998) shows a strong increase around 500 AD, in the 580–950 AD time interval and around 1300 AD. First maximum error is related to the westward drift in declination predicted by this model that is not shown in the PSVC data (see declinations in Fig. 5). The maximum error observed around 1300 AD seems to be produced by the low inclination values generated by this model which seems not to be so low in the input PSVC. The other interval of maximum error is connected to the "Dark Ages". The errors of the CALS7K.2 model are, as said before, related to the over-smoothing of this model. Finally the GUFM model exhibits a higher error in the period 1590–1750 AD owing to the high inclination predicted values. After this period, the error is similar to the one from CALS7K.2 model.

The average angular error in time (the mean of the overall angular error for all the time interval using quadratic error) for the SCHA.DI.00 model is 1.3°, smaller than the calculated from global models: 2.7° for the CALS7K.2 model (Korte and Constable, 2005), 2.5° for the model proposed by Hongre et al. (1998) and 3.4° for the GUFM model (Jackson et al., 2000).

Palaeosecular variation synthetic curves for France, Germany and UK generated by SCHA.DI.00 and by CALS7K.2 and Hongre et al. (1998) models are very similar (Fig. 5). This is expected since these curves (or data) were used for the estimation of these models. In contrast, our model fits better the more recent PSVC of Iberia and Hungary. The average angular error in time for the Iberian and Hungarian synthetic curves obtained from SCHA.DI.00 model are 0.5° (Iberia) and 1.1° (Hungary), while the errors of the curves predicted by the CALS7K.2 and Hongre et al. (1998) models are 3.2° and 3.2° for Iberia and 3.2° and 2.6° for Hungary, respectively.

Fig. 7 shows the PSVC generated from SCHA.DI.00 model with the 95% confidence limit, together with archaeomagnetic dataset and the Bayesian curves. Distribution of the archaeomagnetic data in time is very inhomogeneous. When comparing periods of maximum errors (higher than 1.5°) obtained by SCHA.DI.00 model (Fig. 6b) and the archaeomagnetic data set (Fig. 7), it is possible to conclude that a clear correlation exists: (i) the highest error is observed for the 400–900 AD period when a lower number of archaeomagnetic data are available, (ii) the error observed around the 1625–1700 AD time interval is also correlated with a lack of archaeomagnetic information. Consequently, future archaeomagnetic studies should focus on both periods to obtain a more detailed description of the variations of the Earth's magnetic field.

Another final point that should be carefully taken in consideration concerns the smoothing parameters used to model archaeomagnetic data. This is a very important problem and still an open question. An over-smoothing will obscure real variations of the field. In contrast, anomalous high frequencies can be observed when the number of data is small and are not conveniently smoothed. An apparent variability of the field is then observed which is due to the intrinsic archaeomagnetic errors and temporal distribution of the dataset rather than to genuine field variations. In our case, the smoothing of the predicted curves is basically controlled by the smoothing of the input data (Bayesian Curves), which seems to be too strong.

6.2. PSVC generated by SCHA.DI.00 for Austria (Radstadt), Bulgaria (Sofia), and southern Italy (Etna)

To test the validity of the SCHA.DI.00 model, an independent palaeomagnetic dataset has been used: archaeomagnetic data from Austria, Bulgaria and Italy, which were not used as input data to the model. Figs. 8 and 9 show the PSVC generated for Austria (Radstadt), Bulgaria (Sofia) and Italy (Etna), together with the available archae-

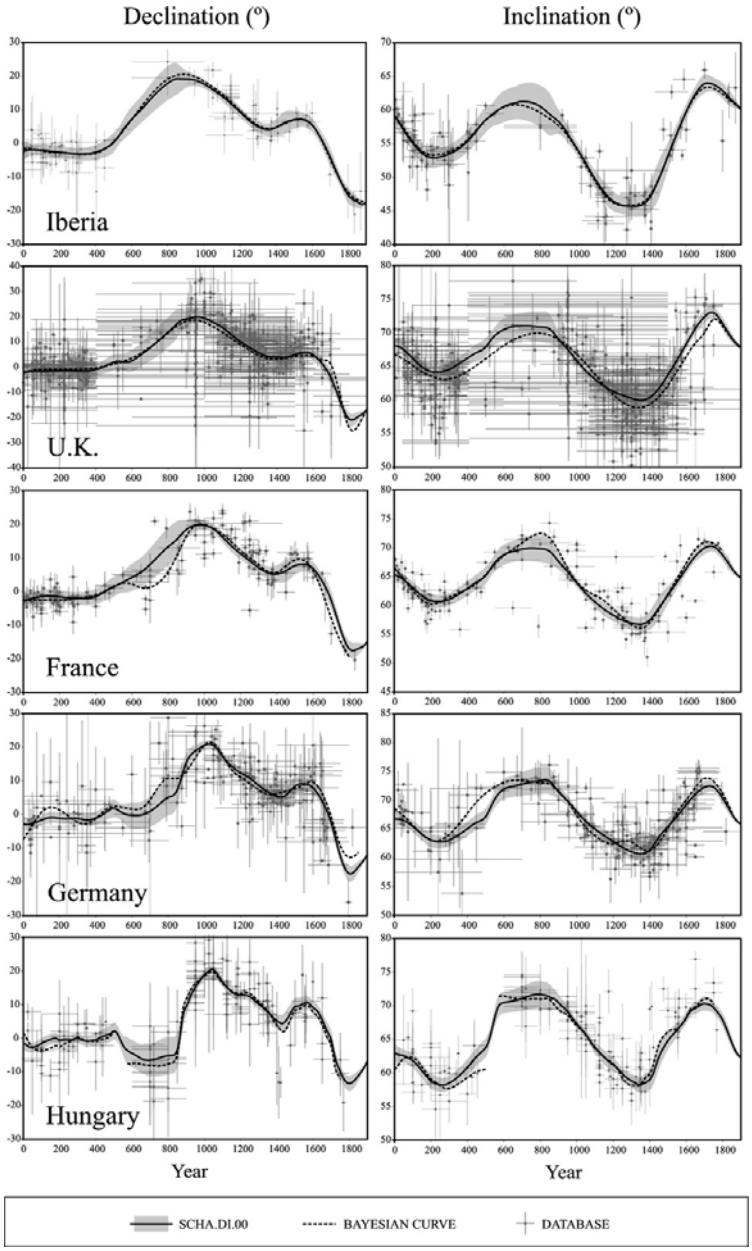

Fig. 7. Declination (left) and inclination (right) curves together with the marginal errors (gray band) for SCHA.DI.00 model, archaeomagnetic databases used for the construction of the PSVC and Bayesian PSVC.

omagnetic data and with predictions from the CALS7K.2 model.

Only a few data from Austria have been recently studied (Schnepp and Lanos, 2006). Six out of the seven studied Austrian sites fit the SCHA.DI.00 model predictions within the confidence limits of the curve and of the archaeomagnetic data. One site (see Fig. 8a) presents an archaeomagnetic direction that differs from the expected value. This site (ST1) was studied, discussed and dated archaeomagnetically by Schnepp and Lanos (2006). These authors produced a date using a new PSVC for Austria computed from archaeomagnetic data of nearby countries. The obtained archaeomagnetic date is 1575–1692 AD, in agreement with our model (Fig. 8a).

We have also estimated the angular error between in situ data and directions calculated from SCHA.DI.00 model and from the new Bayesian Austrian curve (Schnepp and Lanos, 2006) transferred to each site. The anomalous dated site ST1 has been rejected, as well as another site which has an age uncertainty over 300 years. Identical results were obtained for the four sites ranging in age from 250 to 600 AD. Mean angular errors are: $\alpha_{BAY} = 3.2°$ and $\alpha_{SCHA} = 3.6°$. Both are within the uncertainty of the curves, and the palaeomagnetic and age errors.

PSVC generated by SCHA.DI.00 model at Sofia is shown in Fig. 8b. It is important to remark that this dataset was used by Korte and Constable (2005) to produce the CALS7K.2 model, but these data were not used to generate the SCHA.DI.00. Fig. 9b shows the error estimated for both models. For the 400–1000 AD time interval our model fits the archaeomagnetic declination better. In contrast, better results are obtained by the CALS7K.2 model around 1000–1150 AD. Bulgarian data shows a sharp change in declination in this period. The other European datasets, shown in Fig. 7, indicate a high dispersion in declination which is not recorded in the Bayesian curves due to the smoothing parameters used. It would be important for future archaeomagnetic studies to focus on the reliability of this sharp declination variation. Both models seem to be too smoothed to reproduce the variability in declination observed in the Bulgarian dataset.

There is not yet a consensus about the Italian Palaeosecular Variation Curve (Tanguy et al., 2003; Arrighi et al., 2004; Speranza et al., 2004; Principe et al., 2004; Lanza and Zanella, 2005; Tema et al., 2006). Only a few archaeomagnetic data are available at present for the last two millennia (Tema et al., 2006) and most palaeomagnetic studies on Palaeosecular Variation have been focussed on the study of the historical eruptions of Etna and Vesuvius. In the absence of a well-defined PSVC for Italy, the French PSVC transferred to Etna has been used to date some of the volcanic episodes (Tanguy et al., 2003). The estimated relocation error of this process is at present 6.0° (Casas and Incoronato, 2007) which may be too high for dating purposes. In Fig. 9, the PSVC calculated from SCHA.DI.00 and CALS7K.2 models are shown together with palaeomagnetic data from Tanguy et al. (2003), the database for Italy used to develop the CALS7K.2

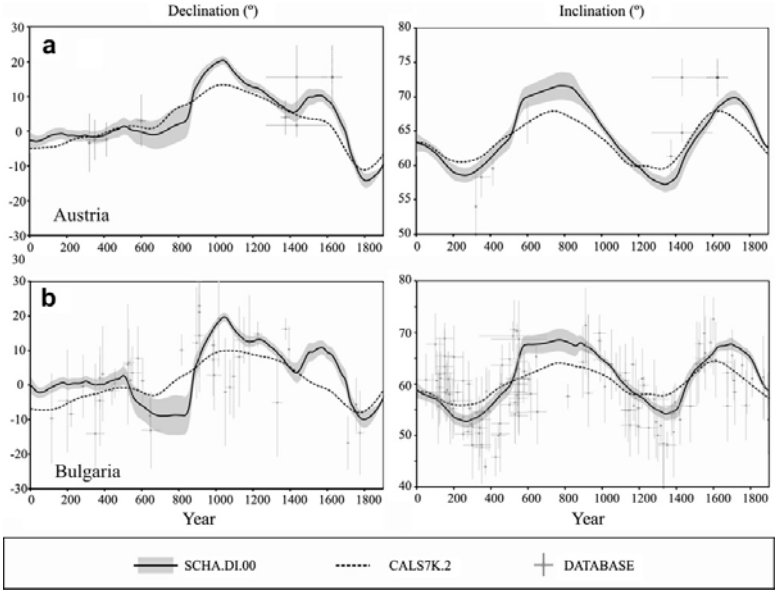

Fig. 8. Declination (left) and inclination (right) curves together with the marginal errors (gray band) for SCHA.DI.00 model, archaeomagnetic databases and CALS7K.2 model (Korte and Constable, 2005): (a) for Austria, all dataset (Schnepp and Lanos, 2006) are reduced to Radstadt (13.45°E, 47.38°N) and (b) for Bulgaria, all dataset (Kovacheva et al., 1998, and references therein) are reduced to Sofia (23.2°E, 42.7°N).

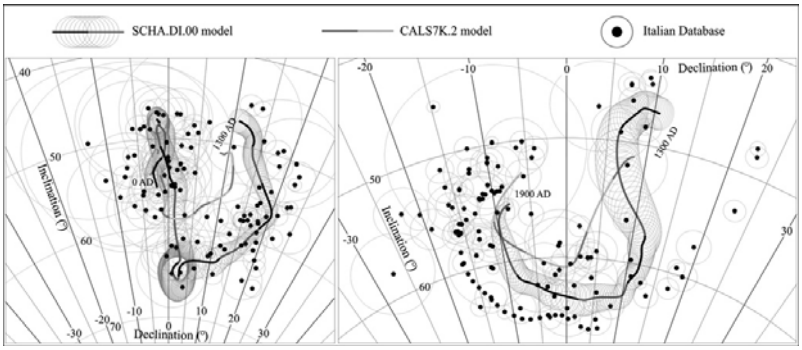

Fig. 9. Secular variation curves from SCHA.DI.00 model, CALS7K.2 model (Korte and Constable, 2005), database of Italy (Tema et al., 2006; Korte et al., 2005; Tanguy et al., 2003) and the instrumental database from Italy (Lanza et al., 2005). All data are reduced to Etna's coordinates (15.00°E, 37.75°N). On the left 0–1300 AD, on the right 1300–1900 AD.

model (Korte et al., 2005), the instrumental database from Italy (Lanza et al., 2005) and recent archaeomagnetic data (Tema et al., 2006). SCHA.DI.00 fits the palaeomagnetic data better than the CALS7K.2 model. This is especially true for the 800–1500 AD time interval (see Fig. 9). It is important to point out that previous global models did not use the new archaeomagnetic catalogue recently published for Iberia (Gómez-Paccard et al., 2006a). The good fit of SCHA.DI.00 model to the Italian data is probably due to this, but it is again necessary to point out that global CALS models use strong smoothing. With the available models and curves the best choice to date volcanic eruptions in Italy seems to be the SCHA.DI.00 model.

SCHA.DI.00 has also been compared with the instrumental database compilation of Lanza et al. (2005) transferred to Etna coordinates. The instrumental data (1625–1900 AD) give values of inclination up to 3° higher than those generated by the SCHA.DI.00 regional model. For recent times, instrumental data are within the confidence uncertainty of SCHA-DI.00 model. For older periods the discrepancy is higher, but it is necessary to take into account that the instrumental error has not been considered.

6.3. Calculation of a palaeosecular variation curve at any locality. A case study: French archaeomagnetic dataset

The main advantage of a regional model like SCHA.DI.00 is the ability to produce an archaeomagnetic palaeosecular calibration curve for any given location. To evaluate this application the French in situ archaeomagnetic database has been used. Synthetic PSVC has been generated for each locality through SCHA.DI.00 and has been compared with original data and with the Bayesian curves transferred via pole to each site. France was selected because it is located near the centre of the cap and consequently, should not be affected by edge effects.

Results are not surprising. The mean angular difference between expected directions and in situ data is the same for both curves ($\alpha_{SCHA} = \alpha_{BAY} = 3.7°$). In fact, curves generated by SCHA.DI.00 model and Bayesian curves transferred to site locations are within 1° of angular distance when the site is up to 4.5° far from the centre of the reference curve (Paris). For these sites the angular errors are: $\alpha_{SCHA} = \alpha_{BAY} = 3.1°$. At angular distances of 5°–6° from Paris, mean angular errors increase ($\alpha_{SCHA} = 5.6°$, $\alpha_{BAY} = 6.0°$) due probably to the relocation process. The SCHA.DI.00 curves are indirectly affected by the relocation error because it used as input data the Bayesian curves that were obtained through the conversion via pole method.

Mean angular difference between expected directions estimated from CALS7K.2 and in situ data for the same region is $\alpha_{CALS7K.2} = 4.2°$, higher than Bayesian or SCHA.DI.00 curves.

We can confirm that, up to present, the SCHA.DI.00 model produces PSVC at any given French site with similar or higher precision than the Bayesian curves used for archaeomagnetic dating.

7. Conclusions

A first regional archaeomagnetic model for Europe for the last two thousand years has been obtained. This model has been calculated by the SCHA regional technique, modified for using only directional data and applying an iterative technique.

Input data (five PSVC) have been compared with the data generated by SCHA.DI.00 model and with the global models of Korte and Constable (CALS7K.2, 2005), Jackson et al. (GUFM, 2000) and Hongre et al. (1998). The obtained average total angular errors are: 1.3° for the SCHA.DI.00, 2.7° for the CALS7K.2 model, 3.4° for the GUFM model and 2.5° for the Hongre et al. (1998) model. The relation between errors and archaeomagnetic data

available indicates the necessity of increasing the number of archaeomagnetic studies in the time intervals with high errors, i.e. during "Dark age" and for 1625–1700 AD periods, characterized by a low density of archaeomagnetic data.

PSVC have been generated from SCHA.DI.00 model in Bulgaria, Austria and Italy, and compared with available palaeomagnetic data. The regional SCHA.DI.00 model obtained fits well the data and, regarding the current data compilation, is the best obtained so far over Europe compared to previous results. To generate a PSVC from SCHA.DI.00 model it is necessary to indicate the latitude and longitude of the site (input data). The output data are the declination and inclination (and their errors at 95% of confidence) versus time in ASCII format (file.dat). The next step in this study will be to consider the archaeomagnetic data in situ to avoid the errors produced by data relocation.

Acknowledgements

The authors benefited from discussions with Juan I. Núñez and Angelo De Santis during the early stages of the approach presented in this work. The authors are also grateful to the Spanish research project CGL2005-00211. Thanks are given to I. Zananiri and E. Tema, for providing updated versions of their databases. We also thank R. Thébault, R. Holme and A. Lodge for constructive reviews which helped to improve the original manuscript.

References

Arrighi, S., Rosi, M., Tanguy, J., Courtillot, V., 2004. Recent eruptive history of Stromboli (Aeolian Islands, Italy) determined from high-accuracy archeomagnetic dating. Geophys. Res. Lett. 31, L19603.

Barraclough, D.R., 1974. Spherical Harmonic analyses of the geomagnetic field for eight epochs between 1600 and 1910. Geophys. J. Int. 36, 497–513.

Bullard, E.C., 1967. The removal of trend from magnetic surveys. Earth Planet Sci. Lett. 2, 293–300.

Casas, Ll., Incoronato, A., 2007. Distribution analysis of errors due to relocation of geomagnetic data using the 'Conversion via Pole' (CVP) method: implications on archaeomagnetic data. Geophys. J. Int. 169 (2), 448–454.

Daly, L., Le Goff, M., 1996. An updated and homogeneous world secular variation data base: 1. Smoothing of the archaeomagnetic results. Phys. Earth Planet. Interiors 93, 159–190.

De Santis, A., Battelli, O., Kerridge, D.J., 1990. Spherical cap harmonic analysis applied to regional field modelling for Italy. J. Geomag. Geoelect. 42, 1019–1036.

Draper, N.R., Smith, H., 1981. Applied Regression Analysis. John Wiley & Sons, New York.

Gallet, Y., Genevey, A., Le Goff, M., 2002. Three millennia of directional variations of the Earth's magnetic field in western Europe as revealed by archaeological artefacts. Phys. Earth Planet. Interiors 131, 81–89.

Gaya-Piqué, L.R., Ravat, D., De Santis, A., Torta, J.M., 2006. New model alternatives for improving the representation of the core magnetic field of Antarctica. Antarctic Sci. 18 (1), 101–109.

Gómez-Paccard, M., Catanzariti, G., Ruiz-Martínez, V.C., McInstosh, G., Núñez, J.I., Osete, M.L., Lanos, Ph., Chauvin, A., Tarling, D.H., Bernal-Casasola, D., Tiritó, J. Archeological Working Group, 2006a. A catalogue of Spanish archaeomagnetic data. Geophys. J. Int. 166, 1125–1143.

Gómez-Paccard, M., Lanos, Ph., Chauvin, A., McInstosh, G., Osete, M.L., Catanzariti, G., Ruiz-Martínez, V.C., Núñez, J.I., 2006b. The first Archaeomagnetic secular variation curve for the Iberian Peninsula. Comparison with other data from Western Europe and with global geomagnetic field models. Geochem. Geophys. Geosyst. 7, Q12001. doi:10.1029/2006GC001476.

Haines, G.V., 1985a. Spherical cap harmonic analysis. J. Geophys. Res. 90 (B3), 2583–2591.

Haines, G.V., 1985b. Spherical cap harmonic analysis of geomagnetic secular variation over Canada 1960–1983. J. Geophys. Res. 90 (B14), 12563–12574.

Haines, G.V., 1988. Computer programs for spherical cap harmonic analysis of potential and general fields. Comput. Geosci. 14 (4), 413–447.

Hongre, L., Hulot, G., Khokhlov, A., 1998. An analysis of the geomagnetic field over the past 2000 years. Phys. Earth Planet. Interiors 106, 311–335.

Hulot, G., Khokhlov, A., Le Mouël, J.L., 1997. Uniqueness of mainly dipolar magnetic fields recovered from directional data. Geophys. J. Int. 129, 347–354.

Jackson, A., Jonkers, A.R.T., Walker, M.R., 2000. Four centuries of geomagnetic secular variation from historical records. Phil. Trans. R. Soc. Lond. A 358, 957–990.

Jonkers, A.R.T., Jackson, A., Murray, A., 2003. Four centuries of geomagnetic data from historical records. Rev. Geophys. 41, 1006. doi:10.1029/2002RG000115.

Korte, M., Constable, C.G., 2003. Continuous global geomagnetic field models for the past 3000 years. Phys. Earth Planet. Interiors 140, 73–89.

Korte, M., Constable, C.G., 2005. Continuous geomagnetic field models for the past 7 millennia: 2. CALS7K. Geochem. Geophys. Geosyst. 6, Q02H16. doi:10.1029/2004GC000801.

Korte, M., Haak, V., 2000. Modelling European magnetic repeat station and survey data by SCHA in search of time-varying anomalies. Phys. Earth Planet. Interiors 122, 205–220.

Korte, M., Genevey, A., Constable, C.G., Frank, U., Schnepp, E., 2005. Continuous geomagnetic field models for the past 7 millennia: 1. A new global data compilation. Geochem. Geophys. Geosyst. 6, Q02H15. doi:10.1029/2004GC000800.

Kovacheva, M., Jordanova, N., Karloukovski, V., 1998. Geomagnetic field variations as determined from Bulgaria Archaeomagnetic data. Part II: the last 8000 years. Sur. Geophys. 19, 431–460.

Lanos, Ph., 2004. Bayesian inference of calibration curves: application to archaeomagnetism. In: Buck, C., Millard, A. (Eds.), . In: Tools for Constructing Chronologies: Crossing Disciplinary Boundaries, vol. 177. Springer-Verlag, London, pp. 43–82.

Lanza, R., Zanella, E., 2005. Comments on "Chronology of Vesuvius' activity from A.D. 79 to 1961 based on archeomagnetism of lavas and historical sources" by C. Principe et al. Bull Volcanol. Bull Volcanol. doi:10.1007/s00445-005-0030-9.

Lanza, R., Meloni, A., Tema, E., 2005. Historical measurements of the Earth's magnetic field compared with the remanence directions from lava flows in Italy over the last four centuries. Phys. Earth Planet. Interiors 148, 97–107.

Le Goff, M., 1990. Lissage et limites d'incertitude des courbes de migration polaire: pondération des données et extension bivariate de la statistique de Fisher. CR Acad. Sci. Paris 311 (Serie II), 1191–1198.

Marton, P., Ferencz, E., 2006. Hierarchical versus stratification statistical analysis of archaeomagnetic directions: the secular variation curve for Hungary. Geophys. J. Int. 164, 484–489.

Noel, M., Batt, C.M., 1990. A method for correcting geographically separated remanence directions for the purpose of archaeomagnetic dating. Geophys. J. Int. 102, 753–756.

Ohno, M., Hamano, Y., 1993. Spherical harmonic analysis of palaeomagnetic secular variation curves. Central Core Earth 3, 205–212.

Principe, C., Tanguy, J.C., Arrighi, S., Paiotti, A., Le Goff, M., Zoppi, U., 2004. Chronology of Vesuvius' activity from A.D. 79 to 1961 based on

archeomagnetism of lavas and historical sources. Bull Volcanol 66, 703–724.

Schnepp, E., Lanos, Ph., 2005. Archaeomagnetic secular variation in Germany during the past 2500 years. Geophys. J. Int. 163, 479–490.

Schnepp, E., Lanos, Ph., 2006. A preliminary secular variation reference curve for archaeomagnetic dating in Austria. Geophys. J. Int. 166 (1), 91–96, doi: 10.111/j.1365-246X.2006.03012.x.

Speranza, F., Pompilio, M., Sagnotti, L., 2004. Paleomagnetism of spatter lavas from Stromboli volcano (Aeolian Islands, Italy): implications for the age of paroxysmal eruptions. Geophys. Res. Lett. 31, L02607.

Tanguy, J.C., Le Goff, M., Principe, C., Arrighi, S., Chillemi, V., LaDelfa, S., Patane, G., 2003. Archeomagnetic dating of Mediterranean volcanics of the last 2100 years: validity and limits. Earth Planet. Sci. Lett. 211, 111–124.

Tema, E., Hedley, I., Lanos, Ph., 2006. Archaeomagnetism in Italy: a compilation of data including new results and a preliminary Italian secular variation curve. Geophys. J. Int. 167, 1160–1171.

Thébault, E., 2003. Modélisation régionale du champ magnétique terrestre. Ph.D. thesis, Univ. Louis Pasteur, Strasbourg, France (in French).

Thébault, E., Schott, J.J., Mandea, M., 2006. Revised spherical cap harmonic analysis (R-SCHA): validation and properties. J. Geophys. Res. 111, B01102. doi:10.1029/2005JB003836.

Torta, J.M., Gaya-Piqué, L.R., De Santis, A. 2006. Spherical cap harmonic analysis of the geomagnetic field with application for aeronautical mapping. In: Rasson, J.L., Delipetrov, T. (Eds.), Geomagnetics for Aeronautical Safety: A Case Study in and around the Balkans. NATO Security Through Science Series – C, pp. 291–307.

Zananiri, I., Batt, C.M., Lanos, Ph., Tarling, D.H., Linford, P., 2007. Archaeomagnetic secular variation in the UK during the past 4000 years and its application to archaeomagnetic dating. Phys. Earth Planet. Interiors 160 (2), 97–107.

5.2 Adición de la arqueointensidad al modelo geomagnético direccional: el modelo SCHA.DI.00-F.

Resumen.

El modelo regional direccional SCHA.DI.00 de campo geomagnético válido para los últimos 2000 años (Pavón – Carrasco et al., 2008a) ha sido actualizado mediante la adición de la paleointensidad. Este modelo inicial, SCHA.DI.00, fue desarrollado aplicando la técnica clásica del análisis armónico en un casquete esférico (SCHA) a las curvas de variación paleosecular europeas generadas mediante la estadística Bayesiana. La comparación entre las curvas de variación paleosecular dadas por el modelo regional con los datos arqueomagnéticos no usados en el desarrollo del modelo mostraron una mejora con respecto al ajuste obtenido con los modelos arqueomagnéticos globales. Las recientes publicaciones en arqueointensidad nos han permitido desarrollar un modelo regional completo (declinación, inclinación e intensidad) del campo arqueomagnético en Europa para los últimos 2000 años: el modelo SCHA.DI.00-F. El modelo regional generado además de contribuir en las nuevas técnicas de datación arqueomagnética, ha podido ser usado para testar la reciente relación propuesta entre la variación secular del campo geomagnético y el cambio climático. Las curvas de variación de la intensidad obtenidas mediante el modelo SCHA.DI.00-F parecen verificar la hipótesis enunciada por Gallet et al. (2005) sobre la posible (causal) conexión entre cambios en la intensidad del campo magnético terrestre y las variaciones climáticas, abriendo nuevas perspectivas en este discutido tema.

Pure appl. geophys. 165 (2008) 1209–1225
0033–4553/08/061209–17
DOI 10.1007/s00024-008-0354-4

Pure and Applied Geophysics

A Regional Archaeomagnetic Model for the Palaeointensity in Europe for the last 2000 Years and its Implications for Climatic Change

Fco. Javier Pavón–Carrasco,[1] Maria Luisa Osete,[1] J. Miquel Torta,[2] and Luis R. Gaya–Piqué[3]

Abstract—The SCHA.DI.00 directional model for the geomagnetic field in Europe for the last 2000 years (Pavón–Carrasco *et al*., 2008) has been updated by modelling the palaeointensity. This model, SCHA.DI.00, was developed from available Bayesian European Palaeosecular Variation Curves using the regional Spherical Cap Harmonic Analysis technique. The comparison of the palaeosecular variation curves, given by the regional model, with available archaeomagnetic data not used in its development showed an improvement with respect to the fit obtained by global archaeomagnetic models. In this paper advantage is taken of recently published palaeointensity databases to develop a complete (direction and intensity) regional archaeomagnetic model for the last 2000 years valid for the European region: the SCHA.DI.00–F model. Not only does this complete model provide an improvement for example for archaeomagnetic data studies, but it is also shown that this new regional model can be used to study the recently proposed link between the centennial secular variation of the geomagnetic field and climate change. The pattern of the archaeosecular variation of the field intensity obtained by SCHA.DI.00–F seems to verify the hypothesis presented by Gallet *et al*. (2005) about a possible (causal) connection between changes in the geomagnetic field intensity and in climate parameters, opening the door for more discussions on this challenging subject.

Key words: Palaeointensity, archaeomagnetism, geomagnetic secular variation, regional models, Europe.

1. Introduction

The long-term variation of the geomagnetic field extending over many years is called secular variation (SV). The temporal change of the geomagnetic field is far from linear, and abrupt changes in the rate of the secular variation change measured at the surface, known as geomagnetic jerks, provide information about the dynamics of the currents flowing in the Earth's outer core (Bloxham *et al*., 2002). When moving into the past, the Secular (or Palaeosecular) Variation Curves generated from archaeomagnetic

[1] Dpto de Geofísica y Meteorología, Universidad Complutense de Madrid, 28040, Madrid. E-mail: fjpavon@fis.ucm.es; mlosete@fis.ucm.es

[2] Observatori de l'Ebre, CSIC – Universitat Ramon Llull, Horta Alta 38, 43520. Roquetes, Spain. E-mail: jmtorta@obsebre.es.

[3] Equipe de Géomagnétisme, Institut de Physique du Globe de Paris, CNRS; Tour 14, 2 place Jussieu, 75005 Paris, France. E-mail: gaya@ipgp.jussieu.fr.

measurements can be used for dating purposes (e.g., LANOS, 2004). Moreover, a link between enhanced secular variation of the geomagnetic field and climate change over centennial time scales recently has been proposed (GALLET *et al.*, 2005, 2006; GALLET and GENEVEY, 2007; COURTILLOT *et al.*, 2007), challenging the role of solar forcing as the unique factor provoking these climatic variations.

The secular variation has been recorded directly through observatory measurements for the last two centuries. Declination (mostly) and inclination data are also available for the last four centuries from shipboard and navigational records (e.g., JACKSON *et al.*, 2000; JONKERS *et al.*, 2003). To extend our knowledge of the geomagnetic field variations into the past, palaeomagnetic studies are needed. The palaeosecular variation (PSV) in a region can be obtained from (a) heated archaeological structures, which are well-dated and not disturbed (archaeomagnetic curves), (b) well–dated volcanic materials, and (c) detailed sedimentary records (directional data or relative intensity). The use of archaeological material is normally preferred for several reasons: 1) The stability and origin of its remanence, commonly a thermo–remanence (TRM) or a partial thermo–remanence (pTRM); 2) the absence of delays in the remanence acquisition mechanism; 3) the stability of the carriers of the remanence; and 4) the facility of some archaeological materials to be accurately dated.

Archaeomagnetic data sets (e.g., the recent compilation of KORTE *et al.*, 2005) comprise directional and palaeointensity observations. The number of directional data is however higher (3787, about 7575 if we consider declination and inclination separately) than the amount of palaeointensity measurements (3206). In addition to this, archaeomagnetic data are not homogeneously distributed around the globe; Europe is the region where the highest record density is available.

Palaeomagnetic global models have been obtained during the last decade (e.g., OHNO and HAMANO, 1993; HONGRE *et al.*, 1998), and more recently by KORTE and CONSTABLE (2003, 2005) by using archaeomagnetic and sedimentary data. Since they are intended to represent the palaeofield on a global scale, these models are usually too smooth to record rapid changes of the Earth's magnetic field (i.e., archaeomagnetic jerks, GALLET *et al.*, 2005) which could be related to climatic changes. Recently the first directional regional model (SCHA.DI.00) to describe the palaeomagnetic field in Europe was proposed (PAVÓN–CARRASCO *et al.*, 2008), which seems to better reproduce the variability of the geomagnetic field over this region for the last 2000 years. The SCHA.DI.00 model was developed using the Spherical Cap Harmonic Analysis (SCHA) technique applied to five of the Bayesian European Palaeosecular Variation Curves (PSVC) (GALLET *et al.*, 2002; SCHNEPP and LANOS, 2005; MARTON and FERENCZ, 2006; GÓMEZ–PACCARD *et al.*, 2006a and ZANANIRI *et al.*, 2007), that are based on archaeomagnetic data. This model provided the directional behavior of the Earth's magnetic field, but no estimation about intensity was supplied because input data only contained directional information. The first spherical cap harmonic (SCH) coefficient, g_0^0, was used to normalize the rest of the coefficients.

In this study the present palaeointensity data set in Europe is used to adjust the first SCH coefficient, g_0^0, of the SCHA.DI.00 model to obtain a regional model for Europe

which also provides palaeointensity values for the last 2000 years. The new model, SCHA.DI.00–F, is compared to the existing global models of HONGRE *et al*. (1998), JACKSON *et al*. (GUFM, 2000), and KORTE and CONSTABLE (CALS7K.2, 2005) and with respect to real archaeointensity records. The use in the development of the regional model of a large amount of data over a restricted region of the planet makes it possible to achieve a higher spatial resolution compared to global models, and therefore the temporal variation of the field can be more accurately accounted for in that particular region. Finally, this new regional model can be used to study the recently proposed link between the centennial secular variation of the geomagnetic field and climate change (GALLET *et al*., 2005).

2. *The Previous SCHA.DI.00 Model*

The SCHA.DI.00 model (PAVÓN–CARRASCO *et al*., 2008) is based on the Spherical Cap Harmonic Analysis technique that was originally presented by HAINES (1985) and applied since to numerous geophysical studies (see Table 2 in TORTA *et al*., 2006, for a list of references). Although this method has been recently revised by THÉBAULT *et al*. (2006), the numerical problems are difficult to solve when only ground data are used, as in the case of archaeomagnetic data sets. Consequently the SCHA.DI.00 model used the classical approach of HAINES (1985), so the model cannot be extrapolated outside the limits of the cap. The SCHA algorithms of HAINES (1988) were adapted to the directional case by using Bauer's method (BARRACLOUGH, 1974), that relates the components X, Y and Z to the declination and inclination values. To produce a directional model (without intensity information) PAVÓN–CARRASCO *et al*. (2008) obtained a system of equations that depend on the declination (D) and inclination (I) data:

$$\begin{aligned}
&\sum_{k,m} G_{k,m}(\alpha_{k,m}\cdot \sin D - \beta_{k,m}\cdot \cos D) = 0\\
&\sum_{k,m} G_{k,m}(\alpha_{k,m}\cdot \sin I - \gamma_{k,m}\cdot \cos D\cos I) = \gamma_{0,0}\cos D\cos I\\
&\sum_{k,m} G_{k,m}(\beta_{k,m}\cdot \sin I - \gamma_{k,m}\cdot \sin D\cos I) = \gamma_{0,0}\sin D\cos I
\end{aligned} \tag{2.1}$$

where $\alpha_{k,m}, \beta_{k,m}, \gamma_{k,m}$ include the radial power, the colatitudinal Legendre, and longitudinal Fourier dependencies and $G_{k,m} = g_k^m/g_0^0$ are the SCH coefficients normalized to the first SCH coefficient g_0^0. This system of equations was introduced in the SCHA routines of HAINES (1988).

The input data of the SCHA.DI.00 model were the PSVC of Europe determined by application of hierarchical Bayesian modelling based on roughness penalty (LANOS, 2004). Five PSVC were used, which correspond to the regions of France, with its reference point located in Paris (GALLET *et al*., 2002); Germany, in Göttingen (SCHNEPP and LANOS, 2005); Hungary, in Budapest (MARTON and FERENCZ, 2006); Iberia, in Madrid (GÓMEZ–PACCARD *et al*., 2006a); and the United Kingdom, in Meriden (ZANANIRI *et al*., 2007). The databases

from Bulgaria (Kovacheva *et al.*, 1998 and references therein), Italy (Tema *et al.*, 2006; Korte *et al.*, 2005 and Tanguy *et al.*, 2003) and Austria (Schnepp and Lanos, 2006) were used to test the model.

The spherical cap expansion of SCHA.DI.00 extends up to $K_{int} = 2$ which, given the size of the spherical cap used (40° half angle), is equivalent, in terms of spatial wavelength, to a maximum degree of approximately 5 in the ordinary Spherical Harmonic Analysis (SHA).

3. SCHA.DI.00–F

The palaeointensity data used as input values for the development of the model were obtained from the global database of Korte *et al.* (2005). This database was updated with new data from Gallet *et al.* (2005) and Gómez–Paccard *et al.* (2006b) corresponding to French and Spanish locations. 611 palaeointensity determinations were available from different European countries for the time interval 0–1900 AD. The distribution of data in Europe is inhomogeneous, with high concentrations in France, England, Bulgaria, and Greece. Locations of the sites from which palaeointensity data have been used are shown in Figure 1.

The temporal distribution of data (Fig. 1, in box) shows a high density in the Roman period (between 100 and 300 AD). Similar to the archaeomagnetic directional database, there is a decrease in the density of data for 600–1000 AD (the so called "Dark Ages"). The palaeointensity data in Europe range between 36 and 106 μT; the average palaeointensity for 0–1900 AD is 60 μT. The mean palaeointensity error is 9 μT (maximum error of 21 μT and minimum of 1 μT). The mean time error is 42 years, with a minimum error of 0 and maximum of 300 years.

We have compared the palaeointensity data (F) compiled with the relative intensity data (f) provided by the directional regional model SCHA.DI.00 (Pavón–Carrasco *et al.*, 2008):

$$f^2 = x^2 + y^2 + z^2 = \left(\sum_{k,m} \alpha_{k,m} \cdot G_{k,m}\right)^2 + \left(\sum_{k,m} \beta_{k,m} \cdot G_{k,m}\right)^2 + \left(\sum_{k,m} \gamma_{k,m} \cdot G_{k,m}\right)^2 \tag{3.1}$$

where x, y and z are the relative Cartesian components of the geomagnetic field expansion in the SCH series, and $G_{k,m}$ represents the spherical cap harmonic coefficients g_k^m and h_k^m normalized to the first SCH coefficient, g_0^0. The relative intensity error can be obtained by applying the SCH coefficients errors to equation (3.1) (see Pavón–Carrasco *et al.*, 2008, Section 3).

From the relative intensity f calculated by the SCHA.DI.00 model at each location (Fig. 1) and for every epoch, the first SCH coefficient g_0^0 and its error were obtained as:

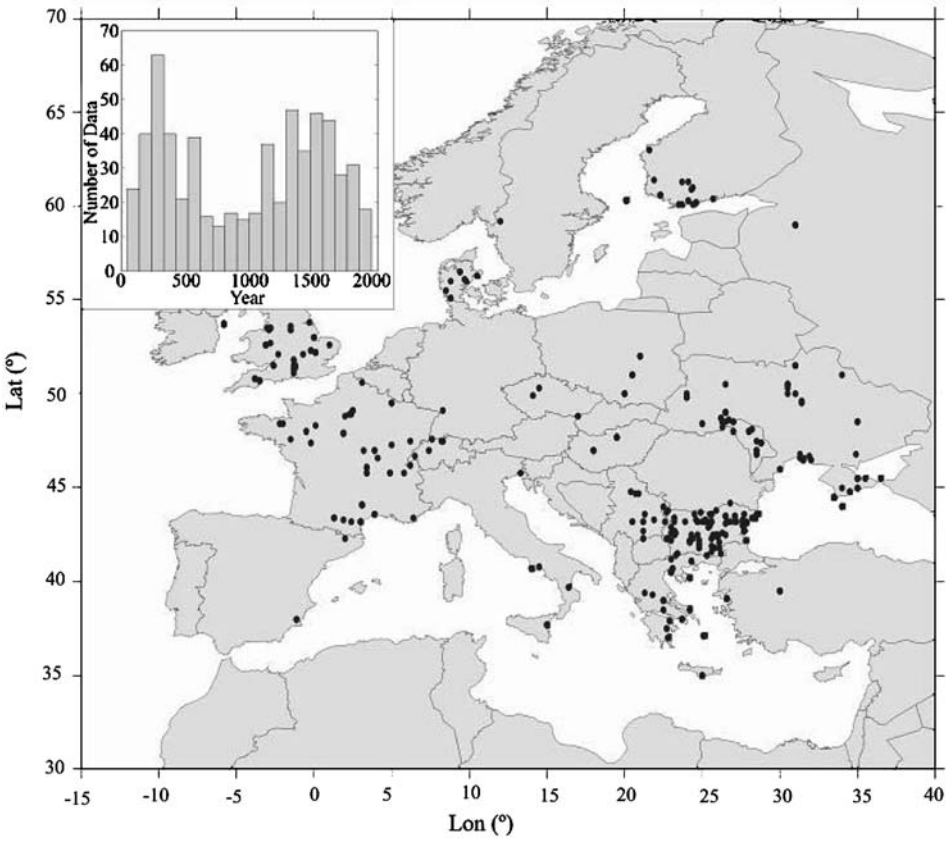

Figure 1
Map showing locations of palaeointensity data (KORTE *et al*., 2005; GALLET *et al*., 2005 and GÓMEZ-PACCARD *et al*., 2006b); and the temporal distribution of the data (in box).

$$g_0^0 = \frac{F}{f}; \quad \Delta g_0^0 = \frac{1}{f}\sqrt{F^2\Delta f^2 + f^2\Delta F^2}, \tag{3.2}$$

where F is the palaeointensity data and ΔF its error of the database of KORTE *et al*. (2005) and f is the relative intensity and Δf its error given by the SCHA.DI.00 model according to the equation (3.1). The g_0^0 coefficient has temporal but not spatial dependence, so these data sets were fitted using a time–dependent function. The temporal error of g_0^0 was considered to be equal to that of the palaeointensity data.

Considering that the mean time error of the palaeointensity data is 42 years, we have used windows of 50 years. The g_0^0 function was developed for each window by a polynomial temporal expansion (cubic splines) with knot points every 50 years. A weight function w_i was added in the inversion and is inversely proportional to the intensity and time errors:

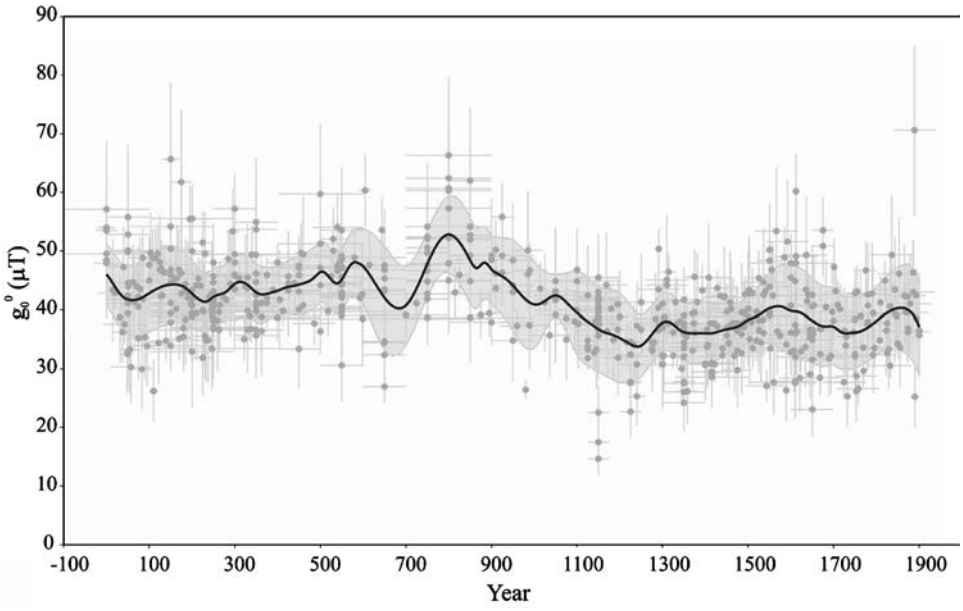

Figure 2
The first SCH coefficient, g_0^0. Dots: g_0^0 calculated by the global database (KORTE *et al.*, 2005; GALLET *et al.*, 2005 and GÓMEZ–PACCARD *et al.*, 2006b) with error bars. Curves: Fitted g_0^0 with error band.

$$w_i = \frac{1}{\rho_i + \tau_i}, \tag{3.3}$$

where ρ_i is the normalized error associated with the intensity and τ_i is the time normalized error. Once the g_0^0 function for the entire time interval is obtained, the rms (the square-root of the sum of the squared differences) was calculated by comparison with the calculated g_0^0 coefficient and input data.

Figure 2 shows the input data (the g_0^0 coefficient for each palaeointensity data measurement) and the g_0^0 time function and its error. The average value of the g_0^0 coefficient in Europe for the entire time interval is 41.5 μT, with a maximum at 800 AD. This age corresponds to abrupt changes in the magnetic field of the Earth, as pointed out by GALLET *et al.* (2005) and COURTILLOT *et al.* (2007).

Once the value of g_0^0 is obtained, we can derive the rest of SCH coefficients by using the expression $g_k^m = g_0^0 \cdot G_{k,m}$. Figure 3 shows the SCH coefficients and their associated errors. Coefficients g_0^0 and g_1^1 represent the main contribution to the Earth's magnetic field values. With this set of SCH coefficients it is possible to obtain the geomagnetic field components and intensity for Europe for the last 2000 years. The declination, inclination, and intensity values given by the SCHA.DI.00–F model for Europe every 100 years from 0 to 1900 AD are shown in the maps of Figure 4.

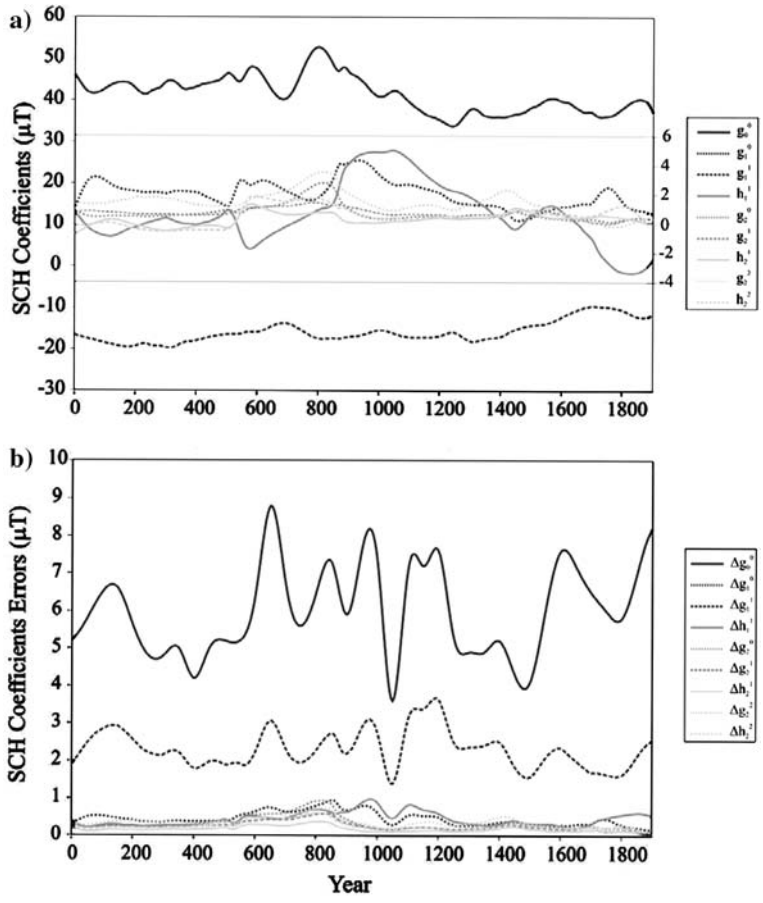

Figure 3
SCH coefficients (a) and their errors (b). The SCH coefficient errors are at 95% of confidence. Left scale corresponds to the SCH coefficients g_0^0 and g_1^1, right scale for the other SCH coefficients.

The new SCHA.DI.00–F and the previous directional SCHA.DI.00 models are available from the web site: http://pc213fis.fis.ucm.es/scha_model_f.html (palaeomagnetism group).

4. Discussion

4.1. The SCHA.DI.00–F Model

The palaeointensity values predicted by the SCHA.DI.00–F model have been compared with the *in situ* input data (we refer to PAVÓN–CARRASCO *et al.*, 2008, for

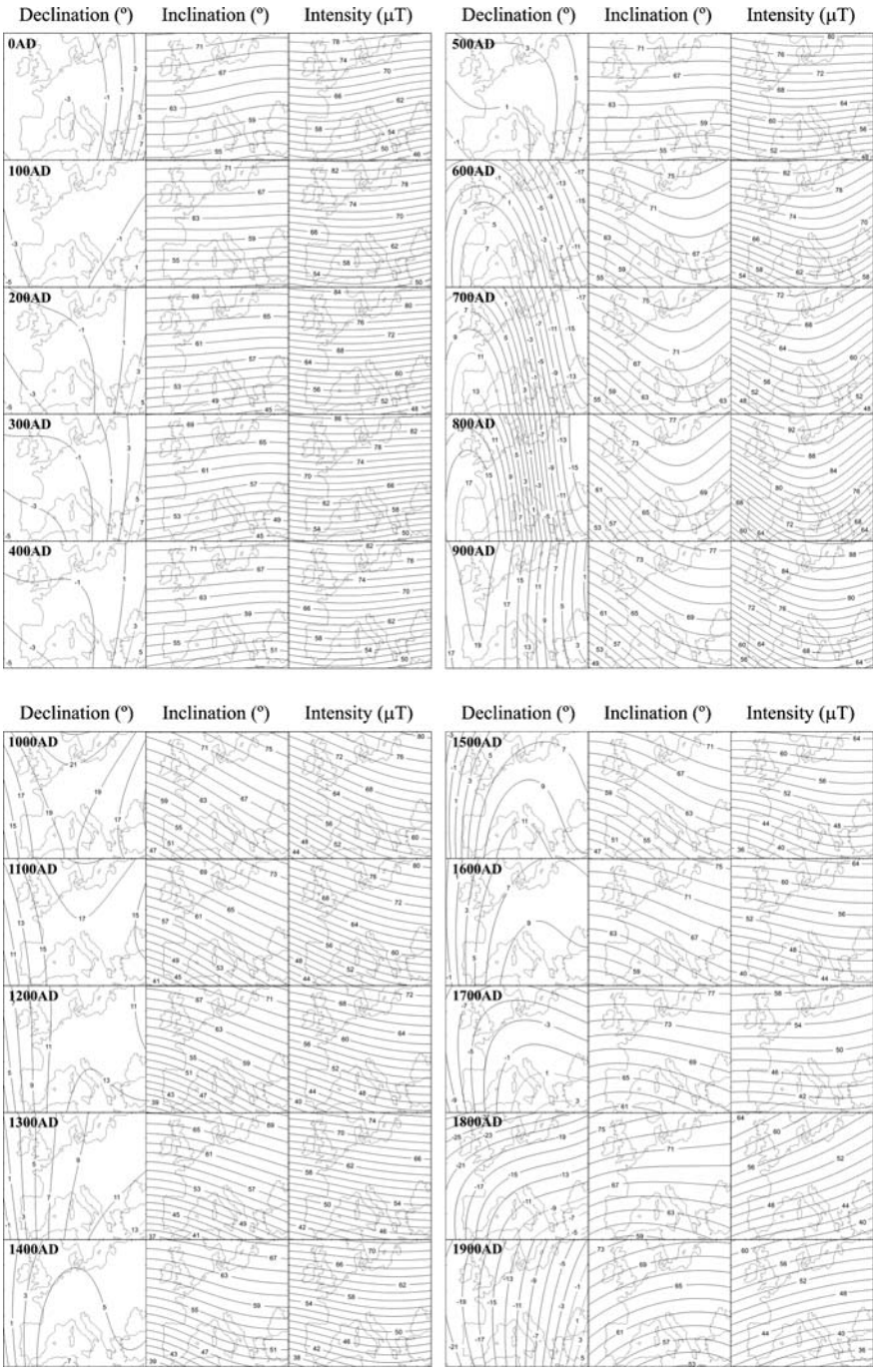

Figure 4
Declination, Inclination and Palaeointensity maps obtained by the SCHA.DI.00–F model at 100 year intervals.

directional data comparisons) and with the estimations from global models (CALS7K.2, KORTE and CONSTABLE, 2005–valid from 5000 BC to 1950 AD; GUFM, JACKSON *et al*., 2000–from 1590 to 1990 AD and HONGRE *et al*., 1998–from 0 to 1700 AD). The GUFM model only uses intensity data post 1840 AD and the authors assume a constant variation of the first SH coefficient ($\Delta g_1^0 = 15$ nT/year). Afterwards, GUBBINS *et al*. (2006) use the palaeointensity database of KORTE *et al*. (2005) from 1590 to 1840 AD to obtain the first SH coefficient g_1^0 in the same way that we have obtained the SCH coefficient g_0^0 in the present study. In this case, these authors propose a constant value in the variation of $g_1^0 = 2.28$ nT/year. For the comparison with the regional model, we have used the GUFM model with the new values of g_1^0 of GUBBINS *et al*. (2006) for the time period 1590–1840.

The error distribution for all these models has been plotted (Figs. 5a and 5b) with those obtained from SCHA.DI.00–F for comparison within the appropriate time period. For the period 0–1900 AD, the CALS7K.2 (KORTE and CONSTABLE, 2005) and the SCHA.DI.00–F models are compared. A total of 611 data have been used. The most frequent error is 5 μT for this regional model. In contrast, the error distribution of the global model exhibits a maximum at 7.5 μT. The mean quadratic error is very similar: 8.7 μT for the SCHA.DI.00–F model and 8.9 μT for CALS7K.2 model. The input data used in both models are also very similar. Therefore, the explanation of differences between the models resides in 1) the global model is also influenced by the data outside Europe and 2) the smoothing parameters used by KORTE and CONSTABLE (2005) seem to be too high to adequately describe brief, but significant Earth's magnetic field variations (this point is discussed later). The main differences between both models are the intervals 0–200, 800–950, and 1000–1100 AD, where the rms error of CALS model is higher than the regional model. Around 1300 and close to 1800 AD, the global model fits the data better than the regional model (Fig. 5b).

For the time interval 0–1700 AD, the distribution of errors of the SCHA.DI.00–F and the global model proposed by HONGRE *et al*. (1998) are shown in Figures 5a (center) and 5b. The mean quadratic errors are 8.7 μT for the regional model and 9.7 μT for the global model. In this case both distributions show a maximum in 5 μT, however the width of the error distribution is higher for the global model. It is important to consider that the input data for both models are very different in this case since many palaeointensity studies have been published in the last decade. This global model presents a poor fitting in the intervals 650–850 and 1400–1500 AD (Fig. 5b).

For the 1590–1900 AD interval the SCHA.DI.00–F model and the global GUFM (JACKSON *et al*., 2000) model are compared. For 1590–1840 AD we have used the modified GUFM model by GUBBINS *et al*. (2006). Mean quadratic error is 9.4 μT for the regional and 8.1 μT for the global model. The rms errors (Fig. 5b) show that the comportment of this global model is similar to the CALS global model for the considerate interval (1590–1900 AD), because the modified GUFM model also used the archaeointensity database of KORTE *et al*. (2005). In this case the global model seems to represent the behavior of the variation of intensity of the magnetic field better for this time period. However the GUFM model does not accurately describe the directional variation of the

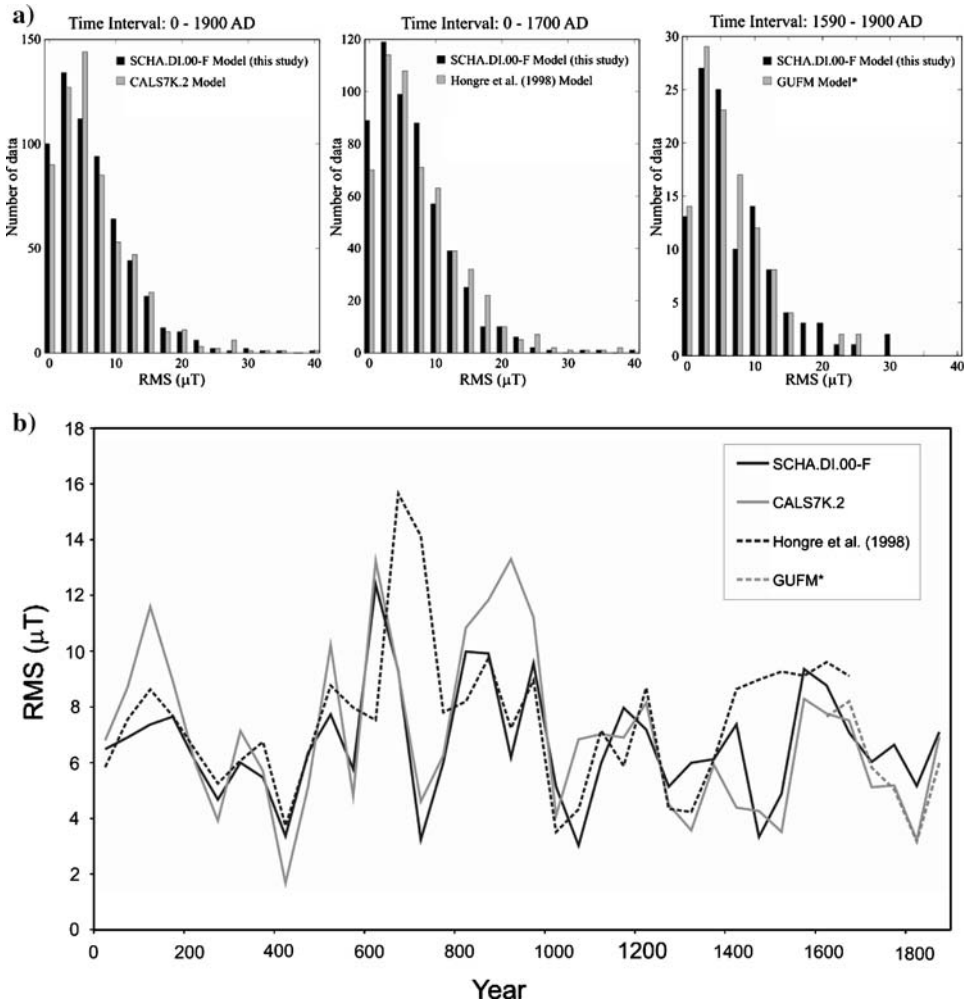

Figure 5

Histograms of errors (a) *versus* number of data and (b) *versus* time. Comparison of the rms errors between the SCHA.DI.00–F model and the global CALS7K.2 model (Korte and Constable, 2005); the global model of Hongre *et al*. (1998) and the global GUFM model (Jackson *et al*., 2000).* The GUFM model has been modified according to Gubbins *et al*. (2006).

geomagnetic field prior to 1700 AD (Pavón–Carrasco *et al*., 2008). Jackson *et al*. (2000) used historical directional observations of the magnetic field (from shipboards). The number of data used in the GUFM model was much higher (e.g., 83000 observations of magnetic declination before 1800 AD, Jackson *et al*., 2000) than those used in this study. For a detailed representation of the Earth's magnetic field a combination of both models should be considered in the future.

The SCHA.DI.00–F model suggests that the Earth's magnetic field in Europe reached 8 maximum peaks between 0–1900 AD at: 160, 320, 590, 820, 1070, 1310–1400, 1570 and 1770–1850 AD. Such a detailed description of the intensity variations of the geomagnetic field during the last 2000 years has not been achieved to date by any other geomagnetic model. This suggests that the smoothing parameters commonly used in constructing global models are too high to show such small wavelength variations.

4.2. Palaeointensity Generated Curves by SCHA.DI.00–F for France and Bulgaria

Palaeointensity data from Europe are inhomogeneously distributed (Fig. 1), most of the data being concentrated in France and Bulgaria. In Figure 6 the palaeointensity curves generated by the SCHA.DI.00–F model are compared with the palaeointensity data from France (KORTE *et al*., 2005 and references therein) after relocation to Paris, and from Bulgaria (KORTE *et al*., 2005 and references therein), relocated to Sofia (by the Virtual Axial Dipole Moment, VADM). The predicted palaeointensity curves generated by global models (KORTE and CONSTABLE, 2005; HONGRE *et al*., 1998 and JACKSON *et al*., 2000) are also shown.

The Bulgarian dataset suggests a higher variability in the intensity of the geomagnetic field than the French dataset. However, the French and Bulgarian datasets are only a part of the much larger amount of data used in the development of the models discussed in this paper. Consequently, they are influenced by the neighboring regions (as is the case of the regional model) or by data over the entire globe (global models). It also should be kept in mind that not all intensity values are determined using a unique method, therefore this could lead to variability in these datasets.

The CALS7K.2 global model (KORTE and CONSTABLE, 2005) is too smoothed to describe fluctuations shown by the data in these two locations. The model proposed by HONGRE *et al*. (1998) also seems to fail in isolating short–term fluctuations, whereas the GUFM model (JACKSON *et al*., 2000; GUBBINS *et al*., 2006) seems to represent the geomagnetic variations for the interval 1700–1900 AD most accurately.

The French and Bulgarian data appear to be in agreement with the SCHA.DI.00–F model except for two intervals. First, between 800–1000 AD, when a maximum in palaeointensity is predicted around 790–820 AD, which seems to be observed later in the Bulgarian database (about 900 AD). This location is mostly influenced by data from Ukraine (KORTE *et al*., 2005 and references therein). In addition, data from the Ukraine and Moldavia regions determined the position of the previous minimum at 690 AD. Second, a strong maximum is observed in the Bulgarian database around 1600–1650 AD (KOVACHEVA, 1997; KOVACHEVA *et al*., 1998), which is not well represented in the rest of the European database. The SCHA.DI.00–F shows a maximum at about 1570 AD but of lower magnitude.

Taking into account the European dataset used, it is suggested that future palaeointensity studies should be focussed in these two periods. The first one corresponds

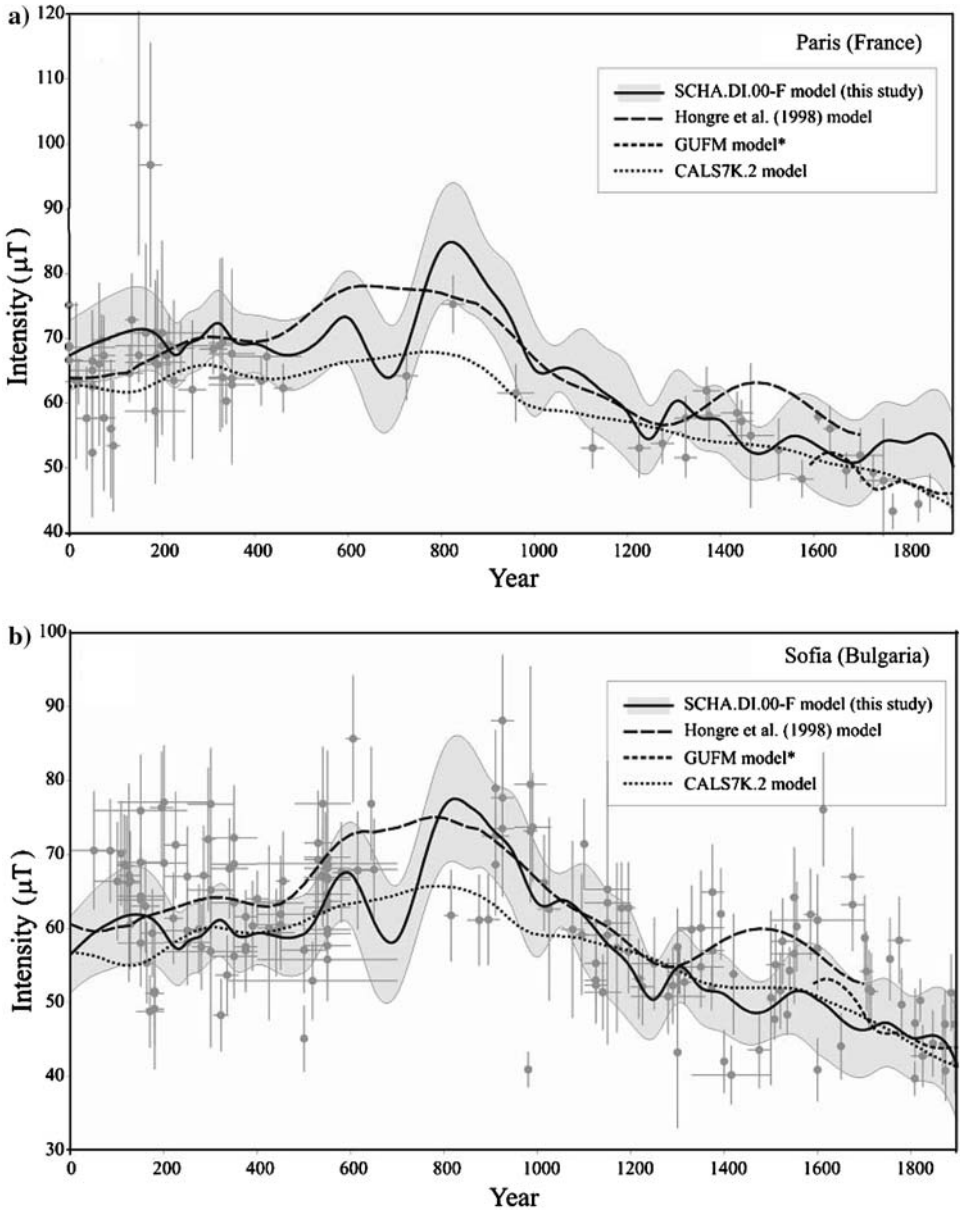

Figure 6

Palaeointensity curves for (a) Paris and (b) Sofia. Dots: Archaeointensity dataset from these regions with their error bars. Solid curve: Palaeointensity curve given by SCHA.DI.00–F model (with the error band) and the global geomagnetic models of Hongre *et al.* (1998), CALS7K.2 (Korte and Constable, 2005), and GUFM (Jackson *et al.*, 2000).* The GUFM model has been modified according to Gubbins *et al.* (2006).

to the "Dark Ages" from which there is less palaeomagnetic information available (see Fig. 1, in box). The second (the maximum around 1600 AD observed in the Bulgarian database, KOVACHEVA, 1997; KOVACHEVA *et al*., 1998) seems to be poorly represented in Western Europe data.

4.3. Palaeointensity during the last 2000 Years and the Climatic Record

The last section of this paper deals with a hot topic of research — the relationship between the geomagnetic field and climate. Many studies have indicated that solar variability is one of the main non–anthropogenic sources for climate alterations in the past, because of the positive correlation between solar irradiance and the temperature at the Earth's surface (e.g., USOSKIN *et al*., 2005), at least until the decade of 1980 AD when anthropogenic causes are assumed to play an important role in climate change (e.g., LE MOUËL *et al*., 2005). The role of the Earth's magnetic field as an agent connected to climate variations has been discussed for decades, but recently the topic generated interest because more archaeomagnetic information are now available (see COURTILLOT *et al*., 2007 for a review). A plausible physical mechanism hypothesized to explain this connection is as follows: A change in the strength of the magnetic field would induce variability in the cosmic ray flux that reaches the troposphere, consequently modifying the rate of production of clouds and therefore altering the temperature at the Earth's surface (GALLET *et al*., 2006; COURTILLOT *et al*., 2007). However, many unanswered issues emerge when entering into details, such as the role of changes in the Earth's magnetic field compared either to CO_2 concentration or to the variation in the cosmic ray flux modulated by solar activity (COURTILLOT *et al*., 2007). GALLET *et al*. (2005) found a good agreement for Western Europe between cooling periods and archaeomagnetic jerks, defined as sharp increases in the intensity of the magnetic field contemporary to abrupt changes in its direction. The authors hypothesize that this may be a causal link, furthermore presenting these geomagnetic variations (a total of six possible archaeomagnetic jerks for the last two millennia) as the triggering events for climate variations which produced cultural changes in societies world wide (GALLET *et al*., 2006; GALLET and GENEVEY, 2007).

Figure 7 represents the palaeointensity curve for Paris generated by our model SCHA.DI.00–F, its error band, and the palaeointensity data from Western Europe (KORTE *et al*., 2005; GALLET *et al*., 2005 and GÓMMEZ–PACCARD *et al*., 2006b) relocated into the location of Paris by the VADM method. The errors associated with the palaeomagnetic measurements correspond to uncertainties in the intensity (vertical bar) and in the date (horizontal bar). The shaded stripes indicate cooling periods as deduced from the advance of the Swiss Alps glaciers (after HOLZHAUSER *et al*., 2005). Following the definition by GALLET *et al*. (2005), and taking into account the figures for the temporal evolution of the magnetic field direction presented in PAVÓN–CARRASCO *et al*. (2008), up to 8 archaeomagnetic jerks can be deduced from this curve. All of these coincide with a cooling period; in more detail, the rising part of each intensity

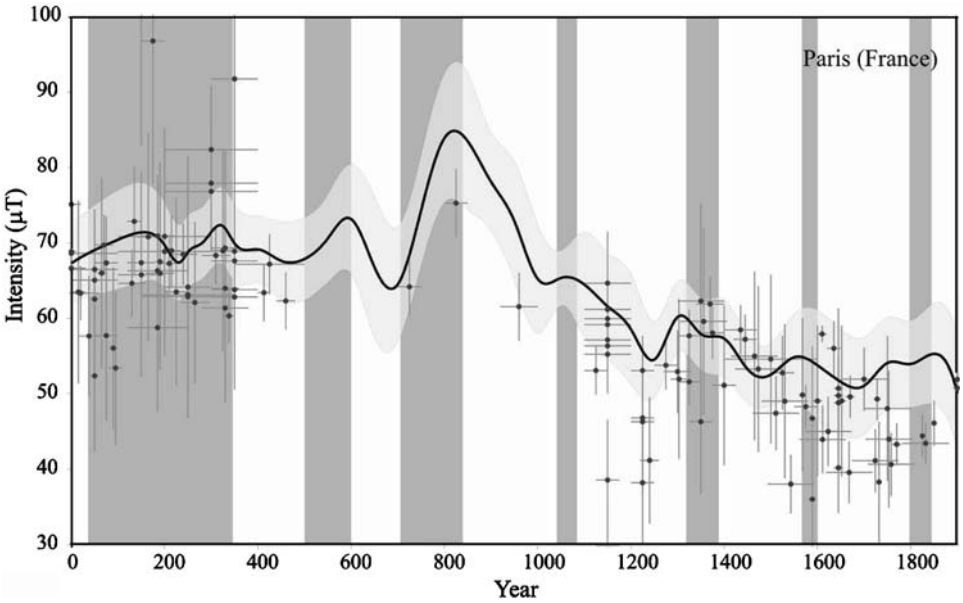

Figure 7
Palaeointensity curve at Paris (with error band) predicted by the SCHA.DI.00–F model. Archaeointensity data from Western Europe (Korte *et al*., 2005; Gallet *et al*., 2005 and Gómmez–Paccard *et al*., 2006b) relocated to Paris by VADM method. Climatic variations summarized by Gallet *et al*. (2005) deduced from retreats and advances of the Alpine Glaciers for the past millennium studied by Holzhauser *et al*. (2005). Cooling periods are indicated by shaded bands. Modified from Gallet *et al*. (2005).

maximum falls into a period of low temperature as shown by the shaded bands. Among these jerks, some of them (those around 820–950 AD, 1540–70 AD, and 1850 AD) are in good agreement with those found by Gallet *et al*. (2005), others (like the one for 1310–20 AD) precede the event detected by Gallet *et al*. (2005), but this event could extend up to 1400. The single jerk detected by Gallet *et al*. (2005) around 200 AD seems to split into two events as suggested by the new model, with maximum intensities and directional changes around 160–190 AD and 320 AD. The event around 590 AD suspected by Gallet *et al*. (2005) is better defined in the new model, therefore it is now considered to be a robust event. Finally, the low intensity maximum around 1070–1100 was not reported by Gallet *et al*. (2005) since no archaeointensity values were available from France for that epoch. The fact that more data are now being used helps to detect jerks more clearly, especially in the new model that incorporates data from other European regions.

If these eight events are real, the repetition time for the archaeomagnetic jerks has been about 250 years for the last 2000 years. This is usually assumed as the characteristic time for the non–dipolar part of the secular variation (e.g., Hulot and Le Mouël, 1994; Hongre *et al*., 1998). However, Korte and Constable (2006) suggest a shorter–term

variability of the dipole field, thus this characteristic time sheds no light on either the dipolar or non–dipolar secular variation. The conclusion from this comparison is that there seems to be a correlation between geomagnetic field variation and climate, although a fuller cross correlation analysis is needed to test if this correlation is robust. This study allows no inference whether the link is causal or not. Neither can it be inferred that the archaeomagnetic jerks are of dipolar or non–dipolar origin. Such assessments require this type of study to be extended to other areas of the world, enabling other regional models to be developed to monitor the extent (global or regional) of this causal–noncausal relationship.

5. Conclusions

This paper shows how the inclusion of *in situ* palaeointensity data improves a regional archaeomagnetic model by providing a complete description of the geomagnetic field over a restricted area for the last 2000 years. Following a similar procedure, when substituting the PSVC directional input data by *in situ* directional data as well, the overall fit will be further improved in the future when a dense compilation will be finished.

The SCHA.DI.00–F model fits the present palaeointensity archaeomagnetic database for Europe more accurately than the global models proposed by Hongre *et al*. (1998) and Korte and Constable (2005) for the 0–1900 AD time interval. The regional model also fits the directional data properly (Pavón–Carrasco *et al*., 2008), and, regarding the current data compilation, is the best model obtained to date over Europe for the 0–1900 AD time period. The model proposed by Jackson *et al*. (2000) seems to represent most accurately the geomagnetic variations for 1700–1900 AD interval.

The new SCHA.DI.00–F model suggests that the Earth's magnetic field strength reached 8 maxima in Europe at: 160, 320, 590, 820, 1070, 1310–1400, 1570 and 1770–1850 AD. The complete model presented in this paper has also provided new insights into a very new and controversial topic of research, i.e., the question of whether connections exist between geomagnetic field changes and global (or regional) climate alterations. Although our results seem to confirm, even amplify, previous studies, it cannot be concluded that such relationships are statistically significant, nor can the existence of causality between both phenomena be considered established.

Acknowledgements

The authors are grateful to the Spanish research project CGL2005–00211, the FPI grant BES-2006-13488 and the IPGP contribution 2603. The paper benefited from the reviews of D. Tarling and A. Lodge, whose comments assisted the enhancement of the manuscript.

References

Barraclough, D.R. (1974), *Spherical Harmonic analyses of the geomagnetic field for eight epochs between 1600 and 1910*, Geophys. J. Int. *36*, 497–513.

Bloxham, J., Zatman, S., and Dumberry, M. (2002), *The origin of geomagnetic jerks,* Nature. *420*, 65–68.

Courtillot, V., Gallet, Y., Le Mouël, J–L., Fluteau, F., and Genevey, A. (2007), *Are there connections between the Earth's magnetic field and climate?* Earth Planet. Sci. Lett. *253*, 328–339.

Gallet, Y. and Genevey, A. (2007), *The Mayans: climate determinism or geomagnetic determinism?* EOS Trans. Am. Geophys. Un. *88*, N. 11, 129–130.

Gallet, Y., Genevey, A., and Le Goff, M. (2002), *Three millennia of directional variations of the Earth's magnetic field in western Europe as revealed by archaeological artefacts*, Phys. Earth Planet. Inter. *131*, 81–89.

Gallet, Y., Genevey, A., and Fluteau, F. (2005), *Does Earth's magnetic field secular variation control centennial climate change?*. Earth Planet. Sci. Lett. *236*, 339–347.

Gallet, Y., Genevey, A., Le Goff, M., Fluteau, F., and Eshraghi, S.A. (2006), *Possible impact of the Earh's magnetic field on the history of ancient civilizations*, Earth Planet. Sci. Lett. *266*, 17–26.

Gómez–Paccard, M., Lanos, Ph., Chauvin, A., McInstosh, G., Osete, M.L., Catanzariti, G, Ruiz–Martínez, V.C., and Núñez, J.I. (2006a), *The first archaeomagnetic secular variation curve for the Iberian Peninsula. Comparison with other data from Western Europe and with global geomantetic field models*, Geochemi., Geophys., Geosyst. *7*, Q12001, doi:10.1029/2006GC001476.

Gómez–Paccard, M., Chauvin, A., Lanos, Ph., Thiriot, J., and Jímenez–Castillo, P. (2006b), *Archeomagnetic study of seven contemporaneous kilns from Murcia* (*Spain*), Phys. Earth Planet Int. *157*, 16–32.

Gubbins, D., Jones, A.L., and Finlay, C.C. (2006), *Fall in Earth's magnetic field is erratic*. Science. *312*. 5775, 900–902.

Haines, G.V. (1985), *Spherical cap harmonic analysis*, J. Geophys. Res. *90* (B3), 2583–2591.

Haines, G.V. (1988), *Computer programs for spherical cap harmonic analysis of potential and general fields*, Comp. Geosci. *14*. 4, 413–447.

Holzhauser, H., Magny, M., and Zümbuhl, H. (2005), *Glacier and lake–level variations in west central Europe over the last 3500 years*, Holocene *15*, 789–801.

Hongre, L., Hulot, G., and Khokhlov, A. (1998), *An analysis of the geomagnetic field over the past 2000 years*, Phys. Earth Planet. Int. *106*, 311–335.

Hulot, G. and Le Mouël, J.L. (1994), *A statistical approach to the Earth's main magnetic field*, Phys. Earth Planet. Int. *82*, 167–183.

Jackson, A., Jonkers, A.R.T., and Walker, M.R. (2000), *Four centuries of geomagnetic secular variation from historical records*, Phil. Trans. R. Soc. Lond. A *358*, 957–990.

Jonkers, A.R.T., Jackson, A., and Murray, A. (2003), *Four centuries of geomagnetic data from historical records,* Rev. Geophys. *41*, 1006, doi:10.1029/2002R G000115.

Korte, M. and Constable, C. G. (2003), *Continuous global geomagnetic field models for the past 3000 years*, Phys. Earth Planet. Inter. *140*, 73–89.

Korte, M., Genevey, A., Constable, C.G., Frank, U., and Schnepp, E. (2005), *Continuous geomagnetic field models for the past 7 millennia: 1. A new global data compilation*, Geochem. Geophys. Geosyst. *6*, Q02H15, doi:10.1029/2004GC000800.

Korte, M. and Constable, C.G. (2005), *Continuous geomagnetic field models for the past 7 millenia: 2. CALS7K*, Geochem. Geophys. Geosyst. *6*, Q02H16, doi:10.1029/2004GC000801.

Korte, M. and Constable, C.G. (2006), *Centennial to millennial geomagnetic secular variation*, Geophys. J. Int. *167*, 43–52.

Kovacheva, M., (1997), *Archaeomagnetic database from Bulgaria: The last 8000 years*, Phys. Earth Planet. Int. *102*, 145–151.

Kovacheva, M., Jordanova, N., and Karloukovski, V. (1998), *Geomagnetic field variations as determined from Bulgaria archaeomagnetic data. Part II: The last 8000 years*, Sur. Geophys. *19*, 431–460.

Lanos, Ph., *Bayesian inference of calibration curves: Application to archaeomagnetism, in Tools for constructing chronologies: Crossing disciplinary boundaries*. (vol. 177, eds. C. Buck, and A. Millard, 2004) pp. 43–82 (Springer–Verlag, London 2004).

LE MOËL, J.–L., KOSSOBOKOV, V., and COURTILLOT, V. (2005), *On long–term variations of simple geomagnetic indices and slow changes in magnetospheric currents; the emergence of anthropogenic global warming after 1990?* Earth Planet. Sci. Lett. *232*, 273–286.

MARTON, P. and FERENCZ, E. (2006), *Hierarchical versus stratification statistical analysis of archaeomagnetic directions: The secular variation curve for Hungary*. Geophys. J. Int. *164*, 484–489.

OHNO, M. and HAMANO, Y. (1993), *Spherical harmonic analysis of palaeomagnetic secular variation curves*, Central Core Earth *3*, 205–212.

PAVÓN–CARRASCO, F.J., OSETE, M.L., TORTA, J.M., GAYA–PIQUÉ, L.R., and LANOS, Ph. (2008), *Initial SCHA.DI.00 regional archaeomagnetic model for Europe for the last 2000 years*, Phys. Chem. Earth A/B/C *33*, 6–7, 596–608.

SCHNEPP, E. and LANOS, Ph. (2005), *Archaeomagnetic secular variation in Germany during the past 2500 years*, Geophys. J. Int. *163*, 479–490.

SCHNEPP, E. and LANOS, Ph. (2006), *A preliminary secular variation reference curve for archaeomagnetic dating in Austria*, Geophys. J. Int. *166* (1), 91–96.

TANGUY, J. C., LE GOFF, M., PRINCIPE, C., ARRIGHI, S., CHILLEMI, V., LADELFA, S., and PATANE, G. (2003), *Archeomagnetic dating of Mediterranean volcanics of the last 2100 years: Validity and limits*, Earth Planetary Sci. Lett. *211*, 111–124.

TEMA, E., HEDLEY, I., and LANOS, Ph. (2006), *Archaeomagnetism in Italy: A compilation of data including new results and a preliminary Italian secular variation curve*, Geophys. J. Int. *167*, 1160–1171.

THÉBAULT, E., SCHOTT, J.J., and MANDEA, M. (2006), *Revised spherical cap harmonic analysis (R–SCHA): Validation and properties*, J. Geophys. Res. *111*, B01102, doi: 10.1029/2005JB003836.

TORTA, J.M., GAYA–PIQUÉ, L.R., and DE SANTIS, A. (2006), *Spherical cap harmonic analysis of the geomagnetic field with application for aeronautical mapping*. In Rasson, J.L. and Delipetrov, T., eds., *Geomagnetics for Aeronautical Safety: A Case Study in and around the Balkans*, NATO Security Through Science Series–C, 291–307.

USOSKIN, I.G., SCHÜSSLER, M., SOLANKI, S.K., and MURSULA, K. (2005), *Solar activity, cosmic rays, and Earth's temperature: A millennium–scale comparison*, J. Geophys. Res. *110*, A10102, doi:10.1029/2004JA010946.

ZANANIRI, I., BATT, C.M., LANOS, Ph., TARLING, D.H., and LINFORD, P. (2007), *Archaeomagnetic secular variation in the UK during the past 4000 years and its application to archaeomagnetic dating*, Phys. Earth Planet. Inter. *160*, 2, 97–107.

(Received June 9, 2007, revised January 24, 2008, accepted January 24, 2008)

Capítulo 6.
Modelo Arqueomagnético Europeo SCHA.DIF.3K para los últimos 3000 años

Este capítulo lo dedicamos a un nuevo modelo regional generado a partir de datos arqueomagnéticos e instrumentales en sus localizaciones originales (datos *in situ*), además en este caso vamos a trabajar conjuntamente con los tres elementos del campo (declinación, inclinación e intensidad de forma conjunta). El nuevo modelo regional, denominado **SCHA.DIF.3K**, junto con varios ejecutables y animaciones, está disponible en la siguiente dirección web: http://pc213fis.fis.ucm.es/scha.dif.3k/index.html

6.1 Modelo geomagnético para los últimos 3000 años para la región europea: El modelo SCHA.DIF.3K.

Resumen

En este trabajo hemos usado la base europea de datos arqueomagnéticos y datos instrumentales para generar un modelo regional de campo geomagnético para Europa para los últimos 3000 años (desde el año 1000 a.C. hasta el 1900 d.D., conectándolo con la época cubierta por los modelos instrumentales IGRF). Este nuevo modelo, llamado SCHA.DIF.3K, constituye una mejora respecto al modelo regional previo SCHA.DI.00-F, ya que éste último fue generado usando datos arqueomagnéticos relocalizados y era válido sólo para los últimos dos milenios. El nuevo modelo ha sido obtenido mediante la inversión de datos paleomagnéticos haciendo uso del método de diferencias absolutas aplicando el análisis de armónicos en un casquete esférico en la parte espacial y el método de ventanas móviles para la parte temporal. Para poder modelar los tres elementos del campo geomagnético, declinación, inclinación e intensidad hemos desarrollado los algoritmos correspondientes. El modelo resultante permite conocer tanto la dirección como la intensidad del campo geomagnético en cualquier punto de Europa y también valido para el oeste de Asia y el norte de África (últimos 3000 años). El modelo regional se ajusta mejor a la base de datos arqueomagnéticos que los modelos globales. Además, el nuevo modelo generado representa un paso más en el desarrollo de la datación arqueomagnética ya que hemos eliminado el proceso de relocalización y, por tanto, eliminado una fuente de error del método clásico de datación. Por otra parte, permite utilizar la técnica en cualquier punto de la región incluida en el casquete esférico. Por último, el modelo ha sido utilizado para analizar las variaciones del campo geomagnético, en concreto los denominados recientemente jerks arqueomagnéticos (variaciones bruscas del campo geomagnético).

Geochemistry Geophysics Geosystems G3
AN ELECTRONIC JOURNAL OF THE EARTH SCIENCES
Published by AGU and the Geochemical Society

Article
Volume 10, Number 3
25 March 2009
Q03013, doi:10.1029/2008GC002244
ISSN: 1525-2027

Click Here for Full Article

A regional archeomagnetic model for Europe for the last 3000 years, SCHA.DIF.3K: Applications to archeomagnetic dating

F. Javier Pavón-Carrasco and Maria Luisa Osete
Grupo de Paleomagnetismo, Departamento de Geofísica y Meteorología, Universidad Complutense de Madrid, E-28040 Madrid, Spain (fjpavon@fis.ucm.es; mlosete@fis.ucm.es)

J. Miquel Torta
Observatori de l'Ebre, CSIC, Universitat Ramon Llull, Horta Alta 38, E-43520 Roquetes, Spain (jmtorta@obsebre.es)

Luis R. Gaya-Piqué
Equipe de Géomagnétisme, Institut de Physique du Globe de Paris, CNRS, Tour 14, 2 place Jussieu, F-75005 Paris, France (gaya@ipgp.jussieu.fr)

[1] The available European database of archeomagnetic field values and instrumental data has been used to produce a regional model for the geomagnetic field in Europe for the last 3000 years (from 1000 B.C. to 1900 A.D., connecting with the epoch covered by the IGRF models). This new model, SCHA.DIF.3K, constitutes an improvement with respect to the previous regional archeomagnetic model SCHA.DI.00-F, which used relocated values and was only valid for the last 2000 years. The new model has been obtained by least sums of absolute deviation inversion of paleomagnetic data using spherical cap harmonics for the spatial representation of the field and sliding windows in time. An algorithm has been developed to jointly model the three archeomagnetic elements declination, inclination, and intensity. The resulting model provides the direction and intensity of the Earth's magnetic field over the European continent, northern Africa, and western Asia for the last 3000 years. The fit to the European archeomagnetic database is more accurate than that provided by global archeomagnetic models. In addition, this model represents a step forward in archeomagnetic dating studies (since the relocation error is avoided) and can also be used to study the rapid changes of the geomagnetic field (archeomagnetic jerks) that have been recently proposed.

Components: 11,416 words, 10 figures, 4 tables.

Keywords: Archaeomagnetism; geomagnetic secular variation; regional models; archaeomagnetic dating; archaeomagnetic jerks; Europe.

Index Terms: 1503 Geomagnetism and Paleomagnetism: Archeomagnetism; 1522 Geomagnetism and Paleomagnetism: Paleomagnetic secular variation; 1532 Geomagnetism and Paleomagnetism: Reference fields: regional, global.

Received 12 September 2008; **Revised** 15 January 2009; **Accepted** 6 February 2009; **Published** 25 March 2009.

Pavón-Carrasco, F. J., M. L. Osete, J. M. Torta, and L. R. Gaya-Piqué (2009), A regional archeomagnetic model for Europe for the last 3000 years, SCHA.DIF.3K: Applications to archeomagnetic dating, *Geochem. Geophys. Geosyst.*, *10*, Q03013, doi:10.1029/2008GC002244.

Geochemistry Geophysics Geosystems G3 PAVÓN-CARRASCO ET AL.: SCHA.DIF.3K EUROPEAN ARCHEOMAGNETIC MODEL 10.1029/2008GC002244

1. Introduction

[2] Paleosecular variation (PSV) describes the long-term temporal changes of the Earth's ancient magnetic field. The study of this variation improves our knowledge about the behavior of the magnetic field and the dynamics of the Earth's core.

[3] To define the geomagnetic field at any location three independent elements are needed. Several combinations are possible, but the measurements made most commonly in historical times were declination (*D*), inclination (*I*), and total intensity (*F*).

[4] Instrumental measurements of the directional (declination and inclination) Earth's magnetic field are available for the last few centuries, e.g., at London, 1570–1900 A.D. [*Malin and Bullard*, 1981]. Early historical measurements do not come from observatories, not even from single same locations, since permanent geomagnetic observatories were not established until the 19th century. These historical data sets are complemented by measurements of declination (mostly) and inclination for shipboard navigational purposes since the end of the 16th century [*Jackson et al.*, 2000; *Jonkers et al.*, 2003]. Instrumental intensity data are scarcer, the first measurements being taken in 1832 A.D. when Gauss invented a method for determining the absolute intensity values. For times prior to instrumental values, paleomagnetic data are needed. These data can be obtained from heated archeological structures (archeomagnetic data), from well-dated volcanic materials (lava flows), and from lake sediments which are well dated and undisturbed. Archeomagnetic data provide both directional and intensity data, whereas lake sediments contribute with directions and relative intensity only.

[5] Global models based on archeomagnetic data have been obtained during the last decade by using the Spherical Harmonic Analysis (SHA) technique, like the one proposed by *Hongre et al.* [1998], and the CALS family of models [*Korte and Constable*, 2003, 2005], which also includes lava flows and lake sediments as input data. These models represent the paleofield at a global scale, but they are usually too smooth to be used as a tool for archeomagnetic dating and to record rapid changes of the Earth's magnetic field (i.e., archeomagnetic jerks [*Gallet et al.*, 2003, 2005]).

[6] There are different reasons for the smoothness of the global models. For example in the model of *Hongre et al.* [1998] the smoothness is due to the small number of paleomagnetic data, and their inhomogeneous distribution around the globe. For the CALS models a trade-off was imposed between both spatial and temporal smoothness and fit to the global data, leading to a damping of variations also in regions and at times with dense data coverage. Very recently [*Lodge and Holme*, 2009], a test has been presented to demonstrate the feasibility of using the same regularized inversion strategy as in the CALS family to generate a viable regional dating tool. However, a definitive model still remains to be built.

[7] A possible solution to describe more accurately the long-term geomagnetic variations comes from the construction of Paleosecular Variation Curves (PSVC). These curves are the classical approach used by paleomagnetists to study the PSV in a region. To build a PSVC, a high density of well distributed in time paleomagnetic data from a small region (usually less than 600–900 km radius) are needed. The archeomagnetic data are then transferred from the sampling place to a reference point by the Conversion Via Pole method (CVP [*Noël and Batt*, 1990]). This relocation process introduces an error that, for the present geomagnetic field, increases with the relocation distance (a maximum of 7° for a 1700 km radius [*Casas and Incoronato*, 2007]).

[8] An intermediate approach between global models and PSVC is the determination of regional models. When analyzing the recent paleomagnetic compilations [e.g., *Korte et al.*, 2005] for the last 3000 years, it is observed that data are not homogeneously distributed around the globe, and the European continent is the region where the highest density of paleomagnetic data (mostly archeomagnetic data) is available: about 198 data/km^2 compared to 41 data/km^2 (Meso-America), 30 data/km^2 (North America), 23 data/km^2 (Asia), 3 data/km^2 (Oceania) and 1 data/km^2 (Africa) (values from *Korte et al.* [2005] and the updated European data set). *Korte et al.* [2005] show the temporal evolution of these data for each region or continent. Consequently a regional model at the European scale seems to be a realistic objective.

[9] In a recent paper, we proposed an initial regional model (the SCHA.DI.00 model [*Pavón-Carrasco et al.*, 2008a]) to describe the directional behavior of the paleomagnetic field in Europe for the last 2000 years, which was afterward updated by also modeling the paleointensity (the SCHA.DI.00-F model [*Pavón-Carrasco et al.*, 2008b]). The

SCHA.DI.00 and SCHA.DI.00-F models were developed using the spherical cap harmonic analysis technique (SCHA [*Haines*, 1985]) applied to directional data from five of the Bayesian European PSVC based on archeomagnetic data [*Pavón-Carrasco et al.*, 2008a, and references therein]. The intensity was added from the recent European paleointensity data set. These regional models seem to better reproduce the variability of the geomagnetic field over this region for the last 2000 years. However, the use of the PSVC as input data implied the inclusion of the relocation error into those models.

[10] In this paper, we propose a new regional archeomagnetic model for the European continent valid for the last 3000 years (1000 B.C. to 1900 A.D.): the SCHA.DIF.3K model (SCHA is the technique used to develop the model, D comes for declination, I for inclination, F for intensity, and 3K stands for the last 3000 years). Only archeological material has been used as input data because of the stability and origin of its remanence, commonly a thermoremanence (TRM) or a partial thermoremanence (pTRM) and because of the facility of some archeological materials to be accurately dated. Since the remanence acquisition mechanism for lake sediments is depositional (or postdepositional) a delay in the remanence acquisition time is expected. In addition, there seems to be some discrepancy in the determination of the paleointensity between the archeomagnetic and the lava flow records (M. Kovacheva, personal communication, 2008). For this reason we opted to use an internally consistent database, and therefore decided not to use any lake sediment and lava flow data in our study.

[11] The main differences between the SCHA.DIF.3K model and the initial SCHA.DI.00-F model [*Pavón-Carrasco et al.*, 2008b] are as follows:

[12] 1. For the input data, we have used the complete (with measurements up to 2007) ''in situ'' archeomagnetic data and three time series of historical observations of geomagnetic field directions, which we have denoted as ''instrumental database.'' By using ''in situ'' data, the model is not affected by the relocation error. The instrumental database includes time series covering the last 4 centuries (from 1600 A.D. to 1900 A.D.) located in three western European countries (the United Kingdom, France and Italy).

[13] 2. The new model has been developed by jointly modeling the three archeomagnetic components (declination, inclination, and intensity). This model is more coherent than the previous regional models, for which in a first step the directional geomagnetic model was developed, and in a second step the intensity was added [see *Pavón-Carrasco et al.*, 2008a, 2008b].

[14] 3. The valid time period has been increased by 1000 years: from 1000 B.C. to 1900 A.D. (the SCHA.DI.00-F model was only valid from year 0 onward).

[15] The paper finishes with a demonstration of the main utility of the model as a tool for archeomagnetic dating and for the analysis of the rapid changes of the geomagnetic field (i.e., the so-called archeomagnetic jerks [*Gallet et al.*, 2003, 2005]) over the last three millennia.

2. Methodology

2.1. SCHA Technique

[16] The spherical cap harmonic analysis (SCHA) presented by *Haines* [1985] has been applied in many different studies [*Torta et al.*, 2006, and references therein]. The technique has been revised by *Thébault et al.* [2006] developing a new technique called revised spherical cap harmonic analysis (R-SCHA), for which a complete boundary value problem is solved. This method represents the magnetic field in a closed conical domain by a complete family of functions. The R-SCHA technique is an exact mathematical method, but the numerical problems are difficult to solve when only ground data are used. Very recently a new method (R-SCHA2D) for regional modeling of geomagnetic data over a spherical cap and at a constant altitude by using R-SCHA has been proposed [*Thébault*, 2008]. A further development of our work will be the study of the differences in the model results by using R-SCHA2D instead of SCHA.

[17] Some modelers prefer to use SHA with a regularized inversion strategy because of the following inherent limitations to SCHA: spatial structure limited by both the average minimum wavelength considered resolvable and by the shape of the limited number of basis functions, and difficulty to adapt the basis functions to irregular distributions of data within the cap. In regularized global inversions, the structure is constrained to minimize a specific measure of complexity in the field, and it is inherently adaptive to provide simple models in regions with few data. In our study, we

Geochemistry Geophysics Geosystems G3 PAVÓN-CARRASCO ET AL.: SCHA.DIF.3K EUROPEAN ARCHEOMAGNETIC MODEL 10.1029/2008GC002244

decided to follow the classical approach by *Haines* [1985], accepting the limitations of SCHA and the fact that the model cannot be extrapolated outside the limits of the cap. To model irregular distributions of data within the cap it is necessary to use a low maximum degree of the expansion. This low degree produces a spatial resolution for the regional archeomagnetic model that could be not too different from that of global models. On the other hand, the SCHA technique imposes an artificial conical boundary and it is not possible to study the power spectrum of the field and its behavior at the core-mantle boundary. In spite of these limitations, we think that a regional approach could better reproduce the variability of the geomagnetic field in Europe.

[18] The SCHA (and the R-SCHA) technique satisfies the Laplace equation and therefore we prefer to use this technique rather than other regional techniques (polynomial or spline modeling). The general solution that satisfies the conditions imposed by Laplace's equation is expressed for a spherical cap by an expansion in terms of spherical harmonics. The internal geomagnetic potential is:

$$V(r,\theta,\lambda) = a\sum_{k=0}^{K_{\text{int}}}\sum_{m=0}^{k}\left(\frac{a}{r}\right)^{n_k+1} P_{n_k}^{m}(\cos\theta) \cdot \left(g_{n_k}^{m}\cos m\lambda + h_{n_k}^{m}\sin m\lambda\right) \quad (1)$$

where $P_{nk}^{m}(\cos\theta)$ are the colatitudinal Legendre functions, $\left(\frac{a}{r}\right)^{n_k+1}$ is the radial dependence (with r the radial distance and a the mean radius of the Earth) and $\cos m\lambda$, $\sin m\lambda$ the longitudinal Fourier functions. g_k^m and h_k^m are the model's coefficients (SCH coefficients). The K_{int} parameter is the maximum degree of the expansion. The indices m and k are integers and the index $n_k(m)$ is real.

[19] In paleomagnetic studies, the elements usually determined for a given location are the declination, the inclination and the intensity. These components cannot be expressed by a linear combination of SCH coefficients. In the next section we will describe how we have solved this problem of linearization.

2.2. SCHA Applied to Directional and Intensity Data

[20] To express the archeomagnetic data as a linear function of the SCH coefficients, we have used the truncated Taylor's series applied to the expressions of the relationship between the declination, inclination and intensity and the Cartesian components of the geomagnetic field:

$$D = \arctan\left(\frac{Y}{X}\right)$$
$$I = \arctan\left(\frac{Z}{\sqrt{X^2+Y^2}}\right)$$
$$F = \sqrt{X^2+Y^2+Z^2} \quad (2)$$

[21] Expanding the series and taking into account equation (2), we obtain the general expression for the elements of the geomagnetic field:

$$\alpha(r,\theta,\lambda,t) = \alpha_0(r,\theta,\lambda,t) + \delta\alpha(r,\theta,\lambda,t) = \alpha_0(r,\theta,\lambda,t) + \left.\frac{\partial\alpha(r,\theta,\lambda,t)}{\partial g}\right|_{\alpha=\alpha_0}\cdot\delta g(t) \quad (3)$$

α (r, θ, λ, t) is the studied archeomagnetic element (declination, inclination or intensity), α_0 (r, θ, λ, t) is the initial value of the element given by a reference geomagnetic field. The variation of the element $\delta\alpha$ (r, θ, λ, t) is given by its derivative with respect to the SCH coefficients and their variation δg(t).

[22] The values of the derivatives of the archeomagnetic element by the SCH coefficients depend only on the initial reference field α_0 (X_0, Y_0 and Z_0):

$$\delta D = \frac{1}{H_0^2}\left(-Y_0\cdot\left(A_X^g, A_X^h\right) + X_0\cdot\left(A_Y^g, A_Y^h\right)\right)\cdot\delta g$$
$$\delta I = \frac{1}{F_0^2}\left(-\frac{Z_0X_0}{H_0}\left(A_X^g, A_X^h\right) - \frac{Z_0Y_0}{H_0}\left(A_Y^g, A_Y^h\right) + H_0\left(A_Z^g, A_Z^h\right)\right)\cdot\delta g$$
$$\delta F = \frac{1}{F_0}\left(X_0\left(A_X^g, A_X^h\right) + Y_0\left(A_Y^g, A_Y^h\right) + Z_0\left(A_Z^g, A_Z^h\right)\right)\cdot\delta g \quad (4)$$

where H_0 is the horizontal intensity and F_0 the total intensity of the reference geomagnetic field, and:

$$\left(A_X^g, A_X^h\right) = \sum_{k=0}^{K_{\text{int}}}\sum_{m=0}^{m=k}\left(\frac{a}{r}\right)^{n+2}\frac{dP_{n_k}^{k}(\cos\theta)}{d\theta}(\cos\lambda, \sin\lambda)$$
$$\left(A_Y^g, A_Y^h\right) = \sum_{k=0}^{K_{\text{int}}}\sum_{m=0}^{m=k}\left(\frac{a}{r}\right)^{n+2}\frac{m\cdot P_{n_k}^{k}(\cos\theta)}{\sin\theta}(\sin\lambda, -\cos\lambda)$$
$$\left(A_Z^g, A_Z^h\right) = \sum_{k=0}^{K_{\text{int}}}\sum_{m=0}^{m=k}\left(\frac{a}{r}\right)^{n+2}(n+1)P_{n_k}^{k}(\cos\theta)(-\cos\lambda, -\sin\lambda) \quad (5)$$

[23] There is an equation for every archeomagnetic data (declination, inclination or intensity) according to equations (4). These equations present spatial and temporal dependence.

[24] Before solving the problem, it is necessary to transform the coordinate system and the geomag-

netic elements to the SCHA reference frame. Two rotations are needed. First, we have transformed the coordinates and geomagnetic elements from geodetic (denoted by subscript gd) to geocentric (subscript gc). After this, we have rotated both coordinates and elements to the cap frame (subscript sch).

[25] For the first rotation, the geodetic longitude and the intensity are invariant; i.e., $\lambda_{gd} = \lambda_{gc}$ and $F_{gd} = F_{gc}$. To transform from geodetic to cap's coordinates the intensity changes along with radius but it is a small effect that cannot be taken account of by the SCH model since it needs data at uniform radius. To obtain the new geocentric colatitude (θ_{gc}), the radial distance (r_{gc}), the declination (D_{gc}) and the inclination (I_{gc}) one can easily adapt the subroutines given by *Haines* [1988]. It should be borne in mind that (1) for the pair declination-inclination, the transformation does not depend on the intensity value and (2) for single inclination values (without declination) we have associated a value to the declination equal to 0°. The maximum error made using this zero value for declination is very low (we have tested this error with synthetic data and it is lower than 0.02°).

[26] For the second rotation the radial distance, the inclination and the intensity are invariant ($r_{gc} = r_{sch}$, $I_{gc} = I_{sch}$ and $F_{gc} = F_{sch}$). The remaining coordinates (longitude λ_{sch} and colatitude θ_{sch}) and the declination (D_{sch}) can be transformed according to *De Santis et al.* [1989]:

$$\begin{aligned}\cos\theta_{sch} &= \cos\theta_0\cos\theta_{gc} + \sin\theta_0\sin\theta_{gc}\cos(\lambda_{gc}-\lambda_0)\\ \tan\lambda_{sch} &= \frac{-\sin\theta_{gc}\sin(\lambda_{gc}-\lambda_0)}{\sin\theta_0\cos\theta_{gc} - \cos\theta_0\sin\theta_{gc}\cos(\lambda_{gc}-\lambda_0)}\\ \tan D_{sch} &= \frac{\tan D_{gc} - \tan\alpha}{1+\tan D_{gc}\cdot\tan\alpha}\end{aligned} \tag{6}$$

where θ_0 and λ_0 are the cap's center coordinates and α is the angle between the north direction and the cap's center direction. This is given by:

$$\cos\alpha = \frac{\cos\theta_0 - \cos\theta_{gc}\cos\theta_{sch}}{\sin\theta_{gc}\sin\theta_{sch}} \tag{7}$$

2.3. Inversion Method

[27] To find the SCH coefficients that minimize the misfit we have to choose an appropriate inversion scheme. In a first attempt we used the classical iterative least squares (LS, L2 norm) inversion method. However, a detailed study of the error distribution showed that this distribution was not Gaussian but double exponential, so the use of the L2 norm was formally inappropriate. Therefore, and following the suggestion by an anonymous referee, we used the iterative least sums of absolute deviation (LAD, L1 norm) inversion. Differences between the L1 and L2 norms are related to the way the outliers are penalized. The L1 norm penalizes the outliers more than the L2 norm, so the residual data distribution is sharper. This type of distribution is called the Laplace (or double exponential) distribution.

[28] The LAD method is based in minimizing the absolute difference between real and modeled data. Taking into account the global data uncertainty (measurement uncertainty and time uncertainty) of the data (σ_i^{obs}), we have to minimize the function (χ_{L1}):

$$\chi_{L1}(t,a) = \sum_{i=1}^{n}\left\|\frac{x_i^{obs}(t,a) - x_i^{\mathrm{mod}}(t,a)}{\sigma_i^{obs}}\right\| \tag{8}$$

where t is the time, a is the location, $x_i^{obs}(t, a)$ is the real datum and $x_i^{mod}(t, a)$ is the modeled datum.

[29] For the inverse problem, we used an iterative approach. First we used an initial model as a reference model or input model (indicated by the subscript 0 in equation (4)) to obtain a new model by minimizing the equation (8). This new model will be used as the input model for a second iteration, and so on for successive iterations. The RMS error for each component of the geomagnetic field has been obtained taking into account the weight of the data $w_i^{obs} = 1/\sigma_i^{obs}$ (the weighting of the data is discussed in section 3.4):

$$rms = \sqrt{\frac{\sum_{i=1}^{n} w_i^{obs}\left(x_i^{obs} - x_i^{\mathrm{mod}}\right)^2}{\sum_{i=1}^{n} w_i^{obs}}} \tag{9}$$

[30] To solve the inverse problem for the temporal part, we have used a sliding windows technique, which is similar to the classical approach to construct paleosecular variation curves. The size of the window is related to the temporal data distribution and the age uncertainties. For each window, we have considered that each SCH coefficient ($g_i(t)$) can be defined by a cubic polynomial function, i.e., for the window i the SCH coefficients are given by:

$$g_i(t) = \sum_{p=0}^{3} g_{i,p}\cdot\left(\frac{t-t_0}{s}\right)^p \tag{10}$$

Geochemistry Geophysics Geosystems G3 PAVÓN-CARRASCO ET AL.: SCHA.DIF.3K EUROPEAN ARCHEOMAGNETIC MODEL 10.1029/2008GC002244

where t_0 is the central time of the window and s the size of the window. Thus, a spatial-temporal SCHA model was constructed for every s-year window. Finally, for every window we only took into account the $g_{i,0}$ parameter, so the resultant only spatial model is assumed valid for the center of the window (time t_0). This main $g_{i,0}$ coefficient is conditioned by all the remaining data into the window. The relation between two sets of consecutive SCH coefficients is smooth, because the windows are overlapping (in our case, we used a step of s/2). The size of the windows and the overlapping step conditioned the temporal resolution of the model. To evaluate how the sliding overlapping windows method affects the modeling results, we have carried out a test using synthetic data from the IGRF model at the same locations as those used in the archaeomagnetic database, and with similar dispersions and uncertainties. Results show that the variations (generated by the sliding windows method) are lower than the real variations given by the SCHA.DIF.3K model (especially for the inclination and intensity values). The temporal resolution, using the sliding windows method, is given by the time distance between 4 consecutive windows. In our case the window is overlapping s/2 years, so the temporal resolution is 3s/2.

3. Database and Input Data

3.1. Archeomagnetic Database

[31] We have used a recent data set of archeomagnetic data for Europe for the last 3000 years. The data set is based essentially on the database of *Korte et al.* [2005], (which consists of globally distributed paleomagnetic data). We have selected only the archeomagnetic data in the considered region (a cap of semiangle 40° center at 48°N and 9°E, i.e., Europe, north of Africa and west of Asia), excluding data from lava flows and sediments.

[32] From 2005 new data have been included in the database, largely because of the AARCH Network Project. These new data correspond to different European countries. For the directional data: Austria [*Schnepp and Lanos*, 2006], Germany [*Schnepp and Lanos*, 2005], Hungary [*Márton and Ferencz*, 2006], France [*Chauvin et al.*, 2000], Italy [*Evans and Hoye*, 2005; *Tema et al.*, 2006], Spain [*Gómez-Paccard et al.*, 2006a; *Ruíz-Martínez et al.*, 2008; G. Catanzariti, personal communication, 2008] and Greece [*Evans*, 2006]. And for the intensity: France [*Gallet et al.*, 2005] and Spain [*Gómez-Paccard et al.*, 2006c]. The initial number of the directional paleomagnetic data considered is 1464 for declination and 2018 for inclination. Intensity data also come from archeomagnetic artifacts. The initial number of archaeointensity data is 927.

[33] We have applied a filter based on the statistical uncertainty of directional paleomagnetic data. The precision of directional data is given by the parameter α_{95}° (value for the 95% confidence cone about the mean direction). The intensity data has precision given by the parameter σ_F. We have rejected all data whose $\alpha_{95°}$ is three times bigger than the mean $\alpha_{95°}$. A similar criterion has been applied to intensity data (three times the mean σ_F). After applying this filter, we have rejected 26 directional data (1 from Poland, 6 from Russia, 5 from Ukraine, 10 from United Kingdom, 2 from Germany, and 2 from Italy) and 12 intensity data (3 from Slovakia, 1 from France, 1 from Serbia, 3 from Egypt, 3 from United Kingdom, and 1 from Russia). The mean values of $\alpha_{95°}$ and σ_F are 4.1° and 3.3 μT, respectively. We have also rejected those data with age uncertainties greater than 500 years (9 data from United Kingdom and 3 from Hungary).

[34] The definitive archeomagnetic database consists of 1437 declination data, 1979 inclination data and 913 intensity data.

3.2. Distribution of Archeomagnetic Input Data

[35] Figure 1 shows the spatial distribution of the archeomagnetic data (declination, inclination and intensity) used as input data for the time interval 1000 B.C. to 1900 A.D. The distribution of data in Europe is inhomogeneous, so in order to visualize the number of data in every region we have represented the spatial distribution of the data according to the latitude and longitude coordinates relative to the cap's center: 48°N latitude and 9°E longitude (orange lines in Figure 1).

[36] The colatitudinal distribution (Figure 2a) of declination and inclination are similar. Both show that the data are distributed inside a cap with semiangle 22° (except for some inclination data, up to 25° away from the cap center). A higher data density is found between 3° and 15° of colatitude, marked with high peaks between 5° and 10°. The inclination registers two other maxima in the number of data at about 11° and 19° of colatitude (corresponding to Bulgarian and eastern European data respectively). Intensity data are concentrated between 11° and 15° of colatitude. There is a second smaller concentration peak around 7°

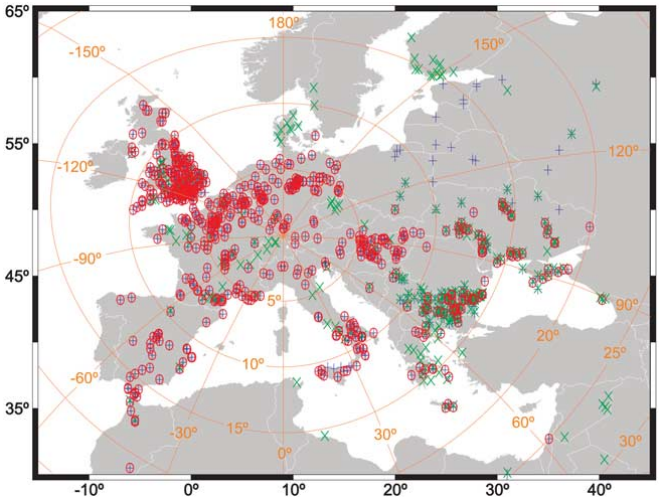

Figure 1. Locations of input data. Declination (red circles), inclination (blue pluses), and intensity (green crosses). Orange grid shows colatitude and longitude relative to the cap's center (48°N, 9°E).

corresponding to Hungarian data. The furthest data are about 28° away from the center of the cap (Middle East).

[37] Figure 2b shows the longitudinal distribution of the data. Again, both declination and inclination distributions are similar. The western European data (negative longitudes) are almost identical, so it is obvious that declination data have inclination data associated. For positive longitudes, i.e., eastern Europe, the number of inclination data is higher than declination data. France and the United Kingdom (about −125° longitude) in the western part of the cap, and Bulgaria and Hungary (between 60° to 90° of longitude) in the eastern part have the highest concentration of archeomagnetic directional data.

[38] The spatial distribution of the intensity data of Figure 2b is very significant since it shows the elevated difference between the number of intensity data from western and eastern Europe. From the 927 initial intensity data, only 139 data are from western countries. This may have consequences for the development of the regional model, because the east intensity data are predominant over the rest of the intensity data. The highest concentration of intensity data are in Greece (50° longitude), Bulgaria (about 70° longitude), and Hungary (90° longitude).

[39] The temporal distribution of data (Figure 2c) shows a high density in the Roman period (between 100 B.C. and 500 A.D.) and between the 9th and 19th centuries A.D. There is a decrease in the density of data for 500–1000 A.D. (the so-called "Dark Ages"). There are more intensity data than directional data before 100 B.C.

[40] In the time interval 1000 B.C. to 1900 A.D., the declination ranges in Europe between −33.7° and 42.9° with an average uncertainty of 4.6° and a standard deviation of 2.5°. Inclination varies between 32.5° and 86.0°, with a mean uncertainty of 2.3° and a standard deviation of 1.1°. The upper and lower limits of intensity are 33.0 μT and 101.0 μT, with 3.4 μT and 2.0 μT of mean uncertainty and standard deviation respectively. The mean age uncertainty for all data is 53.0 years with a standard deviation of 67.0 years. All data uncertainties are given at 68% of confidence.

3.3. Instrumental Data

[41] We have included three historical time series of the direction of the Earth's magnetic field for the last 400 years (∼1600–1900 A.D.) located at London, Paris and many Italian localities (Figure 3). The first series is given by the compilation of *Malin and Bullard* [1981], which reports the direction of the Earth's magnetic field at London from 1570 to

Geochemistry Geophysics Geosystems G3 PAVÓN-CARRASCO ET AL.: SCHA.DIF.3K EUROPEAN ARCHEOMAGNETIC MODEL 10.1029/2008GC002244

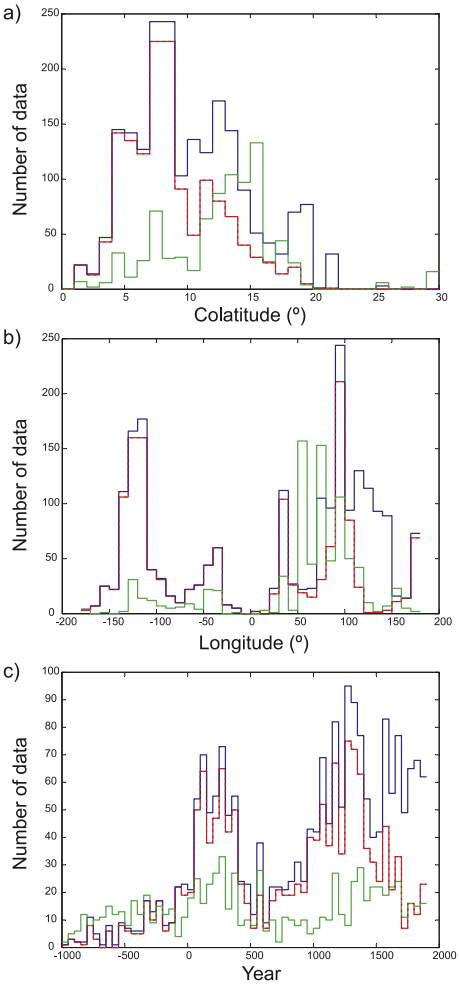

Figure 2. Histograms of declination (red), inclination (blue), and intensity (green) data through (a) colatitude, (b) longitude, and (c) time. Both colatitude and longitude are referred to the cap's center (orange grid in Figure 1). The size of the bins are 1° for colatitude, 10° for longitude, and 50 years for time.

1975 A.D. *Alexandrescu et al.* [1996] compiled the instrumental series of the geomagnetic field direction in Paris (from ~1550 to 1994 A.D.). Finally, the instrumental series from Italy includes historical measurements at many localities since 1640 [*Cafarella et al.*, 1992, and references therein], complemented by the records of the Pola observatory (north of Italy, nowadays in Croatia, from 1881 to 1909 A.D.).

[42] We have assigned a constant value to the uncertainties of the instrumental series. The observatory directional data used have not been corrected for crustal anomalies and they may present an error related to correlation. According to this reason the use of original uncertainties is not appropriate. *Jackson et al.* [2000] indicated that the use of different observation sites can generate about 0.5° noise in the observations, so in order to solve this problem we have assigned a constant uncertainty of 0.5° for all declination and inclination instrumental data.

[43] We have not used instrumental intensity data because they start progressively from 1832 A.D. onward, while our model has an upper limit at 1900 A.D.

[44] Figure 3 shows all instrumental series, which have been reduced (we have used the relocated data as given in the original works) to three reference points (London coordinates for the first series: 51.5°N latitude and 0.1°W longitude), Paris (48.1°N, 2.3°E) for the second and Viterbo (42.5°N, 12.0°E) for the Italian series). They are

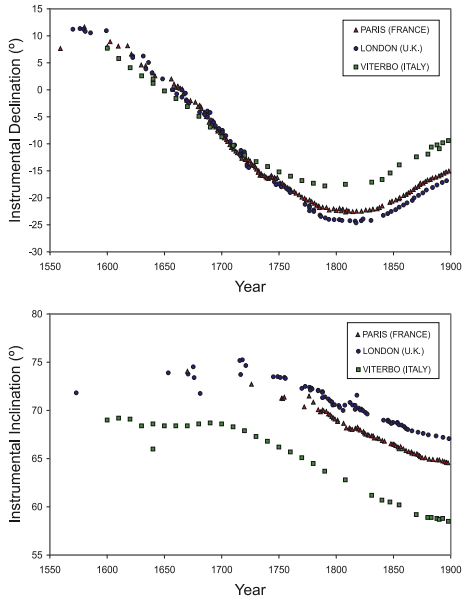

Figure 3. Series of directional instrumental data. All data have been reduced to the reference point (see legend).

in general annual mean values. We have analyzed the relocation error for the three time series: The directional Italian data set comes from many locations distributed all over the country. Using the synthetic data from the GUFM model [*Jackson et al.*, 2000] we have calculated the relocation error for all time interval (1600–1900 A.D.); this error is lower than 0.2° for the declination and 0.1° for the inclination. The French and English data sets are distributed very near to the reference location. We have also calculated the relocation error using GUFM model for the corresponding time interval. These errors are close to zero (0.07° and 0.03° for declination and inclination respectively).

3.4. Weighting of the Data

[45] We have added an additional uncertainty (τ_i) to the measurement uncertainty (ρ_i) depending on the age uncertainty value, applying the same criteria as in the work by *Korte et al.* [2005] but modified because of the use of sliding windows; the final uncertainty is therefore the square root of the sum of the squares of the measurement uncertainty (ρ_i) and the uncertainty associated to age (τ_i). The value of τ_i for each datum has been normalized according to the following scheme. Each datum is given by a mean age t_0 and an age uncertainty t_m, so it spreads over the whole time interval: $[t_0 - t_m, t_0 + t_m]$. To take this into account in the model, we normalized the uncertainty by introducing a factor depending on the location of the datum inside the temporal window. There are 4 possible cases for a window limited by $[t_1, t_2]$.

[46] 1. The datum is completely within the time window: $t_1 < t_0 - t_m$ and $t_0 + t_m < t_2$. In this case the normalization factor is 1. The datum mean age is given by t_0.

[47] 2. Part of the datum is within the window. There are two types: (1) If $t_0 - t_m < t_1$ and $t_0 + t_m < t_2$, the normalization factor is given by $f = 2 \cdot t_m/(t_0 + t_m - t_1)$, and the datum mean age is $(t_0 + t_m + t_1)/2$. (2) If $t_1 < t_0 - t_m$ and $t_0 + t_m > t_2$, the normalization factor is given by $f = 2 \cdot t_m/(t_2 - t_0 + t_m)$, and the mean age is $(t_2 + t_0 - t_m)/2$.

[48] 3. Finally, if $t_0 - t_m < t_1$ and $t_2 < t_0 + t_m$, the normalization factor is $f = 2 \cdot t_m/(t_2 - t_1)$, and the datum mean age is given by the mean time of the window, $(t_1 + t_2)/2$.

[49] Therefore, the final uncertainty (σ_i) is given by:

$$\sigma_i = f \cdot \left(\rho_i^2 + \tau_i^2\right)^{1/2} \tag{11}$$

and the weight of the datum is given by the inverse of the uncertainty:

$$w_i = \frac{1}{\sigma_i} = \frac{1}{f} \cdot \left(\rho_i^2 + \tau_i^2\right)^{-1/2} \tag{12}$$

4. Model Parameters and Result: SCHA.DIF.3K Model

4.1. Model Parameters

[50] Previous studies have shown that, in order to produce a spatial-temporal model from archeomagnetic data using SCHA it is necessary to consider relatively large size caps and a low degree spherical harmonic expansion [*Pavón-Carrasco et al.*, 2008a]. In this new study we keep the same maximum spherical cap harmonic index that was used for the initial model built from the European PSVC [*Pavón-Carrasco et al.*, 2008a], i.e., K = 2. Given the size of the spherical cap used ($\theta_0 = 40°$) and the maximum data resolution, the model represents the same spatial wavelength as a global (SHA) model with maximum degree n = 5.

[51] Taking into account the spatial distribution of data, the cap has been situated centered on Austria, at 48°N latitude and 9°E longitude (see Figure 1). The temporal distribution of data and the associated age uncertainty have conditioned the size of the windows for the temporal expression of the inverse problem. The optimal size of the window is 50 years, because the mean age uncertainty is 53 years. Within each window there are, on average, 29 declination data, 38 inclination data, and 15 intensity data (see Figure 2c), except for two windows which have no declination values (750 B.C. to 700 B.C., and 650 B.C. to 600 B.C.).

[52] For each time window we have applied a spatial-time fitting by the iterative LAD technique using equations (8) and (10). By moving the window at 25 years steps from 1000 B.C. to 1900 A.D., we obtain 117 sets of SCH coefficients.

4.2. Input Models

[53] To obtain the new regional model, we have used two initial reference models (these models are only used in the first iteration) for two time intervals: the SCHA.DI.1-F from 1000 B.C. to 1650 A.D., and the GUFM model [*Jackson et al.*, 2000] from 1650 to 1900 A.D.

[54] The SCHA.DI.1-F is an extension of the SCHA.DI.00-F, since the previous has a temporal

Geochemistry Geophysics Geosystems G3 PAVÓN-CARRASCO ET AL.: SCHA.DIF.3K EUROPEAN ARCHEOMAGNETIC MODEL 10.1029/2008GC002244

Table 1. Number of Initial and Rejected Data

Component	Initial Number of Data	Rejection Criterion	Number of Rejected Data	% of Rejected Data
Declination	1437	$\sigma_D > 3 \cdot 4.9°$	89	6.2%
Inclination	1979	$\sigma_I > 3 \cdot 2.9°$	114	5.8%
Intensity	913	$\sigma_F > 3 \cdot 6.6\ \mu T$	24	2.6%

validity from 0 to 1900 A.D. To build the new model, SCHA.DI.1-F, valid from 1000 B.C. up to 1900 A.D., we have used the European PSVC from 1000 B.C. to 0 (France [*Gallet et al.*, 2002], Germany [*Schnepp and Lanos*, 2005], Hungary [*Márton and Ferencz*, 2006], Iberia [*Gómez-Paccard et al.*, 2006b], and the United Kingdom [*Zananiri et al.*, 2007]) and applied the same procedure described by *Pavón-Carrasco et al.* [2008a, 2008b].

[55] From 1650 A.D. onward we used the GUFM model because this model appears to be the most suitable one after the 17th century. The model has been modified with a new value for the first Gauss coefficient g_1^0 from 1590 A.D. to 1840 A.D. given by *Gubbins et al.* [2006]; the modification thus applies only to the prediction of the intensity before 1840 A.D.

[56] The change in initial reference models was chosen at 1650 A.D. because the minimum difference between both models occurs at this epoch [*Pavón-Carrasco et al.*, 2008a, 2008b]. To estimate the difference between the SCHA.DI.1-F and the modified GUFM model at 1650 A.D. we have calculated the difference between predicted data from both models at the location of the input data from 1625 A.D. to 1675 A.D. Declination shows the most abrupt change, the main difference being 4.7° with a deviation of 3.2°. The differences for inclination and intensity are more reasonable: 1.9° ± 1.0° and 2.2 μT ± 1.5 μT, respectively. Despite these differences, the final SCHA.DIF.3K model shows a smooth behavior in the time period from 1600 A.D. to 1700 A.D. The reason is that the difference between SCHA.DI.1-F and modified GUFM models at 1650 A.D. is smaller than the uncertainties of the archeomagnetic data in the window 1625–1675 A.D.

[57] To evaluate how the input model affects the final model, we performed tests using the following three archaeomagnetic models: (1) CALS7K.2 model, (2) SCHA.DI.1-F model, and (3) a simple dipolar model. This dipolar model was obtained from the relocation of all the data at the cap's center and calculating the average Fisher direction and the average intensity (in the same way as a palaeosecular curve is generated).

[58] The study showed that for temporal windows with a high data density, the final model was similar for all three cases. However, for windows with a low density of data (for B.C. windows), the input model determined the final model. For this reason, we decided to use the most suitable model according to the updated input data, i.e., the regional archaeomagnetic model SCHA.DI.1-F.

4.3. SCHA.DIF.3K Model

[59] The SCHA.DIF.3K has been obtained following an iterative procedure in which outliers are rejected. A first SCHA model is obtained and used to remove those data with residuals greater than 3 times the average value of RMS misfit error. Table 1 shows the number of rejected data. No data from historical series have been rejected.

[60] With the selected database, the regional SCHA.DIF.3K model has been finally obtained after an average of 6 iterations per window. Table 2 shows the initial and final RMS misfits for every temporal window and the number of iterations. The optimal model is given by the iteration not varying the RMS misfit by more than 1% of its value.

[61] To obtain the model uncertainty (at 95% of confidence) of the predicted values for the regional model, we have used a spatial function, $C(t, \varphi, \lambda)$, for every element, i.e., declination, inclination and intensity. This function is obtained by the spatial-time distribution of the RMS misfits for each window by using a gridding method (polynomial in space and time). The $C(t, \varphi, \lambda)$ function defines the prediction uncertainty for the three components of the Earth's magnetic field at any location and time (at 95% of confidence). Figure 4 shows the $C(t, \varphi, \lambda)$ function for different locations in the valid time period.

Table 2. Initial and Final RMS Misfits and Number of Iterations for Every Temporal Window[a]

t_0	Number of Iterations	Initial RMS	Final RMS
−975	5	0.81	0.50
−950	5	0.63	0.41
−925	5	0.58	0.39
−900	6	0.67	0.48
−875	6	0.65	0.49
−850	5	0.67	0.50
−825	6	0.73	0.60
−800	7	0.76	0.65
−775	6	0.71	0.60
−750	6	0.79	0.67
−725	8	0.79	0.64
−700	9	0.90	0.71
−675	7	0.97	0.82
−650	7	0.87	0.71
−625	7	0.89	0.73
−600	6	0.90	0.80
−575	6	0.81	0.70
−550	8	0.90	0.76
−525	6	0.82	0.71
−500	7	0.86	0.72
−475	9	0.86	0.70
−450	9	0.99	0.81
−425	6	0.98	0.87
−400	9	1.20	1.06
−375	7	1.13	1.03
−350	7	1.18	1.05
−325	6	1.19	1.09
−300	5	1.16	1.06
−275	5	1.09	1.01
−250	5	1.05	0.95
−225	7	0.93	0.81
−200	8	0.53	0.41
−175	7	0.85	0.71
−150	7	0.94	0.72
−125	4	0.93	0.83
−100	11	0.85	0.70
−75	4	0.87	0.83
−50	4	0.63	0.58
−25	5	0.80	0.74
0	5	0.69	0.52
25	6	0.91	0.80
50	6	0.91	0.79
75	6	1.01	0.93
100	5	0.86	0.81
125	4	0.80	0.78
150	6	0.82	0.74
175	5	0.84	0.80
200	7	0.86	0.77
225	7	0.93	0.86
250	6	0.91	0.81
275	7	0.83	0.75
300	4	0.60	0.58
325	5	0.85	0.80
350	5	0.89	0.83
375	5	0.92	0.85
400	6	0.74	0.66
425	5	0.76	0.70
450	6	0.71	0.62
475	7	0.86	0.75
500	7	0.78	0.59
525	6	1.11	1.00
550	7	1.09	0.90
575	7	0.88	0.77
600	6	0.48	0.38
625	6	0.62	0.53
650	4	0.44	0.39
675	5	0.63	0.55
700	4	0.59	0.50
725	4	0.78	0.70
750	4	0.62	0.59
775	4	0.69	0.66
800	5	0.58	0.50
825	4	0.74	0.72
850	4	0.71	0.68
875	4	0.83	0.78
900	5	0.75	0.66
925	4	0.58	0.54
950	5	0.57	0.52
975	5	0.69	0.63
1000	6	0.68	0.62
1025	3	0.72	0.70
1050	4	0.73	0.70
1075	4	0.82	0.78
1100	5	0.84	0.80
1125	4	0.88	0.85
1150	4	0.82	0.79
1175	5	0.81	0.77
1200	6	0.77	0.71
1225	5	0.94	0.87
1250	4	0.85	0.83
1275	4	1.01	0.98
1300	4	1.09	1.07
1325	5	1.20	1.15
1350	5	0.99	0.94
1375	6	0.98	0.90
1400	5	0.87	0.81
1425	4	1.03	0.97
1450	5	0.91	0.84
1475	6	1.02	0.96
1500	7	1.04	0.95
1525	5	1.18	1.03
1550	7	1.05	0.93
1575	3	1.00	0.96
1600	5	1.24	1.16
1625	5	1.54	1.45
1650	7	2.24	1.84
1675	8	2.14	1.61
1700	4	1.06	1.02
1725	6	1.02	0.94
1750	5	0.88	0.85
1775	4	1.14	1.11
1800	5	1.34	1.28
1825	5	1.36	1.31
1850	3	0.92	0.91
1875	5	1.44	1.38

[a] The window is denoted by the central time t_0.

[62] The spatial-temporal distribution of the input data, the uncertainty of the data and the technique used for modeling define the spatial and temporal resolution of the model. For the spatial resolution,

Geochemistry Geophysics Geosystems G3 PAVÓN-CARRASCO ET AL.: SCHA.DIF.3K EUROPEAN ARCHEOMAGNETIC MODEL 10.1029/2008GC002244

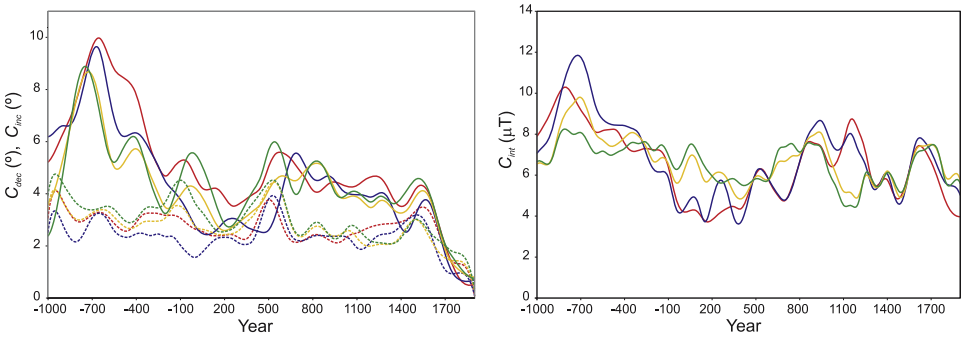

Figure 4. $C(t, \lambda, \varphi)$ error functions for (left) declination (C_{dec}, solid lines) and inclination (C_{inc}, dashed lines) and (right) intensity (C_{int}) components. This function has been calculated at different locations over Europe: north (red lines), 52°N latitude, 9°E longitude; west (blue lines), 44°N latitude, −4°W longitude; south (yellow lines), 40°N latitude, 12°E longitude; and east (green lines), 42°N latitude, 23°E longitude.

according to the model parameters (maximum degree and size of the cap), the model can reproduce wavelengths not lower than ∼5000 km [*Thébault et al.*, 2006]. Furthermore, the use of the sliding windows method with s = 50 years and 25 years overlapping between windows limits the temporal resolution to 75 years (3s/2).

[63] Figure 5 shows the declination, inclination and intensity maps for Europe and adjacent areas every 100 years from 1000 B.C. to 1900 A.D. Furthermore, an animation with declination, inclination and intensity maps is available as auxiliary material.[1]

[64] The obtained continuous geomagnetic field model for Europe and adjacent areas is available from the Web site: http://pc213fis.fis.ucm.es/scha.dif.3k_model.html. To generate a PSVC from SCHA.DIF.3K model it is only necessary to indicate the latitude and longitude of the site (input data). The output predictions are the declination, inclination and intensity (and their prediction uncertainties at 95% of confidence) versus time in ASCII format from 1000 B.C. to 1900 A.D.

5. Discussion: SCHA.DIF.3K Model and Input Data and Comparison With Global Models

[65] Values predicted by the model have been compared with the input data. The RMS misfit for data over the whole cap, averaged in 50 year bins, for declination, inclination and intensity are given in Figure 6. For comparison, we have added the spatial RMS misfit associated to the CALS7K.2 model [*Korte and Constable*, 2005] and the input models SCHA.DI.1-F and GUFM model (*Jackson et al.* [2000] modified according to *Gubbins et al.* [2006]).

[66] For the declination (Figure 6a) the RMS misfits of the regional model vary from 0.3° in 1875 ± 25 A.D. to 11.9° for 425 ± 25 B.C. The RMS error for CALS7K.2 model strongly increases between 1000 B.C. and 600 B.C. The distribution of the residual individual data has a Laplacian behavior with an average of −0.3° and a standard deviation of 4.0°. In Figure 6b, we have plotted the Laplace distribution curve (red curve) obtained with these statistical parameters. We have also calculated the cumulative distribution of the residual data and we have compared it with the theoretical Laplace cumulative distribution (Figure 6c). This comparison shows that the Laplace distribution is the suitable distribution for the actual residuals.

[67] The inclination RMS misfits are lower than the declination RMS misfits in absolute value (Figure 6d). For the regional model, the RMS error exhibits two maxima at 125 ± 25 B.C. (5.4°) and at 525 ± 25 A.D. (5.2°, which is bigger than the RMS errors from CALS7K.2), and two minima in 825 ± 25 B.C. (0.7°) and 1875 ± 25 A.D. (0.8°). The intensity errors (Figure 6g) show minima between 1025 and 1175 A.D. (∼ 4 μT) and maxima about 11.6 μT at 275 B.C. Figures 6e and 6h show the distribution of the individual data residuals for inclination and intensity, respectively. The Laplacian parameters for inclination and intensity residuals are −0.2°/0.1 μT (averaged residual) and 3.2°/7.5 μT (standard deviation). In this case,

[1] Auxiliary materials are available in the HTML. doi:10.1029/2008GC002244.

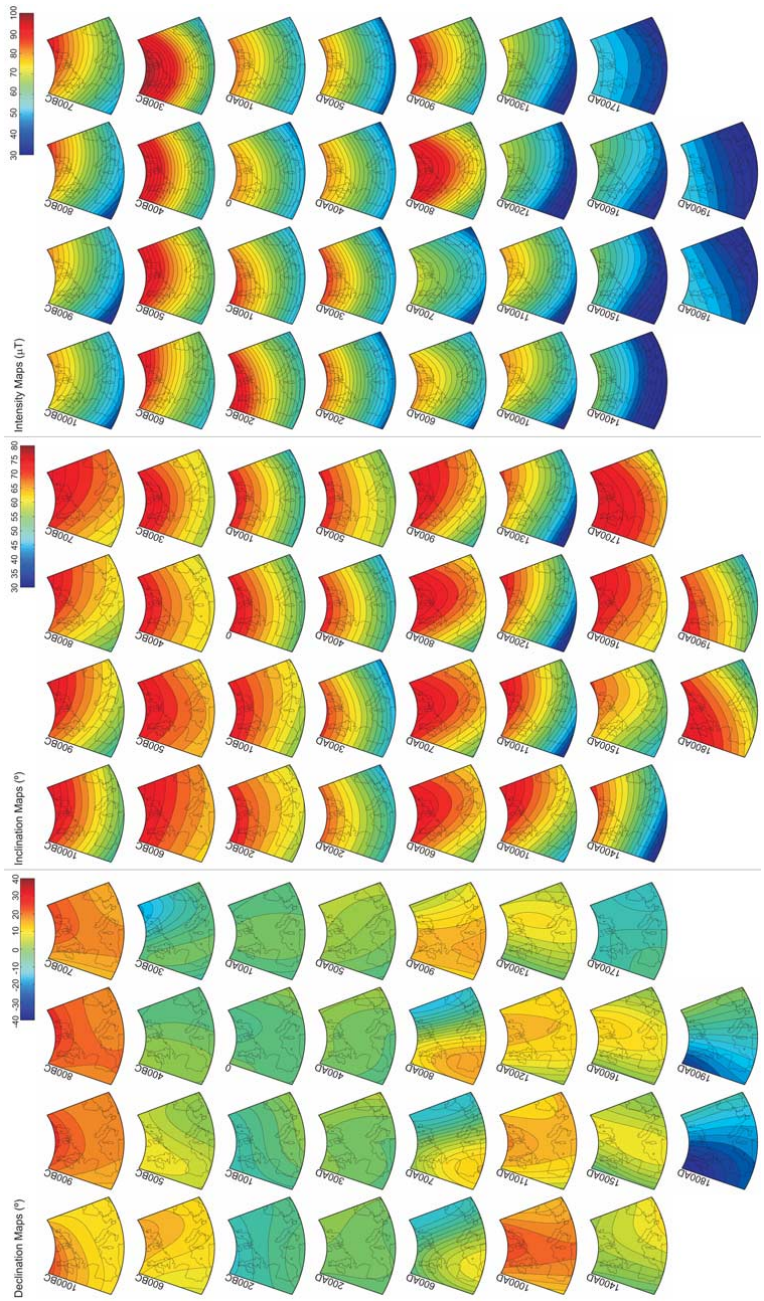

Figure 5. Snapshots from the SCHA.DIF.3K model for each 100 year interval. An animation is available as auxiliary material.

Geochemistry Geophysics Geosystems G3 PAVÓN-CARRASCO ET AL.: SCHA.DIF.3K EUROPEAN ARCHEOMAGNETIC MODEL 10.1029/2008GC002244

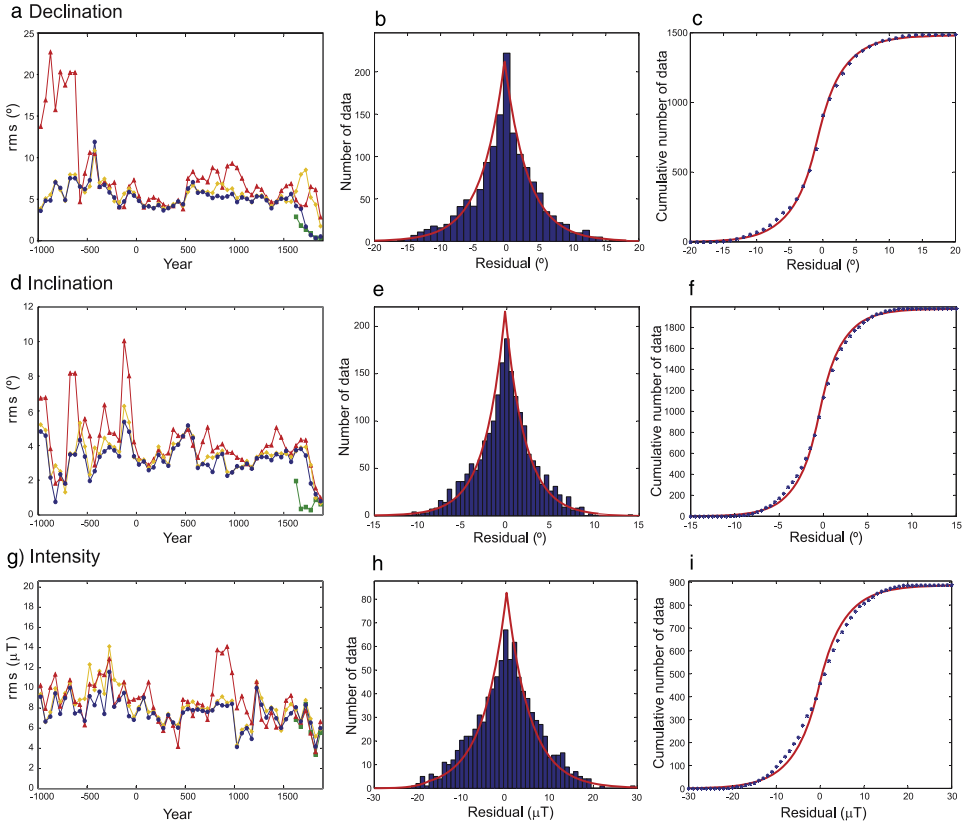

Figure 6. (a–c) Declination, (d–f) inclination, and (g–i) intensity RMS misfits (Figures 6a, 6d, and 6g), the residual distribution (Figures 6b, 6e, and 6h), and cumulative residual distribution (Figures 6c, 6f, and 6i). Figures 6a, 6d, and 6g show the RMS misfits (averaged for windows of 50 years) from the SCHA.DIF.3K model (blue line), from the CALS7K.2 (red line), from the SCHA.DI.1-F (yellow line), and from the GUFM model (green line). Figures 6b, 6e, and 6h show histograms of residual data; red lines are the Laplace distributions with the same mean and standard deviation. Figures 6c, 6f, and 6i show cumulative residual distribution (blue stars) and theoretical cumulative Laplace distributions (red lines).

the cumulative intensity residuals show a little difference with respect to the theoretical curve (Figure 6i) because of the high dispersion of this component. No major differences are observed between the RMS misfits associated with the regional and CALS7K.2 models for the inclination (except for the time interval 725 B.C. to 25 B.C.), but the RMS errors of the regional model are generally lower than the RMS errors of the CALS7K.2 global model for the intensity (especially between 700 A.D. and 1250 A.D.).

[68] We have compared the SCHA.DIF.3K model with the input models. The new regional model improved the previous model (SCHA.DI.1-F) for all the time interval (Figures 6a, 6d, and 6g). This improvement is clear for the declination after 1600 A.D. The RMS errors from the GUFM model are similar to the RMS errors from the regional model; an obvious result, since the global model is very similar to the regional one for the considered 1650–1900 period. Table 3 summarizes the averaged spatial-temporal RMS misfits for each element of the geomagnetic field and for the different models.

[69] To plot the SCHA.DIF.3K model with the input data, we have selected seven reference points to give predicted PSVC. These areas are shown in Figure 7. We have transferred both directional and

Geochemistry Geophysics Geosystems G3 PAVÓN-CARRASCO ET AL.: SCHA.DIF.3K EUROPEAN ARCHEOMAGNETIC MODEL 10.1029/2008GC002244

Table 3. Comparison of the Averaged Spatial-Temporal RMS Misfits Between SCHA.DIF.3K and Global Models CALS7K.2 and GUFM[a]

Models	RMS D (deg)	RMS I (deg)	RMS F (μT)
From 1000 B.C to 1900 A.D.			
SCHA.DIF.3K	2.4	2.3	7.6
CALS7K.2	5.3	3.3	8.8
From 1650 to 1900 A.D.			
SCHA.DIF.3K	1.2	1.4	6.3
GUFM[a]	1.2	1.1	6.4

[a] The GUFM model of *Jackson et al.* [2000] modified according to *Gubbins et al.* [2006].

intensity data from each site to the reference point by CVP and VADM methods respectively (VADM is the Virtual Axial Dipole Moment, i.e., an axial dipole field is assumed to transfer the intensity data to a reference point). The maximum distance between the site and the reference point was decided to be 700 km. Figure 8 shows the curves predicted by the regional model for each of the seven locations, along with their prediction uncertainty intervals at 95% of confidence. For comparison, we have also plotted the CALS7K.2 [*Korte and Constable*, 2005] and GUFM [*Jackson et al.*, 2000] global models and the input SCHA.DI.1-F model.

[70] Declination and inclination curves, i.e., directional curves show different behaviors in western Europe (Iberia, France, United Kingdom) and eastern Europe (Hungary, Bulgaria and Greece). The density of directional data is concentrated in the western area. The declination (Figure 8, left) in Europe shows several maximum peaks (easterly declinations), concentrated mainly in two time periods, around 800 B.C. and 1000–1100 A.D. The declination curves for the eastern side (Hungary and Bulgaria-Greece) show a significant maximum at 1575 A.D. For the Roman period, the declination has low values and little variation (see also Figure 5, from 100 B.C. to 400 A.D.). The minima declination values (westerly declinations) are achieved at 400 B.C., 600 A.D. and at recent times, around the 18th century.

[71] The global model CALS7K.2 shows a similar variation to declination as the regional model, but underfitting all peaks because of the strong smoothing of the model. This smoothing is clearly visible for the period 1000 B.C. to 500 B.C., where the global model gives declination values close to zero, while the regional model records its highest maximum of declination (between 23° and 25° for the whole European area). The biggest differences between global and regional models are recorded during this time period; however, it is worth remembering that input data from this epoch are extremely scarce (CALS7K.2 model used lake sediments data for this epoch).

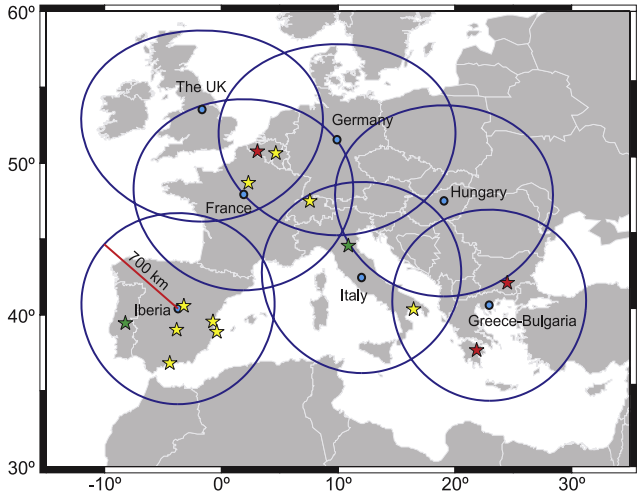

Figure 7. Considered areas (blue circles) to compare the SCHA.DIF.3K model to the input data. Blue points are the reference site (see text for details). Locations of archeomagnetic dating studies with all geomagnetic components (D, I, and F, red stars) and directional components (D and I, green stars). Location of the new intensity data (yellow stars).

Geochemistry Geophysics Geosystems G3 PAVÓN-CARRASCO ET AL.: SCHA.DIF.3K EUROPEAN ARCHEOMAGNETIC MODEL 10.1029/2008GC002244

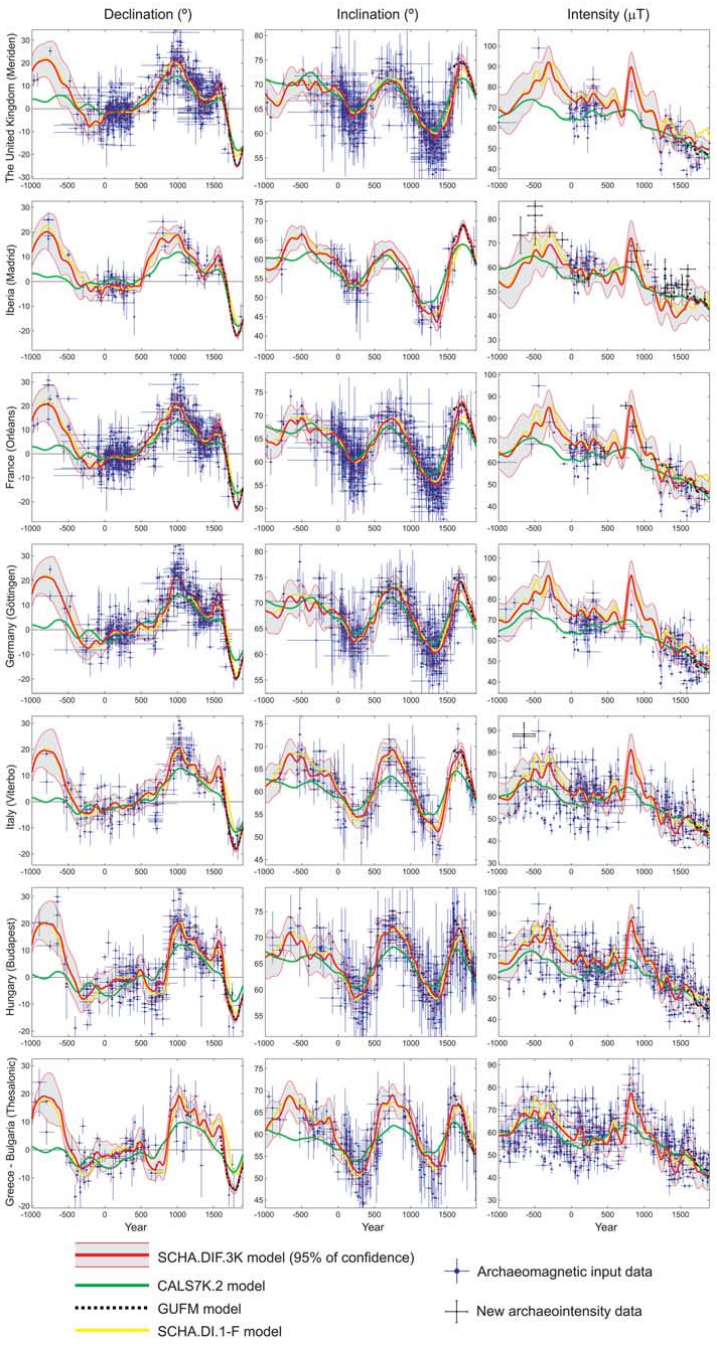

Figure 8

[72] The inclination curves (Figure 8, middle) show a sinusoidal appearance with maximums peaks at 500 B.C., 750 A.D. and 1700 A.D. The most relevant minimum peaks are found around 320 A.D. and 1325 A.D. This behavior is also reflected in the CALS7K.2 global model, but the predicted curves again show underfitting for these peaks (especially for Italy, Hungary and Greece-Bulgaria). The greatest discrepancy between the regional and global models occurs again during the years B.C.

[73] The density of intensity values (Figure 8, right) is higher in eastern Europe (Hungary, Bulgaria and Greece) than in western Europe, where data are mainly divided into two time periods: 0–400 A.D. and 1250–1800 A.D. This could indicate an underfitting of intensity data in western Europe. To evaluate this problem, we have considered intensity data from western European countries not included in the regional model (yellow stars in Figure 7). These data come from recent publications [*Nachasova et al.*, 2007, and references therein; *Gómez-Paccard et al.*, 2008] and from archeointensity studies product of the European AARCH project [*Batt et al.*, 2008, and references therein]. These new intensity data have been plotted in Figure 8 reduced by VADM to the nearby reference point. As shown in Figure 8, the predictions by the regional model are in agreement with the new intensity data, especially in the maxima around 500–300 B.C. and $\sim$ 800 A.D. Therefore, we think that the model predicts the intensity over Europe in a proper manner. The intensity curves generated by the SCHA.DIF.3K model have a common behavior throughout Europe.

[74] The regional model suggests that the Earth's magnetic field strength reached 10 maxima in Europe at 600–500 and 275 B.C., and at 160, 325, 580, 820, 1310, 1550–1700 and 1780 A.D. On the other hand, the CALS7K.2 global model [*Korte and Constable*, 2005] is too smoothed to describe fluctuations shown by the data at these locations. This global model exhibits only two maxima, around 500 B.C. and 800 A.D.

[75] The comparison between the new regional model and the input models (Figure 8) shows that the difference is due to the data density and their temporal distribution. The new model is close to the input models when the data density is low, which is logical. Before 200 B.C., both new and input models are very similar for the three components in western Europe, again in agreement with the low data density there (Figure 2c). However, for this time interval, differences are found in the inclination and intensity curves from eastern Europe, where the density of inclination and intensity data is higher (Figures 2b and 2c). The new regional model agrees with the GUFM model modified according to *Gubbins et al.* [2006].

6. Applications

6.1. Archeomagnetic Dating

[76] One of the immediate applications of SCHA.DIF.3K regional model is its use as tool for archeomagnetic dating. So far the PSVC determined for a region have been used for archeomagnetic dating. The limitation of this application is the distance from the dating point to the location of the reference curve (the relocation error). In addition it must be borne in mind that the PSVC are individually generated for each region, so there is no consistency enforced between curves from neighboring areas.

[77] The use of the SCHA.DIF.3K model as a tool for archeomagnetic dating represents an improvement for several reasons. First of all, the regional model has been generated considering all elements of the geomagnetic field (declination, inclination and intensity). Second, the regional model is built with an in situ archeomagnetic database. Furthermore, the database covers the whole time period from 1000 B.C. to 1900 A.D., while the database used in the PSVC has gaps of data for any time interval. Finally, and more important, we can generate a PSVC at the location of the archeological structure, avoiding in this way the relocation error associated with traditional PSVC.

[78] To demonstrate the utility of the regional SCHA.DIF.3K model, we have used it to date five archeological structures which have also been dated by the classical archeomagnetic method [*Lanos*, 2004]. Therefore the studied selected sites are located close to the available Bayesian reference PSVC. Archeological evidence has estab-

Figure 8. (left) Declination, (middle) inclination, and (right) intensity data (blue points with uncertainty bars) and model predictions (solid red line) with the prediction uncertainty (gray shading) for the last 3000 years. The CALS7K.2 (green line) and the input models SCHA.DI.1-F (yellow line) and GUFM (green line) have been plotted. New intensity values (black points with error bars) have been plotted in different intensity curves (see text for details).

Geochemistry Geophysics Geosystems G3 PAVÓN-CARRASCO ET AL.: SCHA.DIF.3K EUROPEAN ARCHEOMAGNETIC MODEL 10.1029/2008GC002244

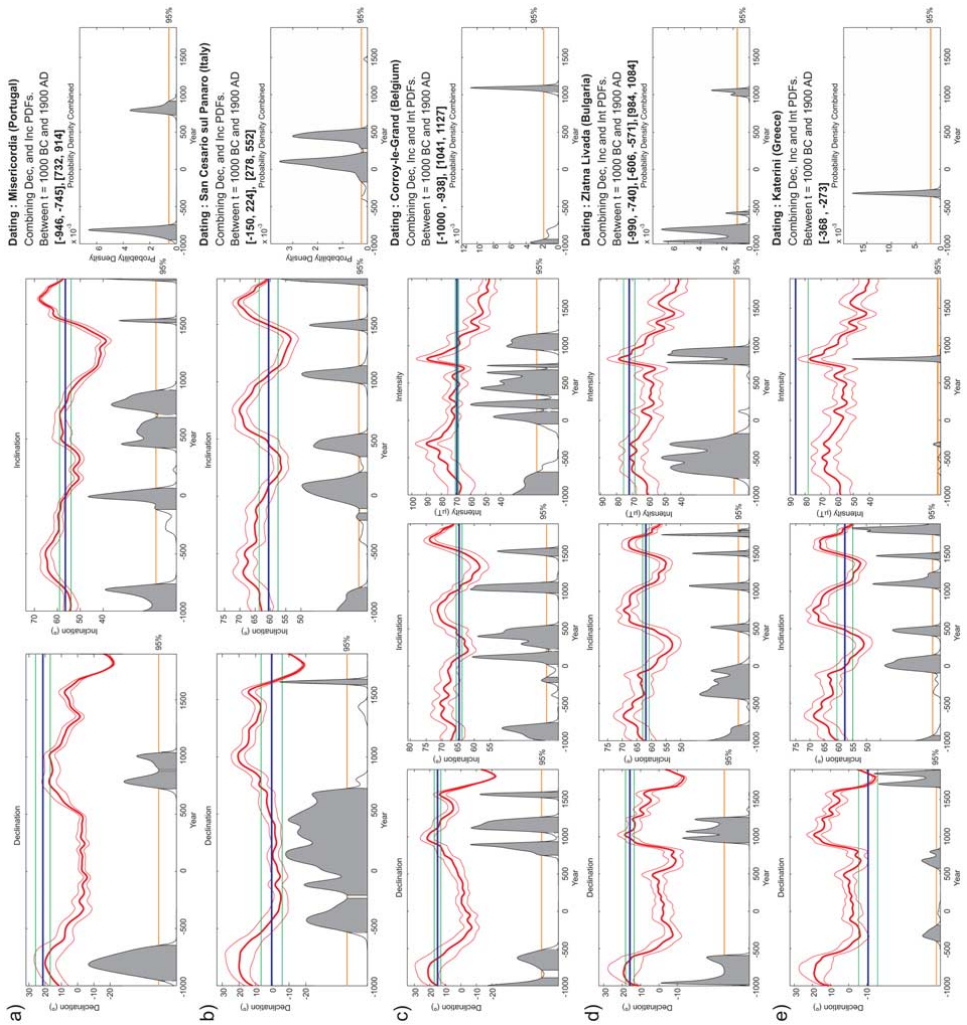

Figure 9

Table 4. Archeomagnetic Dating by SCHA.DIF.3K Model[a]

Site	Archeological Estimation	Archeomagnetic Dating by PSVC	Archeomagnetic Dating by SCHA.DIF.3K Model
Misericordia (Portugal)	Late Bronze Age, first half of C9 B.C. until C8 B.C.	[−834, −709]	[−946, −745]
San Cesario sul Panaro (Italy)	From C3 to C4 A.D.	[−99, 650]	[−150, 224] * [278, 552]
Corroy-le-Grand (Belgium)	Second half of C10 until C12 A.D.	[1022, 1167]	[1041, 1127]
Zlatna Livada (Bulgaria)	C11–C12 A.D.	[826, 1004]	[984, 1084]
Katerini (Greece)	Late C4 B.C. to early C2 B.C.	[−505, −287]	[−368, −273]

[a] See text for details.

lished the age of each structure (age of the last usage). Archeomagnetic data (declination, inclination and/or intensity) from these structures have not been included in the generation of the regional model, so they constitute an independent set of data. The studied structures correspond to five European sites: Misericordia (Serpa, Portugal [*Catanzariti et al.*, 2008]); San Cesario sul Panaro (Bazzano, Italy [*Tema and Lanza*, 2008]); Corroy-le-Grand (Belgium [*Spassov et al.*, 2008]); Katerini (Greece [*De Marco et al.*, 2008]) and Zlatna Livada (Bulgaria [*Herries et al.*, 2008]). Two of the five sites (Misericordia and San Cesario sul Panaro) have only directional data (declination and inclination). The location of each structure is shown in Figure 7.

[79] The archeomagnetic dating has been carried out according to the mathematical method of *Lanos* [2004], where archeomagnetic data are compared with a PSVC. In our case, the PSVC is generated by the regional SCHA.DIF.3K model avoiding the relocation error. So, we can obtain the probability density functions (PDF) for each data (D, I and/or F), whose combination generates the final PDF (combined PDF). The combined PDF is used to define the dating period time at 95% of confidence.

[80] Figure 9 shows the five archeomagnetic datings along with the PDF of each archeomagnetic element and the combined PDF, with the determined confidence intervals at 95% of probability. Table 4 summarizes these time intervals, the archeological information and time intervals obtained from the archeomagnetic dating with PSVC close to the sampling site. The structures used for this application are located close to the published Bayesian PSVC, therefore the relocation error should be small and both archeomagnetic methods should produce similar results. For all cases there is a good agreement between the archeomagnetic dating by SCHA.DIF.3K model, by the PSVC, and by the archeological information.

[81] This new method can also be applied in other European regions where reference PSVC are not available.

6.2. Archeomagnetic Jerks

[82] Archeointensity data from Europe covering the last three millennia show coincidence between sharp changes in the direction of the geomagnetic field with intensity maxima during short periods of less than 1 century: archeomagnetic jerks (AMJ) according to *Gallet et al.* [2003, 2005] with a time scale between geomagnetic jerks (years) and excursions (thousands of years). *Gallet et al.* [2005] analyzed the intensity data from western Europe and the eastern Mediterranean. They detected 4 AMJ for the last three millennia, around 800 B.C., 200 A.D., 750 A.D., and 1400 A.D. However, the evidence for these jerks is limited, given the density of data used by *Gallet et al.* [2003, 2005]. *Snowball and Sandgren* [2004] concluded, from high resolution sedimentary data, that significant century scale increases and decreases in relative field intensity between 4000 and 2000 cal B.P.

Figure 9. Archeomagnetic dating. The PSVC from SCHA.DIF.3K model (red curve) at each location and the archeomagnetic data (blue line). Their uncertainty envelopes are shown in red and green, respectively. The probability density functions (a and b) for declination and inclination and (c–e) for intensity and combined declination-inclination (Figures 9a and 9b) and declination-inclination-intensity (Figures 9c–9e) are shaded at the 95% (orange line in probability density functions). The most probable age for every site is shown in brackets.

Geochemistry Geophysics Geosystems G3 PAVÓN-CARRASCO ET AL.: SCHA.DIF.3K EUROPEAN ARCHEOMAGNETIC MODEL 10.1029/2008GC002244

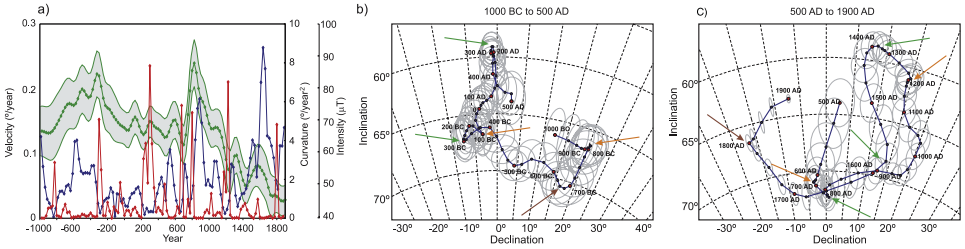

Figure 10. Archeomagnetic jerks: (a) Velocity (blue line) and curvature for the directional curve (red line) and intensity curve (green line) with the prediction uncertainty band (gray band) at the center of Europe (48°N, 9°E). Directional curve plotted in an equal area diagram (b) from 1000 B.C. to 500 A.D. and (c) from 500 A.D. to 1900 A.D. with the prediction uncertainty (gray ellipses). Red circles are marked every 100 years. Green arrows indicate proposed jerks according to *Gallet et al.* [2003, 2005] (coincidence between sharp changes in the direction of the geomagnetic field with intensity maxima). Orange arrows indicate abrupt changes in the direction (small or no intensity maxima). Brown arrows indicate possible jerks.

were associated with abrupt changes (jerks) in the direction of the geomagnetic vector.

[83] The regional SCHA.DIF.3K allows for the study of potential AMJ by analyzing the intensity maxima, the magnitude of directional velocity, or angular rate of change of direction and the maximum curvature of the archeomagnetic curve. We have calculated the velocity and curvature of the directional curve at the center of the cap (48°N of latitude and 9°E of longitude). Results are shown in Figure 10, along with the intensity curve for this location.

[84] We can see 5 epochs where a maximum in intensity coincides with a maximum of curvature and a minimum in velocity (Figure 10) around 300 B.C., and 300, 800, 1350, and 1600 A.D. And a less well defined event could also have occurred around 1800 A.D. (small intensity maxima). Another event characterized by a directional change together with a small intensity maxima occurred around 650 B.C.; and rapid directional changes associated with velocity minima (but no intensity maxima) took place around 825 B.C., 125 B.C., 650 A.D. and 1200 A.D.

[85] According to *Gallet et al.*'s [2003, 2005] definition of AMJ, we can propose five clear AMJ around 275–325 B.C. (AMJ-300), 275–325 A.D. (AMJ300), 775–825 A.D. (AMJ800), 1350 A.D. (AMJ1350) and 1550–1600 A.D. (AMJ1600) and a suspected jerk at 1775–1800 A.D. (AMJ1800).

[86] It is important to point out that the AMJ1350 is best defined in western Europe, while the AMJ1600 is evidenced from eastern Europe studies. This is due to the inhomogeneous distribution of data in Europe already mentioned. More archeomagnetic information, well distributed in Europe and well dated, is necessary in both periods to better define these events. Similarly, an additional possible AMJ is suspected around 650–700 B.C. (AMJ-650), but it needs to be confirmed with more data. During the period 600–900 A.D. two AMJ could have occurred instead of the only one that we propose here, but during the "dark ages" the number of archeomagnetic data is small and the confidence in dating is low.

[87] The AMJ proposed by *Gallet et al.* [2005] around 800 B.C. correspond to an abrupt directional change (maximum curvature and minimum velocity), but no global intensity maximum is observed. It has to be noted that *Gallet et al.* [2005] only had a single intensity datum for that epoch. More studies are necessary to investigate this event. Other abrupt directional changes are observed around 125 B.C. and 1200 A.D.

7. Conclusions

[88] We have developed a new regional archeomagnetic model for Europe for the last 3000 years. The model has been calculated by using the SCHA regional technique, modified for modeling the three elements of the geomagnetic field together: declination, inclination and intensity. The SCHA.DIF.3K model allows a complete description of the geomagnetic field over Europe and adjacent areas for the last 3000 years, and suggests that the Earth's magnetic field has experienced a minimum of 5 archeomagnetic jerks in Europe for the last 3000 years (AMJ-300, AMJ300, AMJ800, AMJ1350, AMJ1600) and a suspected jerk (AMJ1800). These events are

characterized by intensity maxima, velocity minima and a sharp change in curvature. Other events are observed around 825 B.C., 650–700 B.C., 125 B.C., 600–650 A.D. and 1175–1200 A.D. which seem "directional jerks," but need to be confirmed with more data. We have also demonstrated that the regional model is an appropriate tool for archeomagnetic dating, since a PSVC can be generated at the location of the archeological structure, thus avoiding the traditional relocation error. The model fits the present archeomagnetic database for Europe more accurately than the global model proposed by *Korte and Constable* [2005] for the 1000 B.C. to 1900 A.D. time interval. The discrepancies with CALS7K.2 reflect the difference in the data sets used and uncertainties assigned, the choice of least sums of absolute deviation versus regularized inversion in the spatial domain, and the use of sliding windows versus continuous time variations.

Acknowledgments

[89] The authors are grateful to the Spanish research projects CGL2005-00211 and CGL2008-02203/BTE and the FPI grant BES-2006-13488. Constructive comments and suggestions from Catherine Constable, Monika Korte, and a third anonymous reviewer have highly improved the manuscript and are therefore gratefully acknowledged. All algorithms have been developed in Matlab® codec (Matlab 7.0.4, R14) along with the figures and animations.

References

Alexandrescu, M., V. Courtillot, and J.-L. Le Mouël (1996), Geomagnetic field direction in Paris since the mid-sixteenth century, *Phys. Earth Planet. Inter.*, *98*, 321–360, doi:10.1016/S0031-9201(96)03194-9.

Batt, C. M., I. Zananiri, and D. H. Tarling (2008), Preface: Archaeomagnetic applications for the rescue of cultural heritage, *Phys. Chem. Earth*, *33*, 403–406, doi:10.1016/j.pce.2008.02.015.

Cafarella, L., A. De Santis, and A. Meloni (1992), *The Historical Italian Geomagnetic Data Catalogue*, 160 pp., Ist. Naz. di Geofis. e Vulcanol., Rome.

Casas, L., and A. Incoronato (2007), Distribution analysis of errors due to relocation of geomagnetic data using the 'Conversion via Pole' (CVP) method: Implications on archaeomagnetic data, *Geophys. J. Int.*, *169*(2), 448–454, doi:10.1111/j.1365-246X.2007.03346.x.

Catanzariti, G., G. McIntosh, A. M. Monge Soares, E. Díaz-Martínez, P. Kresten, and M. L. Osete (2008), Archaeomagnetic dating of a vitrified wall at the Late Bronze Age settlement of Misericordia (Serpa, Portugal), *J. Archaeol. Sci.*, *35*, 1399–1407.

Chauvin, A., Y. Garcia, P. Lanos, and F. Laubenheimer (2000), Paleointensity of the geomagnetic field recovered on archaeomagnetic sites from France, *Phys. Earth Planet. Inter.*, *120*, 111–136, doi:10.1016/S0031-9201(00)00148-5.

De Marco, E., S. Spassov, D. Kondopoulou, I. Zananiri, and E. Gerofoka (2008), Arcaheomagnetic study and dating of a Hellenistic site in Katerini (N. Greece), *Phys. Chem. Earth*, *33*, 481–495.

De Santis, A., D. J. Kerridge, and D. R. Barraclough (1989), A spherical cap harmonic model of the crustal magnetic anomaly field in Europe by Magsat, in *Geomagnetism and Paleomagnetism*, edited by F. J. Lowes et al., pp. 1–17, Kluwer, Dordrecht, Netherlands.

Evans, M. E. (2006), Archaeomagnetic investigations in Greece and their bearing on geomagnetic secular variation, *Phys. Earth Planet. Inter.*, *159*, 90–95, doi:10.1016/j.pepi.2006.06.005.

Evans, M. E., and G. S. Hoye (2005), Archaeomagnetic results from southern Italy and their bearing on geomagnetic secular variation, *Phys. Earth Planet. Inter.*, *151*, 155–162.

Gallet, Y., A. Genevey, and M. Le Goff (2002), Three millennia of directional variations of the Earth's magnetic field in western Europe as revealed by archaeological artefacts, *Phys. Earth Planet. Inter.*, *131*, 81–89, doi:10.1016/S0031-9201(02)00030-4.

Gallet, Y., A. Genevey, and V. Courtillot (2003), On the possible occurrence of archeomagnetic jerks in the geomagnetic field over the past three millennia, *Earth Planet. Sci. Lett.*, *214*, 237–242, doi:10.1016/S0012-821X(03)00362-5.

Gallet, Y., A. Genevey, and F. Fluteau (2005), Does Earth's magnetic field secular variation control centennial climate change?, *Earth Planet. Sci. Lett.*, *236*, 339–347, doi:10.1016/j.epsl.2005.04.045.

Gómez-Paccard, M., et al. (2006a), A catalogue of Spanish archaeomagnetic data, *Geophys. J. Int.*, *166*, 1125–1143, doi:10.1111/j.1365-246X.2006.03020.x.

Gómez-Paccard, M., P. Lanos, A. Chauvin, G. McInstosh, M. L. Osete, G. Catanzariti, V. C. Ruiz-Martínez, and J. I. Núñez (2006b), First archaeomagnetic secular variation curve for the Iberian Peninsula: Comparison with other data from western Europe and with global geomagnetic field models, *Geochem. Geophys. Geosyst.*, *7*, Q12001, doi:10.1029/2006GC001476.

Gómez-Paccard, M., A. Chauvin, P. Lanos, J. Thiriot, and P. Jiménez-Castillo (2006c), Archeomagnetic study of seven contemporaneous kilns from Murcia (Spain), *Phys. Earth Planet. Inter.*, *157*, 16–32, doi:10.1016/j.pepi.2006.03.001.

Gómez-Paccard, M., A. Chauvin, P. Lanos, and J. Thiriot (2008), New archeointensity data from Spain and the geomagnetic dipole moment in western Europe over the past 2000 years, *J. Geophys. Res.*, *113*, B09103, doi:10.1029/2008JB005582.

Gubbins, D., A. L. Jones, and C. C. Finlay (2006), Fall in Earth's magnetic field is erratic, *Science*, *312*(5775), 900–902, doi:10.1126/science.1124855.

Haines, G. V. (1985), Spherical cap harmonic analysis, *J. Geophys. Res.*, *90*(B3), 2583–2591, doi:10.1029/JB090iB03p02583.

Haines, G. V. (1988), Computer programs for spherical cap harmonic analysis of potential and general fields, *Comput. Geosci.*, *14*(4), 413–447, doi:10.1016/0098-3004(88)90027-1.

Herries, A. I. R., M. Kovacheva, and M. Kostadinova (2008), Mineral magnetism and archaeomagntic dating of a mediaeval oven from Zlatna Livada, Bulgaria, *Phys. Chem. Earth*, *33*, 496–510.

Hongre, L., G. Hulot, and A. Khokhlov (1998), An analysis of the geomagnetic field over the past 2000 years, *Phys. Earth Planet. Inter.*, *106*, 311–335, doi:10.1016/S0031-9201(97)00115-5.

Jackson, A., A. R. T. Jonkers, and M. R. Walker (2000), Four centuries of geomagnetic secular variation from historical

records, *Philos. Trans. R. Soc. London, Ser. A*, *358*, 957–990, doi:10.1098/rsta.2000.0569.

Jonkers, A. R. T., A. Jackson, and A. Murray (2003), Four centuries of geomagnetic data from historical records, *Rev. Geophys.*, *41*(2), 1006, doi:10.1029/2002RG000115.

Korte, M., and C. G. Constable (2003), Continuous global geomagnetic field models for the past 3000 years, *Phys. Earth Planet. Inter.*, *140*, 73–89, doi:10.1016/j.pepi.2003.07.013.

Korte, M., and C. G. Constable (2005), Continuous geomagnetic field models for the past 7 millennia: 2. CALS7K, *Geochem. Geophys. Geosyst.*, *6*, Q02H16, doi:10.1029/2004GC000801.

Korte, M., A. Genevey, C. G. Constable, U. Frank, and E. Schnepp (2005), Continuous geomagnetic field models for the past 7 millennia: 1. A new global data compilation, *Geochem. Geophys. Geosyst.*, *6*, Q02H15, doi:10.1029/2004GC000800.

Lanos, P. (2004), Bayesian inference of calibration curves: Application to archaeomagnetism, in *Tools for Constructing Chronologies: Crossing Disciplinary Boundaries*, vol. 177, edited by C. Buck and A. Millard, pp. 43–82, Springer, London.

Lodge, A., and R. Holme (2009), Towards a new approach to archaeomagnetic dating in Europe using geomagnetic field modelling, *Archaeometry*, doi:10.1111/j.1475-4754.2008.00400.x, in press.

Malin, S. R. C., and E. C. Bullard (1981), The direction of the Earth's magnetic field at London, 1570–1975, *Philos. Trans. R. Soc. London, Ser. A*, *299*, 357–423, doi:10.1098/rsta.1981.0026.

Márton, P., and E. Ferencz (2006), Hierarchical versus stratification statistical analysis of archaeomagnetic directions: The secular variation curve for Hungary, *Geophys. J. Int.*, *164*, 484–489, doi:10.1111/j.1365-246X.2006.02873.x.

Nachasova, I. E., K. S. Burakov, and A. J. Lorrio (2007), Archaeomagnetic study of ceramics from the El Molon Archaeological Monument (Spain), *Izv. Phys. Solid Earth*, *43*(10), 830–835.

Noël, M., and C. M. Batt (1990), A method for correcting geographically separated remanence directions for the purpose of archaeomagnetic dating, *Geophys. J. Int.*, *102*, 753–756, doi:10.1111/j.1365-246X.1990.tb04594.x.

Pavón-Carrasco, F. J., M. L. Osete, J. M. Torta, L. R. Gaya-Piqué, and P. Lanos (2008a), Initial SCHA.DI.00 regional archaeomagnetic model for Europe for the last 2000 years, *Phys. Chem. Earth*, *33*(6–7), 596–608.

Pavón-Carrasco, F. J., M. L. Osete, J. M. Torta, and L. R. Gaya-Piqué (2008b), A regional archaeomagnetic model for the palaeointensity in Europe for the last 2000 years and its implications for climatic change, *Pure Appl. Geophys.*, *165*(6), 1209–1225, doi:10.1007/s00024-008-0354-4.

Ruíz-Martínez, V. C., F. J. Pavón-Carrasco, and G. Catanzariti (2008), First archaeomagnetic data from northern Iberia, *Phys. Chem. Earth*, *33*, 566–577.

Schnepp, E., and P. Lanos (2005), Archaeomagnetic secular variation in Germany during the past 2500 years, *Geophys. J. Int.*, *163*, 479–490, doi:10.1111/j.1365-246X.2005.02734.x.

Schnepp, E., and P. Lanos (2006), A preliminary secular variation reference curve for archaeomagnetic dating in Austria, *Geophys. J. Int.*, *166*(1), 91–96, doi:10.1111/j.1365-246X.2006.03012.x.

Snowball, I., and P. Sandgren (2004), Geomagnetic field intensity changes in Sweden between 9000 and 450 cal BP: Extending the record of "archaeomagnetic jerks" by means of lake sediments and the pseudo-Thellier technique, *Earth Planet. Sci. Lett.*, *227*, 361–376, doi:10.1016/j.epsl.2004.09.017.

Spassov, S., J. Hus, R. Geeranerts, and F. Heller (2008), Archaeomagnetic dating of a High Middle Age likely iron working site in Corroy-le-Grand (Belgium), *Phys. Chem. Earth*, *33*, 544–556.

Tema, E., and R. Lanza (2008), Archaeomagnetic study of a lime kiln at Bazzano (northern Italy), *Phys. Chem. Earth*, *33*, 534–543.

Tema, E., I. Hedley, and P. Lanos (2006), Archaeomagnetism in Italy: A compilation of data including new results and a preliminary Italian secular variation curve, *Geophys. J. Int.*, *167*, 1160–1171, doi:10.1111/j.1365-246X.2006.03150.x.

Thébault, E. (2008), A proposal for regional modelling at the Earth's surface, R-SCHA2D, *Geophys. J. Int.*, *174*, 118–134, doi:10.1111/j.1365-246X.2008.03823.x.

Thébault, E., J. J. Schott, and M. Mandea (2006), Revised spherical cap harmonic analysis (R-SCHA): Validation and properties, *J. Geophys. Res.*, *111*, B01102, doi:10.1029/2005JB003836.

Torta, J. M., L. R. Gaya-Piqué, and A. De Santis (2006), Spherical cap harmonic analysis of the geomagnetic field with application for aeronautical mapping, in *Geomagnetics for Aeronautical Safety: A Case Study in and Around the Balkans*, edited by J. L. Rasson and T. Delipetrov, pp. 291–307, Springer, Dordrecht, Netherlands.

Zananiri, I., C. M. Batt, P. Lanos, D. H. Tarling, and P. Linford (2007), Archaeomagnetic secular variation in the UK during the past 4000 years and its application to archaeomagnetic dating, *Phys. Earth Planet. Inter.*, *160*(2), 97–107.

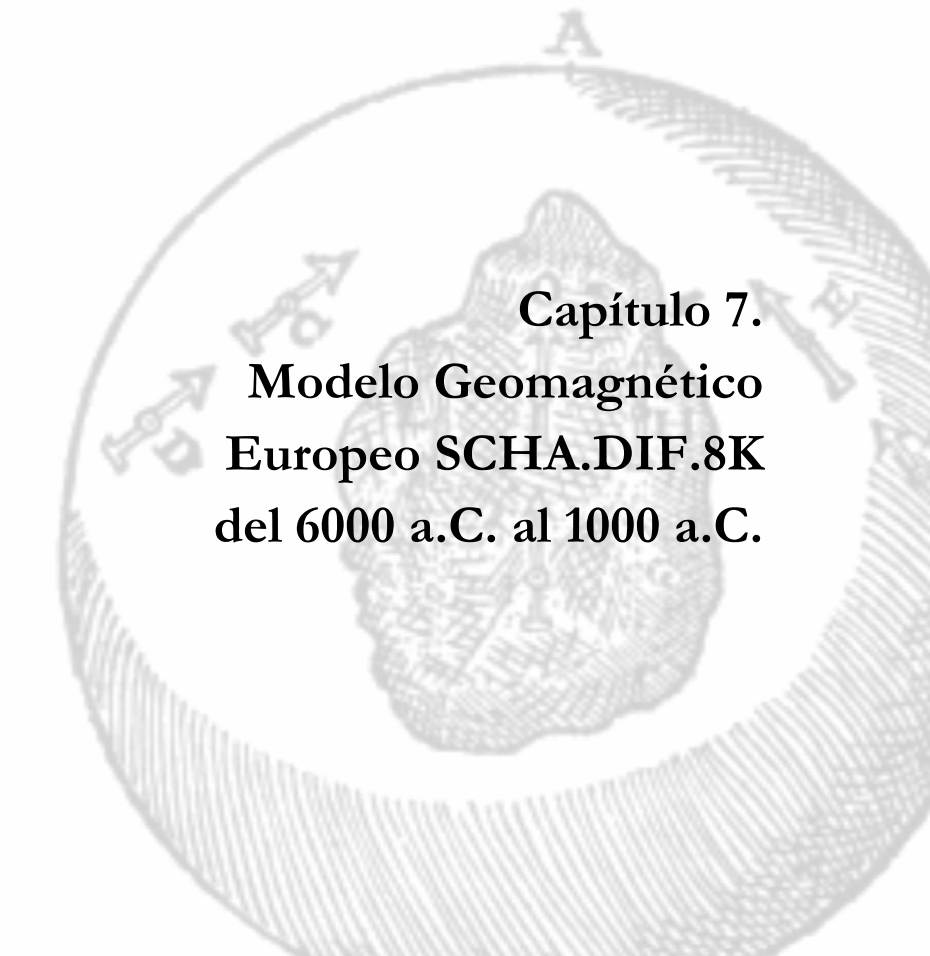

Capítulo 7.
Modelo Geomagnético Europeo SCHA.DIF.8K del 6000 a.C. al 1000 a.C.

En capítulos anteriores hemos desarrollado diferentes modelos que permiten tener un conocimiento del Campo Principal en la región europea para los últimos 2000 y 3000 años. Estos modelos están basados en datos arqueomagnéticos, cuya densidad es muy pobre para períodos anteriores. Sin embargo, existe la posibilidad de generar modelos más amplios temporalmente si se utilizan otro tipo de datos paleomagnéticos que proporcionan un registro temporal más largo: los registros que proporcionan los sedimentos lacustres. Este tipo de sedimentos se almacenan en el fondo de lagos y mediante procesos de imanación deposicional (y/o post-deposicional) registran el campo geomagnético presente en el momento de la deposición. No son los mejores registros del campo, pues los datos arqueomagnéticos tienen mucha más calidad, sin embargo, son los únicos que permiten analizar el campo geomagnético hasta edades que van más allá de los últimos 12000 años.

Los datos de sedimentos lacustres de la región europea y los datos arqueomagnéticos disponibles han sido utilizados para generar un nuevo modelo que nos permite conocer el comportamiento del campo en Europa desde el año 6000 a.C. El nuevo modelo regional obtenido, denominado **SCHA.DIF.8K**, junto con varios ejecutables y animaciones, está disponible en la siguiente dirección web: http://pc213fis.fis.ucm.es/scha.dif.8k/index.html

7.1 Datos de sedimentos lacustres de los últimos 8000 años.

Los sedimentos lacustres pueden adquirir una remanencia magnética en presencia de un campo magnético. El tipo de remanencia magnética que presentan es la denominada detrítica y puede ser adquirida por alineamiento con el campo magnético durante la deposición (Deposicional, DRM) y/o por reorientación durante la consolidación del sedimento (pDRM). Los granos magnéticos que forman el conjunto sedimentario tienden a alinearse bajo las líneas de fuerza del campo magnético circundante durante el proceso de deposición en el fondo lacustre (o marino). Este alineamiento se preserva a través de procesos de deposición y se bloquea para una cierta profundidad sedimentaria. El proceso puede ser complejo y el número de agentes que lo pueden perturbar es muy alto (ver Tauxe, 1993 para una revisión).

Los datos sedimentarios aportan largos registros temporales del campo geomagnético, principalmente para el período del Holoceno (últimos 12000 años). Los largos testigos extraídos del fondo de los lagos permiten un análisis

cuasi-continuo de las variaciones del campo geomagnético. Una vez obtenida la información paleomagnética del testigo, hay que establecer una correlación entre la profundidad del dato sedimentario y la edad absoluta (o relativa). Para efectuar la datación cobran especial relevancia los materiales orgánicos, los elementos que permiten realizar análisis isotópicos, etc.

Debido al tipo de remanencia magnética (que incluye un cierto retraso en el bloqueo de la magnetización con respecto a la edad del sedimento), al propio proceso de muestreo, a la débil magnetización que presentan y a la posible existencia de reimanaciones, los registros sedimentarios presentan fuertes dispersiones y se debe aplicar sobre ellos un fuerte filtro de suavizado. Consecuentemente, proporcionan variaciones muy suavizadas del campo geomagnético. Sin embargo, aunque los sedimentos lacustres no sean los más precisos para definir el comportamiento del Campo Principal en el pasado, son la única opción cuando queremos analizar el Campo Principal más allá de los últimos 3000 años, ya que los datos arqueomagnéticos son escasos a partir de dicha época.

Donadini et al. (2009) actualizaron la base de datos de sedimentos lacustres del Holoceno anteriormente establecida por Korte et al. (2005). En la figura 7.1 se muestra la localización de todos los datos obtenidos de sedimentos lacustres para los últimos 8000 años. Vemos que la mayoría se encuentran en el hemisferio norte y están concentrados en América del Norte y Eurasia. Los registros más largos aportan información del campo geomagnético de los últimos 35000 años. Uno de los registros más amplio es el obtenido de la Laguna de Trébol en Argentina (Irurzun et al., 2006)

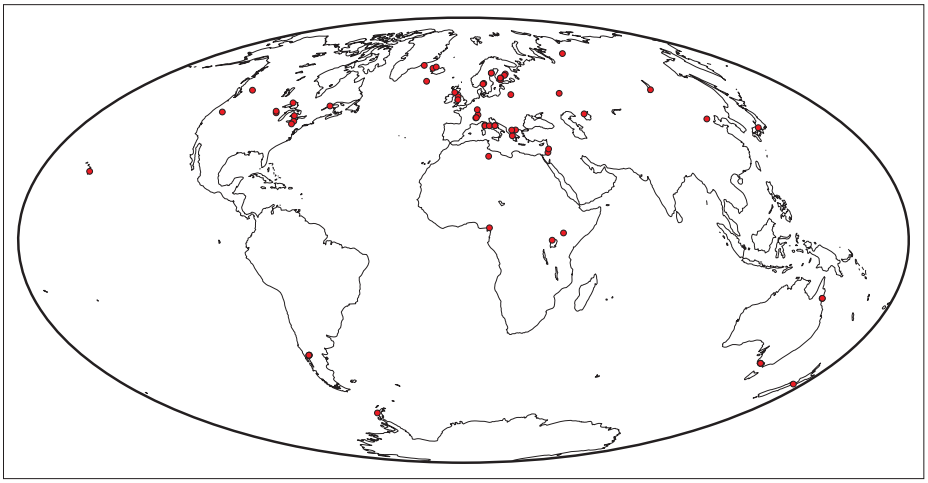

Figura 7.1. Localización de sedimentos lacustres para el Holoceno. Datos de Donadini et al., (2009).

En la siguiente sección veremos cómo gracias a los registros de sedimentos lacustres en la región Europea, podemos ampliar el período temporal del modelo regional SCHA.DIF.3K en unos 5000 años, abarcando los últimos 8000 años.

7.2. Modelo geomagnético para la región europea para el período 6000 a.C. – 1000 a.C.: el modelo SCHA.DIF.8K.

Resumen

En este trabajo se ha generado un primer modelo de campo geomagnético de bajo grado armónico válido para la región europea en el período temporal 6000 a.C. – 1000 a.C. El nuevo modelo regional proporciona información sobre la dirección (declinación e inclinación) y la intensidad del Campo Principal en Europa durante 5000 años. Al conectar dicho modelo con el previo SCHA.DIF.3K, válido desde el año 1000 a.C. hasta el 1900 d.C., y con el IGRF, proporcionamos información del Campo Principal en Europa para los últimos 8000 años. El nuevo modelo, llamado SCHA.DIF.8K, ha sido desarrollado usando la versión revisada del método SCHA en 2 dimensiones (R-SCHA2D) y la norma del Campo Principal para constreñir el problema inverso. El tamaño del casquete esférico elegido es 22º y el máximo índice de expansión armónica es 2. El problema de linealización se resuelve usando series truncadas de Taylor aplicadas a la relación entre la declinación, inclinación e intensidad y las componentes cartesianas del campo geomagnético. Como modelo inicial se ha usado el Campo Dipolar Axial Geocéntrico (GAD). Para la parte temporal se ha hecho uso de ventanas móviles de 100 años movidas cada 50 años. El modelo obtenido se ha comparado con los datos de entrada, con el modelo global CALS7K.2 y con nuevos datos independientes. El modelo regional muestra un mejor ajuste a los datos de entrada y a los datos independientes que el modelo global, especialmente en intensidad. Se ha calculado el Momento Virtual Axial Dipolar del campo geomagnético (VADM) a partir del modelo regional y se ha comparado con estudios realizados por otros autores en la región europea, obteniéndose resultados similares. Mediante la correlación de máximos de intensidad y cambios de curvatura en la región Europea, hemos determinado los cambios bruscos o jerks arqueomagnéticos del campo geomagnético para los últimos 8000 años. Por último, a partir del modelo generado, se ha comprobado la validez de la hipótesis del GAD para la región Europea.

Submitted to Geochemistry, Geophysics, Geosystems (Under Review)

Regional modelling of the Geomagnetic Field in Europe from 6000 BC to 1000 BC

F. Javier Pavón-Carrasco and Maria Luisa Osete

Grupo de Paleomagnetismo, Departamento de Física de la Tierra I: Geofísica y Meteorología, Universidad Complutense de Madrid, E-28040, Madrid, Spain (fjpavon@fis.ucm.es; mlosete@fis.ucm.es)

J. Miquel Torta

Observatori de l'Ebre, CSIC, Universitat Ramon Llull, Horta Alta 38, E-43520 Roquetes, Spain (jmtorta@obsebre.es)

[1] We have developed a first low-degree regional geomagnetic model for the European Continent valid for the period 6000 BC to 1000 BC from a selected compilation of sedimentary and archaeomagnetic data (the SCHA.DIF.8K model). This model provides information about the direction (declination and inclination) and intensity of the Earth's magnetic field in Europe during a period of 5000 years. By connecting it with our previous model, SCHA.DIF.3K, valid from 1000 BC to 1900 AD and the IGRF, we furnish continuous geomagnetic field information for the last 8000 years. It has been developed using the Revised Spherical Cap Harmonic Analysis in 2 Dimensions technique (R-SCHA2D) and using the norm of the Earth's magnetic field to constrain the inversion problem. The size of the cap is 22º and the maximum degree of the expansion is 2. The linearization problem was solved using the truncated Taylor's series applied to the expressions representing the relationship between the declination, inclination and intensity data and the Cartesian components of the geomagnetic field. We used the Geocentric Axial Dipole (GAD) field as our initial or reference field. We used the classical sliding overlapping window method for time. The size of the window was set to 100 years shifted 50 years. We compared the model's prediction with the input data, with the global CALS7K.2 model, and with new independent data. The regional model shows a better fit to the input and independent data than the global model, especially in terms of intensity, and agrees with the virtual axial dipole moment given by other studies. For the last 8000 years, the palaeosecular variation of the European geomagnetic field has recorded rapid changes or archaeomagnetic jerks and satisfies the GAD hypothesis.

Components: 9,032 words, 12 figures, 3 tables.

Keywords: Archaeomagnetism; geomagnetic secular variation; regional models; archaeomagnetic jerks; Europe.

Index Terms: 1503 Geomagnetism and Paleomagnetism: Archeomagnetism; 1522 Geomagnetism and Paleomagnetism: Paleomagnetic secular variation; 1532 Geomagnetism and Paleomagnetism: Reference fields: regional, global.

Pavón-Carrasco, F. J., M. L. Osete, and J. M. Torta (2010), Regional modelling of the Geomagnetic Field in Europe from 6000 BC to 1000 BC, for submitting to Geochem. Geophys. Geosyst.

1. Introduction

[1] Global and regional models based on palaeomagnetic, historical and instrumental data allow us to understand the behaviour of the geomagnetic field in the past. For recent times (the last 400 years), a high resolution model has been developed (GUFM1, Jackson et al., 2000) from historical data. However, if we want to understand the behaviour of the geomagnetic field for the last 10 millennia, i.e. the Holocene epoch, palaeomagnetic data must be used. Palaeomagnetic models (Hongre et al., 1998, Korte & Constable, 2003, 2005, Pavón-Carrasco et al., 2008a, 2008b, 2009; Korte et al., 2009) do not achieve the accuracy given by instrumental/historical models, but they are the only way to study the secular variation of the geomagnetic field on a millennial time scale.

[2] Palaeosecular variation curves (PSVCs) are one-dimensional models, which can be generated when a high density of palaeomagnetic data is available from a small area (with a radius no greater than 600-700 km). At present several European PSVCs have been constructed following the Bayesian approach given by Lanos (2004) (Schneep and Lanos, 2005, Gómez-Paccard et al., 2006, Tema et al., 2006, Zananiri et al., 2007, De Marco et al., 2009). However, models of this kind exclude spatial distribution of the data, and only take the temporal variation into account. Therefore they contain limited information of the geomagnetic field. In addition to this, the relocation error, which could be important (Casas and Incoronato, 2007), is not often considered in these models.

[3] Global models using the Spherical Harmonic Analysis (SHA) technique have been obtained during the last decade (Hongre et al., 1998, Korte & Constable, 2003, 2005, Korte et al., 2009). The present reference model for the last 7000 years is the CALS7K.2 (Korte & Constable, 2005) which used archaeomagnetic data, lava flows and lake sediment records as input data. However, discrepancies have been observed between recent archaeomagnetic data and model predictions (Genevey et al., 2008, Kovacheva et al., 2009).

[4] When the palaeomagnetic data are concentrated in a considerably large area, such as the European region, an intermediate approach between global models and PSVC is offered by the determination of regional models. Regional models based on exclusively archaeomagnetic data have been developed for the study of the European region during the last two or three millennia (Pavón-Carrasco et al., 2008a, 2008b, 2009). The model SCHA.DIF.3K (Pavón-Carrasco et al., 2009) is based on in situ archaeomagnetic data and is valid from 1000 BC to 1900 AD. With the aim of extending our knowledge of the geomagnetic field variations in Europe backwards in time, in this study we present a regional model for the European region covering 5 millennia from 6000 BC to 1000 BC, which then connects with the SCHA.DIF.3K. The model is constructed by applying the Revised Spherical Cap Harmonics in 2 Dimensions (R-SCHA2D, Thébault, 2008) to selected archaeomagnetic and lake sediment databases.

2. Input data

[5] The palaeomagnetic datum is constituted by one, two or three elements of the geomagnetic field (declination/inclination/intensity) associated with the geographical coordinates (latitude/longitude) and time. Heated archaeological artefacts (such as kilns, pottery, etc) are the preferred records because they can, usually, be accurately dated and the mechanism of remanence acquisition is better understood (the thermo-remanence process). However, prior to 1000 BC, there are not enough archaeomagnetic data in the European region (e.g. database of Korte et al., 2005) to perform the regional modelling process. Additional data must be considered. Data from lava flows are also scarce and the best sequences from Etna and Vesuvius have originated a considerable debate (e.g. Lanza and Zanella, 2005). Cautiously, we have not considered these data in our analysis. Lake sediment records are smoothed and magnetization is delayed due to the remanence acquisition process (e.g., Tauxe, 1993, Snowball et al., 2007 and references therein). However, to study the geomagnetic field prior to 1000 BC sedimentary records must be used. Table 1 contains information about the initial database used in this study (location, type and number of data and references).

A considerable scattering is observed in the data. To reject the outliers we used a preliminary model. The rejection criterion is explained in section 4.

2.1. Archaeomagnetic data

[6] Directional archeomagnetic data (declination and inclination) are provided by the global databases of Korte et al. (2005) and Donadini et al. (2009). For the intensity, we used the global compilation of Genevey et al. (2008). Recent data from Bulgaria have also been included (Kovacheva et al., 2009). The resulting initial archaeomagnetic database for this study contains: 232 declination, 242 inclination and 505 intensity data (see Table 1), All located within the spherical cap shown in Figure 1. Directional palaeomagnetic uncertainties are given by the semi angle of confidence α_{95} (value for the 95% confidence cone about the average fisherian direction, Fisher, 1953). The uncertainty σ_F (for archeointensities) is the standard deviation. Age uncertainties are deduced from archaeological considerations, radiocarbon and/or dendrochronology dating.

[7] An initial filter based on their statistical uncertainty has been applied. All archeomagnetic data with α_{95} /σ_F three times bigger than the mean α_{95} /σ_F value have been rejected. In addition, data with age uncertainties greater than 500 years were not considered. The filtered database contains a total of 959 archeomagnetic data (225 declination, 235 inclination and 499 intensity data). Mean values of the data uncertainties were: α_{95} = 4.0º (direction), σ_F = 3.5 μT (intensity) and 85 years (age).

2.2 Lake sediment records

[8] The lake sediment database of the Holocene (Korte et al., 2005 and Donadini et al., 2009) was updated with new sedimentary data from Italy (Vigliotti, 2006). The resulting compilation contains mainly directional data, some of which include relative (or standardized relative) intensity data. The considered sedimentary series into the spherical cap are given in Table 1.

[9] Sedimentary data from neighbouring regions are often combined to obtain a continuous and smoothed paleosecular variation curve (master curve). We have used three master curves: (i) the Scandinavian master curve: FENNOSTACK (directional information) and FENNORPIS (relative standardized intensities) (Snowball et al., 2007), based on the sedimentary sequences: FRG, FUR, MOT, SAR, NAU, BYE, and SAV (Table 1). The curve was developed by a running time window of 150 years from 7750 BC up to 1550 AD. (ii) The United Kingdom's master curve (Turner and Thomson, 1981), which shows the variation of the geomagnetic field for the last 10000 years. It was obtained from 10 cores from three sites (WIN, GEI and LOM lakes in Table 1). The calibrated ages were provided by radiocarbon methods and pollen analyses. (iii) The master curve of Belarus (Nourgaliev et al., 2005) that recorded the geomagnetic variations during the last 12000 years. It is based on results from 9 cores from Naroch and Svir lakes (NAR lake in Table 1).

[10] In addition, individual lake sediment records from Italy (AD1, AD2, TY1, TY2, NEMI, JON1, JON2 and MEZ lakes in Table 1), Greece (BEG and TRI lakes), Israel (BIR and DES lakes), Finland (VUK and POH lakes) and Germany (MEE lake) were also included.

[11] In summary, a total of 18 directional (including the 3 master curves) and 6 relative intensity lake sediment records were included in the initial database for our study.

2.3. Data distribution

[12] The geometry of the spherical cap was defined by the data distribution. We have restricted the analysis region to a spherical cap of semi angle 22º centred at 45ºN and 15ºE, including Europe, north Africa and west Asia. Figure 1 shows the spatiotemporal distribution of data. The archaeomagnetic dataset contains more intensity (Figure 1a – right) than directional data (Figure 1a – left). Eastern Europe (Bulgaria and Ukraine) is the region with the highest density of archaeomagnetic data. Lake sediment records are distributed around the spherical cap (Figure 1a, red points). The highest densities are observed in Italy, the United Kingdom, and the Scandinavian Peninsula regions. The amount of directional lake sediment data is higher than the amount of directional archaeomagnetic data, and represents

Table 1. Lake sediment records and archaeomagnetic data from 6050 BC to 950 AD.

Lake sediment records		
Country	**Lake**	**D/I/F**
Italy	AD1	I/F
	AD2	I/F
	TY1	D/I
	TY2	D/I
	NEMI**[1]	D/I
	JON1**[1]	I
	JON2**[1]	I
	MEZ	D/I/F
Greece	BEG	D/I
	TRI	D/I
Israel	BIR	D/I/F
	DES	D/I
Sweden	FGR[2]	D/I/F
	FUR[2]	D/I/F
	MOT[2]	D/I/F
	SAR[2]	D/I/F
	BYE**[2]	D/I/F
Finland	NAU[2]	D/I/F
	SAV[2]	D/I
	VUK	D/I
	POH	D/I/F
Germany	MEE	D/I
The U.K.	GEI[3]	D/I
	WIN[3]	D/I
	LOM[3]	D/I
Belarus	NAR[4]	D/I

Archaeomagnetic data		
Country	**Nº D/I**	**Nº F**
The U.K.	8/8	-
Bulgaria	110/110	126
Egypt	-/4	54
Georgia	16/22	88
Greece	29/29	79
Hungary	1/1	1
Serbia	6/6	13
Turkey	1/1	5
Ukraine	49/49	37
Cyprus	-	3
Czech Republic	-	14
Finland	-	3
Romania	-	2
Spain	-	50
Syria	3/3	12
France	-	1
Israel	-	2
Moldova	1/1	14
Switzerland	1/1	1
Austria	1/1	-
Germany	3/3	-
Italy	3/3	-

** Data are not included in the database of Donadini et al. (2009).
1. L. Vigliotti (personal communication, 2009)
2. Escandinavian master curve (Fennostack and Fennorpis).
3. UK master curve.
4. Belarus master curve.

93% of the total number of directional data. While the 54% of the intensity data correspond to relative palaeointensities obtained from lake sediment data.

3. R-SCHA2D technique and modelling process

[13] In the present work, we used the updated version of the classical SCHA technique: the revised spherical cap harmonic analysis in two dimensions, R-SCHA2D (Thébault, 2008). It is a particular case of the R-SCHA method (Thébault et al., 2006), when data are available at a constant altitude. The main difference between both modelling techniques, R-SCHA and SCHA, consists in the addition of a new set of basis functions: the Mehler conical functions. These functions allow both, a better definition of the geomagnetic field within the cap, and a better convergence in the modelling process. More specific information on the differences between the revised and classical SCHA methods can be found in Thébault and Gaya-Piqué (2008).

[14] The general solution of the Laplace equation is expressed (in the spherical cap) by an expansion in terms of spherical cap harmonics and the Mehler functions:

$$V(r,\theta,\lambda) = a\sum_{k=0}^{K_{max}}\sum_{m=0}^{k}\left(\frac{a}{r}\right)^{n_k+1} P_{n_k}^m(\cos\theta)\cdot(g_{n_k}^{m,i}\cos m\lambda + h_{n_k}^{m,i}\sin m\lambda) +$$
$$+a\sum_{k=0}^{K_{max}}\sum_{m=0}^{k}\left(\frac{r}{a}\right)^{n_k} P_{n_k}^m(\cos\theta)\cdot(g_{n_k}^{m,e}\cos m\lambda + h_{n_k}^{m,e}\sin m\lambda) + \quad [1]$$
$$+a\sum_{m\geq 0}^{M} R(r)\cdot P_{-1/2}^m(\cos\theta)\cdot(G_{-1/2}^m\cos m\lambda + H_{-1/2}^m\sin m\lambda).$$

with

$$R(r) = \frac{1}{2}\sqrt{\frac{a}{r}}\left(\ln\left(\frac{r}{a}\right)+2\right) \quad [2]$$

where r, θ and λ are the radius, the colatitude and the longitude of the data in the cap's reference frame. a is the average radius of the Earth. $P_{nk}^m(\cos\theta)$ are associated Legendre functions of real degree n_k and integer order m. $P_{-1/2}^m(\cos\theta)$ are a special case of the Mehler functions. $R(r)$ is a radial function (see Thébault, 2008). $g_{nk}^{m,i-e}$ and $h_{nk}^{m,i-e}$ are the SCH coefficients (Haines, 1985), with the subindex i indicating the internal potential and e the external potential. $G_{-1/2}^m$ and $H_{-1/2}^m$ are the new coefficients introduced by Thébault (2008). The new potential equation does not include both sets of basis Legendre functions (with $k - m$ even and $k - m$ odd), because the revised version of the SCHA method only takes into account the Legendre functions with $k - m$ even. The other set of basis functions is replaced by the Mehler functions.

[15] In palaeomagnetic studies, only the main field is considered and the declination, inclination and intensity are the elements usually analysed. These elements cannot be expressed by linear combinations of the spherical cap coefficients ($g_n^{m,i-e}$, $h_n^{m,i-e}$, $G_{-1/2}^m$ and $H_{-1/2}^m$). We solved this linearization problem using the truncated Taylor's series approach applied to the expressions of the relationship between the declination, inclination and intensity data and the Cartesian components of the geomagnetic field. A complete description of the linearization problem is given in Pavón-Carrasco et al. (2009). Here is an example for the declination (D) data:

$$D(r,\theta,\lambda,t) = D_0(r,\theta,\lambda,t) + \delta D(r,\theta,\lambda,t) =$$
$$= D_0(r,\theta,\lambda,t) + \left.\frac{\partial D(r,\theta,\lambda,t)}{\partial m}\right|_{\alpha=\alpha_0}\cdot\delta m(t) \quad [3]$$

where D_0 is an initial value of the declination, $\partial D/\partial m$ is the Frechet derivative matrix of the declination's expression and m is related to the vector of the SCH coefficients.

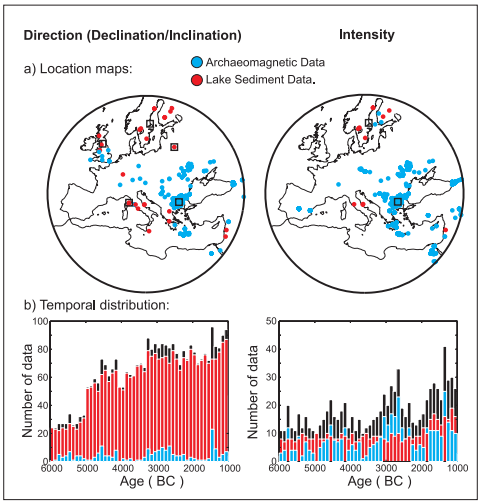

Figure 1. Spatial (a) – Temporal (b) distribution of the input data. Red: lake sediment data. Blue: archaeomagnetic data. Black histograms in (b): all data. Black squares: location of the PSVCs (5 directional and 2 intensity curves) used in the construction of the *model.0*. (see text for details).

[16] The initial values must be provided by a previous geomagnetic field model. We used the simplest geomagnetic field as our initial input model: the Geocentric Axial Dipole field (GAD). In this case the declination D_0 is zero and the inclination and intensity only depend on the geographic latitude ϕ : $I_0 = \text{atan}(2\cdot\tan\phi)$ and $F_0 = C\sqrt{1+3\cdot\sin^2\phi}$. The parameter C is a constant value that we established as:

$$C = \frac{< F_C >}{\sqrt{1+3\cdot\sin^2\phi_0}} \quad [4]$$

where $<F_C>$ is the average value of the intensity at the cap's centre and ϕ_0 is the latitude of the cap's centre. This parameter is an estimation of the first Gauss coefficient g_1^0 (for the spherical global analysis).

[17] Considering the present database error distribution (Gaussian) the L2 norm (least squares) has been applied to solve the inverse problem equation:

$$\chi^2 = < d - f(m) >^2 + \varsigma < B^2 > \quad [5]$$

where d is the actual data, $f(m)$ the modelled data and the second term is a roughness constraint.

[18] This roughness constraint is given by the norm of the geomagnetic field in the spherical cap $<B^2>$ and ς is a scalar which must be fixed in order to determine the best compromise between model complexity and the misfit (see e.g., Jackson et al., 2000). We can transform the norm of the geomagnetic field into a product of the SCH coefficients vector m and the constraint matrix M_R (see Appendix B in Thébault, 2008):

$$< B^2 >= m^T M_R m \qquad [6]$$

Expressing the data uncertainty (measurement uncertainty) as a covariance matrix C, the final matrix equation becomes:

$$m = (\varsigma M_R + A^T C^{-1} A)^{-1} A^T C^{-1} d \qquad [7]$$

[19] For the temporal modelling, we used the classical sliding overlapping window method. The size of the window is related to the temporal data distribution and the age uncertainties.

[20] Finally, the normalized *rms* misfit was obtained by taking into account the data uncertainty (σ_i) in accordance with the following expression:

$$rms = \sqrt{\frac{1}{n}\sum_{i=1}^{n}\left(\frac{d_i - f_i(m_i)}{\sigma_i}\right)^2} \qquad [8]$$

4. The rejection criterion

[21] A new filter was designed to reject the outlier data. It is based on a filtering model, called *model.0*, which was developed by using the "best" data: the Bulgarian palaeosecular variation curve based on the recent compilation of Kovacheva et al. (2009) and the best lake sediment records.

[22] To select the best lake sediment data, we assumed the following hypothesis: if a directional lake sediment record fits reasonably well to the directional predictions given by accurate archaeomagnetic data sited in the same region for the last 3000 years, then this sedimentary record has the potential to describe the behaviour of the geomagnetic field for that region in a previous time. Consequently, the available European directional sedimentary data for the last 3000 years (from 1000 BC to 1900 AD) has been compared with the geomagnetic field elements provided by the regional SCHA.DIF.3K archaeomagnetic model (Pavón-Carrasco et al., 2009).

[23] We only used sedimentary data which, besides covering the last 3000 years, also provide information prior to 1000 BC. A total of 17 directional temporal data series satisfy this requirement (see Table 2). The time-average angular deviation (α), defined by the angle between the directional sedimentary data and the model prediction, is also shown in Table 2.

[24] We selected the time-series of sedimentary data whose average angular deviations were lower or equal than 5º. Only 4 lake sediment records passed our first selection criteria: the master curve from the United Kingdom (Turner and Thompson, 1981), the reference curve from the Scandinavian Peninsula (FENNOSTACK, Snowball et al., 2007), the reference curve from Belarus (Nourgaliev et al., 2005) and the lake sediment records from the Tirreno Sea in Italy (Vigliotti, 2006).

Table 2. Lake sediment records and the average angular deviation α (* SD is the standard deviation of α).

Lake/Master Curve	Average α	SD* α
AD1	5.5	4.9
AD2	9.7	5.9
TY1	10.8	4.8
TY2	5.0	3.3
NEMI	13.3	4.5
MEZ	11.0	4.8
BEG	6.9	4.0
TRI	8.3	4.3
BIR	13.7	6.1
DES	17.4	6.3
FENNOSTACK	4.8	1.7
VUK	8.9	9.9
POH	8.3	4.9
MEE	15.0	11.2
UK master	4.6	2.6
Belarus master	4.1	2.8

[25] The reference curve from the Scandinavian Peninsula also gives relative standardized intensity values (FENNORPIS curve). We relocated all the archaeointensity data at the location of the Scandinavian reference curve using the virtual axial dipole moment (VADM) method (or the

virtual dipolar moment (VDM) when inclination data are provided). After that, we recalibrated the relative intensity data using the relocated archaeointensity by a linear fitting which is shown in Figure 2. Using the selected sedimentary data and a new PSVC for Bulgaria calculated from the updated dataset given by Kovacheva et al. (2009) we obtained the filtering *model.0*.

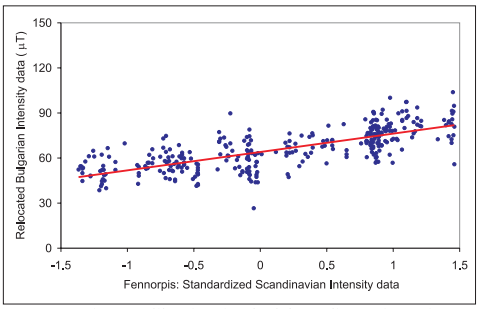

Figure 2. Linear calibration for the lake sediment intensity.

[26] The selected palaeosecular variation curves (five directional and two intensity curves) allow a smooth and continuous evolution in time to facilitate the stability in the inversion process. They are situated at five different locations, well-distributed geographically within the spherical cap (Figure 1). All PSVCs covered the time period from 6000 BC to 1000 BC, except the Italian directional curve which does not provide information prior to 3300 BC.

[27] Taking into account the number of input data for each epoch, we used the lowest degree in the spherical cap harmonic expansion, i.e. $K_{int} = K_{ext} = M = 1$ (eq. 3.1). Moreover, a regularization matrix was included in the inversion process following the details given in section 3. The GAD model was used as the initial model for the truncation of the Taylor's series of the geomagnetic field elements and for the Frechet derivative matrix (eq. 3.3). A total of 101 knot points were fixed over the whole time span (5000 years) every 50 years and we applied the regional method to obtain snapshot models at these knot points. The continuity between adjacent models was given by the smoothness of the input PSVCs. The obtained regional *model.0* was used to filter the database (both archaeomagnetic and lake sediment data) and to calibrate the relative intensity data. Directional data with angular deviations higher than 15º, and intensity data with deviations higher than 10 μT were rejected. All archaeomagnetic data satisfy our rejection criteria, but the ~16% of the lake sediment data were rejected. Finally, we retained 2367 declination, 2724 inclination and 452 intensity lake sediment data covering the whole time span.

5. The SCHA.DIF.8K model

[28] With the selected data, we obtained the regional model over 100-year windows shifted 50 years from 6050 BC to 950 BC. The model is called SCHA.DIF.8K because, by connecting it with our previous SCHA.DIF.3K model valid from 1000 BC to 1900 AD and the IGRF, we furnish continuous geomagnetic field information for the last 8000 years.

[29] Following Donadini et al. (2009) we assigned a minimum data uncertainty for the geomagnetic field elements. A minimum α_{95} of 4.3º/6.0º is fixed for the archaeomagnetic/sedimentary data uncertainty and a minimum σ_F of 5 μT is fixed for the intensity uncertainty. The maximum expansion degree in this final model was taken to be 2 for the classical internal and external potential ($K_{int} = K_{ext} = 2$, in eq. 3.1) and 1 for the potential given by the Mehler function ($M = 1$, in eq. 3.1), providing a total of 14 SCH coefficients. In order to estimate the damping parameter ς in (3.7) that allows the best prediction of the model in areas without input data, we applied our algorithm to synthetic data from the global CALS7K.2 model. These tests with synthetic data also allowed us to evaluate the sliding overlapping windows method. Results show that the variations (generated artificially by the sliding windows method) are lower than the actual variations given by the regional model.

[30] The constant C (eq. 3.5) of the GAD field model is calculated using the intensity data in the spherical cap. Figure 3 shows the value obtained for C using the 100-year windows shifted 50 years. The time-average value is 32.5 μT and a linear fitting of C shows a rate variation of 2.4 nT per year.

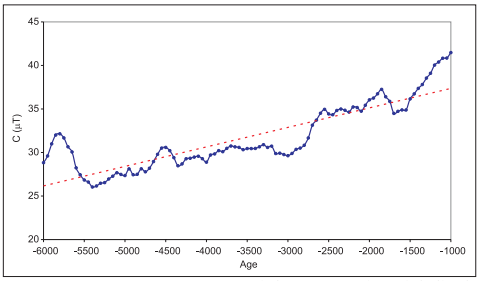

Figure 3. Average constant *C* of the geocentric axial dipole field model for all individual intensity data. Blue line: the average *C* using 100-year windows shifted 50 years. Red dashed line: linear interpolation of individual *C* data.

[31] The normalized rms misfits (Figure 4a) range around 1 for the three geomagnetic elements individually and taken together which shows a good fit of the data according to their uncertainties. The time averaged rms values are close to 1 for each element (rms_D = 1.2, rms_I = 1.3, rms_F = 1.0) and the overall value is rms_{DIF} = 1.2. The histograms of Figure 4b show the residuals between the input data and the modelled data. The residuals were binned in 50-year intervals and compared with the normalized probability density function calculated with the same mean and standard deviation (red curves). The declination residuals show a mean of – 0.1º and a standard deviation of 7.2º. Their distribution contains values between -20º and 20º and the theoretical normal distribution (red line) fits the histogram fairly well. The inclination residuals are characterized by a mean value of 0.5º and 4.3º of standard deviation. In this case, the histogram looks more like an exponential rather than a normal distribution (red curve). The intensity residual histogram is more asymmetric, with more overestimations than underestimations for the actual data. – 0.5 μT (5.6 μT) is the mean (standard deviation) of the intensity residual data.

[32] Following our previous work (Pavón-Carrasco et al., 2009), we have calculated a polynomial spatial function $\Phi(t, \phi, \lambda)$ for every window using the rms misfit data. This function defines the prediction (at 65% or 95%) uncertainty for the three geomagnetic field elements at any location and epoch.

[33] Figure 5 shows the declination, inclination and intensity maps for Europe and adjacent areas every 1000 years from 6000 BC to 1000 BC. In addition, an animation with declination, inclination and intensity maps is available as auxiliary material. The SCHA.DIF.8K model we obtained is available from the Web site: http://pc213fis.fis.ucm.es/scha.dif.8k_model.html. By indicating the latitude and longitude of the site, the output predictions are the declination, inclination and intensity (and their uncertainties at 95% of confidence) from 1000 BC to 1900 AD.

6. The SCHA.DIF.8K model prediction.

[34] The regional SCHA.DIF.8K model predictions (from 5000 BC to 1000 BC) have been compared with the input data at representative locations. Directional palaeosecular curves have been obtained at four sites within the cap (NW, SW, NE and SE), while palaeointensity curves have been calculated for the north and the south of the cap (see insets of figures 6, 7 and 8). Data have been relocated to the selected localities. Directional data (declination and inclination) have been translated using the conversion via pole method (Noël and Batt, 1990) and the intensity data using the virtual axial dipole moment, VADM (see Merrill et al., 1996). Results are shown in figures 6, 7 and 8. The predictions given by the CALS7K.2 global model have also been plotted.

[35] Declination and inclination maxima and minima have also been compared with the events labelled by Turner and Thomson (1981) from the United Kingdom master curve. We denote these marks following the same criteria used by Turner and Thomson (1981): *type* – *age*, where *type* is given by a Latin/Greek word for the declination/inclination curve and *age* is the date established by Turner and Thomson (1981) for the corresponding event. Table 3 contains a summary of the different declination and inclination events predicted by the SCHA.DIF.8K model at the four selected European regions and the ages assigned to each of them.

6.1 Declination Curves.

[36] The SCHA.DIF.8K master declination curves, in general, lie within the 95% confidence level

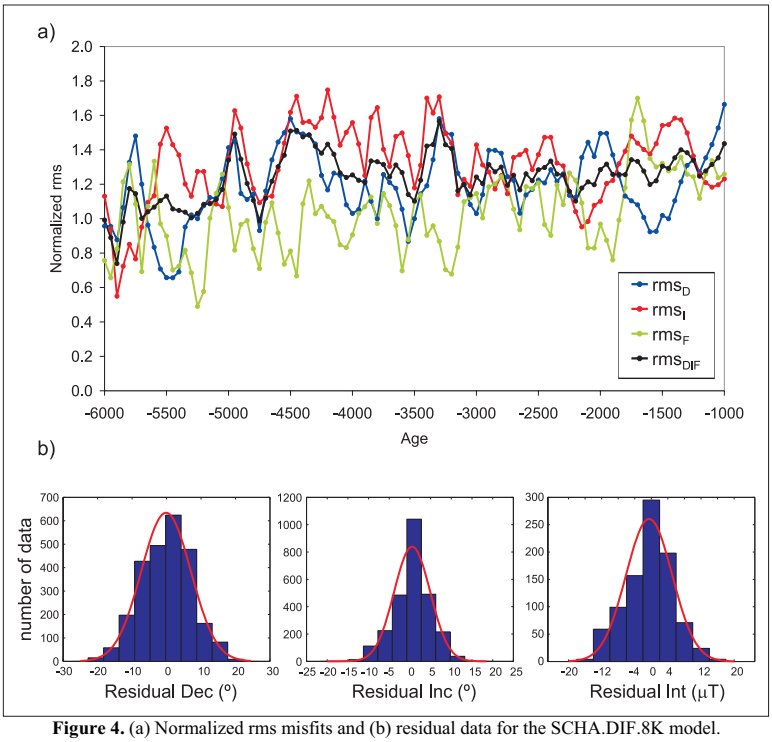

Figure 4. (a) Normalized rms misfits and (b) residual data for the SCHA.DIF.8K model.

(error bands) of the input data (Figure 6). Westerly declinations are observed around 6000 BC. The value of the declination increases continuously and a maximum (easterly declination) is reached about 5200 BC (western region) in agreement with the maximum *h – 5215 BC* proposed by Turner and Thomson (1981) from the UK master curve. In the eastern European region (NE and SE in Figure 6) the recorded maximum is broader, extending from around 5100 BC up to 4200 BC.

[37] The minimum *g′ – 3600 BC* is clearly recognized in all curves around 3600 BC. While the *g – 2910 BC* event given by the UK master curve is less pronounced but still recognized in the western region.

[38] Around 2300 BC there is a clear inflection point and declination moved more rapidly to the East in the European region. In the eastern region a maximum is observed around 1900 BC, followed by a minimum (1500 BC). Finally, the declination increases until 1000 BC. In contrast, in the western region no minima are observed, but a change in the slope of the declination variation around 1900 BC. The CALS7K.2 global model lies, in general, within the 95% confidence level of the SCHA.DIF.8K predictions, except for 3700 BC (eastern region) and 2300 BC (northern region).

6.2 Inclination Curves.

[39] Both regional and global models provide consistent inclination values (into the 95% of confidence level) for the considered time span. But differences in the ages of the relative maxima and minima are observed (figure 7). All synthetic SCHA.DIF.8K curves show a maximum at the beginning of time window, around 5900 BC. This peak could be related to the maximum *λ - 6350 BC* described by the UK master curve. It is followed by two consecutive minima: the first around 5100 BC and the second at 4300 BC. These minima are

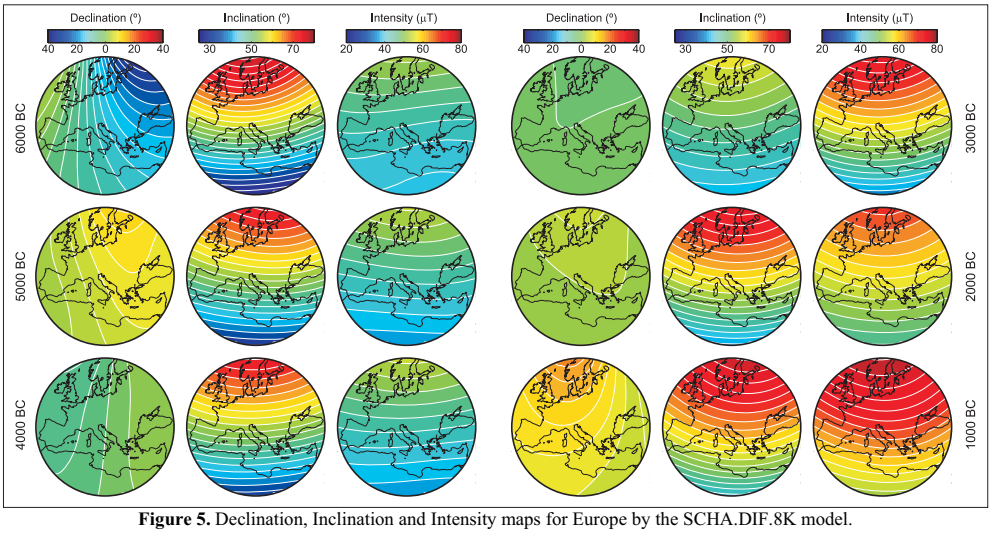

Figure 5. Declination, Inclination and Intensity maps for Europe by the SCHA.DIF.8K model. Maps every 1000 years from 6000 BC to 1000 BC.

correlated with the event κ – *5050 BC* recorded in the UK master curve.

[40] Around 3450 BC all synthetic regional curves show a maximum. This maximum agrees with the maximum proposed by Snowball et al. (2007) from the FENNOSTACK curve. However, this event seems to correspond to the ι – *4050 BC* event recorded in the UK master curve. Similarly, all the curves have a small minimum at 2900 BC while the minimum of the UK master curve, the θ - *3250 BC* event, is observed 350 years before.

[41] From 2900 BC up to 1600 BC small variations in the inclination values are predicted by the regional model. The maximum η - *2250 BC* event is not clear recorded in the synthetic curves, it is only slightly suggested in the southern region around 2200 BC. The ζ – *2050 BC* event (minimum) is observed with a temporal delay of 450 years (1600 BC) in the SW and SE curves and does not appear in the NW and NE curves.

[42] Finally, all curves tend towards a maximum at the end of the time span which is correlated with the ε – *1320 BC* event recorded in the UK master curve. See Table 3 for more details.

6.3 Intensity Curves

[43] Figure 8 shows two synthetic intensity curves for the cases of Northern and Southern Europe at 55ºN and 35ºN of latitude, respectively (both at 15ºE of longitude). The regional SCHA.DIF.8K curves agree with the input intensity data at 95% of confidence level. The global CALS7K.2 model predicts lower intensity values. The highest discrepancies between the two models are observed in two time intervals: 4500 - 3000 BC period and 2500 - 1500 BC time window. The variability of both northern and southern curves is very similar. We have to keep in mind that the Bulgarian intensity data have more weight in the model construction, because they represent most of the archaeomagnetic data and, in addition, the relative intensity data provided by sedimentary records have been rescaled using the Bulgarian data. The general behaviour of the synthetic intensity curves is that of a steady increase throughout the 5400 BC to 1000 BC time span with a linear rate of variation of 5.4/4.5 nT per year for the northern/southern region. The slope of the increase in intensity seems to have a change around 2900 BC, being the variation rate of 3.4/2.7 nT per year for the 5400−2900 BC period and of 8.8/7.5 nT/year for the 2900−1000 BC time interval (see Figure 8).

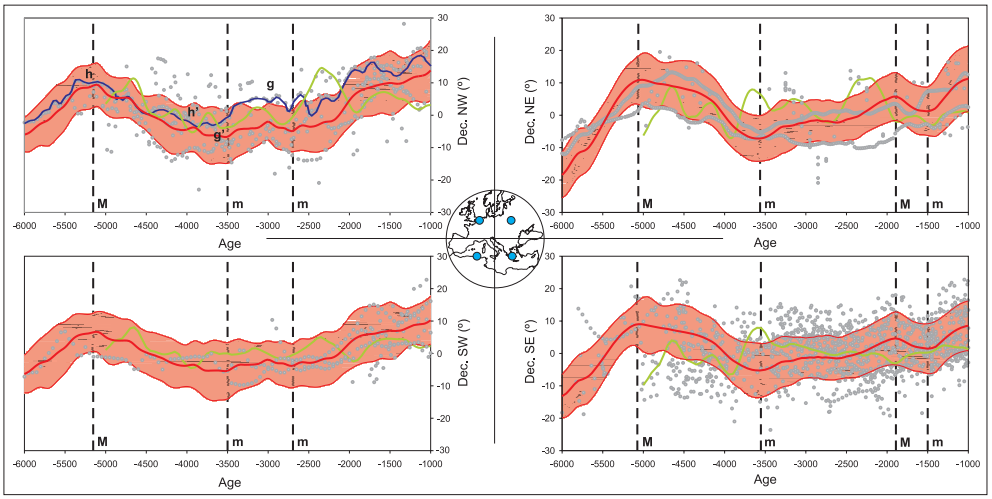

Figure 6. Comparison of the model predictions with the declination data (grey points) at the four locations shown in the inset map (on the NW, SW, NE and SE of the region). Red: SCHA.DIF.8K model with error band at 95% of confidence level. Green: CALS7K.2 model. For comparison, the UK master curve (GEI, WIN, LOM lakes) and its events are included in the NW region. Vertical dashed lines: maxima (M) and minima (m) declination from the regional model. See text for details.

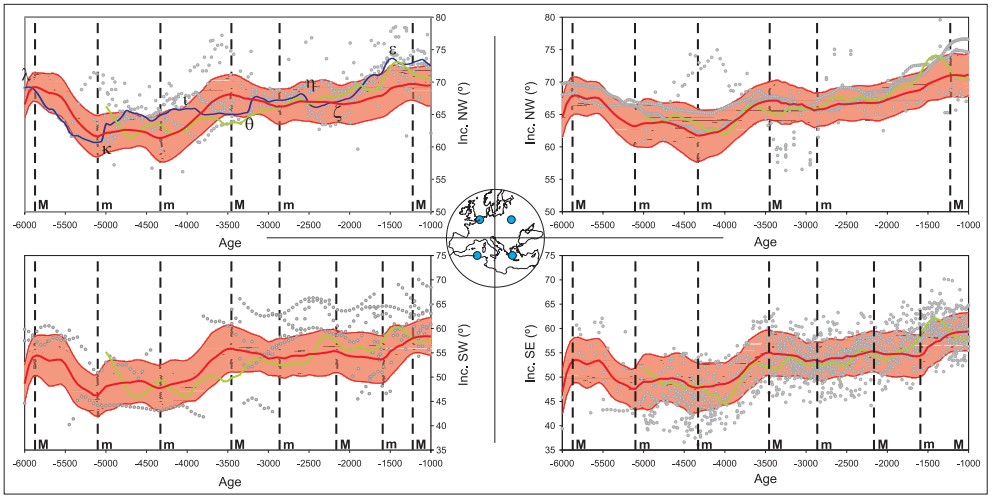

Figure 7. Comparison of the model predictions with the inclination data (grey points) at the four locations shown in the inset map (on the NW, SW, NE and SE of the region). Red: SCHA.DIF.8K model with error band at 95% of confidence level. Green: CALS7K.2 model. For comparison, the UK master curve (GEI, WIN, LOM lakes) and its events are included in the NW region. Vertical dashed lines: maxima (M) and minima (m) inclination from the regional model. See text for details.

6.4 Testing the SCHA.DIF.8K model with independent data

[44] To investigate the validity of the regional model, we have compared it with new independent data (not used in the construction of the model). The new data considered correspond to a calibrated curve obtained from eight cores from two neighbouring lakes (63.6º N of latitude and 29.0ºE of longitude) in eastern Finland (Haltia-Hovi et al., 2010) and new directional archaeomagnetic data from Hungary (Marton, 2009). Comparisons are shown in Figure 9, in which the synthetic curves from the global CALS7K.2 model are also included.

[45] The new sedimentary declination record from Finland agrees reasonably well with the declination values given by the regional SCHA.DIF.8K model. The synthetic curve from the CALS7K.2 model looks more irregular than the calibrated sedimentary curve and differs from new data around 2250 BC (Figure 9a).

[46] The inclination master curve from eastern Finland runs around 5º lower than would be expected from the regional SCHA.DIF.8K model prediction (Figure 9b). The low inclination behaviour is discussed by Haltia-Hovi et al. (2010), suggesting two possible explanations: (i) it is due to the remanence acquisition process in lake sediment records, since the depositional remanent magnetization (DRM) is assumed to cause inclination flattening (Tauxe, 2005), or (ii) the inclination master curve represents a true geomagnetic feature due to the non-dipolar contribution in this region.

[47] When comparing the inclination master curve with our regional model prediction at this location, we can observe that both curves have similar variations but with an offset of 5º. Adding 5º to the inclination master curve, it fits very well with our synthetic curve (Figure 9b). Consequently we favour the first explanation given by Haltia-Hovi et al. (2010). In addition, if the second explanation was plausible, the close FENNOSTACK inclination curve (Snowball et al., 2007) should record this non-dipolar contribution and it does not.

[48] New archaeomagnetic data from Hungary have been recently published (Marton, 2009). These new data agree with our model prediction at 47.0ºN latitude and 20.0ºE of longitude (Figure 9c and 9d). There is only an isolated declination datum around 1800 BC whose value is anomalous in comparison with the regional model but also differs from the other archaeomagnetic data with similar ages. Consistency is observed between the regional model inclination predictions and the trend of the new data. However, the new archaeomagnetic data for the 5000 BC to 4000 BC time interval exhibit lower values than the synthetic curve. This effect could be due to the use of lake sediment data in our regional model which tend to smooth the variation pattern.

7. The European geomagnetic field for the last 8000 years

[49] The present regional model SCHA.DIF.8K along with the previous regional archaeomagnetic model SCHA.DIF.3K, provide information about the palaeosecular variation of the Earth's magnetic field for the last 8000 years. In this section we analyse the variation of the virtual axial dipole moment (VADM) and its rapid changes (archaeomagnetic jerks), and the GAD hypothesis.

7.1. The Virtual Axial Dipole Moment for Europe for the last 8000 years

[50] Figure 10 shows the average synthetic VADM estimated from our regional models (SCHA.DIF.8K and SCHA.DIF.3K: Pavón-Carrasco et al., 2009), the VADM calculated from individual input archaeointensity data and the average VADM determined from different studies (Genevey et al. 2008, Yang et al., 2000). For comparison we have also included regional values calculated from different global models. In the following discussion the limits of our analysis must be considered. Genevey et al. (2008) indicated that it is necessary to be careful when the VADM/VDM is used as a tool to investigate the behaviour of the Earth's magnetic field, because the regional analysis from average VADM/VDM cannot be extrapolated to global scales. In this sense, our results are only valid for the European region.

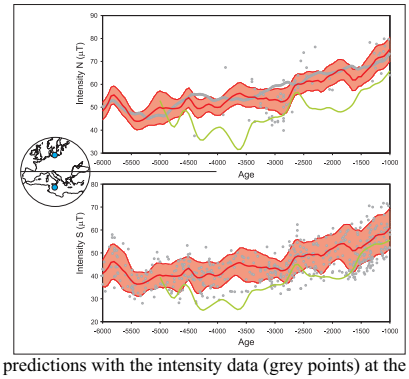

Figure 8. Comparison of the model predictions with the intensity data (grey points) at the two locations shown in the inset map (on the N and S of the region). Red: SCHA.DIF.8K model with error band at 95% of confidence level. Green: CALS7K.2 model. See text for details.

[51] For the regional study we used the SCHA.DIF.8K model for the 6000 BC to 1000 BC time period and the SCHA.DIF.3K model (Pavón-Carrasco et al., 2009) for the last 3000 years. The global CALS7K.2 and CALS3K.3 models have been considered for the intervals: 5000 BC−1000 BC and 1000 BC−1990 AD, respectively. Finally, for the instrumental/historical period we used the global GUFM1 model (Jackson et al., 2000) modified by Gubbins et al. (2006) and the last IGRF-11th (IAGA, 2009). These synthetic VADMs were generated using synthetic intensity values calculated over a homogeneous grid within the European spherical cap considered in this study. Individual VADMs were computed every 50 years and averaged over time.

[52] For the first time span, 6000 BC - 1000 BC, the synthetic VADM curve obtained from our regional SCHA.DIF.8K model fits, within the 95% of confidence level, the individual VADMs estimated from archaeointensity studies and those given by Yang et al. (2000). The synthetic average VADM curve given by the CALS7K.2 model underestimates all the other VADM data and curves. The regional model VADM curve from the regional model provides higher values than the estimations given by Genevey et al. (2008) in two different epochs: around 3700 BC and around 1900 BC. Genevey et al. (2008) used palaeointensity data with latitudes between 0°N and 70°N and longitudes from 10ºW to 80ºE to generate the average curve, which corresponds to a region much larger than that given by our spherical cap (Figure 1). This can be enough to explain the discrepancies.

Table 3. Directional events.

Declination					
Events	**NW curve**	**SW curve**	**NE curve**	**SE curve**	**Type***
h – 5215 BC	5200 BC	5200 BC	5100 BC	5100 BC	Max
g′ – 3600 BC	3500 BC	3500 BC	3500 BC	3500 BC	Min
g – 2910 BC	2700 BC	2700 BC	-	-	Min
-	-	-	1900 BC	1900 BC	Max
-	-	-	1500 BC	1500 BC	Min
Inclination					
Events	**NW curve**	**SW curve**	**NE curve**	**SE curve**	**Type**
λ - 6350 BC	5900 BC	5900 BC	5900 BC	5900 BC	Max
κ – 5050 BC	5100 BC	5100 BC	5100 BC	5100 BC	Min
	4300 BC	4300 BC	4300 BC	4300 BC	Min
ι – 4050 BC	3450 BC	3450 BC	3450 BC	3450 BC	Max
θ - 3250 BC	2900 BC	2900 BC	2900 BC	2900 BC	Min
η - 2250 BC	-	*2200 BC*	-	*2200 BC*	Max
ζ – 2050 BC	-	1600 BC	-	1600 BC	Min
ε – 1320 BC	1200 BC	1200 BC	1200 BC	1200 BC	Max

*Type: Max: Maximum and Min: minimum.

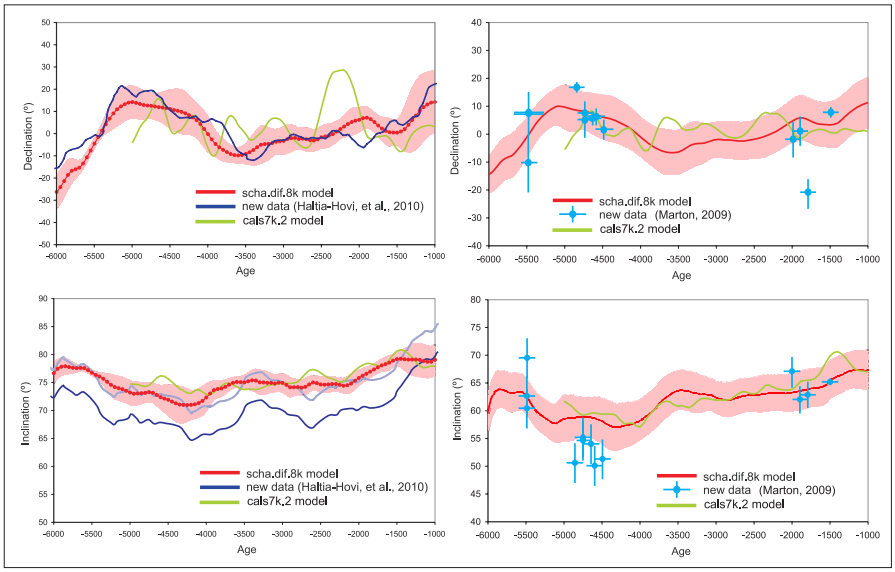

Figure 9. (a) Blue: Declination and (b) inclination master curves from eastern Finland (Haltia-Hovi et al., 2010). (c) Blue points: declination data and (d) inclination data given by Marton (2009). Red: SCHA.DIF.8K model with error band at 95% of confidence level. Green: CALS7K.2 model. The dashed blue curve is the Finland inclination master curve plus 5º. See text for details.

[53] From 1000 BC to 1600 AD, both synthetic VADM curves obtained with the regional SCHA.DIF.3K and global CALS3K.3 models, the average VADMs given by Genevey et al. (2008) and Yang et al. (2000), and the individual VADM data show a good agreement. And finally, for the historical/instrumental time span (1600 AD - 2010 AD), a high consistency is also observed between synthetic curve models, average VADMs and individual VADM data (except for the average VADM of Yang et al. 2000 which shows a higher value). The agreement is partially due to the fact that for this epoch, both palaeomagnetic (global and regional) models have been constrained by the historical GUFM1 model.

[54] Considering all the previous information, we divided the European VADM characterization into different time periods. The first time period, from 6000 BC to 5400 BC, is characterized by a decay of the VADM with a linear variation rate of $-3.5 \cdot 10^{19}$ Am^2/year. After 5400 BC the European VADM increases at different rates: $0.5 \cdot 10^{19}$ Am^2/year up to 2900 BC, around $1.2 \cdot 10^{19}$ Am^2/year from 2900 BC to 1000 BC and $4.6 \cdot 10^{19}$ Am^2/year for the time interval 1000 BC – 500 BC. Between 500 BC and 800 AD the VADM shows a sort of parabolic behaviour with a minimum around 200 AD. And finally, a linear variation rate of $-3.5 \cdot 10^{19}$ Am^2/year indicates a strong decay of the European VADM for the last 1200 years.

7.2. Rapid changes of the geomagnetic field in Europe

[55] There are different ways to describe the rapid changes or archaeomagnetic *jerks* of the palaeosecular variation of the Earth's magnetic field (Gallet et al., 2003, 2005, 2009a and 2009b; Snowball and Sandgren, 2004; Mandea and Olsen, 2009) and several theories about the origin of them have been suggested (see Gallet et al., 2009b and references therein for a review). However, it is still necessary that the scientific community establishes a consensus definition which is, up to date, absent. In this study, we follow the Gallet et al's (2003) definition: simultaneous occurrence of intensity maxima and directional curvature changes, To find the maxima intensity $M_F(t)$ and directional curvature $\rho_D(t)$ in an individual PSVC (declination,

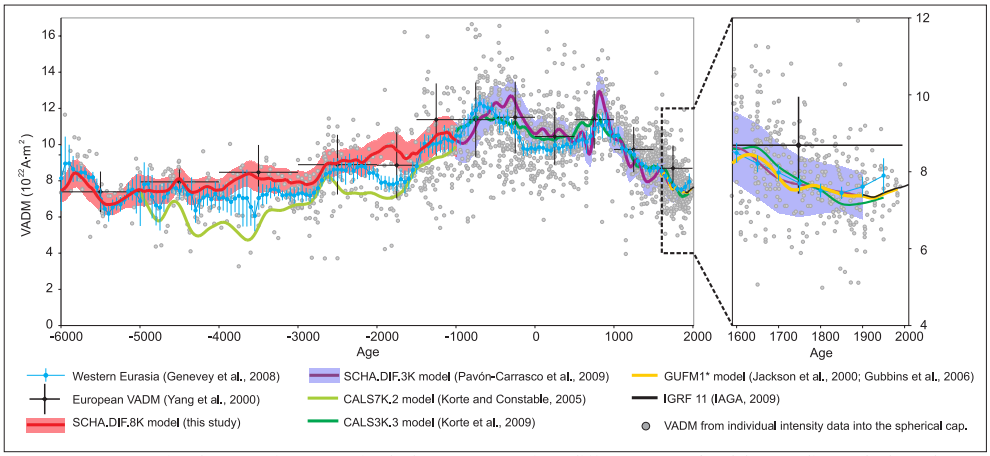

Figure 10. Regional VADM for Europe for the last 8000 years from different sources/models according to the legend.

inclination and intensity curves) we applied the following expressions:

$$M_F(t) = -sign(\ddot{F}(t))\frac{1}{|\dot{F}(t)|} \quad [9]$$

$$\rho_D(t) = \frac{|\dot{D}(t)\cdot\ddot{I}(t) - \dot{I}(t)\cdot\ddot{D}(t)|}{[\dot{D}(t)+\dot{I}(t)]^{3/2}} \quad [10]$$

where $\dot{D}(t)$, $\dot{I}(t)$ and $\dot{F}(t)$ are the first derivatives of the declination, inclination and intensity in time respectively, and $\ddot{D}(t)$, $\ddot{I}(t)$ and $\ddot{F}(t)$ are the second derivatives with time. The *sign* function is *sign(x) = x/abs(x)*. Pavón-Carrasco et al. (2009) used the SCHA.DIF.3K model to find 6 archaeomagnetic *jerks* over the last 3000 years using the PSVC at the centre of Europe (48ºN of latitude and 9ºE of longitude). In this study, instead of using the PSVC of the centre of Europe, we calculated the spatial averaged maxima intensity and curvature over Europe. To do that, we averaged expressions 9 and 10 into the spherical cap for the whole time interval 6000 BC – 1900 AD, using both SCHA.DIF.8K and SCHA.DIF.3K models.

[56] Figure 11 shows the calculated intensity maxima and the directional curvature changes for the last 8000 years. Results show a different behaviour before and after 1000 BC, that clearly reflects the use of the two different regional models and the input data considered. The SCHA.DIF.8K model gives maxima wider than those given by the SCHA.DIF.3K model. The reason for this discrepancy is the number and type of input data used for generating the models. For the present SCHA.DIF.8K model, both, lake sediment records and archaeomagnetic data have been used as input data, while only archaeomagnetic data were considered for determination of the SCHA.DIF.3K model. The sedimentary records are smooth, consequently, only broad peaks are expected.

[57] A correlation study was carried out to establish the occurrence of archaeomagnetic *jerks* (figure 11c). The new analyses give 6 AMJs for the last 3000 years (the same described in Pavón-Carrasco et al., 2009) as well as several AMJs prior to 1000BC (see Figure 11c).

7.3. The averaged directional and intensity field: the GAD field

[58] A principal assumption in palaeomagnetism is that of considering the geomagnetic field as a geocentric axial dipole (GAD) field when the palaeosecular variation is averaged over sufficient time, i.e., around 10000 years (Merrill and McFadden, 2003, for a review). This GAD model of the field is a fundamental tool for palaeomagnetic studies. The characteristics of the geomagnetic field elements of the GAD field are given in section 3. To test this hypothesis we

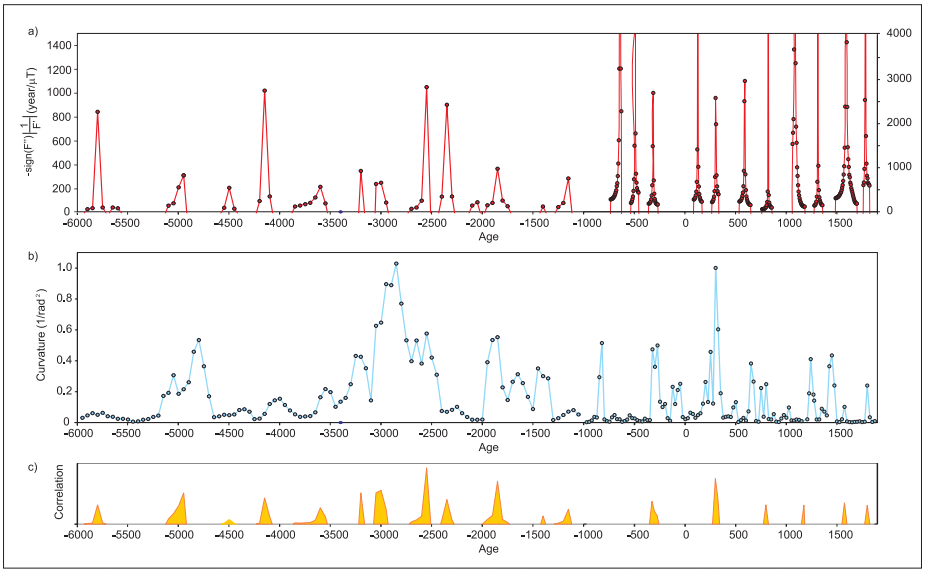

Figure 11. Archaeomagnetic jerks: a) Maxima intensity, b) directional curvature and c) correlation for the last 8000 years by SCHA.DIF.3K and SCHA.DIF.8K models (see text for details).

averaged the palaeosecular variation of the geomagnetic field over Europe for the last 8000 years using the present SCHA.DIF.8K and our previous SCHA.DIF.3K models.

[59] Synthetic curves were generated in a regular grid in the spherical cap to simulate the record of the palaeosecular variation. The directional and intensity curves were averaged over time to obtain one averaged value for each location and for the whole time interval (6000 BC – 1900 AD). Fisherian statistics was used for averaging the directional curves. Figure 12 shows the obtained average regional models for the last 8000 years and the GAD field. Results show that, for the last 8000 years, the palaeosecular variation of the Earth's magnetic field is approximately averaged to a GAD field. The intensity map of the GAD field in Figure 12 was scaled with a first Gauss coefficient equal to 35 μT. This is, in fact, the averaged value of *C* calculated in section 5 - in that case, for the period from 6000 BC to 1900 AD.

8. Conclusions

[60] In this study we have developed a first regional model of the geomagnetic field for Europe, Northern Africa and Western Asia from 5000 BC to 1000 BC. The model was constructed using archaeomagnetic data and lake sediment records. Although the sedimentary data show a smooth behaviour of the geomagnetic field, they are essential for our knowledge of the palaeosecular variation of the geomagnetic field. Through several tests we have proved that the R-SCHA2D technique can be applied to this type of data using a roughness constraint in the inversion process. Our results provide an alternative to the global modelling approach which, thanks to the density of data over the European continent, is superior in terms of a better fitting.

[61] The resulting model, SCHA.DIF.8K, provides the values of the three elements of the geomagnetic field (declination, inclination and intensity) for any European location. The directional secular variation given by the regional model shows good agreement with the United Kingdom master curve proposed for the Holocene (Turner and Thomson, 1981) and with new independent data not used in the modelling process. For the last 8000 years, the average regional European VADM is characterized by periods of increase between 5000 BC and 500 BC and an abrupt decay, confirmed in previous

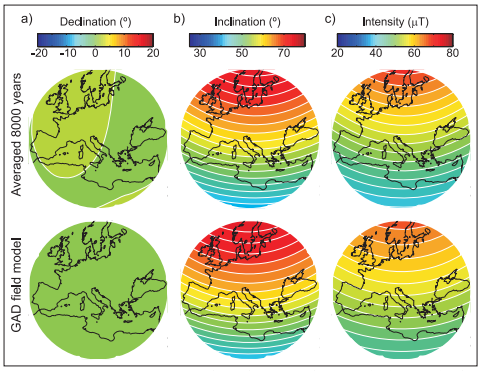

Figure 12. (a) Averaged palaeosecular variation of the Geomagnetic Field in the European region using both SCHA.DIF.3K and SCHA.DIF.8K models for the last 8000 years, and (b) the GAD field. See text for details.

studies, for the last 1200 years. A correlation study of the simultaneous occurrence of intensity maxima and directional curvature changes shows that the Earth's magnetic field has recorded several archaeomagnetic *jerks* over the last 8000 years. Moreover, we have demonstrated the GAD hypothesis for the European region based on regional modelling.

Acknowledgments

[62] The authors are grateful to the Spanish research project CGL2008-02203. F.J. Pavón-Carrasco thanks the Spanish FPI BES-2006-13488 grant for allowing him a stay of six months at IPG Paris. He would like to thank Erwan Thébault for providing the set of Mehler functions and especially for his help and discussions concerning the R-SCHA2D technique when F.J. Pavón-Carrasco was at the IPG Paris. We are also grateful to L. Vigliotti who provided the Italian lake sediment data.

References

Casas, Ll. and A. Incoronato (2007), Distribution analysis of errors due to relocation of geomagnetic data using the 'Conversion via Pole' (CVP) method: implications on archaeomagnetic data. Geophys. J. Int., 169 (2), 448 – 454.

De Marco, E., E. Tema, Ph. Lanos, and D. Kondopoulou (2009), A directional Secular Variation Curve for Greece for the last 4500 years: Comparison with regional and global geomagnetic field models. Abstracts AGU Fall Meeting 2009.

Donadini, F., M. Korte, and C. G. Constable (2009), Geomagnetic field for 0–3 ka: 1. New data sets for global modeling, Geochem. Geophys. Geosyst., 10, Q06007, doi:10.1029/2008GC002295.

Fisher, R.A. (1953), Dispersion on a sphere. Proc. Roy. Soc. London A 271, 295–305.

Gallet, Y., A. Genevey, and V. Courtillot (2003), On the possible occurrence of archeomagnetic jerks in the geomagnetic field over the past three millennia, Earth Planet. Sci. Lett. 214, 237– 242.

Gallet, Y., A. Genevey, and F. Fluteau (2005) Does Earth's magnetic field secular variation control centennial climate change? Earth Planet. Sci. Lett. 236, 339–347.

Gallet, Y., G. Hulot, A. Chulliat, and A. Genevey (2009), Geomagnetic field hemispheric asymmetry and archeomagnetic jerks, Earth Planet. Sci. Lett. 284, Issues 1-2, 179-186.

Gallet, Y., A. Genevey, M. Le Goff, J.G-A. Warmé, and A. Lefèvre (2009b), On the use of archaeology in geomagnetism, and vice-versa: Recent developments in archaeomagnetism. C.R. Physique 10, 630 – 648.

Genevey, A., Y. Gallet, C.G. Constable, M. Korte, G. Hulot (2008), ArcheoInt: An upgraded compilation of geomagnetic field intensity data for the past ten millennia and its application to the recovery of the past dipole moment. Geochem. Geophys. Geosyst, Vol. 9, Number 4.

Gómez-Paccard, M., Ph. Lanos, A. Chauvin, G. McInstosh, M.L. Osete, G. Catanzariti, V.C.Ruiz-Martínez and J.I. Núñez (2006), The first Archaeomagnetic secular variation curve for the Iberian Peninsula. Comparison with other data from Western Europe and with global geomantetic field models. Geochem. Geophys. Geosyst., VOL. 7, Q12001, doi:10.1029/2006GC001476.

Gubbins, D., Jones, A.L. and C.C. Finlay (2006), Fall in Earth's Magnetic Field is erratic. Science. Vol. 312. no. 5775, pp. 900 – 902.

Haines, G.V. (1985), Spherical Cap Harmonic Analysis. J. Geophys. Res. 90 (B3), 2583 – 2591.

Haltia-Hovi,E., N. Nowaczyk, and T. Saarinen (2010), Holocene palaeomagnetic secular variation recorded in multiple lake sediment cores from eastern Finland. Geophys. J. Int. (2010) 180, 609–622.

Hongre, L., G. Hulot and A. Khokhlov (1998), An analysis of the geomagnetic field over the past 2000 years. Phys. Earth Planet. Int., 106, 311 – 335.

IAGA (2009), 11th generation of the Internacional Geomagnetic Referente Field. http://www.ngdc.noaa.gov/IAGA/vmod/igrf.html

Jackson, A., A.R.T. Jonkers and M.R. Walker (2000),Four centuries of geomagnetic secular variation from historical records. Phil. Trans. R. Soc. Lond. A 358, 957 – 990.

Korte, M., A. Genevey, C.G. Constable, U. Frank, and E. Schnepp (2005), Continuous geomagnetic field models for the past 7 millennia: 1. A new global data compilation. Geochem. Geophys. Geosyst., 6, Q02H15, doi:10.1029/2004GC000800.

Korte, M., and C. G. Constable (2003), Continuous global geomagnetic field models for the past 3000 years. Phys. Earth Planet. Inter.140 73-89.

Korte, M. and C. G. Constable (2005), Continuous geomagnetic field models for the past 7 millenia: 2. CALS7K. Geochem. Geophys. Geosyst, 6, Q02H16, doi:10.1029/2004GC000801.

Korte, M., F. Donadini, and C. G. Constable (2009), Geomagnetic field for 0–3 ka: 2. A new series of time-varying global models, Geochem. Geophys. Geosyst., 10, Q06008, doi:10.1029/2008GC002297.

Kovacheva, M., Y. Boyadziev, M. Kostadinova, N. Jordanova, and F. Donadini (2009), Updated archeomagnetic data set of the past 8 millennia from the Sofia laboratory, Bulgaria, Geochem. Geophys. Geosyst., 10, Q05002, doi:10.1029/2008GC002347.

Lanos, Ph. (2004), Bayesian inference of calibration curves: application to archaeomagnetism, in Tools for constructing chronologies: crossing disciplinary boundaries. Vol. 177, edited by C. Buck, and A. Millard, pp. 43 – 82, Springer-Verlag, London.

Lanza, R., and E. Zanella (2005), Comments on ‘‘Chronology of Vesuvius’ activity from A.D. 79 to 1961 based on archeomagnetism of lavas and historical sources” by C. Principe et al. Bull Volcanol. Bull Volcanol. doi:10.1007/s00445-005-0030-9.

Mandea, M., and N. Olsen (2009), Geomagnetic and Archeomagnetic Jerks: Where Do We Stand?. - Eos, Transactions, American Geophysical Union, 90, 24, 208-208

Marton, P (2009), Prehistorical archaeomagnetic directions from Hungary in comparison with those from south-eastern Europe. Earth Planets Space, 61, 1351–1356.

Merrill, R.T., M.W McElhinny, and P.L. McFadden (1996), The magnetic field of the Earth, Ed. Academic Press.

Merrill, R.T. and P.L. McFadden (2003), The geomagnetic axial dipole field assumption. Phys. Earth Planet. Int. Volume 139, 171–185

Noël, M. and C.M. Batt (1990), A method for correcting geographically separated remanence directions for the purpose of archaeomagnetic dating. Geophys. J. Int., 102, 753 – 756.

Nourgaliev, D., F. Heller, A. Borisov, P. Yasonov, I. Chernova, and I. Hajdas (2005), Principal features (master curve) of geomagnetic field variations in Belorussia during the last 12 thousand years, Russ. J. Earth Sci., 7, 1–16.

Pavón–Carrasco, F.J., M.L. Osete, J.M. Torta, L.R. Gaya–Piqué, and Ph. Lanos (2008a), Initial SCHA.DI.00 regional archaeomagnetic model for Europe for the last 2000 years. Phys. Chem. Earth., Vol. 33, Issues 6-7, 596 – 608.

Pavón–Carrasco, F.J., M.L. Osete, J.M. Torta, and L.R. Gaya–Piqué (2008b), A regional archaeomagnetic model for the palaeointensity in Europe for the last 2000 years and its implications for Climatic Change. Pure and Applied Geophysics, Vol. 165, nº6, 1209 - 1225.

Pavón–Carrasco, F.J., Osete, M.L., Torta, J.M. and, Gaya–Piqué, L.R., 2009. A regional archeomagnetic model for Europe for the last 3000 years, SCHA.DIF.3K: applications to archeomagnetic dating. Geochem. Geophys. Geosyst., 10, Q03013, doi:10.1029/2008GC002244.

Schnepp, E. and Ph. Lanos (2005), Archaeomagnetic secular variation in Germany during the past 2500 years. Geophys. J. Int., 163, 479 – 490.

Snowball, I., L. Zillen, A. Ojala, T. Saarinen, and P. Sandgren (2007), FENNOSTACK and FENNOPRIS: Varve dated Holocene palaeomagnetic secular variation and relative palaeointensity stacks for Fennoscandia, Earth Planet. Sci. Lett., 255, 106–116.

Tauxe, L. (1993), Sedimentary records of relative paleointenisty of the geomagnetic field in sediments: theory and practice, Rev. Geophys., 31,319-354, 1993.

Tauxe, L. (2005), Inclination flattening and the geocentric axial dipole hypothesis, Earth planet. Sci. Lett., 233, 247–261.

Tema, E., I. Hedley and Ph. Lanos (2006), Archaeomagnetism in Italy: a compilation of data including new results and a preliminary Italian secular variation curve. Geophys. J. Int. 167, 1160 – 1171.

Thébault, E. (2008), A proposal for regional modelling at the Earth's surface, R-SCHA2D, Geophys. J. Int., 174, 118–134.

Thébault, E., J.J. Schott and M. Mandea (2006), Revised spherical cap harmonic analysis (R-SCHA): Validation and properties. J. Geophys. Res., Vol. 111, B01102, doi: 10.1029/2005JB003836.

Thébault, E. and L.R. Gaya-Piqué (2008), Applied comparisons between SCHA and R-SCHA regional modeling techniques. Geochem. Geophys. Geosyst., Vol. 9, Number 7.

Turner, G. M., and R. Thomson (1981), Lake sediment record of the geomagnetic secular variation in Britain during Holocene times, Geophys. J. R. Astron. Soc., 65, 703–725.

Vigliotti, L. (2006), Secular variation record of the Earth’s magnetic field in Italy during the Holocene: Constrain for the construction of a master curve, Geophys. J. Int., 165, 414 – 429.

Yang, S., H. Odah, and J. Shaw (2000), Variations in the geomagnetic dipole moment over the last 12000 years, Geophys. J. Int., 140, 158–162.

Zananiri, I., C.M. Batt, Ph. Lanos, D.H. Tarling, and P. Linford (2007), Archaeomagnetic secular variation in the UK during the past 4000 years and its application to archaeomagnetic dating. Phys. Earth Planet. Int. Volume 160, Issue 2, p. 97 – 107.

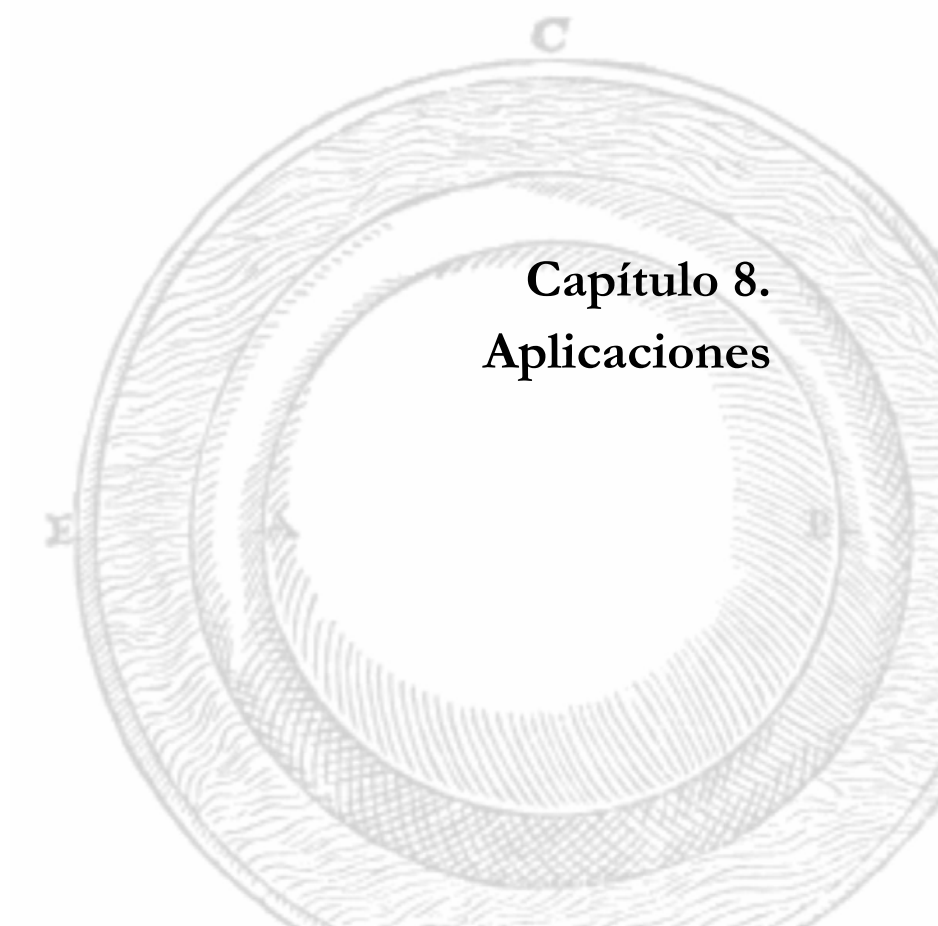

Capítulo 8.
Aplicaciones

Los dos últimos modelos regionales generados cubren el período temporal de los últimos 8000 años: el modelo SCHA.DIF.8K desde el 6000 a.C. hasta el 1000 a.C. y el modelo SCHA.DIF.3K desde el 1000 a.C. hasta el 1900 d.C. Ambos modelos pueden ser usados para evaluar las variaciones del campo geomagnético en la región Europea, Norte de África y oeste de Asia. Debemos tener en cuenta la naturaleza de ambos modelos, pues el primero está basado en la combinación de datos sedimentarios y arqueomagnéticos y el segundo es puramente arqueomagnético. La utilización de datos sedimentarios conlleva un mayor suavizado del modelo SCHA.DIF.8K respecto del 3K y ello tiene consecuencias que serán analizadas en el presente capítulo. Además, en este capítulo se presentan algunas de las aplicaciones directas de los modelos regionales obtenidos, como es el detectar y estudiar cambios bruscos en la variación paleosecular, su posible relación con el clima y finalmente el uso de los modelos para la datación arqueomagnética/paleomagnética.

8.1. Variaciones bruscas del Campo Principal: *jerks* arqueomagnéticos.

En los capítulos 6 (sección 6.2) y 7 (sección 7.2) vimos la posibilidad del uso de los modelos SCHA.DIF.3K y SCHA.DIF.8K para analizar las variaciones rápidas del campo geomagnético que han ocurrido en los últimos 8000 años y detectadas en Europa. Para ello hemos realizado un análisis conjunto de los tres elementos geomagnéticos (declinación, inclinación e intensidad) proporcionados por los modelos regionales.

Existen numerosas formas de definir la variación brusca del campo geomagnético observada a partir de estudios arqueomagnéticos (*jerk* arqueomagnético) y determinar su origen (Gallet et al., 2009 y referencias internas). Actualmente es un tema de discusión en la comunidad científica (ver, por ejemplo, Mandea y Olsen, 2009). En nuestro trabajo hemos considerado la definición dada por Gallet et al. (2003), que considera el *jerk* arqueomagnético como aquel definido por máximos en intensidad y máximos en la curvatura direccional, es decir, variaciones direccionales bruscas.

Hay que tener en cuenta que la variación paleosecular varía en el espacio, por lo que se debe tener cuidado a la hora de explorar los resultados y, por otra parte, se debe tener también en cuenta al afrontar este estudio. Si queremos, por ejemplo, analizar los cambios rápidos de la variación paleosecular en un punto

geográfico en concreto, debemos usar la PSVC determinada por el modelo en dicho lugar. Sin embargo, si queremos analizar las variaciones rápidas del campo geomagnético en toda la región Europea, se deben promediar los resultados en todo el área de estudio. En el capítulo 6 (sección 6.2) analizamos los *jerks* arqueomagnéticos a partir de la curva de variación paleosecular obtenida en el centro del casquete (48ºN de latitud y 9ºE de longitud), sin embargo, en el capítulo 7 (sección 7.2) se hizo uso de todas las PSVCs de la región Europea para obtener un resultado global para la región de estudio.

i) Máximos en intensidad. Para determinar los máximos de intensidad debemos tener en cuenta la derivada temporal primera (denotada con un punto) y segunda (dos puntos) de las curvas de variación paleosecular de la intensidad *F(t)*. Para una localización dada (latitud ϕ y longitud λ) dichos máximos se pueden calcular como:

$$M_F(t) = -sig(\ddot{F}(t))\frac{1}{\left|\dot{F}(t)\right|} \qquad [8.1]$$

Siendo *sig* la función signo. Sin embargo, si queremos calcular el valor máximo dentro de un área circular de semiángulo esférico θ_0, debemos promediar su valor como:

$$\bar{M}_F(t) = \frac{1}{2\pi \sin\theta_0}\iint M_F(t,\phi,\lambda)d\Omega \qquad [8.2]$$

Donde $d\Omega$ es el diferencial de superficie esférica: $d\Omega = \sin\phi d\phi d\lambda$.

ii) Máximos en la curvatura direccional. En este caso, debemos calcular las derivadas temporales primera (un punto) y segunda (dos puntos) de la declinación *D(t)* e inclinación *I(t)*. Para el caso particular de una localización concreta (latitud ϕ y longitud λ), dicha curvatura viene expresada como:

$$\rho_{direc}(t) = \frac{\left|\dot{D}(t)\cdot\ddot{I}(t) - \dot{I}(t)\cdot\ddot{D}(t)\right|}{[\dot{D}(t)+\dot{I}(t)]^{3/2}} \qquad [8.3]$$

De nuevo, si queremos analizar la curvatura en una región, debemos promediar la curvatura en dicha región mediante una integral de superficie:

$$\bar{\rho}_{direc}(t) = \frac{1}{2\pi \sin\theta_0}\iint \rho_{direc}(t,\phi,\lambda)d\Omega \qquad [8.4]$$

En nuestro caso hemos considerado una malla regular en la región Europea, donde hemos calculado para cada punto de malla las PSVCs dadas por el modelo regional SCHA.DIF.3K y SCHA.DIF.8K. Estas curvas han sido usadas para calcular los máximos en intensidad y curvatura promediados dentro del área de interés (ec. 8.2 y 8.3). Los *jerks* arqueomagnéticos han sido determinados

mediante la correlación de ambas funciones. La figura 8.1 muestra los máximos obtenidos así como la ocurrencia de jerks (figura 8.1c) establecida por la correlación de los máximos de intensidad y curvatura. Vemos que existe una clara diferencia de las gráficas antes y después del año 1000 a.C. Los máximos se ensanchan para épocas anteriores al año 1000 a.C. Ello es debido al uso de datos sedimentarios en el modelo SCHA.DIF.8K que suavizan las variaciones del campo geomagnético. Como se puede observar, el campo geomagnético ha sufrido numerosos *jerks* arqueomagnéticos en los últimos 8000 años.

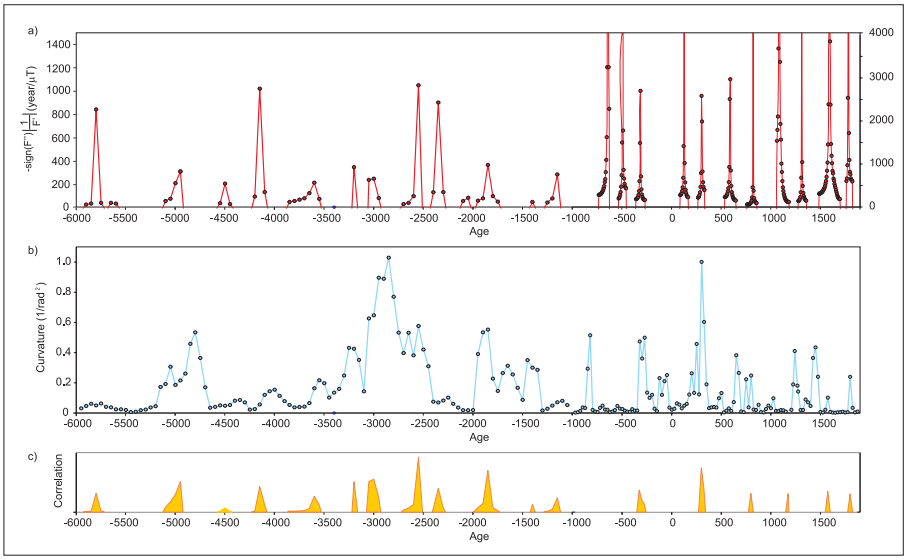

Figura 8.1. Jerk arqueomagnéticos: (a) máximos de intensidad, (b) curvatura direccional promediados en la región Europea según los modelos SCHA.DIF.3K y SCHA.DIF.8K; y (c) su correlación.

8.2. Arqueomagnetismo y Clima.

Gallet et al. (2006) y Courtillot (2007) sugieren un mecanismo de conexión entre el campo geomagnético y el clima. Dichos autores proponen que los cambios en intensidad del Campo Principal afectan a la dosis de rayos cósmicos que penetran en la atmósfera y esto influye en la generación de nubes y en consecuencia, el clima de nuestro planeta. Según sus postulados, los períodos de alta intensidad geomagnética deben estar asociados a períodos fríos y viceversa. Gallet et al. (2009) revisa dicha relación comparando los datos de intensidad de Europa occidental (últimos 2000 años) y de Oriente Medio (4000 a.C. – 1000 d.C.) y con la información climática proporcionada por el avance y retroceso de glaciares alpinos (ver capítulo 5.2, sección 4.3) y con datos paleoclimáticos del Noreste atlántico.

En el capítulo 5 (sección 5.2) corroboramos la hipótesis de Gallet et al. (2005) para los últimos 2000 años. Nosotros comparamos la curva de intensidad que proporcionaba el modelo SCHA.DI.00-F con los períodos fríos y cálidos dados por el avance y retroceso de glaciares para los últimos 2000 años. Ahora, vamos a comparar la curva de intensidad dada por los modelos SCHA.DIF.3K y SCHA.DIF.8K (últimos 8000 años) con los eventos climáticos considerados por Gallet et al. (2009). La figura 8.2 muestra la curva de intensidad a la latitud de París (48.9ºN) y la curva de intensidad en Medio Oriente (en la latitud de la antigua ciudad de Mari, 34.5ºN), ambas son comparadas con datos de avance y retroceso de glaciares alpinos y de índices climáticos de testigos de hielo del Noreste Atlántico, respectivamente (Gallet et al., 2009).

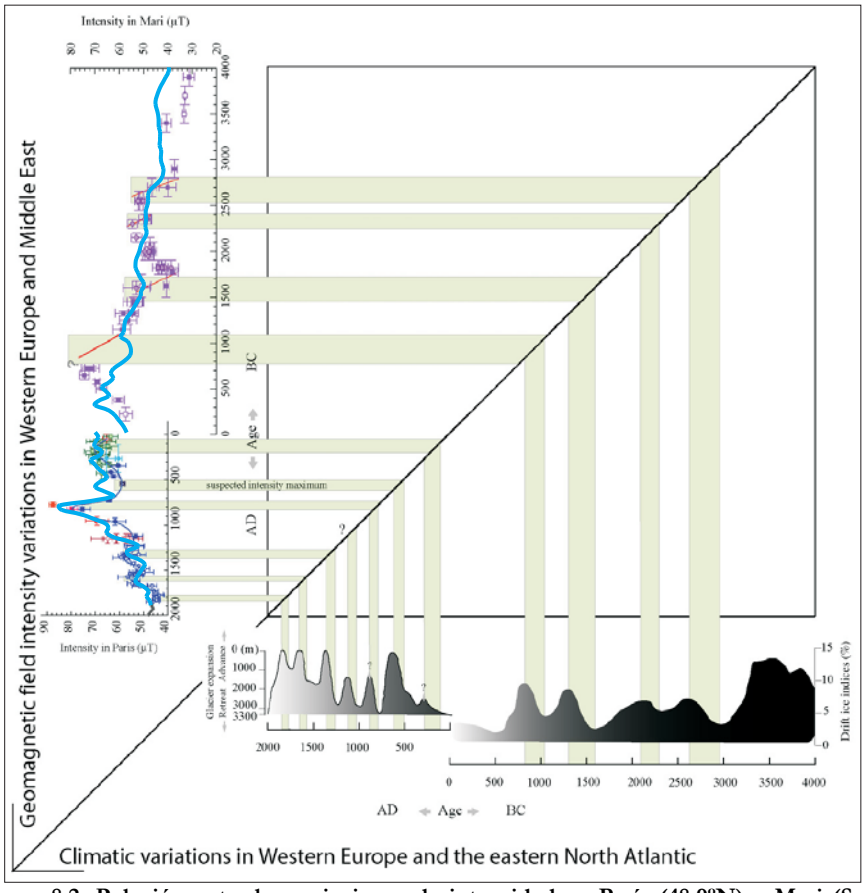

Figura 8.2. Relación entre las variaciones de intensidad en París (48.9ºN) y Mari (Syria, 34.5ºN) con los datos climáticos del avance de glaciares alpinos y testigos de hielo del Noreste Atlántico. (Figura modificada de Gallet et al., 2009). Curvas de intensidad en azul indican los modelos regionales de este trabajo: SCHA.DIF.3K y SCHA.DIF.8K.

Vemos que para los últimos 2000 años, nuestro modelo SCHA.DIF.3K (al igual que el previo SCHA.DI.0-F, sección 5.2), corrobora dicha relación e incluso se confirman los máximos supuestos por Gallet et al. (2005) entorno al 650 d.C. y 1100 d.C. Sin embargo la correlación es más compleja para el intervalo temporal: 4000 a.C. – 1000 d.C. Puede que la falta de una correlación clara sea debida al uso de datos sedimentarios en el modelo SCHA.DIF.8K, que como ya hemos explicado, hace que se suavicen las variaciones del campo geomagnético y que disminuya la resolución temporal o que simplemente sea casual y no causal la correlación observada en los dos últimos milenios. Para poder obtener un modelo del campo geomagnético con mayor resolución, que permita abordar este tipo de estudios, es necesario disponer de más datos arqueomagnéticos de alta precisión. Para poder así establecer modelos robustos, además de establecer correlaciones con otros parámetros climáticos.

8.3. Datación arqueomagnética.

Resumen

En este trabajo se aporta un software informático generado en código Matlab para realizar dataciones arqueomagnéticas. La base de la datación arqueomagnética es la comparación de la dirección (y/o intensidad) de la magnetización remanente obtenida en un yacimiento arqueológico con una curva de variación paleosecular (PSVC, del inglés *Palaeosecular Variation Curve*) de referencia para la región (regiones entorno a 10000 km^2). Clásicamente, el método requiere disponer de una PSVC bien definida para esa región, curva que se genera a partir del estudio arqueomagnético de estructuras arqueológicas bien datadas en esa zona. Por tanto, sólo se puede aplicar esta técnica a regiones con una gran densidad de estudios arqueomagnéticos y que estén bien distribuidos temporalmente. La incorporación de modelos regionales en el proceso de datación arqueomagnética permite, por una parte, extender la técnica de datación a toda la región Europea (y norte de África), incluso a aquellas zonas cuya densidad y distribución temporal de los datos no permitan definir una PSVC precisa. Y por otra parte, en el proceso de datación se elimina el error de relocalización que está presente, tanto en la generación de las PSVCs clásicas, como en el traslado del nuevo dato al punto de referencia de la curva.

El proceso de datación usado es el definido por Lanos (2004), que está basado en la combinación de funciones de densidad temporal de probabilidad de cada uno de los tres elementos geomagnéticos. En este trabajo hemos desarrollado una herramienta interactiva en código Matlab para realizar dataciones arqueomagnéticas comparando el dato arqueomagnético (o lava) de edad desconocida con una PSVC de referencia. Las PSVCs incluidas dentro del software son el grupo de curvas Bayesianas de la región Europea y las que son generadas a partir de modelos regionales y globales del campo geomagnético.

Para analizar cómo afecta al proceso de datación el usar una u otra PSVC, hemos llevado a cabo un estudio datando una misma estructura arqueológica con todas las PSVCs disponibles. Además se ha analizado la precisión en la datación arqueomagnética, así como el efecto del error de relocalización en la región Europea. Los resultados muestran que algunas PSVCs Bayesianas y aquellas dadas in situ por los modelos puramente arqueomagnéticos regionales y globales son las más adecuadas para obtener dataciones más precisas. Además, la datación debe realizarse usando los tres elementos del campo geomagnético (cuando éstos estén disponibles), ya que ello contribuye a restringir más el intervalo de edad buscado.

A MATLAB TOOL FOR ARCHAEOMAGNETIC DATING

FCO. JAVIER PAVÓN-CARRASCO[1*], JUAN RODRÍGUEZ-GONZÁLEZ[1], MARÍA LUISA OSETE[1] and J. MIQUEL TORTA[2]

[1]*Dpto. de Física de la Tierra I: Geofísica y Meteorología, Universidad Complutense de Madrid, 28040, Madrid, Spain. Corresponding author: fjpavon@fis.ucm.es (phone: +34 913945190 - Fax: +34 913944398).*

[2]*Observatori de l'Ebre, CSIC – Universitat Ramon Llull, Horta Alta 38, 43520. Roquetes, Spain. jmtorta@obsebre.es*

A Matlab tool for archaeomagnetic dating has been developed in this work. Well-dated palaeosecular variation curves (PSVCs) can be used to date archaeological artefacts with an unknown age. The archaeomagnetic direction (declination and/or inclination) and the archaeointensity obtained from the archaeological artefact are compared with a master PSVC. In addition, historical lava flows with controversial age can be dated using this methodology. The dating process follows the descriptions given by Lanos (2004), which is based on the combination of temporal probability density functions of the three geomagnetic field elements. Here, we develop an interactive tool in Matlab code to carry out an archaeomagnetic dating comparing the undated archaeomagnetic (or lava flow) data with a master PSVC. The master PSVCs included into the Matlab tool are the different European Bayesian curves and those generated using both regional and global geomagnetic field models. A case study using all the PSVCs available in Europe and some undated archaeomagnetic data has been carried out to analyze how the different PSVCs affect the dating process. In addition, the dating uncertainty and the relocation error have been analyzed in the European region. Results show that some regional Bayesian PSVCs and both regional and global archaeomagnetic model are the best choices to obtain an accurate date. Moreover, when it is available, the full geomagnetic field vector must be used for archaeomagnetic dating.

KEYWORDS: ARCHAEOMAGNETIC DATING, GEOMAGNETIC SECULAR VARIATION, GEOMAGNETIC FIELD MODELLING

INTRODUCTION

The geomagnetic field varies in both space and time over the Earth's surface. For what concerns internal fields, it shows a long–term variation, called secular (or palaeosecular) variation. This physical phenomenon, along with the ability of certain archaeological artefacts (e.g. ceramics, bricks, burnt horizons, etc), lava flows and sediments, to acquire a stable remanent magnetisation at the time of its last use (heated archaeological materials) or its formation (rocks), are the principal grounds of the palaeomagnetic dating. When the studies are carried out in archaeological materials they are referred as archaeomagnetic investigations and the dating technique as archaeomagnetic dating.

Since the ancient geomagnetic field can be recorded in a wide variety of materials (archaeological structures, sediments, etc) which can be independently dated, a compilation of these types of data allows us to construct a Palaeosecular Variation Curve (PSVC) for any particular region. If the curve is sufficiently well-defined it can be used as relative dating tool for archaeological features from the same region (see e.g. Aitken 1990, Eighmy and Sternberg, 1990 or McIntosh and Catanzariti for more details).

To determine the most probable age of the last use of an archaeological artefact its remanent magnetisation is compared with a reference PSVC. This classical approach to archaeomagnetic dating can be completed by the use of PSVCs generated by global or regional models (Lodge and Holme, 2009; Pavón-Carrasco et al., 2009).

The classical technique requires a high density of archaeomagnetic data concentrated in a region of about $2 \cdot 10^5$ km^2. The use of synthetic PSVCs generated by geomagnetic models allows extending the archaeomagnetic dating technique to regions where there is not enough density of data to construct a classical PSVC, or there are important gaps in its temporal distribution. In these cases the classical dating archaeomagnetic tool could not be applied or would provide a high uncertainty. However if the behaviour of the geomagnetic field is well defined at a continental scale where the region is located (or at a global scale) a synthetic PSVC can be estimated exactly for the locality of the archaeological site. In addition, this new approach avoids the relocation error included when data are relocated to a reference point to construct the PSVC and when the site to date is also relocated for comparison with the PSVC.

Recently new, and more refined, global (Korte et al., 2009) and regional models for the European region (Pavón-Carrasco et al., 2009; 2010) have been published; therefore this new technique can be implemented as routine dating tool for archaeological sites. The main goal of this paper is to develop a Matlab tool for archaeomagnetic dating using different sources of PSVCs.

The methodology followed to obtain the most probable age for an archaeological structure is that of Lanos (2004), with which statistical probability density functions of the geomagnetic field are analyzed. A description of the Matlab tool for users is given in the paper, along with an illustrated example. To analyze how the selection of a PSVC could affect the dating process, we discuss several examples of archaeomagnetic dating obtained by using different PSVCs to the same undated archaeological site. We also analyze the accuracy in the dating process by using Bayesian PSVCs and the SCHA.DIF.3K European regional model. Finally, we carry out a study showing how the relocation error affects the archaeomagnetic dating.

PALAEOSECULAR VARIATION CURVES AND REFERENCE MODELS

A well-dated reference palaeosecular variation curve (master PSVC) is needed for dating an archaeomagnetic datum with unknown date. There are currently three different sources of archaeomagnetic PSVCs: the classical regional PSVCs determined for a region (or country), the regional archaeomagnetic models and the global models.

Regional palaeosecular variation curves (classical approach)

Well-dated archaeomagnetic data for a given region are translated to a common place (reference point) to construct a PSVC. The area must not be bigger than $2 \cdot 10^5$ km^2 because a dipolar geomagnetic field is assumed to translate the data from the archaeological site to the reference point. Directional data (declination and inclination) are transferred by the Conversion Via Pole method (CVP, Noël and Batt, 1990), while intensity data are relocated by calculating the Virtual Axial Dipole Moment (VADM) or the Virtual Dipole Moment (VDM) when the intensity datum is associated with an inclination value.

The relocation procedure introduces an error, the relocation error, which is independent to the data measurement and increases with the distance from the archaeological site to the reference point. This error is related to the dipolar geomagnetic field assumption. For directional data the error is about 7º per 1700 km (Casas and Incoronato, 2007) and about 3 μT per 1000 km for the intensity data (Gómez-Paccard et al., 2008). It is assumed that for small regions the relocation error is within the palaeomagnetic uncertainty, but it is not considered in the error propagation calculations.

During the last years a considerable effort has been carried out to obtain detailed PSVCs from several countries (e.g., France, Gallet et al., 2002 and Chauvin et al., 2000; Germany, Schnepp and Lanos, 2005; Iberia, Gómez-Paccard et al., 2006; Italy, Tema et al., 2006; the United Kingdom, Zananiri et al., 2007; Western North America, Hagstrum and Blinman, 2010). Especially relevant is the case of Europe, from where several PSVCs have been recently updated thanks to the high density of archaeomagnetic data (see Figure 1). We have included some of these new PSVCs into the Matlab tool. They have been constructed by using the Bayesian approach of Lanos (2004). This method provides smooth and continuous PSVCs for a region or country.

Table 1 shows the PSVCs which have been included into the Matlab tool along with the region/country, the validity time interval, the reference location and the type of data used in the construction. The considered curves, generally, cover the last 3000 years and contain the directional elements (i.e., declination and inclination) of the Earth's magnetic field. The PSCVs used in the Matlab tool have been taken from the original publications which provide a mean value of the geomagnetic field element (declination or inclination or intensity) and its uncertainty at 95% of confidence.

The classical PSVCs from Bulgaria, Greece and Hungary have not been included in the program since they have not been constructed with the same Bayesian homogeneous procedure as the PSVCs from western European countries. According to the recently updated database from Bulgaria (Kovacheva et al., 2009) and the density of archaeomagnetic data from Eastern Europe, probably new classical Bayesian PSVCs will be published in the next future, which will be incorporated in the proposed Matlab dating tool.

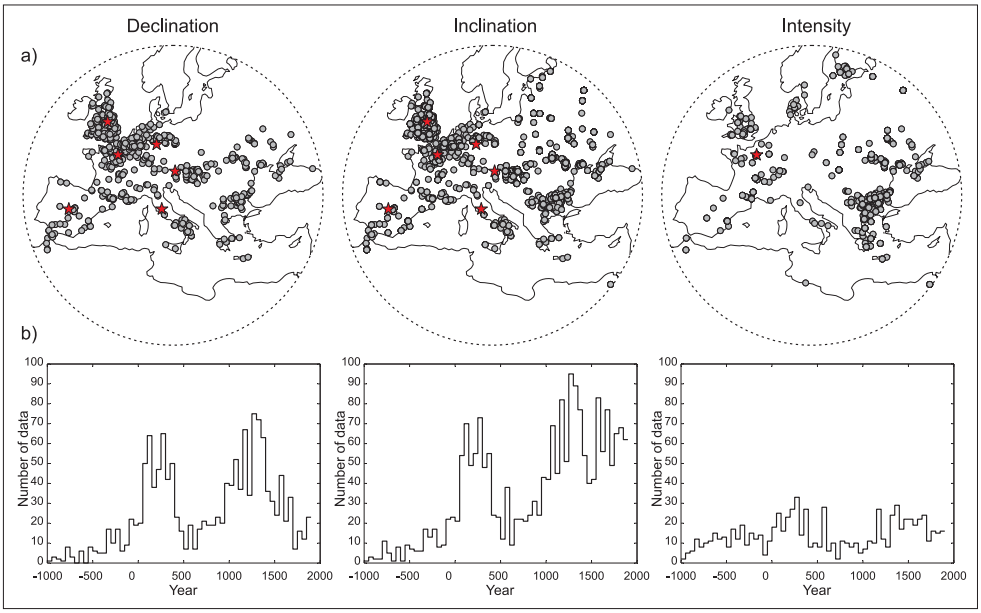

Figure 1. Spatial (a) and temporal (b) distribution of the European archaeomagnetic data (last 3000 years, database of Donadini et al, 2009). Red stars: Location of the Bayesian PSVCs.

It is important to note that in the construction of each PSVC no assumptions on the spatial nature of the geomagnetic field are considered (except that it behaves as dipolar at small distances). Therefore neighbouring curves could show different behaviours which are more related to the database used in the construction of the curve (quantity and quality of data) than to the characteristics of the geomagnetic field. Figure 2 shows all directional European Bayesian PSVCs: France, England, Italy, Austria, Germany and Iberia. All PSVCs look similar during most of the past three millennia. However, a closer inspection reveals some significant differences in the detail of the curves, for example, the uncertainties.

We also include in the program the Bayesian intensity PSVC for Western Europe recently compiled by Gómez-Paccard et al. (2008). The program allows combining this master curve with the western directional curves to obtain more accurate archaeomagnetic dating. In addition to the master curves included in the program, the Matlab routine allows us to include any other PSVC.

F.J.Pavón – Carrasco, J.Rodríguez-González, M.Osete and J.M.Torta

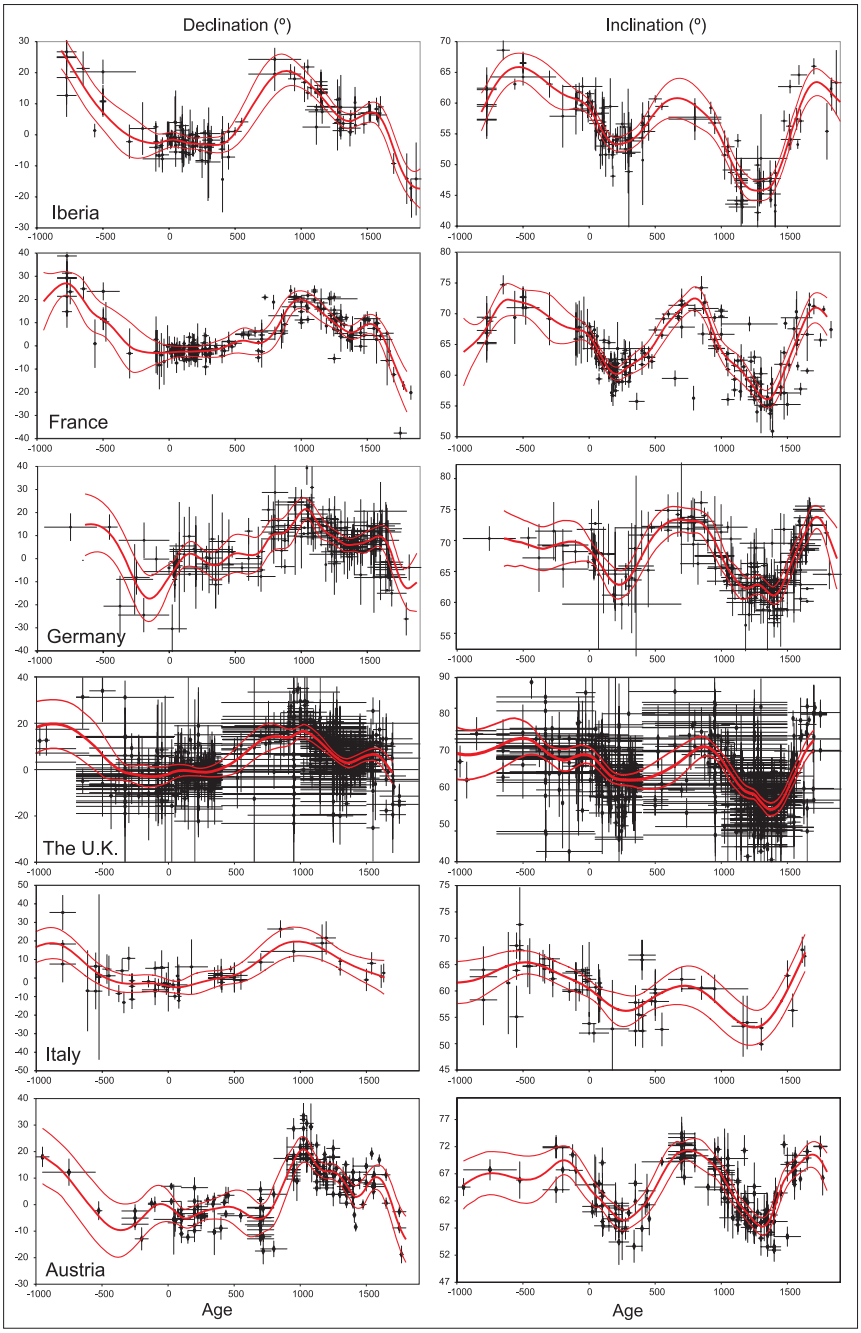

Figure 2. European Bayesian palaeosecular variation curves (declination and inclination curves), in red, along with the data that were used for their construction (dots) and their uncertainties. See text for details and references. The red thin lines show the curve's uncertainty at 95%.

Regional models

When a high density of archaeomagnetic data are concentrated in a considerably large area, such as the European region, regional models using in situ data can be developed. Recently a first generation of European regional models based on Spherical Cap Harmonic Analysis (SCHA) have been published: the SCHA.DIF.3K model (Pavón–Carrasco et al., 2009), valid for the last 3000 years; and the SCHA.DIF.8K model (Pavón–Carrasco et al., 2010), valid for the time period from 6000 BC to 1000 BC. These models provide information of the three geomagnetic field elements (and their uncertainties at 95%) for any point at the European continent, north of Africa and Western Asia (see Table 1). Figure 3 shows the synthetic PSVCs of the declination, inclination and intensity at the centre of Europe (45ºN, 15ºE) for the last 8000 years generated from such models.

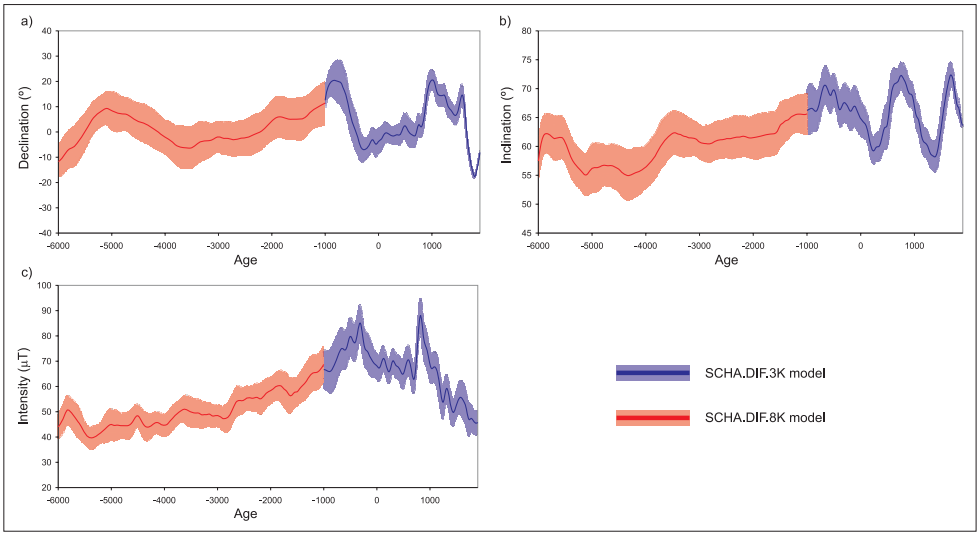

Figure 3. Synthetic palaeosecular variation curves at 45ºN, 15ºE for the (a) declination, (b) inclination and (c) intensity from SCHA.DIF.3K (blue curves) and SCHA.DIF.8K (red curves) regional models (Pavón-Carrasco, 2009, 2010). Bands show the prediction uncertainty at 95% of confidence.

The first model, SCHA.DIF.3K, is based only on archaeomagnetic data (lava flows were not included as input data), while the SCHA.DIF.8K model is based on lake sediment records and archaeomagnetic data. Selected lake sediment palaeomagnetic data were included in the second model to overcome the low density of available archaeomagnetic data from 6000 BC to 1000 BC. Differences observed in the smoothing of the two curves are related to the use of the sedimentary records prior to 1000 BC (see Figure 3).

By using the regional models to date archaeological artefacts a synthetic PSVC is compiled at the site location. Therefore the relocated error associated with the translation of the data is avoided (the same applies for the global models).

Another important benefit of the use of regional modelling is the inclusion of a spatial relation between the geomagnetic field components, i.e., the Laplace equation. This allows us to calculate a PSVC even in regions where the density of archeomagnetic data is low, as is the case of Italy (see Figure 2), or when the uncertainties of the input data are high and consequently the Bayesian PSVC is poorly defined (as is the case of the U.K., Figure 2). Nevertheless, there are regions where the regional model prediction agrees with the classical PSVC, as the case of France. Figure 4 shows the synthetic curves generated by the SCHA.DIF.3K model for France (at Paris) and Italy (at Viterbo), together with the Bayesian PSVCs.

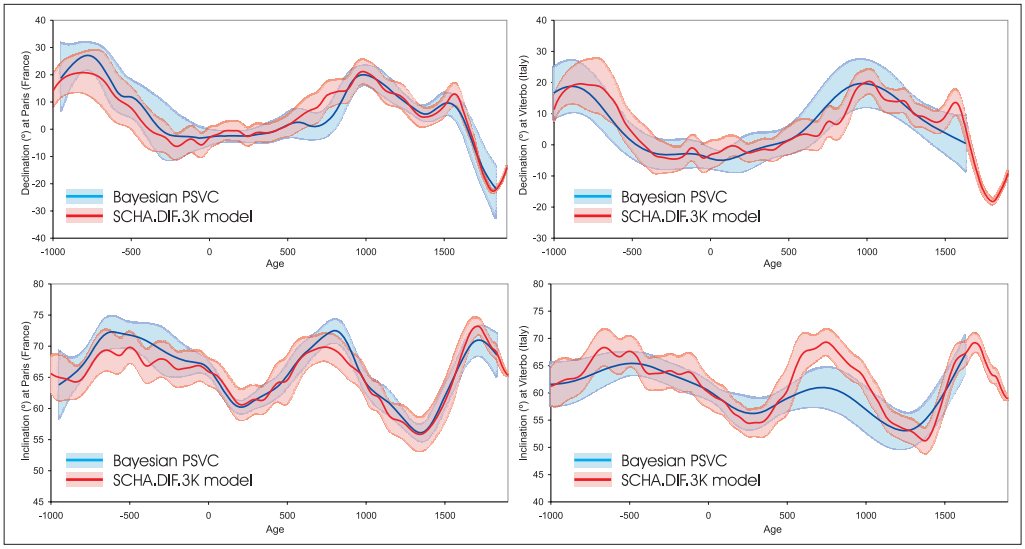

Figure 4. Synthetic directional palaeosecular variation curves for France (left) and Italy (right) from SCHA.DIF.3K (red curves) regional model and the classical Bayesian PSVCs (blue curves). Bands show the prediction uncertainty at 95% of confidence.

Global models

Korte et al. (2009) give a new generation of global models for the last 3000 years using different palaeomagnetic databases (Donadini et al., 2009). They are generically known as CALS models. Three new models can be used to obtain the geomagnetic field components including the uncertainty at 65% at any point all around the world (see Table 1). The first model, called ARCH3K.1, was developed using only archaeomagnetic input data. This model covers the same period and agrees with the regional SCHA.DIF.3K for Europe.

The lake sediment database was used to obtain the second model: SED3K.1. This model shows a highly smooth behaviour of the geomagnetic field. Therefore, it is not the best option to obtain an accurate archaeomagnetic dating. However, the model can be used for correlation with other sedimentary data.

Finally, with the complete database (archaeomagnetic data, lava flows and lake sediment data) Korte et al. (2009) obtained the CALS3K.3 model. Its authors prefer using this model for global studies of the geomagnetic field, because the model was derived from a more homogeneous and complete distribution of data. However, the ARCH3K.1 model is the best option for archaeomagnetic dating, because it is not disturbed with the lake sediment data. Figure 5 shows the different synthetic PSVCs, for the three geomagnetic field elements, obtained using the three models at 45ºN of latitude and 45ºE of longitude.

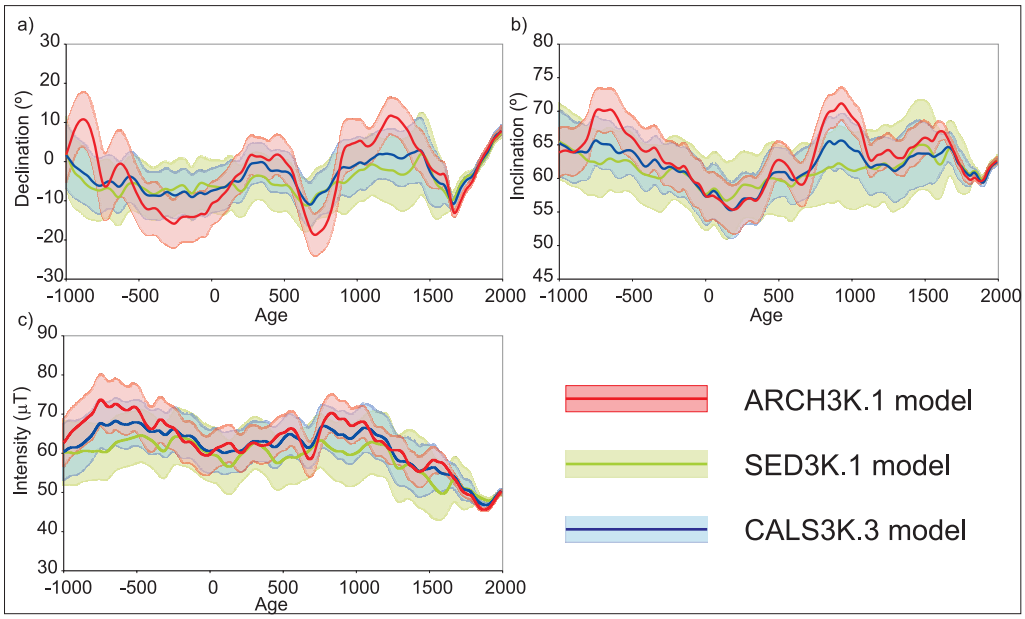

Figure 5. Palaeosecular variation curves for the (a) declination, (b) inclination and (c) intensity at 45ºN of latitude and 45ºE of longitude. Model predictions are given by the ARCH3K.1 (red curve), SED3K.1 (green curve) and CALS3K.3 (blue curve) models (Korte et al., 2009). Bands show the model uncertainties at 65% of confidence.

ARCHAEOMAGNETIC DATING: METHODOLOGY

In this work we have followed the methodology described by Lanos (2004) using the probability density functions of the three geomagnetic field elements: declination, inclination and intensity. The undated archeomagnetic element D is considered normally distributed at a fixed time t, with mean value $G_D(t)$ and standard deviation error σ_D, i.e., $D \sim N(G_D(t),\sigma_D^2)$. In the same way, the geomagnetic field element provided by the master curve $G_D(t)$ at the same fixed time is supposed normally distributed with mean and standard deviation given by $\bar{G}_D(t)$ and σ_G: $G_D(t) \sim N(\bar{G}_D(t),\sigma_G^2(t))$. At the time t, the conditional probability density (or likelihood) of the observation (non-dated archaeomagnetic element) is given by the following equation, where $p(x/y,t)$ is the conditional probability function of x over y in the time t:

$$PDF_D(t) = p(D|\bar{G}_D,t) = \int_{-\infty}^{+\infty} p(D|G_D,\bar{G}_D,t)\cdot p(G_D|\bar{G}_D,t)\cdot dG_D \qquad [1]$$

In order to illustrate the above formulation, Figure 6 shows a visual example. On the left (upper panel) we have plotted the probability density map for the non-dated archaeomagnetic data, in this case the declination element. The probability is equal over the whole time interval, with a mean value of 20º and standard deviation of 2º. On the right (upper panel) the probability density map of the master PSVC (declination curve is given by the SCHA.DIF.3K model at 40ºN of latitude and 4ºW of longitude) is plotted. By combining both maps we can obtain the final probability density map (Figure 6c). The integration, over the declination values of the final map, gives the Probability Density Function (PDF) of the undated declination (Figure 6d). To find the most probable age of the archaeomagnetic data we have to combine the probability density functions (PDFs) of the geomagnetic field elements.

Table 1. Master palaeosecular variation curves and reference models included into the Matlab tool. Type of data: A archaeomagnetic data, LF lava flows and LS lake sediment data. SCHA: Spherical Cap Harmonic Analysis. R-SCHA: Revised Spherical Cap Harmonic Analysis.SHA: Spherical Harmonic Analysis. SOW: sliding overlapping windows. CS: cubic splines

Regions/Countries	Initial time	Final time	Reference Location	Type of data	Method	References
Palaeosecular Variation Curves						
Austria	-940	1850	Radstadt (47.38ºN/13.45ºE)	A	Bayesian	Schnepp and Lanos (2006)
France	-950	1830	Paris (48.9ºN/2.3ºE)	A	Bayesian*	Chauvin et al. (2000) Gallet et al. (2002)
Germany	-625	1900	Göttingen (51.53ºN/9.93ºE)	A	Bayesian	Schnepp and Lanos (2005)
Iberia	-815	1959	Madrid (40.4ºN/-3.7ºW)	A	Bayesian	Gómez-Paccard et al. (2006)
Italy	-1160	1630	Viterbo (42.45ºN/12.03ºE)	A + LF	Bayesian	Tema et al. (2006)
The United Kingdom	-1890	1990	Meriden (52.43ºN/-1.64ºW)	A	Bayesian	Zananiri et al. (2007)
West Europe	-100	1975	Paris (48.9ºN/2.33ºE)	A	Bayesian	Gómez-Paccard et al. (2008)
Regional Models						
Europe, Nothern Africa and Western Asia (SCHA.DIF.3K)	-1000	1900	Any point into the selected region	A	SCHA in space and SOW in time	Pavón-Carrasco et al. (2009)
Europe, Nothern Africa and Western Asia (SCHA.DIF.8K)	-6000	-1000	Any point into the selected region	A+ LS	R-SCHA in space and SOW in time	Pavón-Carrasco et al. (2010)
Global Models						
Global (ARCH3K.1)	-1000	1990	Any point all around the World	A + LF	SHA in space and CS in time	Korte et al. (2009)
Global (SED3K.1)	-1000	1990	Any point all around the World	LS	SHA in space and CS in time	Korte et al. (2009)
Global (CALS3K.3)	-1000	1990	Any point all around the World	A + LF + LS	SHA in space and CS in time	Korte et al. (2009)

** The French Bayesian curve was calculated using the directional data of Chauvin et al. (2000) and Gallet et al. (2002).*

Declination and inclination are the most typical measurements carried out in palaeomagnetic laboratories, since the process to obtain intensity information is more complex (for more details on palaeointensity studies see Thellier and Thellier, 1959). Thus in archaeomagnetism, generally, one deals with directional information only. However, to obtain more accurate dates we must consider the full

geomagnetic field vector (declination, inclination and intensity). If the intensity data are not available, the directional vector (declination and inclination) will also suit.

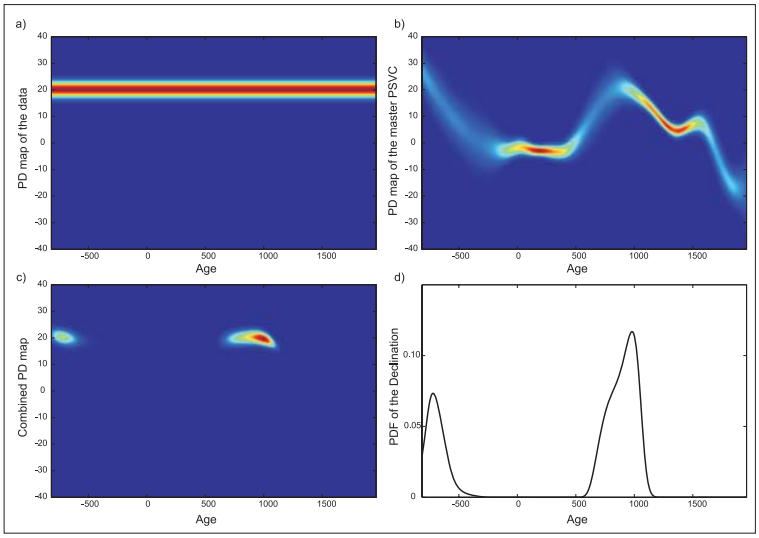

Figure 6. Probability density (PD) maps of the undated archaeomagnetic data (a) and of the master PSVC (b). (c) Combined PD map and (d) final Probability Density Function (PDF) for the data. Dark blue: zero probability (p = 0 in eq. 1). Dark red: maximum probability (p = 1).

An important factor in the archeomagnetic dating process is related with the behaviour of the geomagnetic field itself, which is shown by the PSVCs. Data from periods of rapid changes would provide more precise dating than those from slow change epochs. In addition, similar direction/intensity can be observed for different periods. This can generate non-unique problems. In these cases additional information should be considered (archaeological information, stratigraphy, context, and typology) to select between alternative ages.

USING THE MATLAB TOOL

The developed software contains a package of different routines in Matlab code. The programs package and related material are included as complementary files. It they are also available online at http://pc213fis.fis.ucm.es/archaeo_dating/index.html. After downloading the compressed file *archaeo_dating.rar*, the decompressed folder must be put into the Matlab working folder: *work* (usually in *C:\Matlab\RXXX\work*).

To run the Matlab tool, write in the *Command Window* of Matlab *archaeo_dating* and an interactive window will appear (Figure 7). Three different colour areas are shown in the interactive window. Red area should contain the archaeomagnetic information to the site to be dated. It is divided into two parts: (i) the directional and intensity values with their respective uncertainties (declination, inclination, α_{95}, intensity and σ_F) and (ii) the location information (the latitude, the longitude and the name of the archaeological sample). The user can choose the archaeomagnetic elements to be used, and set their values. If an element is not available, as it can be the case of the intensity, the user must not select that element.

The master PSVC used for dating is selected in the blue area. Four buttons show the different sources of the PSVCs: (i) the available European Bayesian PSVCs, (ii) the global models of Korte et al. (2009), (iii) the European regional models of Pavón-Carrasco et al. (2009, 2010) and (iv) a last button

gives the possibility to include a new master PSVC by the user. After pressing a button, a new window will appear to select the different PSVCs or models described in the previous section. If the user uses a new PSVC (not included into the Matlab tool) the software asks for the new file. When a Bayesian PSVC is selected, it is transferred from the reference location to the site location. This does not occur for the PSVCs given by the regional and global models, because they are calculated at the site location.

After including the archeomagnetic information and the master PSVC, the user can define the time interval used for dating and the statistical probability estimation. These parameters are into the green area. Finally, the button *Dating* must be pressed to obtain the results.

Figure 8 is an example obtained with the Matlab tool. This example is taken from a kiln in Belgium studied by Spassov et al. (2008) which will be dated by using the SCHA.DIF.3K regional model. The undated structure comes from Corroy-le-Grand site, at 50.66ºN of latitude and 4.68ºE of longitude. Directional values are: 15.0º for declination and 65.7º for inclination and its uncertainty (α_{95}) is 0.9º. The palaeointensity is 69.4 ± 1.1 μT. Archaeological considerations suggest that the most probable age for the archaeological artefact is around the 11th century AD.

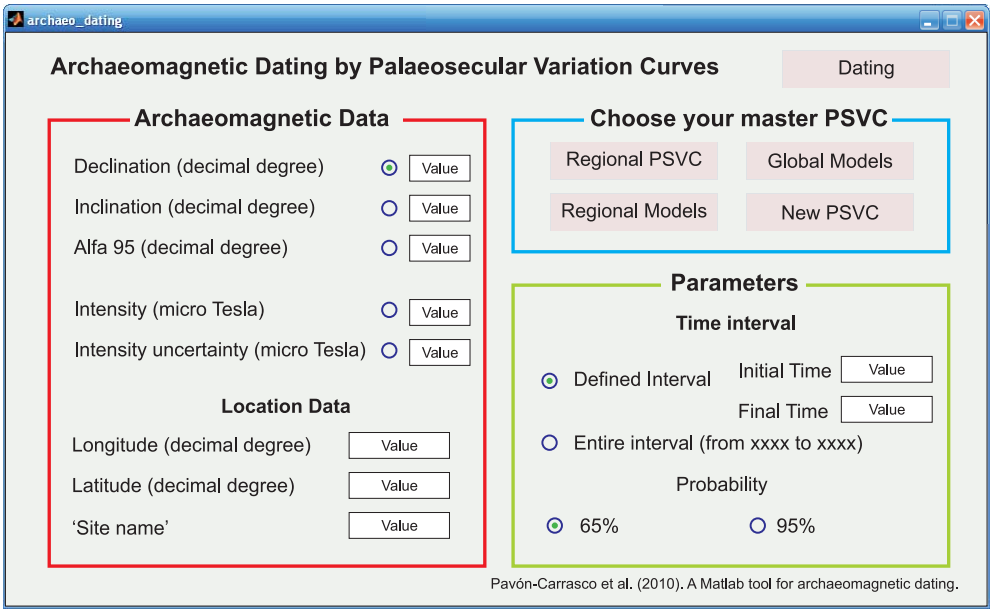

Figure 7. Matlab interactive window. Red area: archaeomagnetic data information. Blue area: buttons with the different PSVCs and regional/global models. Green area: the time interval and statistical probability. See text for details.

The figure contains all the information related to the dating process. It is divided into 9 sections. On the top we have plotted the comparison between the different master PSVCs of the declination (left), inclination (centre) and intensity (right) with the non-dated archaeomagnetic data. In the middle, the PDFs of the declination (left), inclination (centre) and the intensity (right) are given with the most probable age for each archaeomagnetic element. On the bottom, on the left we have plotted a regional map with the data and master PSVC locations. The combined PDF (normalised multiplication of the three previous PDFs) showing the most probable age of the last use of the archaeological artefact is plotted on the centre. Finally, on the right, the figure shows the archaeomagnetic dating information. In this case, we have two different intervals of probable ages: [1000 BC – 938 BC] and [1040 AD – 1127 AD]. Archaeological additional information allows discriminating between the two options: the structure can

not be from the BC period. The most probable age is given by the second time interval which, in addition, is in agreement with the archaeological date (Spassov et al., 2008).

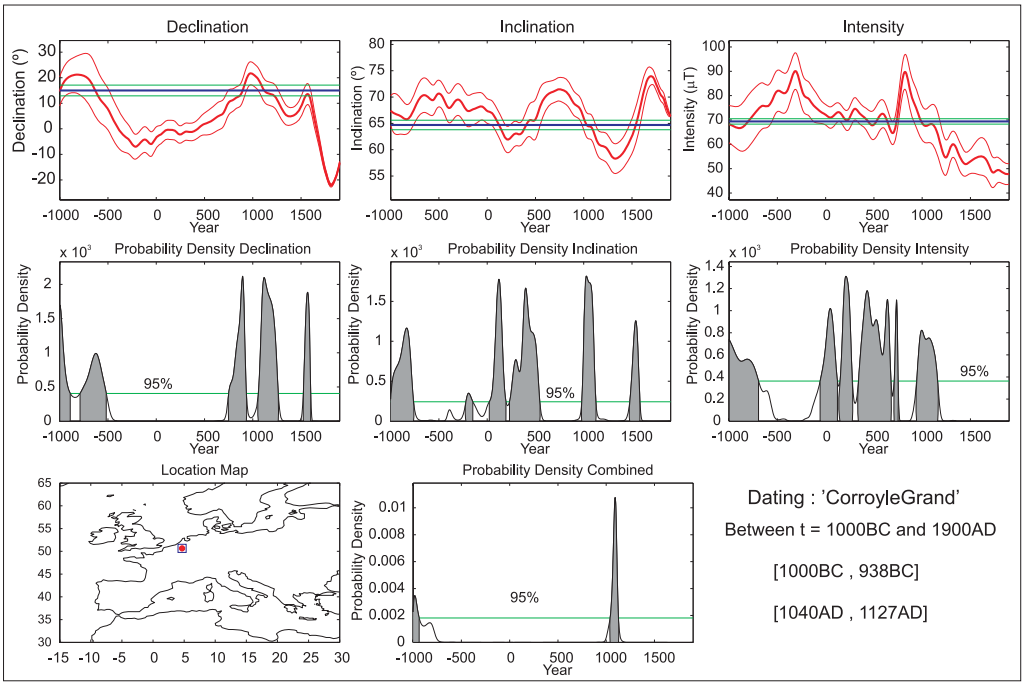

Figure 8. Result after dating. Top: master PSVCs (red curves with red error bands) of the declination (left), inclination (centre) and intensity (right) and the undated archaeomagnetic data (blue line with green error bands). Middle: the individual PDFs for the declination (left), inclination (centre) and intensity (right). The green lines indicate the different thresholds for each element at the given level of probability chosen. Bottom: Regional map (left) of the data location (red point) and the master PSVC location (blue square); combined PDF marked with the green line of probability (centre); and archaeomagnetic dating information (right). See text for details.

A CASE OF ARCHAEOMAGNETIC DATING

In order to test the dating process by using the different master PSVCs included in the program (classical Bayesian curves and synthetic curves generated from the models), we have carried out an archaeomagnetic dating to the same non-dated archaeomagnetic data (given in the previous example) by using all PSVCs from 0 to 1900 AD.

First we have calculated the most probable age obtained by using only the directional information (declination and inclination). Figure 9 shows the combined declination and inclination PDFs resulted from applying the classical method (the Bayesian PSVCs (figure 9a), and those obtained by the use of synthetic curves generated by the regional SCHA.DIF.3K model and by the CALS models (figure 9b).

In the analysis of the obtained results by using the classical PSVCs we must consider: i) the PSVC uncertainty, which depends on the database used to construct the curve (number and internal coherence of data, quality of measurements and dating accuracy); ii) the relocation error related with the distance between the reference point of the PSVC and the site location (see Figure 9c), and iii) the geomagnetic directional variation itself, that is to say, how the archaeomagnetic data constrain the PSVC in the expected time interval.

F.J.Pavón – Carrasco, J.Rodríguez-González, M.Osete and J.M.Torta

Consistent results are obtained by the use of the directional PSVCs from France, Germany and Iberia. Two possible dating time intervals are obtained: from 940 – 1200 AD and from 1480 to 1570 AD. The first is in agreement with the archaeological information (around 11th century AD). But, due to the behaviour of the geomagnetic field, there is another possible age around 16th century AD. The resulted PDFs from the Italian and the United Kingdom PSVCs show a remarkable wider expected time interval: from 550 AD to 1200 AD, which can be explained by the high uncertainty of these PSVCs for the Middle Age (Tema et al., 2006 and Zananiri et al., 2007, see Figure 2). In this case, it seems that the main source of the inaccurate dating is the poor definition of the curves.

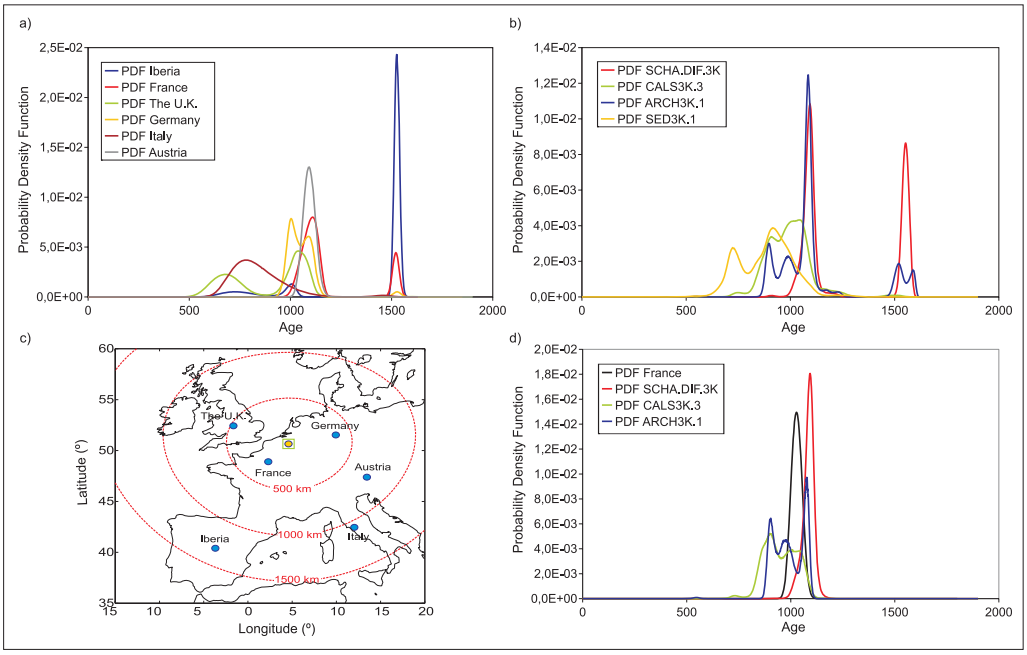

Figure 9. Result after dating. a) PDFs of the directional Bayesian curves, b) PDFs of the directional PSVCs obtained by the regional SCHA.DIF.3K and the CALS models. c) Location map: blue points show the location of the Bayesian PSVCs and yellow point (and green square) is the location of the undated archaeomagnetic data (or site). Dashed red lines indicate the distance to the site location. d) PDFs of the full geomagnetic vector of the French directional Bayesian curve (with the western Europe intensity curve) and the PDFs of the PSVCs given by the regional SCHA.DIF.3K and the CALS models at the site location.

Both the archaeomagnetic regional SCHA.DIF.3K and global ARCH3K.1 models agree in the dating results (Figure 9b). Two possible dating intervals are also obtained, although the first time interval given by the global model is less defined (it begins at 850 AD). The PDFs from SED3K.1 and CALS3K.1 global models show a much longer expected time interval (i.e. less precise dating) than the archaeomagnetic models. This is due to smoothness of both PSVCs resulting from the inclusion of lake sediment records as input data.

In summary, by using the PSVCs constructed from archaeomagnetic data we have found two distinguishable time intervals as possible ages for the archaeological artefact. To solve this controversy, which is based on the behaviour of the geomagnetic field directional variation, additional constraints are required. For example, we would need to fix the archaeological information. But, another possibility is to include the other geomagnetic field element in the archaeomagnetic dating process: the palaeointensity.

The intensity may help to constrain the results. In this case, the undated archaelogical site also provided intensity information, thus we could obtain the combined directional and intensity PDF.

Figure 9d shows the new archaeomagnetic dating results obtained by using the full geomagnetic vector (declination, inclination and intensity). We have used the nearest directional PSVCs to the site location, i.e., the directional French PSVC, along with the Bayesian intensity curve for Western Europe (Gómez-Paccard et al., 2008), and the regional SCHA.DIF.3K model and the global ARCH3K and CALS3K models. The combined PDF of the Bayesian French and German curves agrees with the PDF of the SCHA.DIF.3K regional model, both showing narrow PDFs around 11th century AD. The inclusion of the intensity information has removed the second time interval constraining the dating. The PDF from the ARCH3K.1 model exhibits a longer dating time interval. Insignificant changes have been observed between the previous directional PDF and the present PDF for the CALS3K.3 global model. According to this example, this model does not provide enough accuracy for archaeomagnetic dating.

We have evidenced how archeomagnetic dating strongly depends on the master PSVC used in the dating process and, accordingly, one must be careful to this respect. The narrower results from both archaeomagnetic regional SCHA.DIF.3K model and the Bayesian French curve let us conclude that they are the best candidates to provide master PSVCs for this particular archaeological site and archaeomagnetic study. But if an accurate classical PSVC close to the archaeological site is not available the only option is the use of synthetic curves based on archaeomagnetic models. Models based on sedimentary records or on combining sedimentary and archaeomagnetic data are not appropriate for archaeomagnetic dating.

DISCUSSION ON THE ACCURACY OF ARCHAEOMAGNETIC DATING

The problem of the resolution and reliability of archaeomagnetic dating is difficult. The spatiotemporal distribution of the input database, the uncertainty of the database, its internal coherence and the technique used for modelling (classical PSVCs or global or regional models), define the resolution of the PSVC and, consequently, the resolution in archeomagnetic dating. In addition to this, the relocation error introduces a bias in the dating process which is often not considered.

In this Section, we have estimated the dating uncertainty of the classical Bayesian curves in Europe and compared it with the dating uncertainty obtained by the use of synthetic curves (at the same reference point) compiled from the regional SCHA.DIF.3K model. It is necessary to point out that this calculation does not mean that higher accuracies could not be reached at one individual dating site. This would be the case, for example, of data whose field parameters are close the sharp segments of the PSVC, or even outliers (with intersecting uncertainties).

In this analysis we consider that any PSVC strictly represents the geomagnetic field variations and that the site to be dated is exactly characterized by the values predicted by the curves, i.e., the uncertainty of the palaeomagnetic study is considered negligible. Results of this analysis are plotted in Figure 10. The dating uncertainty (semi-length of the dating interval) is high for the oldest periods and more accurate dating is reached for the last millennium (Figure 10).

When different Bayesian directional PSVCs are compared (Figure 10a) it is obvious that the Italian curve, which has the higher uncertainties, is the less accurate for archaeomagnetic dating. This is mainly due to the low number of archeomagnetic studies carried out in the region (see Figure 2). The U.K. curve is also poorly defined. Mean dating accuracy is over 200 years up to around 1000 AD. After this epoch the accuracy remains between 50 and 100 years. In the case of the U.K. curve the high uncertainty seems to be related with the inaccuracy in the dating of the archaeomagnetic database used to construct the curve (see Figure 2). In general, mean dating accuracy is over 140 years, except for the most recent times (after 1300 AC), and it could reach up to 300 years around 250 BC (maximum in the Austrian PSVC). According to our analysis, the French curve is the one that would provide the most accurate dating.

The dating uncertainties by synthetic curves (using the SCHA.DIF.3K model) are more homogeneous, as it is expected since all were derived from a unique model (Figure 10b). From 1000 BC up to 100 BC the mean accuracy is around 150 years, with time intervals less defined as it is from 400 BC

up to 100 BC (reaching up to an uncertainty of 250 years). This is due to the low number of palaeomagnetic data from this period included in the database. During the Roman times the number of archaeomagnetic data is moderate, but the dating error is still high. The source of this uncertainty is the behaviour of the geomagnetic field variation during this period: declination remains nearly constant during 5 centuries and only variations in inclination are observed, which originates a nearly symmetric path and, consequently, no resolution in dating is obtained. From 400 AD up to 1400 AD typical uncertainties are about 125 years and from this time up to present days the uncertainties diminish considerably, being below 50 years for the last 5 centuries.

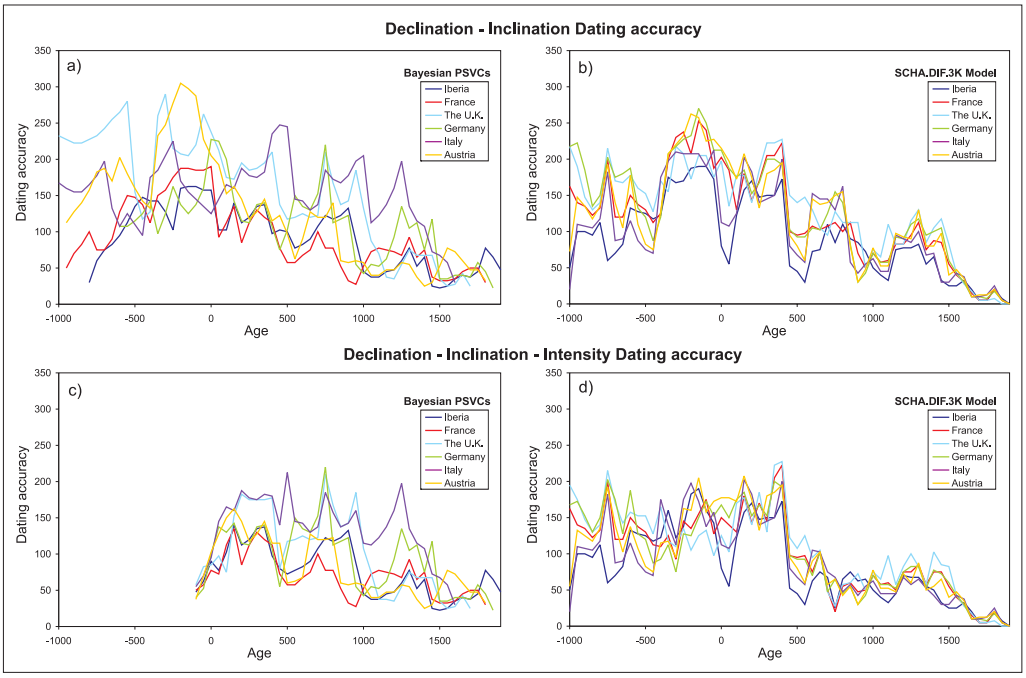

Figure 10. Dating accuracy for the classical Bayesian PSVCs (left) and for the synthetic PSVCs from SCHA.DIF.3K model (right). Top/bottom: directional/full vector information.

When intensity information is also considered in the archaeomagnetic dating, i.e., the full geomagnetic vector, the accuracy of the method by using the regional SCHA model increases considerably (Figure 10d). The uncertainty is typically below 55 years from 400 AD up to present, and it is about 140 years for previous times. However, introducing the palaeointensity in the dating tool based on classical PSVCs does not improve substantially the accuracy (Figure 10c). More constrained dating would be only obtained for the roman period.

In the previous discussion we have analysed the locations with a classical Bayesian PSVC. The case is different if the archaeological site to date is far from the mentioned reference points. The directional relocation error has been discussed by Casas and Inconorato (2007) and it is assumed around 7º per 1700 km. But, as it has been already mentioned, usually the relocation error is not considered in the archaeomagnetic dating. In the following we will discuss an example in which the relocation process introduces an error in the dating procedure.

This relocation error would introduce a shift in the age and an uncertainty which depend on the spatial behaviour of the geomagnetic field at that time. We have evaluated this artefact by using synthetic directional data from the regional SCHA.DIF.3K model. The directional data are calculated at 900 AD for

different longitudes (10ºW – 20ºE, with the latitude of Paris: 48.9ºN) and latitudes (35ºN – 60ºN, with the longitude of Paris: 2.3ºE). All synthetic data have been relocated to Paris (48.9ºN, 2.3ºE).

French Bayesian curve seems the most accurately defined and, therefore, it would be the best option for referring any new archaeological site to date close to Paris. Using this PSVC we have dated all the relocated data. Results are plotted in Figure 11. As expected, the distance to the reference point (Paris), i.e., the relocation error, generates a shift in the archaeomagnetic age (see Figure 11). For example, if the datum to date is in Alger (36.8ºN, 3.0ºE), the archaeomagnetic dating would give an age around 1130 AD ± 80 years. Similarly, if the archaeological site is located near to Prague (50.0ºN, 14.1º E) the archaeomagnetic dating would propose ages of about 735 AD ± 100 years. In both cases, the archaeomagnetic ages are different to the proposed age, i.e., 900 AD. This is a clear example in which it is easy to see the limits of the use of classical PSVCs to date and the artefacts produced by the relocation procedure. It is probably the most extreme case, but it is necessary to point out that the French curve has been traditionally used to date recent lavas from Italy, for example, and that the relocation error has not been considered (Tanguy et al., 2003).

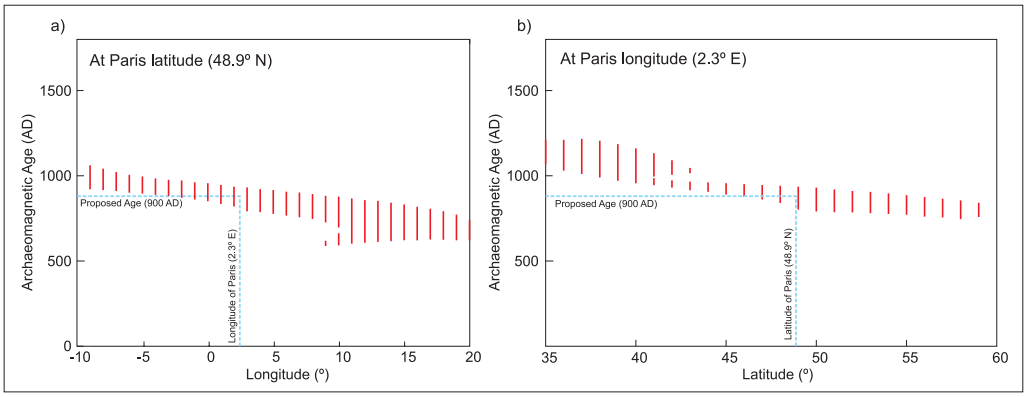

Figure 11. Red lines: archaeomagnetic dating versus longitude (a) and latitude (b). Blue dashed line shows the proposed age (900 AD) and the coordinates of the reference PSVC used for dating, i.e., the French PSVC at Paris.

In order to improve the accuracy of the archaeomagnetic dating tool better dated archaeomagnetic data are still necessary. According to our analysis more directional data are necessary for the following periods: prior to 100 BC, between 600 AD and 900 AD and from 1100 AD to 1400 AD. The roman period is well studied (directionally) and the low accuracy in archaeomagnetic dating observed in this time is due to the behaviour of the geomagnetic field. No higher precisions would be achieved by performing more directional archaeomagnetic studies in most of Europe from this time. This would not be the case for Northern Africa, from where only few data are available.

CONCLUSIONS

We have developed a Matlab code for archaeomagnetic dating. The software is presented as an interactive window where the user can add and change the dating parameters. A set of Bayesian PSVCs and archaeomagnetic models have been included into the Matlab tool. In addition, the program offers the possibility of using a new PSVC. We have also studied how the different PSVCs affect the dating process and results show that the archaeomagnetic dating strongly depends on the used master PSVC, because they show different behaviours in many occasions since they were, by nature, differently constructed.

The dating uncertainty has been analysed by using both classical and synthetic PSVCs. The synthetic curves are obtained from the regional European SCHA.DIF.3K model. Regions with scarce data, as Italy,

or with high age uncertainties, as the U.K., show the highest dating uncertainty. On the contrary, the French PSVC seems to be the most accurate PSVC. The synthetic curves show similar dating uncertainties because all of them are obtained from the same regional model. With the exception of France, where similar dating resolutions are obtained by using both classical and synthetic curves, in general, the use of the SCHA.DIF.3K regional model provides more accuracy in archaeomagnetic dating than classical PSVCs in the European region. Dating by means of the regional model is clearly the best option in regions where the PSVCs are still not well defined as Italy or the U.K. and it is the only possibility for archaeological sites from Northern Africa or Northern Europe.

Our study also reveals that palaeointensity information would help the dating procedure considerably when the synthetic curves are generated by the SCHA model. To improve the method new data are welcome from all epochs, but they can be especially relevant for times prior to 100 BC and for the time interval 400 AD – 900 AD.

Finally, we have carried out a study to evaluate how the relocation error affects to the archaeomagnetic dating. Results show that the relocation error, i.e., the distance between the archaeological site and the reference location of the PSVC, creates a shift in the archaeomagnetic dating. In this sense, an archaeomagnetic dating using the regional SCHA.DIF.3K model improves the results, because the relocation error is avoided.

The Matlab tool and online material in this paper are available as supplementary material and at: http://pc213fis.fis.ucm.es/archaeo_dating/index.html.

ACKNOWLEDGEMENTS

The authors are grateful to the Spanish research project CGL2008-02203 and the FPI grant BES-2006-13488. All algorithms were developed using Matlab 7 R2008. The Matlab tool presented in this work runs in Matlab 6 and newest versions.

REFERENCES

Aitken M.J., 1990. Science-based Dating in Archaeology. Longman, London-New York: 280pp.

Casas, Ll. and A. Incoronato, 2007. Distribution analysis of errors due to relocation of geomagnetic data using the 'Conversion via Pole' (CVP) method: implications on archaeomagnetic data. Geophys. J. Int., 169 (2), 448 – 454.

Chauvin, A., Y. Garcia, Ph. Lanos, and F. Laubenheimer (2000), Paleointensity of the geomagnetic field recovered on archaeomagnetic sites from France, Phys. Earth Planet. Inter., 120, 111-136.

Donadini, F., M. Korte, and C. G. Constable (2009), Geomagnetic field for 0–3 ka: 1. New data sets for global modeling, Geochem. Geophys. Geosyst., 10, Q06007, doi:10.1029/2008GC002295.

Eighmy J.L. and Sternberg R.S., 1990. Archaeomagnetic Dating. University Arizona, Tucson: 450pp.

Gallet, Y., A. Genevey and M. Le Goff, 2002. Three millennia of directional variations of the Earth's magnetic field in western Europe as revealed by archaeological artefacts. Phys. Earth Planet. Int., 131, 81 – 89.

Gómez-Paccard, M., Ph. Lanos, A. Chauvin, G. McInstosh, M.L. Osete, G. Catanzariti, V.C.Ruiz-Martínez and J.I. Núñez, 2006. The first Archaeomagnetic secular variation curve for the Iberian Peninsula. Comparison with other data from Western Europe and with global geomantetic field models. Geochem. Geophys. Geosyst., VOL. 7, Q12001, doi:10.1029/2006GC001476.

Gómez-Paccard, M., A. Chauvin, Ph. Lanos and J. Thiriot, 2008. New archeointensity data from Spain and the geomagnetic dipole moment in western Europe over the past 2000 years. J. Geophys. Res, 113, B09103, doi:10.1029/2008JB005582.

Korte, M., F. Donadini, and C. G. Constable, 2009. Geomagnetic field for 0–3 ka: 2. A new series of time-varying global models, Geochem. Geophys. Geosyst., 10, Q06008, doi:10.1029/2008GC002297.

Lanos, Ph., 2004, Bayesian inference of calibration curves: application to archaeomagnetism, in Tools for constructing chronologies: crossing disciplinary boundaries. Vol. 177, edited by C. Buck, and A. Millard, pp. 43 – 82, Springer-Verlag, London.

Hagstrum, J. T., and E. Blinman, 2010. Archeomagnetic dating in western North America: An updated reference curve based on paleomagnetic and archeomagnetic data sets. Geochem. Geophys. Geosyst., doi:10.1029/2009GC002979, in press.

Kovacheva, M., Y. Boyadziev, M. Kostadinova, N. Jordanova, and F. Donadini, 2009. Updated archeomagnetic data set of the past 8 millennia from the Sofia laboratory Bulgaria Geochem. Geophys. Geosyst.10 Q05002 doi:10.1029/2008GC002347.

Lodge, A. and R. Holme, 2009. Towards a new approach to archaeomagnetic dating in Europe using geomagnetic field modelling. Archaeometry, 51(2), 309-322.

McIntosh, G. and G. Catanzariti, 2006. An introduction to archaeomagnetic dating. Geochronometria. Vol. 25, pp 11-18.

Noël, M. and C.M. Batt, 1990. A method for correcting geographically separated remanence directions for the purpose of archaeomagnetic dating. Geophys. J. Int., 102, 753 – 756.

Pavón–Carrasco, F.J., Osete, M.L., Torta, J.M. and, Gaya–Piqué, L.R., 2009. A regional archeomagnetic model for Europe for the last 3000 years, SCHA.DIF.3K: applications to archeomagnetic dating. Geochem. Geophys. Geosyst., 10, Q03013, doi:10.1029/2008GC002244.

Pavón–Carrasco, F.J., Osete, M.L., and Torta, J.M., 2010. Regional Modelling of the Geomagnetic Field in Europe from 6000 BC to 1000 BC. Submitted to Geochem. Geophys. Geosyst.

Schnepp, E. and Ph. Lanos, 2005. Archaeomagnetic secular variation in Germany during the past 2500 years. Geophys. J. Int., 163, 479 – 490.

Schnepp, E. and Ph. Lanos, 2006. A preliminary secular variation reference curve for archaeomagnetic dating in Austria. Geophys. J. Int. 166 (1), 91-96.

Spassov, S., J. Hus, R. Geeranerts and F. Heller. 2008. Archaeomagnetic dating of a High Middle Age likely iron working site in Corroy-le-Grand (Belgium). Phys. Chem. Earth, 33, 544 – 556.

Tanguy, J.C., M. Le Goff, C. Principe, S. Arrighi, V. Chillemi, A. Paiotti, S. La Delfa, and G. Patane, 2003. Archeomagnetic dating of Mediterranean volcanics of the last 2100 years: validity and limits. Earth and Planetary Science Letters 211, 111-124.

Tema, E., I. Hedley and Ph. Lanos, 2006. Archaeomagnetism in Italy: a compilation of data including new results and a preliminary Italian secular variation curve. Geophys. J. Int. 167, 1160 – 1171.

Thellier, E., and O. Thellier, 1959. Sur l'intensité du champ magnétique terrestre dans le passé historique et géologique. Ann. Goephys. 15: 285-376.

Zananiri, I., Batt, C.M., Lanos, Ph., Tarling, D.H. and Linford, P., 2007. Archaeomagnetic secular variation in the UK during the past 4000 years and its application to archaeomagnetic dating. Phys. Earth Planet. Int. Volume 160, Issue 2, p. 97 – 107.

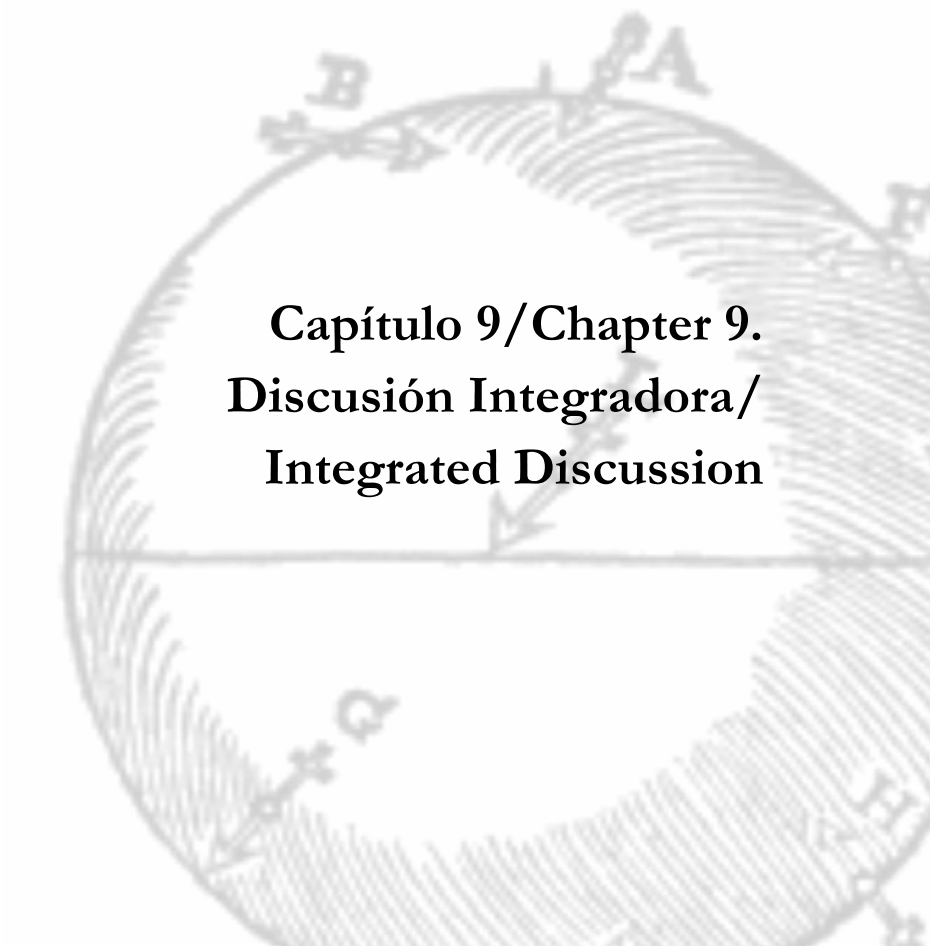

Capítulo 9/Chapter 9. Discusión Integradora/ Integrated Discussion

Discusión Integradora.

1. Bases de datos arqueomagnéticos y paleomagnéticos. Contribución a la base de datos arqueomagnéticos de Iberia.

En tanto que representa la fuente de información esencial que permite describir el comportamiento del campo geomagnético en el pasado, el dato arqueomagnético cobra importancia en esta memoria de Tesis Doctoral. Como se ha descrito en el capítulo 4, el campo geomagnético de origen nuclear, o Campo Principal, puede ser registrado en las estructuras arqueológicas que hayan sufrido un importante calentamiento y posterior enfriamiento en presencia del campo magnético terrestre. Las mejores estructuras con potencial arqueomagnético son los hornos, y los mejores materiales los adobes y ladrillos. Estas hipótesis se han corroborado en el estudio arqueomagnético de 8 sitios diferentes de los dos yacimientos arqueológicos de la Venta del Gallo y del castro de Chao Samartín (Principado de Asturias, España) investigados en este trabajo y detallados en el capítulo 4 (sección 4.1). La mayor parte de las estructuras estudiadas presentaban una termorremanencia debida a calentamientos superiores a los 500/600ºC y, en ocasiones, una termorremanencia parcial en aquellas estructuras donde se observó que el gradiente térmico era importante (figura 5, sección 4.1). Este último comportamiento fue encontrado en los hogares investigados. Pero el fuerte gradiente térmico no ha impedido poder aislar la componente característica del campo geomagnético debido al último calentamiento de la estructura. El análisis llevado a cabo mediante el lavado térmico y por campos alternos decrecientes de las muestras indica una clara componente arqueomagnética con temperaturas de desbloqueo que indicanque la magnetita y la maghemita son, probablemente, las portadoras de la remanencia magnética en los adobes y ladrillos (figura 5, sección 4.1).

Consideraciones arqueológicas y dataciones de C^{14} han establecido la edad de 6 de las 8 estructuras estudiadas arqueomagnéticamente. Dichas edades oscilan entre el s. I a.C. y el s. III d.C., es decir, el período Romano en la península Ibérica. Las direcciones medias obtenidas para estas estructuras son, en su mayoría, indistinguibles entre sí estadísticamente, según el test de McFadden y Lowes (1981), lo cual es compatible con el comportamiento conocido del campo geomagnético para dicha época que tiene aproximadamente valores constantes durante todo el período Romano (tabla 3, sección 4.1). Los resultados obtenidos son, además, comparables con la base de datos arqueomagnéticos de la península Ibérica (Gómez-Paccard et al., 2006a).

Con este estudio arqueomagnético hemos alcanzado los dos primeros objetivos propuestos en el proyecto de tesis doctoral. En primer lugar, conocer la técnica arqueomagnética realizando un estudio paleomagnético completo que incluye trabajo de campo, de laboratorio y el posterior análisis de los resultados. El trabajo realizado me ha permitido aprender a valorar el dato arqueomagnético y conocer sus principales fuentes de error. Y, en segundo lugar, el estudio realizado ha contribuido a aumentar la base de datos arqueomagnéticos de Iberia, en una zona donde no existía ningún dato previo (Norte de Iberia).

La distribución espaciotemporal de datos arqueomagnéticos en Iberia es muy inhomogénea. Así, por ejemplo, en la mitad norte de Iberia solo se cuenta con los datos del período Romano proporcionados por este trabajo (capítulo 4). Además, se debe mejorar en Iberia la cobertura temporal, pues hay períodos en los que apenas hay datos, especialmente entre el 500 – 1000 d.C.

Esta distribución inhomogénea de datos arqueomagnéticos y paleomagnéticos no solo se da en Iberia. En los capítulos 1, 2 y 6 se hace una revisión de la cobertura espaciotemporal de los datos paleomagnéticos. Se puede observar que, a escala global, la densidad de datos aún es muy pobre para el Holoceno (figuras 1.1 y 2.6). Hemos calculado el ratio de número de datos arqueomagnéticos por km^2 para diferentes continentes (capítulo 6). Europa es el continente más densamente investigado, con una densidad de 198 dato/km^2. Mucho mejor que Centro-América (41 dato/km^2), América del Norte (30 dato/km^2) y Asia (23 dato/km^2). Oceanía solo cuenta con 3 dato/km^2 en y África con 1 dato/km^2. En general se observa una gran acumulación de datos arqueomagnéticos y paleomagnéticos en la zona euroasiática y una escasez muy alta en el hemisferio sur, llegando en ocasiones a no existir datos en regiones muy extensas. Los cálculos anteriores fueron llevados a cabo con la base de datos arqueomagnéticos de Korte et al. (2005) para los últimos 3000 años (ver capítulo 6).

La pobre densidad de datos arqueomagnéticos se acentúa para épocas anteriores al año 500 a.C. (figura 2, capítulo 6). Este problema puede ser solventado parcialmente con el uso de datos paleomagnéticos de sedimentos lacustres (figura 1, capítulo 7) con lo que se mejora la cobertura espaciotemporal. Sin embargo, esto conlleva un aumento en el suavizado de los modelos, tanto globales como regionales, generados a partir de este tipo de datos.

De hecho, tanto la pobre distribución espaciotemporal de datos paleomagnéticos, como el uso de sedimentos lacustres, son los responsables del suavizado de los primeros modelos globales de la familia CALS (ver capítulo 2): los modelos CALS3K.1 y CALS3K.2 válidos para los últimos 3000 años y los modelos CALS7K.1 y CALS7K.2 para los últimos 7000 años (Korte y Constable,

2003, 2005). Además, este suavizado en los modelos globales afecta incluso a áreas con alta densidad de datos arqueomagnéticos, como es la región Europea (ver capítulos 6 y 7).

2. Modelos regionales.

Debido a la alta distribución de datos arqueomagnéticos en el continente Europeo, se han ido construyendo a lo largo de los últimos 5 años las curvas de variación paleosecular mediante la estadística bayesiana descrita por Lanos (2004). Estas curvas muestran, en general, el comportamiento de los elementos direccionales (declinación e inclinación) del campo geomagnético para los últimos 3000 años (sección 5.1 y capítulo 8). El hecho de que la medida de arqueointensidad lleve asociado un proceso de laboratorio más complejo y con escasos niveles de éxito, hace que se tengan más datos direccionales que de intensidad y que, de momento, sólo se disponga de una única curva bayesiana de intensidad para la región occidental de Europa (Gómez-Paccard et al., 2008).

La alta distribución de datos paleomagnéticos en la región Europea sugiere que un método regional a gran escala (escala continental) podría ser el mejor camino para analizar el campo geomagnético en dicha región. En el capítulo 2 de esta memoria se han detallado numerosas técnicas de modelado regional, pero de todas ellas nos quedamos con la técnica de modelado regional del análisis armónico en un casquete esférico (SCHA), descrita con gran en detalle en el capítulo 3 (donde hemos indicado sus beneficios y limitaciones).

El proceso de inversión de datos paleomagnéticos ha sido abordado de tres formas diferentes, y ha proporcionado tres modelos regionales (válidos para la misma región: Europa, norte de África y Oeste de Asia) en distintos intervalos temporales:

a) En el primer caso, los datos de entrada fueron las curvas direccionales bayesianas de Europa como si de observatorios geomagnéticos se trataran. Se modificó la técnica SCHA para usar solo datos direccionales (sección 5.1 y anexo 1). El proceso de inversión fue iterativo (sección 5.2), aumentando el grado (y orden) en el desarrollo del potencial geomagnético en el casquete esférico (eq. 3.10 considerando sólo el potencial interno) desde el mínimo posible (grado n = 1, orden m = 1) hasta el grado 2, orden 2. Este proceso iterativo es el método de regularización que permite la inversión de datos arqueomagnéticos, además del uso de casquetes esféricos grandes, entorno a 40º. El resultado de este estudio es el modelo direccional SCHA.DI.00 válido para los últimos 2000 años. Mediante la aplicación del teorema de Hulot et al. (1997) se ha añadido la arqueointensidad al modelo direccional anterior, obteniéndose un modelo completo válido para los últimos 2000 años, el modelo SCHA.DI.00-F (sección 5.2).

b) En un segunda parte, se ha abordado el problema de inversión usando conjuntamente, *in situ*, todos los datos arqueomagnéticos disponibles (abandonando el uso de las curvas de variación secular que introducen un error de relocalización). Para el modelado conjunto de los tres elementos del campo: declinación, inclinación e intensidad, hemos aplicado el desarrollo en serie de Taylor de los mismos (capitulo 6 y anexo 2). Este método necesita un modelo inicial de partida o modelo base. En este caso, el proceso de inversión está regulado por el gran tamaño del casquete esférico (40º), el grado y orden del desarrollo en armónicos del potencial hasta $n = m = 2$, y fundamentalmente por el uso del modelo SCHA.DI.00-F como modelo de partida para obtener el modelo final, SCHA.DIF.3K, válido para los últimos 3000 años. Los datos históricos de observatorios de los últimos 400 años fueron incluidos en el modelo y se usó como modelo de partida el modelo histórico GUFM (Jackson et al., 2000) modificado según Gubbins et al. (2006).

c) Finalmente, se ha desarrollado un modelo válido para los últimos 8000 años (capítulo 7) en el que se modelan conjuntamente los tres elementos del campo geomagnético, manteniendo el mismo orden y grado del desarrollo armónico que en el modelo previo SCHA.DIF.3K, pero usando una revisión de la técnica de modelado SCHA: la técnica R-SCHA2D (Thébault, 2008), que permite disminuir el tamaño del casquete hasta el tamaño óptimo (de acuerdo con la distribución espacial de los datos) de 22º. A los datos arqueomagnéticos se le han sumado los procedentes de sedimentos lacustres para tener una mejor cobertura espaciotemporal. La regulación en este caso ha sido proporcionada por la norma del campo geomagnético dentro del casquete esférico. Este hecho permite que el modelo inicial de partida en el desarrollo de Taylor de los elementos geomagnéticos sea el más simple posible, i.e., el modelo geocéntrico dipolar axial (GAD). Como resultado se ha obtenido un modelo regional para el período temporal 6000 a.C. al 1000 a.C. llamado SCHA.DIF.8K.

3. Modelos regionales versus modelos globales.

Se ha comparado el modelo global CALS7K.2 (Korte y Constable, 2005) con los cuatro modelos regionales desarrollados en este trabajo (los tres primeros son puramente arqueomagnéticos y el cuarto es mixto, i.e., constituido por datos arqueomagnéticos y de sedimentos lacustres) en diferentes intervalos temporales:

a) Para los últimos 2000 años, el modelo global CALS7K.2 se ha comparado con los modelos regionales SCHA.DI.00 y SCHA.DI.00-F propuestos en el capítulo 5 (ver figura 5 en la sección 5.2 para el caso direccional y figura 6 en la sección 5.3 para el caso de la arqueointensidad).

b) Para los últimos 3000 años, el modelo global es comparado con el modelo SCHA.DIF.3K (figura 8 del capítulo 6). El suavizado a escala global ha sido

recientemente analizado mediante la última familia de modelos globales CALS de Korte et al. (2009), que proporcionan valores de los elementos del campo geomagnético para los últimos 3000 años. Dichos modelos son revisados en detalle en los capítulos 2 y 8 de la memoria y fueron publicados con posterioridad a nuestro modelo regional SCHA.DIF.3K. El nuevo modelo global ARCH3K.1 ha sido construido solo con datos arqueomagnéticos y muestra un gran acuerdo con nuestro modelo regional arqueomagnético SCHA.DIF.3K en la región Europea. Sin embargo, el modelo global tiene una variabilidad muy elevada (incluso superior a nuestro modelo) que puede ser un artefacto matemático más que un producto de la variabilidad del campo magnético terrestre.

c) Y finalmente, para el período 5000 a.C. – 1000 a.C. se ha comparado el modelo global con el modelo regional SCHA.DIF.8K (figuras 7, 8 y 9, de la sección 7.2). En este caso la intensidad del modelo CALS7K.2 muestra valores más bajos y anómalos de los esperados para todo el período temporal analizado (figura 9, sección 7.2).

El efecto de suavizado se encuentra también a escala regional, ya que el modelo mixto regional SCHA.DIF.8K (capítulo 7.2) ha sido generado con datos arqueomagnéticos y de sedimentos lacustres. La figura 2 de la sección 8.3 muestra la clara diferencia en suavizado de este modelo respecto del puramente arqueomagnético SCHA.DIF.3K para los tres elementos del campo geomagnético: declinación, inclinación e intensidad. Como veremos después, este alto suavizado cobra importancia en el proceso de datación arqueomagnética cuando se usan las PSVCs generadas por este tipo de modelos (capítulo 8).

4. Variación paleosecular en Europa durante los últimos 8000 años.

El modelo SCHA.DIF.8K, junto con el modelo SCHA.DIF.3K, son denotados como Modelos de Campo Geomagnético en el pasado para Europa. Ellos permiten analizar el Campo Principal y su variación paleosecular en Europa en los últimos 8000 años. Los modelos SCHA.DI.00 y SCHA.DI.00-F pasan a un segundo plano, por ser menos robustos e incluir errores de relocalización debido al uso de las curvas de variación paleosecular. El modelo SCHA.DIF.3K es más riguroso y robusto y, por tanto, sustituye a ambos modelos iniciales.

Las variaciones del campo geomagnético de los últimos 3000 (modelo 3K) años están mejor definidas debido al uso exclusivo de datos arqueomagnéticos, en contraste con la combinación de datos arqueomagnéticos y de sedimentos lacustres anteriores del año 1000 a.C. (ver figura 2 en sección 8.3), que hacen que el modelo 8K de amplitudes de la variación del campo geomagnético más suaves.

En cuanto a dirección (declinación e inclinación), la variación paleosecular en la región europea ha registrado numerosos máximos y mínimos en los últimos 8000 años (capítulos 6 y 7). Los máximos en declinación se alcanzan en varias épocas: entorno al 5000 a.C., en el 800 a.C., el 1000 d.C. y entorno al 1600 d.C. Existe un mínimo pronunciado entorno al 3700 a.C. y otro entorno al año 1800 d.C. La inclinación muestra máximos entorno al 5700 a.C., 3500 a.C., 800 a.C, 850 d.C y entorno al 1700 d.C. Mínimos de inclinación son encontrados entre el 5000 – 4000 a.C, entorno al 300 d.C. y en 1300 d.C. Los eventos de máximos y mínimos direccionales coinciden con aquellos propuestos por la curva patrón de variación secular del Holoceno dada por sedimentos lacustres de los lagos Loch Lomond (Escocia), Windermere (Norte Inglaterra) y Llyn Geirionydd (Norte de Wales) de Turner y Thomson (1981). La figura 9.1 representa la PSVC direccional en el Reino Unido (54.3ºN de latitud y 3.0ºW de longitud) generada por los modelos regionales SCHA.DIF.3K y SCHA.DIF.8K, donde hemos marcado los eventos descritos por Turner y Thomson, (1981). Ver capítulos 7 y 8 para más detalle.

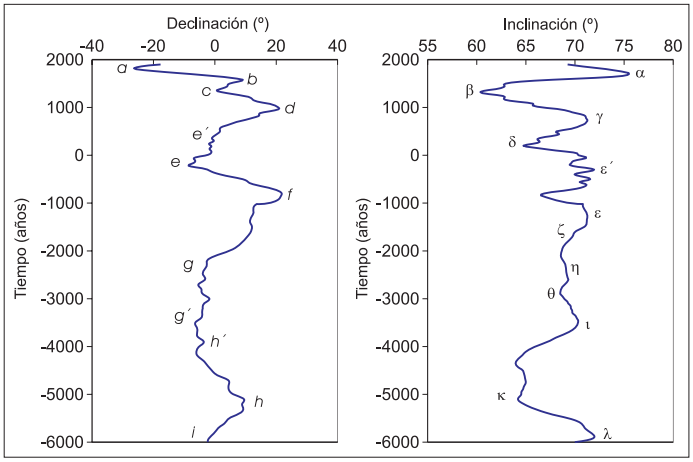

Figura 9.1. CVPS de los modelos SCHA.DIF.3K y SCHA.DIF.8K para el Reino Unido (54.3ºN latitud, 3.0ºW longitud) con los eventos descritos en Turner y Thomson (1981) para la curva patrón del Reino Unido.

La intensidad en Europa muestra numerosos máximos en los últimos 8000 años. Cabe destacar los dos máximos entorno al año 600 a.C. y el del 850 d.C. (figuras 8 del capítulo 6 y figura 9 del capitulo 7). A partir de la intensidad, se ha calculado el momento axial dipolar virtual (VADM) que proporciona un valor aproximado del momento dipolar regional del área Europea. El VADM regional se caracteriza por un decrecimiento hasta el año 5000 a.C. seguido de un incremento continuo durante 4500 años hasta el 500 a.C. Entre el 500 a.C. y el 800 d.C. tiene un mínimo relativo en el 200 d.C. y finalmente, a partir del 900 d.C. muestra una caída brusca hasta la actualidad (figura 11 del capitulo 7).

Un análisis conjunto de los tres elementos geomagnéticos (declinación, inclinación e intensidad) proporcionados por los modelos SCHA.DIF.3K y .8K sugieren que el campo geomagnético observado en Europa ha sufrido variaciones rápidas en los últimos 8000 años (sección 8.1). Estos cambios bruscos de la variación paleosecular o *jerks* arqueomagnéticos están en pleno debate y se necesita una definición consensuada de los mismos (Mandea y Olsen, 2009). En nuestro caso hemos determinado los *jerks* siguiendo la definición de Gallet et al. (2003). El modelo SCHA.DIF.3K muestra 5 *jerks* arqueomagnéticos (entorno al 300 a.C., 300 d.C., 800 d.C., 1350 d.C. y 1600 d.C.) y un posible *jerk* entorno al 1800 d.C. Estos eventos están caracterizados por una intensidad del campo máxima y fuertes cambios en la curvatura direccional (según Gallet et al., 2003). Otros eventos direccionales (*"jerks direccionales"*) se han observado entorno al 825 a.C., 650–700 a.C., 125 a.C., 600–650 d.C. y 1175–1200 d.C., aunque se necesitan más datos para precisar en detalle las variaciones del campo geomagnético (figura 10, capítulo 6). El modelo SCHA.DIF.8K muestra también *jerks arqueomagnéticos* (figuras 11 del capitulo 7 y figura 8.1 del capítulo 8), pero su definición es menos clara y precisa, porque en los datos de entrada se han incluido datos paleomagnéticos de sedimentos lacustres, con lo que los modelos obtenidos están más suavizados.

5. Variaciones del campo magnético terrestre y cambios climáticos.

Numerosos trabajos en la última década indican que las variaciones rápidas pueden estar relacionadas con importantes cambios climáticos (Gallet et al., 2003, 2005, 2009 y referencias interiores) ya que el comportamiento del Campo Principal podría modular la mayor o menor entrada de rayos cósmicos en la atmósfera, cuya interacción con la misma, modifica el grado de generación de nubes (Gallet et al., 2006, Courtillot et al., 2007). Las nubes tienen dos efectos simultáneos y opuestos en el balance radiativo del planeta: por un lado reflejan la radiación solar de longitud de onda corta hacia el espacio exterior (efecto de enfriamiento) y por otro evitan que la emisión de longitud de onda larga de la Tierra escape hacia el espacio (efecto de calentamiento). En promedio se considera que el efecto de enfriamiento domina sobre el de calentamiento (p.e. Curto et al., 2009 y referencias interiores). En general, pues, se asume que máximos de intensidad geomagnética deben estar asociados a períodos fríos y viceversa.

Siguiendo las consideraciones de Gallet et al. (2005, 2009) hemos comparado la intensidad del campo magnético terrestre proporcionada por el modelo SCHA.DI.00-F y SCHA.DIF.3K para los últimos 2000 años con los eventos climáticos considerados por Gallet et al. (2005) (sección 5.3). Los resultados parecen corroborar la hipótesis de Gallet et al. (2005) (figura 7, sección 5.2). Sin embargo creemos que son necesarios muchos más datos paleomagnéticos (principalmente arqueomagnéticos) de alta calidad para que las correlaciones

establecidas con los datos paleoclimáticos sean más robustas (sección 8.2). Hecho que se ha corroborado en la comparación de la intensidad del modelo SCHA.DIF.8K con eventos climáticos de testigos de hielo (ver capitulo 8, sección 8.2).

6. Confirmación de la hipótesis del Dipolo Axial Geocéntrico (GAD).

Un último análisis (capitulo 7) de la variación paleosecular confirma la principal hipótesis en la que se basa el Paleomagnetismo: la hipótesis del dipolo geocéntrico axial (GAD). Ésta indica que la variación paleosecular del Campo Principal se anula cuando se promedia en un intervalo de tiempo próximo a los 10000 años, es decir, cuando el campo se promedia en estos períodos de tiempo. El resultado es un campo dipolar axial geocéntrico. Esta hipótesis se debe cumplir tanto a escala global como a escala regional. Mediante el uso de los modelos SCHA.DIF.3K y SCHA.DIF.8K hemos promediado la variación paleosecular en Europa para los últimos 8000 años. El resultado muestra que en estos 8000 años se cumple la hipótesis GAD a escala regional. La figura 9.2 muestra los valores promediados de la dirección (declinación e inclinación) y de intensidad del campo geomagnético en la región Europea para los 8000 años de validez de los dos modelos regionales. También hemos representado para las mismas coordenadas geográficas los valores dados por el modelo GAD. La hipótesis GAD queda corroborada con un valor del primer coeficiente de Gauss g_1^0 para los últimos 8000 años de unos 35 μT (ver capítulo 2 para detalles).

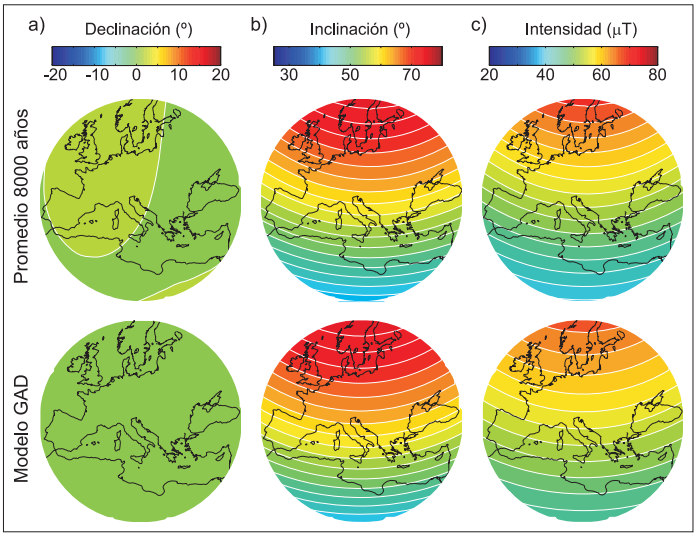

Figura 9.2. Promedio de la variación paleosecular en Europa según los modelos SCHA.DIF.3K y SCHA.DIF.8K (arriba) para los últimos 8000 años. Modelo GAD suponiendo el primer coeficiente de Gauss g_1^0 = 35 μT (abajo). Mapas de (a) declinación, (b) inclinación e (c) intensidad.

7. Utilización de modelos regionales en la datación arqueomagnética.

Finalmente, una de las aplicaciones más directas de los modelos generados de variación paleosecular del campo geomagnético en Europa es su uso como herramienta de datación arqueológica. Para desarrollar esta aplicación hemos generado una herramienta en código Matlab descrita en la sección 8.3 de la presente memoria.

Se ha desarrollado una herramienta versátil que puede utilizar como curvas de referencia las PSVCs bayesianas, las curvas generadas a partir de los modelos globales de Korte et al. (2009) y las calculadas por los modelos regionales desarrollados en este trabajo.

Existen numerosas fuentes que implican una mayor incertidumbre en la datación. A continuación se indican las principales fuentes de incertidumbre en la datación arqueomagnética. Entre ellas cabe destacar:

a) La principal fuente de incertidumbre es la del propio dato paleomagnético y la precisión de la curva de referencia utilizada. Esta curva de referencia puede ser generada a partir de diferentes técnicas (curvas bayesianas u otras técnicas estadísticas, modelos globales o regionales, etc.), pero se basan en los datos paleomagnéticos bien fechados disponibles, es decir, en las bases de datos de referencia. Ya se ha analizado, a lo largo de este trabajo, que aún existen importantes lagunas en la distribución espaciotemporal de las bases de datos actuales. Europa es la región que ha sido más ampliamente investigada y, por tanto, es el área en el que la técnica de datación arqueomagnética puede utilizarse con mayor fiabilidad. No obstante hay que señalar que existen importantes lagunas, a destacar la escasa densidad de datos arqueomagnéticos anteriores al año 500 a.C. y la necesidad de más datos que cubran el período 500 d.C – 1000 d.C. (época oscura).

b) La inhomogénea distribución de los datos arqueomagnéticos de referencia disponibles en Europa hacen que sea aconsejable la utilización de modelos globales o regionales para generar curvas de variación paleosecular de referencia, ya que por una parte se elimina el error de relocalización y, por otra, se puede emplear la técnica aún cuando en esa zona no hay datos paleomagnéticos disponibles.

c) Las curvas generadas a partir de modelos basados en la combinación de datos arqueomagnéticos y sedimentarios no son los más indicados para efectuar dataciones, ya que son muy suaves. La mejor opción es usar las curvas bayesianas arqueomagnéticas más próximas al yacimiento arqueológico; y si estamos en la región Europea, el modelo puramente arqueomagnético SCHA.DIF.3K (para los últimos 3000 años).

d) También contribuye a la incertidumbre de la datación el propio comportamiento del campo geomagnético. Por ejemplo, en el estudio arqueomagnético del capítulo 4 hemos visto como algunas de las direcciones obtenidas para el período Romano tienen direcciones indistinguibles en todo el período 100 a.C. - 500 d.C. Ello se debe a que los elementos direccionales del campo geomagnético permanecen aproximadamente constantes en dicho período de tiempo. Este hecho puede ocurrir también para otros períodos temporales (figura 10, capítulo 6).

e) La incertidumbre disminuye si se dispone, además de los datos direcciones del yacimiento a datar, de información de paleointensidad.

8. Modelos regionales para otras áreas.

Con el trabajo desarrollado en esta presente memoria de Tesis Doctoral se ha analizado y puesto a punto el método regional SCHA para ser aplicado a datos paleomagnéticos y obtener modelos robustos del campo geomagnético para la región Europea en el pasado. Una vez alcanzado este objetivo, se ha aplicado también la técnica a la segunda región mundial con mayor densidad de datos arqueomagnéticos: el continente Asiático (ver figura 1.1). Este modelo preliminar del campo geomagnético para Asia válido para los últimos 2000 años se detalla en el Anexo 3.

Integrated Discussion.

1. The archaeomagnetic and palaeomagnetic databases. New data for the Iberian archaeomagnetic database.

The main source of information for generating models of the ancient geomagnetic field is the archaeomagnetic datum. For this reason, the archaeomagnetic datum takes a special interest in the present PhD Thesis. The internal geomagnetic field, called Main Field, can be recorded on archaeological artefacts which have been heated. Baked clay and brick samples are shown to be the best carriers of the magnetic remanence. This hypothesis has been corroborated in the chapter 4 (section 4.1) which contains an archaeomagnetic study of 8 different structures in two archaeological sites: *la Venta del Gallo* and the hill-fort *Chao Samartín* (Principado de Asturias, Spain). All studied structures showed a thermoremanence with unblocking temperature higher than 500/600ºC and, in some cases, the direction of the thermal gradients in fireplaces has been detected, suggesting partial-thermoremanences as the origin of remanent magnetization (figure 5, section 4.1). However, this partial-thermoremanence has not prevented isolating the characteristic component of the Earth's magnetic field due to the last heating of the structure. Detailed thermal and alternating field demagnetization have been applied to the samples. Results showed a main archaeomagnetic component characterized by a low coercitivity and a moderate unblocking temperature phase, such as magnetite/maghemite, that seem to be the carriers of the archaeomagnetic signal in the baked clay/brick samples (figure 5, section 4.1).

Archaeological considerations and radiocarbon dating have established the age of 6 out of 8 structures. These ages range from the 1st century BC to the 3rd century AD, i.e. the Roman period in the Iberian Peninsula. The mean directions are mostly statistically indistinguishable according to the test of McFadden and Lowes (1981) and the reason could be due to the behaviour of the geomagnetic field for that period, which shows approximately constant directional elements for the entire Roman period (table 3, section 4.1). The results are comparable to those given in the archaeomagnetic database of the Iberian Peninsula (Gómez-Paccard et al., 2006).

With this study we have achieved our fist two goals. First, to analyze and better understand the behaviour of the archaeomagnetic data and their main

source of errors. And second, to increase the archaeomagnetic database in areas which were empty (the northern Iberia).

The spatiotemporal distribution of the archaeomagnetic data in the Iberian Peninsula is very inhomogeneous. For example, there are only the Roman directional data provided by the archaeomagnetic study of chapter 4 (figure 1, section 4.1). Moreover, it is necessary to improve the temporal distribution of the data in the Iberian Peninsula, especially, for the time interval 500 AD – 1000 AD.

The inhomogeneous distribution of archaeomagnetic and palaeomagnetic data does not only occur in the Iberian Peninsula. In chapters 1, 2 and 6 we analysed the poor spatial and temporal global distribution of palaeomagnetic data for the Holocene period (figures 1.1 and 2.6). We also computed the distribution ratio (data per km^2) for different continents (chapter 6). Europe has the largest ratio with 198 data/km^2, followed by Mesoamerica - 41 data/km^2 -, Northern America – 30 data/km^2 -, and Asia – around 23 data/km^2 -. The lowest number of data comes from Oceania with 3 data/km^2 and Africa with 1 data/km^2. In general, there is a large accumulation of archaeomagnetic data in the Eurasian region and, there are practically no data in the southern hemisphere. The above calculations were carried out using the archaeomagnetic database of Korte et al. (2005) for the last 3000 years (see chapter 6).

In order to improve the poor archaeomagnetic data distribution prior to 500 BC (figure 2, chapter 6) the lake sediment data can be used (figure 1, chapter 7). However, this kind of data increases the smoothness of both global and regional models.

Both effects, the limited spatiotemporal distribution of the palaeomagnetic data and the use of lake sediments, have imposed a high smoothness in the construction process of the CALS family of global models (see chapter 2): the CALS3K.1 and CALS3K.2 models covering the past 3000 years, and the CALS7K.1 and CALS7K.2 models for the last 7000 years (Korte and Constable, 2003, 2005). Moreover, this smoothness even affects areas with high density of archaeomagnetic data, such as the European region.

2. Regional model.

The high number of archeomagnetic data in Europe has allowed constructing different PSVCs using the Bayesian statistics of Lanos (2004). These curves generally contain the directional elements (declination and inclination) of the geomagnetic field for the last 3000 years (section 5.1 and chapter 8). There is only a Bayesian intensity curve for the Western Europe (Gomez-Paccard et al., 2008).

The large distribution of palaeomagnetic data in the European region suggests that a regional approach (at continental scale) could be the best way to analyze the geomagnetic field in this region. Numerous regional modelling techniques have been detailed in chapter 2. Among them, we preferred the spherical cap harmonic analysis method (SCHA) described in chapter 3, because this method satisfies the Laplace equation.

The inversion process of the palaeomagnetic data has been carried out at three different steps, each one associated with different treatments of the palaeomagnetic data and regularization methods. Each level has provided a different regional model for the same region, i.e., Europe, Northern Africa and Western Asia, but for different time intervals:

a) In the first step, the inversion process was iterative (section 5.2), increasing the degrees k and m of the geomagnetic potential expansion from $k = 1$ and $m = 1$, up to $k = 2$, $m = 2$. The iterative process, along with the low degree and the large size of the spherical cap (around 40º), turned out to be the regularization method that allowed us to obtain the regional model. The directional Bayesian European PSVCs were used as input data. These curves allow a smooth and continuous evolution of the directional geomagnetic field elements in time to facilitate the stability in the inversion process. The SCHA technique was modified for using only directional information (section 5.1 and Appendix 1). The directional SCHA.DI.00 regional model resulted from this first step. By using a theorem given by Hulot et al. (1997), the archaeointensity was added to the previous directional model, obtaining a complete model valid for the last 2000 years: the SCHA.DI.00-F model (section 5.2).

b) For the next step, all directional and intensity *in situ* data were used to obtain a new regional model for the last 3000 years: the SCHA.DIF.3K model. The linearization problem was solved using the truncation Taylor's series applied to the expressions of the relationships between the declination, inclination and intensity data and the Cartesian components of the geomagnetic field (chapter 6 and appendix 2). This approach needs an initial model. In this case, the inversion process is constrained by the large size of the spherical cap (40º), the low degree of the harmonic expansion and the use of the previous SCHA.DI.00-F model as initial model. Historical data, for the last 400 years, from geomagnetic observatories were included in the modelling process. For this time period we have used the historical GUFM global model (Jackson et al., 2000), modified by Gubbins et al. (2006), as initial model.

c) Finally, we have used the recent R-SCHA method in 2 dimensions (R-SCHA2D, Thébault, 2008) to develop a new regional model of the ancient geomagnetic field (chapter 7). This new method reduces the size of the spherical

cap until an optimal size (according to the spatial data distribution) of 22 º. The inversion process is constrained by the norm of the geomagnetic field into the spherical cap. This regularization method allowed us to use the simplest field, i.e., the geocentric axial dipole field (GAD field) as the initial model (in the Taylor expansion of the geomagnetic field elements). The lake sediment data were included in order to improve the spatiotemporal distribution of the archaeomagnetic data. The new regional model, called SCHA.DIF.8K, is valid from 6000 BC to 1000 BC.

3. Regional models *versus* global models.

We have compared the CALS7K.2 global model (Korte and Constable, 2005) with the four regional models developed in the present work (the first three models are purely archaeomagnetic and the fourth is a mixed model, i.e., constructed with archaeomagnetic data and lake sediment records) for different time intervals:

a) For the past 2000 years, the CALS7K.2 global model has been compared with the SCHA.DI.00 and SCHA.DI.00-F regional models proposed in chapter 5 (see figure 5 in section 5.2 for the direction and figure 6 in section 5.3 for the intensity).

b) For the past 3000 years, the global model is compared with the SCHA.DIF.3K regional model (figure 8, chapter 6). At global scale, the smooth behaviour has been recently analyzed by Korte et al. (2009) using the new family of CALS global models, which provide values of the geomagnetic field elements for the last 3000 years (we want to recall that this new family of global models were published after our SCHA.DIF.3K regional model). More details of these new global models are given in both chapters 2 and 8 of the present work. One of these models, called ARCH3K.1, is developed using only archaeomagnetic data and agrees with our regional SCHA.DIF.3K archaeomagnetic model for the European region. However, the global model variability is very high (even higher than our model) and it seems to be a mathematical artefact rather than a product of the variability of the Earth's magnetic field.

c) And finally, for the time period 5000 BC - 1000 BC, we have compared the global model with the SCHA.DIF.8K regional model (figures 7, 8 and 9, section 7.2). In this case, the intensity provided by the CALS7K.2 model show anomalous values, which are lower than those given by the regional model for the studied time period (figure 9, section 7.2).

This smoothness also appears at regional scale when lake sediment data are included as input data. The SCHA.DIF.8K regional model (chapter 7.2) shows this smooth behaviour because this model was generated using archaeomagnetic

data and lake sediment records. Figure 2 in section 8.3 shows the clear difference between this model and the purely SCHA.DIF.3K archaeomagnetic model for the three elements of the geomagnetic field: declination, inclination and intensity. In chapter 8, we have demonstrated that the smoothness becomes important in the archaeomagnetic dating process.

4. Palaeosecular variation in Europe for the last 8000 years.

The SCHA.DIF.8K model, along with the previous SCHA.DIF.3K model, are denoted as the Geomagnetic Field Models for Europe for the last 8000 years. They allow us to analyze the main field and its paleosecular variation in Europe for the last 8000 years. The SCHA.DI.00 and SCHA.DI.00-F regional models, valid for the last 2000 years, were initial models and they include the relocation error due to the use of PSVCs. In this sense, the new SCHA.DIF.3K regional model is more robust and thus it replaces both initial models.

The palaeosecular variation of the European geomagnetic field for the last 3000 years shows more abrupt changes due to the exclusive use of archaeomagnetic data, in contrast to the combination of these data and the lake sediments records prior to 1000 BC (see figure 2 in section 8.3). In direction (declination and inclination), the paleosecular variation in the European region records different maxima and minima for the past 8000 years (chapters 6 and 7). Declination maxima appear around 5000 BC, 800 BC, 1000 AD and close to 1600 A.D. In addition, there is a pronounced minimum around 3700 BC and another around 1800 A.D. Different inclination maxima are found around 5700 BC, 3500 BC, 800 BC to 850 AD and 1700 AD, with minima between 5000 BC and 4000 BC, at 300 AD and around 1300 A.D. These directional events (maxima and minima) agree with those proposed by Turner and Thomsom (1981) for the Holocene master curve of the United Kingdom. This directional master curve was obtained from lake sediment data from the Loch Lomond (Scotland), Windermere (North England) and Llyn Geirionydd (North Wales) lakes. Figure 9.1 shows the directional PSVC for the U.K. (54.3ºN latitude and 3.0ºW longitude) generated by the SCHA.DIF.3K and SCHA.DIF.8K regional models, where we have marked the events described by Turner and Thomson, (1981). See chapters 7 and 8 for more detail.

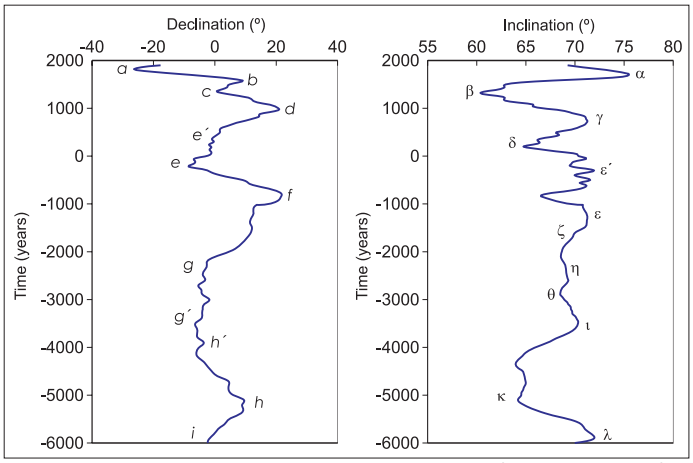

Figure 9.1. Directional PSVC for the United Kingdom (54.3°N latitude, 3.0°W longitude), using the SCHA.DIF.3K and SCHA.DIF.8K models, with the events described by Turner and Thomson (1981).

The intensity of the Earth's magnetic field shows several maxima for the last 8000 years in the European region, e.g., there are two maxima around 600 BC and 850 AD (figures 8 and 9 in chapter 6 and 7, respectively). In order to analyze the European geomagnetic field strength for the last 8000 years, we have calculated the virtual axial dipole moment (VADM) using the intensity values and the different regional and global models (figure 11, chapter 7). The average regional VADM, obtained by our regional models, is characterized by periods of increase between 5000 BC and 500 BC followed by a strong decay for the last 1200 years (figure 11 in chapter 7).

A joint analysis of the three geomagnetic field elements (declination, inclination and intensity) has been carried out using the SCHA.DIF.3K and SCHA.DIF.8K regional models. Results show that the geomagnetic field over Europe has registered some rapid changes for the last 8000 years (section 8.1). These rapid changes of the palaeosecular variation, the so-called archaeomagnetic *jerks*, are a *hot topic* of research and it is necessary to establish a consensus definition of its origin (Mandea and Olsen, 2009). These events are characterized by simultaneous occurrence of intensity maxima and directional curvature changes (Gallet et al., 2003). The SCHA.DIF.3K archaeomagnetic model reproduces 5 archaeomagnetic *jerks* around 300 BC, 300 AD, 800 AD, 1350 AD and 1600 AD and a possible *jerk* around 1800 AD. Other directional events (directional *jerks*) were observed around 825 BC, 650 - 700 BC, 125 BC, 600 - 650 AD and 1175 - 1200 AD. However, more archaeomagnetic data are needed to confirm these directional events (figure 10, chapter 6). We have also found several archaeomagnetic *jerks* using the SCHA.DIF.8K regional model (figures 11 and 8.1 in chapter 7 and 8, respectively), but the results look less

robust due to the use of lake sediment records, which generate a smooth behaviour of the palaeosecular variation of the geomagnetic field.

5. The Earth's magnetic field variations and the climatic changes.

Numerous studies (Gallet et al., 2003, 2005, 2009 and references therein) suggest that the rapid changes of the Earth's magnetic field could be related to the climate change. The link between geomagnetism and climate still remains uncertain, but Gallet et al. (2006) and Courtillot et al. (2007) suggest that the geomagnetic field variation of internal origin can modulate the cosmic ray flux and, in consequence, produce significant changes in cloudiness. Although the clouds have two simultaneous and opposite effects on the Earth's radiative balance (on one hand they reflect the solar radiation of short wavelength - cooling effect and, on the other hand, they prevent the emission of long wavelengths - heating effect), on average, the cooling effect dominates over the heating (e.g. Curto et al., 2009 and references therein). In this sense, geomagnetic intensity maxima should be associated with cool periods and vice versa. Following the considerations of Gallet et al. (2005, 2009) we have compared the intensity prediction provided by the SCHA.DI.00-F, SCHA.DIF.3K and SCHA.DIF.8K regional models and the cooling events marked by glacier advances on land and increases in ice-rafted debris in deep-sea sediments (sections 5.3 and 8.2). Our results seem to corroborate this theory for the last 2000 years (figure 7, section 5.2 and figure 8.2, section 8.2). However, we think that more well-dated and accurate palaeomagnetic data are needed (mainly archaeomagnetic data) to establish a more robust correlation with several climate or palaeoclimate events (section 8.2).

6. The Geomagnetic Axial Dipole field hypothesis.

The last analysis of the palaeosecular variation of the European geomagnetic field is related with the main palaeomagnetic assumption: the GAD field hypothesis (chapter 7). The hypothesis indicates that the palaeosecular variation must be averaged over sufficient time, i.e., around 10000 years, and the result is the Geocentric Axial Dipole field. This condition must be satisfied at both global and regional scale. We have used our SCHA.DIF.3K and SCHA.DIF.8K regional models to study the average variation of the geomagnetic field in Europe for the last 8000 years. Results show that, for the last 8000 years, the European geomagnetic field is approximately averaged to a GAD field. Figure 9.2 shows the average values of the direction (declination and inclination) and intensity of the European geomagnetic field for the 8000 years. We have also represented the values given by the GAD model. For the intensity, the GAD field model is rescaled with a value of the first Gauss coefficient g_1^0 for the last 8000 years of 35 μT (see chapter 2 for details).

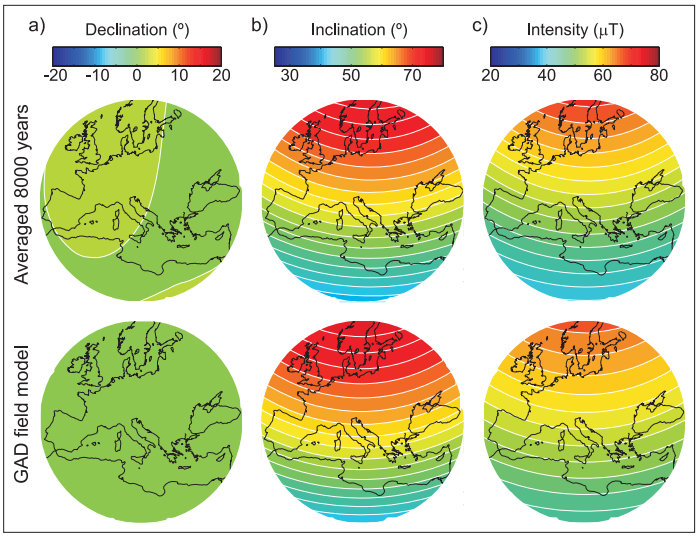

Figure 9.2. (Top) Average paleosecular variation in Europe for the last 8000 years using the SCHA.DIF.3K and SCHA.DIF.8K regional models and (Bottom) the GAD field model assuming the first Gauss coefficient equal to 35 μT. (a) Declination, (b) inclination and (c) intensity maps.

7. Regional models as a tool for archaeomagnetic dating.

Finally, the most direct application of the obtained regional models of the geomagnetic field is its use as a tool for archaeological dating. In this sense, we have generated a Matlab tool which is detailed in section 8.3. To obtain an archaeomagnetic dating the software can use the Bayesian European PSVCs, the PSVCs generated by the global models of Korte et al. (2009), or the regional models provided in this PhD Thesis (or another new PSVC).

There are different sources of error involved in the dating process. Some of them are as follows:

a) The error of the PSVCs: this error is related with the measurement and age uncertainties of the archaeomagnetic data, as it happens with the global and regional models. This error also depends on the spatiotemporal distribution of the archaeomagnetic data.

b) The inhomogeneous distribution of the archaeomagnetic reference data in the European region indicates to use the global or regional models for obtaining the PSVCs, since the relocation error is avoided and the possibility of obtaining a PSVC in areas where palaeomagnetic data are not available.

c) For archaeomagnetic dating, the models based on the combination of sedimentary and archaeomagnetic data are not the best option, since they are

highly smoothed. The Bayesian PSVCs close to the archaeological site and the SCHA.DIF.3K regional model (for the last 3000 years) seem to be the best choice for this purpose.

d) The behaviour of the geomagnetic field also contributes to the uncertainty of the archaeomagnetic dating. In chapter 4, we have seen how different archaeological artefacts with ages into the Roman period (100 BC - 500 AD) show indistinguishable directions. The reason is the behaviour of the directional geomagnetic field elements, which remain approximately constant in that time period. This can occur also for the intensity and for other time periods (figure 10, chapter 6).

e) Finally, the use of the full geomagnetic vector (declination, inclination and intensity values) allows us to obtain a more accurate date.

8. Regional model for other areas.

With the present work we have analyzed and tested the regional SCHA/R-SCHA2D methods and their application to palaeomagnetic data in order to obtain robust models of the ancient geomagnetic field for the European region. We have also applied the regional technique to the second global region with a large density of archaeomagnetic data: the Asian continent (see figure 1.1). This initial model of the geomagnetic field for Asia covers the last 2000 years and is detailed in the Appendix 3.

Capítulo 10/Chapter 10. Conclusiones y perspectivas futuras /Conclusions and Outlook

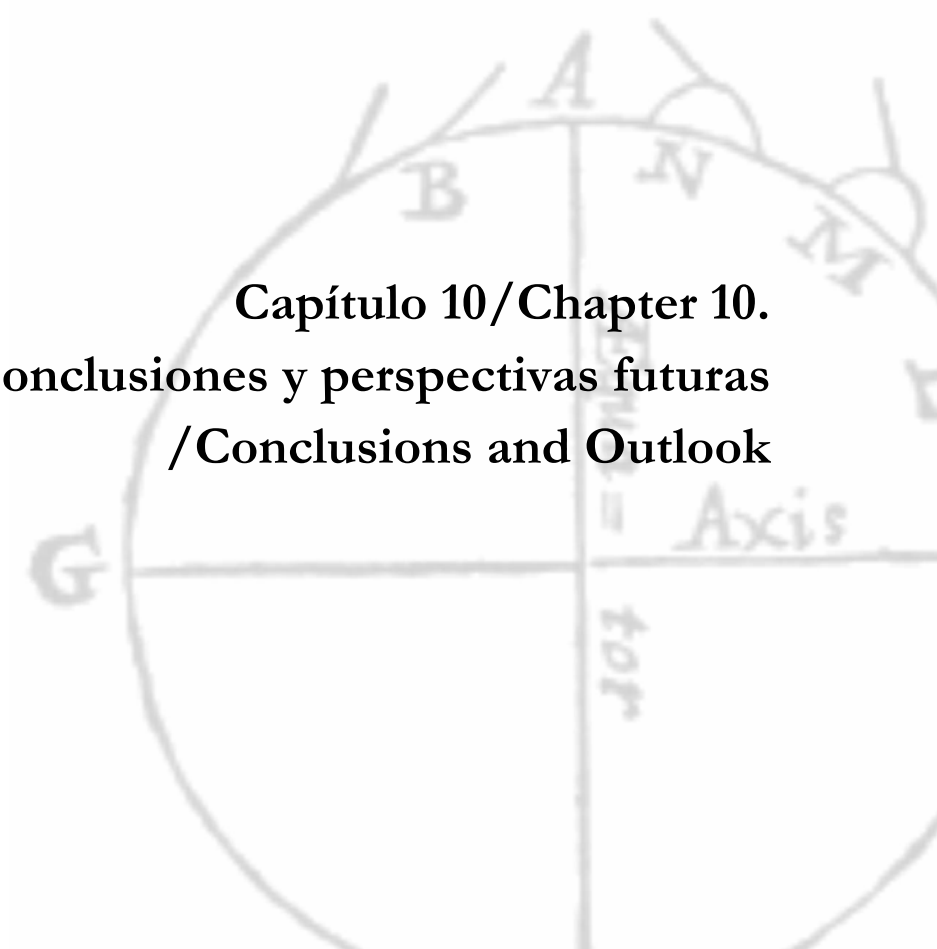

Conclusiones.

Las principales conclusiones y contribuciones de este trabajo son las siguientes:

Análisis de la base europea de datos arqueomagnéticos:

• La actual base mundial de datos arqueomagnéticos muestra grandes lagunas espaciotemporales. Es necesario un mayor número de datos arqueomagnéticos, sobre todo en el hemisferio sur, para mejorar su distribución y poder, así, obtener modelos arqueomagnéticos globales más precisos.

• Europa es la región con la mayor para los últimos 12000 años, lo que le hace idónea para la realización de estudios regionales. Este trabajo muestra que el modelado regional es el mejor procedimiento para analizar el campo geomagnético en Europa para los últimos 8000 años.

Obtención de nuevos datos arqueomagnéticos:

• Se ha realizado un estudio sobre ocho diferentes estructuras arqueológicas procedentes de Asturias (norte de España), región de la que no había datos hasta el momento. Este trabajo, además de proporcionar nuevos datos, ha permitido conocer en profundidad el método arqueomagnético, valorando así las potencialidades y limitaciones de este tipo de datos. Ello ha ayudado a establecer adecuadamente los criterios de selección de datos de entrada al proceso de modelización.

• Los experimentos de magnetismo de rocas indican que la magnetita/maghemita es la portadora de la remanencia magnética característica. Algunos especimenes presentaban una termorremanencia parcial, lo que se ha interpretado por la existencia de importantes gradientes térmicos en los hogares y termas. Esta interpretación es consistente con los valores de los coeficientes Q_n obtenidos.

• La magnetización remanente característica se ha aislado adecuadamente mediante el lavado térmico y por campos alternos decrecientes. Las direcciones medias obtenidas presentaban buenos parámetros estadísticos y se han incluido en la base de datos utilizada.

• Las direcciones medias obtenidas han sido comparadas con la base de datos de Iberia para el período Romano. El estudio muestra las limitaciones de la técnica de datación arqueomagnética durante el período Romano, ya que la dirección del campo geomagnético permanece muy estable durante ese período temporal.

• Para reducir los errores de las curvas de variación paleosecular y que la técnica de datación arqueomagnética tenga mayor precisión, son necesarios más datos arqueomagnéticos de alta calidad.

Obtención de los modelos regionales previos para Europa (modelos SCHA.DI.00 y SCHA.DI.00-F):

• El modelo direccional SCHA.DI.00 utiliza como datos de entrada cinco curvas bayesianas de variación paleosecular. El modelo se ajusta mejor a los datos arqueomagnéticos que los modelos globales de Hongre et al. (1998), y Korte y Constable (2005).

• La relación entre el error rms del modelo SCHA.DI.00 y los datos arqueomagnéticos indican la necesidad de aumentar los datos en dos períodos temporales: la llamada "Época oscura" (500 – 900 d.C.) y el período comprendido entre 1625 d.C. y 1700 d.C.

• El modelo regional SCHA.DI.00-F completa el modelo anterior incorporando datos de intensidad.

• El modelo SCHA.DI.00-F reproduce la actual base europea de datos de arqueointensidad de forma más precisa que los modelos globales de Hongre et al. (1998) y Korte and Constable (2005) para el período temporal 0 – 1900 d.C.

• El modelo SCHA.DI.00-F proporciona una visión completa del campo geomagnético para los últimos 2000 años. Este modelo indica que el campo magnético de la Tierra ha registrado 8 máximos de intensidad en la región europea en los últimos 2000 años en: 160, 320, 590, 820, 1070, 1310–1400, 1570 y 1770–1850 d.C. El modelo permite también analizar la reciente y discutida conexión entre las variaciones del campo geomagnético y el cambio climático.

Modelo arqueomagnético para Europa para los últimos 3000 años (SCHA.DIF.3K):

• Se ha actualizado la base de datos arqueomagnéticos de los últimos 3000 años. A partir de estos datos y de datos históricos, se ha desarrollado un nuevo modelo regional para Europa, norte de África y oeste de Asia. El modelo, llamado SCHA.DIF.3K, ha sido obtenido mediante la aplicación de la técnica SCHA

conjuntamente a los tres elementos del Campo Geomagnético y cubre los últimos 3000 años, desde el año 1000 a.C. hasta el 1900 d.C. Este modelo ofrece una visión de las variaciones del campo magnético terrestre más detallada, y que mejor se ajusta a los datos, que los modelos globales.

• El modelo SCHA.DIF.3K indica que en Europa se ha producido al menos 5 *jerks* arqueomagnéticos o variaciones bruscas en los últimos 3000 años (AMJ-300, AMJ300, AMJ800, AMJ1350, AMJ1600) y un supuesto *jerk* entorno al 1800 d.C. (AMJ1800). Estos eventos están caracterizados por una intensidad del campo máxima y fuertes cambios direccionales. Otros eventos ("*jerks* direccionales") fueron observados entorno al 825 a.C., 650–700 a.C., 125 a.C., 600–650 d.C. y 1175–1200 d.C.

Modelo geomagnético para Europa para los últimos 8000 años:

• El modelo regional previo (SCHA.DIF.3K) ha sido ampliado temporalmente mediante un segundo modelo llamado SCHA.DIF.8K. Este modelo ha sido desarrollado mediante la técnica R-SCHA2D y tiene una cobertura temporal desde el 6000 a.C. hasta el 1000 a.C.

• Se ha analizado y completado la base de datos paleomagnéticos europea para los últimos 8000 años. El número de datos sedimentarios es muy superior al de datos arqueomagnéticos para el Holoceno. Aunque el registro sedimentario suaviza las variaciones del campo geomagnético, estos datos son esenciales para el conocimiento de la variación paleosecular. Se ha confeccionado una base de datos y filtrados que incluye datos arqueomagnéticos y de sedimentos lacustres. Esta ha sido la información de entrada para el desarrollo del modelo SCHA.DIF.8K.

• El modelo regional SCHA.DIF.8K reproduce los datos arqueomagnética y de sedimentos lacustres de la región europea y áreas vecinas de forma más precisa que el modelo global de Korte y Constable (2005) para los últimos 8000 años.

• Las curvas de variación paleosecular direccionales generadas a partir del modelo SCHA.DIF.8K están en acuerdo con la curva master del Holoceno del Reino Unido (Turner y Thomson, 1981) y con nuevos datos independientes no usados en el desarrollo del modelo.

• Se ha obtenido el Momento Axial Dipolar Virtual (VADM) regional a partir de los modelos regionales SCHA.DIF.3K y SCHA.DIF.8K. El VADM regional aumenta entre el 5000 a.C. y el 500 a.C. y presenta una abrupta caída en los últimos 1200 años.

• Mediante la correlación de máximos de intensidad y curvatura direccional se ha analizado la ocurrencia de jerks arqueomagnéticos en la región Europea para los últimos 8000 años. Los modelos regionales demuestran que se verifica la hipótesis GAD para la región europea en los últimos 8000 años.

Aplicaciones:

• Se ha desarrollado en código Matlab una herramienta para la datación arqueomagnética. Para Europa, el modelo puramente arqueomagnético SCHA.DIF.3K parece ser el más adecuado para su uso en dataciones arqueomagnéticas.

• Los modelos SCHA.DIF.3K/8K pueden ser usados para estudiar los cambios rápidos en la variación paleosecular del campo geomagnético. La utilización de estos modelos permitirá analizar de forma más rigurosa la posible relación entre las variaciones del campo magnético de la Tierra y el cambio climático.

• Se han generado diferentes sitios webs que contienen toda la información de cada uno de los modelos y de los programas desarrollados:

SCHA.DI.00, http://pc213fis.fis.ucm.es/scha_model_00.html

SCHA.DI.00-F, http://pc213fis.fis.ucm.es/scha_model_f.html

SCHA.DIF.3K, http://pc213fis.fis.ucm.es/scha.dif.3k/index.html

SCHA.DIF.8K, http://pc213fis.fis.ucm.es/scha.dif.8k/index.html

Herramienta Matlab para la datación arqueomagnética,
http://pc213fis.fis.ucm.es/archaeo_dating/index.html

• Finalmente, haciendo uso de la técnica R-SCHA2D, hemos propuesto un primer modelo preliminar para Asia para los últimos 2000 años.

Perspectivas futuras.

• **Base de datos arqueomagnéticos de la Península Ibérica.** Son necesarios nuevos datos arqueomagnéticos en toda la Península Ibérica, cobrando importancia aquellos situados en el tercio norte peninsular y Portugal. Esta línea de trabajo seguirá siendo clave para el grupo de Paleomagnetismo de la UCM.

• **Aplicación a datos nuevos**. Se están obteniendo en la Península Ibérica los primeros datos arqueomagnéticos anteriores al 1000 a.C. mediante estudios de cenizas quemadas de Atapuerca (Burgos). Dichas cenizas presentan potencial arqueomagnético. Con el modelo SCHA.DIF.8K obtenido en la presente memoria se está probando la coherencia del modelo con las direcciones obtenidas. Este trabajo se está llevando a cabo con el grupo de Paleomagnetismo de la Universidad de Burgos (Drs. A. Carrancho y J.J. Villalaín).

• **Precisión del dato arqueomagnético.** La técnica regional aplicada a datos arqueomagnéticos puede ser usada como test para distribuciones regionales de datos. Estos tests estarán enfocados a analizar en profundidad la precisión de los datos arqueomagnéticos en dos vertientes: (i) determinar qué áreas son más susceptibles a la necesidad de nuevos datos arqueomagnéticos para un cierto período temporal y (ii) establecer relaciones entre el error del dato arqueomagnético (error en la medida y en la edad) y la precisión de éste para contribuir en la modelización del campo geomagnético.

• **Nueva estadística de modelado.** En las técnicas SCHA o R-SCHA2D se han usado los métodos de mínimos absolutos (norma L1) y cuadrados (norma L2) los cuales permiten conocer el valor estimado del coeficiente SCH y su desviación estándar. Sin embargo, podemos analizar con mayor profundidad los coeficientes mediante la aplicación de la estadística Bayesiana (método de Cadena de Marcov), permitiendo definir funciones de densidad de probabilidad para cada coeficiente SCH. En esta línea de trabajo y la anterior se está ya trabajando en colaboración con los Drs. E. Thébault y Y. Gallet (IPG Paris).

• **Modelos en otras regiones.** Una vez puesta a punto la técnica regional SCHA (o R-SCHA2D) para datos arqueomagnéticos, ésta se ha aplicado de forma preliminar a otra región con alta densidad de datos arqueomagnéticos: Asia. Una revisión de dicho modelo preliminar proporcionará un modelo robusto para el continente asiático. También, en colaboración con los Drs. A. Soler y A. Gogichaishvili (Universidad Autónoma de México), se pretende aplicar dicha técnica regional a Mesoamérica.

• **Análisis de la base de datos volcánica de Italia.** Los datos volcánicos italianos no han sido usados en los modelos regionales debido a las características complejas de dichos datos y a la controversia sobre las edades de los eventos volcánicos. Pretendemos analizar la base de datos volcánicos mediante los modelos regionales ya generados y así determinar posibles edades de los eventos y contrastarlos con las edades propuestas en la literatura. Este trabajo se está llevando a cabo en colaboración de los Drs. R. Lanza y E. Tema (Universidad de Torino, Italia).

Conclusions.

The main conclusions and contributions of the present work can be summarised as follows:

The European archaeomagnetic database:

• The present global archaeomagnetic database shows large gaps of data distribution in both time and space. Many new archaeomagnetic directional and intensity data are needed, particularly in the southern hemisphere, to improve the spatiotemporal accuracy in the global modelling approaches.

• Europe is the region with the largest density of archaeomagnetic data for the Holocene (the last 12000 years). A regional modelling approach turns out to be the best way to describe the behaviour of the Earth's magnetic field for the last 8000 years over Europe.

New data contribution:

• In order to analyze and better understand the behaviour of the archaeomagnetic data, a study has been carried out in eight different structures of two different archaeological locations from Asturias, northern Spain.

• Rock magnetic experiments and unblocking temperature spectra inspections reveal a low coercivity and moderate T_{ub} phase in the baked clay/brick samples, such as magnetite/maghemite, that seem to be the carriers of the archaeomagnetic signal. The direction of the thermal gradients in fireplaces has been detected, suggesting (partial) thermoremanences as the origin of remanent magnetization, which is consistent with Q_n values.

• Detailed full demagnetization of the archaeomagnetic remanences led to site-mean Fisherian directions that have been calculated following the hierarchical approach. These new data improve the distribution of sites by contributing new archaeomagnetic sites from northern Spain, an area currently not represented.

• Archaeomagnetic results have been compared, applying Fisherian distribution tests, among themselves and with Roman age entries of the Spanish archaeomagnetic database. This comparison shows that the archaeomagnetic

dating precision during Roman times is problematic because the directional geomagnetic field does not change in these times.

• More high quality archaeomagnetic data (from very well-dated structures) are needed in order to reduce the errors associated with the reference palaeosecular variation curve and the archaeomagnetic dating technique, particularly between 0 and 500 AD.

Initial European archaeomagnetic models (SCHA.DI.00 and SCHA.DI.00-F):

• The directional SCHA.DI.00 model fits the input data (the Bayesian paleosecular variation curves) better than the Hongre et al. (1998) and Korte and Constable (2005) global models. These five European Bayesian PSVCs used for constructing the SCHA.DI.00 model show coherence between themselves although they were obtained for individual region/countries.

• The relation between errors and available archaeomagnetic data indicates the necessity of increasing the number of archaeomagnetic studies in the time intervals with high errors, i.e. during the "Dark age" and for the 1625–1700 AD period, which are characterized by a low density of archaeomagnetic data.

• The directional archaeomagnetic model was completed using the in situ archaeointensity data. The new model, SCHA.DI.00-F, provides a complete description of the geomagnetic field over Europe for the last 2000 years.

• The SCHA.DI.00–F model fits the present intensity archaeomagnetic database for Europe more accurately than the global models proposed by Hongre et al. (1998) and Korte and Constable (2005) for the 0–1900 AD time interval.

• The SCHA.DI.00–F model suggests that the Earth's magnetic field strength reached 8 maxima in Europe at: 160, 320, 590, 820, 1070, 1310–1400, 1570 and 1770–1850 AD. The model has also provided new insights on a very new and controversial topic of research, i.e., the question of whether there exist connections between geomagnetic field changes and global (or regional) climate alterations.

Archaeomagnetic field model for Europe for the last 3000 years (SCHA.DIF.3K):

• Using the present archaeomagnetic database for the last 3000 years and historical data, we have developed a regional archaeomagnetic model for Europe, Northern Africa and Western Asia. The model, called SCHA.DIF.3K, has been

calculated using the SCHA regional technique and spans the last 3000 years, from 1000 BC to 1900 AD.

• The SCHA.DIF.3K model suggests that the Earth's magnetic field has experienced a minimum of 5 archaeomagnetic jerks in Europe for the last 3000 years (AMJ-300, AMJ300, AMJ800, AMJ1350, AMJ1600) and a suspected jerk (AMJ1800). These events are characterized by intensity maxima, velocity minima and a sharp change in curvature. Other events are observed around 825 B.C., 650–700 B.C., 125 B.C., 600–650 A.D. and 1175–1200 A.D. which seem "directional jerks," but need to be confirmed with more data.

Geomagnetic field model for Europe for the last 8000 years:

• The previous SCHA.DIF.3K model is complemented by a second reference model called SCHA.DIF.8K. This model was developed by using the R-SCHA2D regional technique from 6000 BC to 1000 BC.

• The number of sedimentary data is higher than the archaeomagnetic data. Although these data show a smooth behaviour of the geomagnetic field, they are essential for the knowledge of its palaeosecular variation.

• The directional secular variation given by the SCHA.DIF.8K model shows a good agreement with the United Kingdom master curve proposed by the Holocene (Turner and Thomson, 1981) and with new independent data not used in the modelling process.

• The calculated average regional VADM allows us to know the behaviour of the geomagnetic field's strength in the European region, showing how it has changed over the past 8000 years. The average regional VADM, from both SCHA.DIF.3K and SCHA.DIF.8K models, is characterized by a period of increase between 5000 BC and 500 BC and an abrupt decay, confirmed in previous studies, for the last 1200 years.

• A correlation study of the simultaneous occurrence of intensity maxima and directional curvature changes show that the Earth's magnetic field has recorded several archaeomagnetic *jerks* for the last 8000 years. Moreover, we have demonstrated the GAD hypothesis for the European region based on regional modelling.

• Both regional models fit the present archaeomagnetic database (and lake sediment data set) for Europe and adjacent areas more accurately than the global model proposed by Korte and Constable (2005) for the last 8000 years.

Applications:

- We have developed a Matlab code for archaeomagnetic dating. The archaeomagnetic dating strongly depends on the used master PSVC, because they show different behaviours in many occasions since they were, by nature, differently constructed. For Europe, the SCHA.DIF.3K model turns out to be the best way to obtain PSVCs for archaeomagnetic dating.

- Both regional models, SCHA.DIF.3K/8K can be used for studying rapid changes of the palaeosecular variation of the geomagnetic field for the last 8000 years and they could allow us to establish links between the Earth's magnetic field behaviour and palaeoclimate.

- Different web sites have been developed for all the models information and programs:

SCHA.DI.00, http://pc213fis.fis.ucm.es/scha_model_00.html

SCHA.DI.00-F, http://pc213fis.fis.ucm.es/scha_model_f.html

SCHA.DIF.3K, http://pc213fis.fis.ucm.es/scha.dif.3k/index.html

SCHA.DIF.8K, http://pc213fis.fis.ucm.es/scha.dif.8k/index.html

Matlab tool for archaeomagnetic dating,
http:// pc213fis.fis.ucm.es/archaeo_dating/index.html

- Finally, we propose a first preliminary regional geomagnetic model for Asia for the last 2000 years, using the R-SCHA2D technique.

Outlook

• **Archaeomagnetic data.** New archaeomagnetic data are needed in the Iberian Peninsula, especially those from the northern Peninsula and Portugal. This is a priority work line in the Palaeomagnetism's group of Madrid (UCM).

• **Application to new data.** New archaeomagnetic studies in burn ashes are being obtained in the Iberian Peninsula from Atapuerca (Burgos) with ages older than 1000 BC. The regional SCHA.DIF.8K model is used to test these new data. This work is being carried out with the paleomagnetism's group of the University of Burgos (Drs. A. Carrancho and J.J. Villalaín).

• **Testing the accuracy of the archaeomagnetic data.** The regional technique applied to archaeomagnetic data can be used as test for regional data distributions. These tests will be focused on the analysis of the archaeomagnetic data in two ways: (i) to determine which areas are more susceptible to the need of new archaeomagnetic data in a time period and (ii) to establish relationships between error (measurement and age errors) and accuracy of the data for contributing to the geomagnetic field modelling.

• **New statistical approach.** We have applied the L1 and L2 norms in the SCHA or R-SCHA2D techniques. Both statistical methods allow us to know the estimated values of the SCH coefficients and their standard deviations. However, the coefficients can be better analyzed by applying the Bayesian statistics (method of Markov's Chain), which allows to define probability density functions for each coefficient. This and the previous work lines are being developed in collaboration with the Drs. E. Thébault and Y. Gallet (IPG Paris).

• **New models in other regions.** The R-SCHA2D technique has been applied to another region characterized with a high density of archaeomagnetic data: the Asian continent. A revision of the obtained preliminary model will provide a robust model for Asia for the last 2000 years. Moreover, in collaboration with Drs. A. Soler and A. Gogichaishvili (Autonomous University of Mexico) we plan to apply this technique to the archaeomagnetic data distribution of the Mesoamerican region.

• **Testing the Italian volcanic database.** The Italian volcanic data have not been used in regional models because of the complexities of such data and the controversial discussions about the ages of the volcanic events. The archaeomagnetic regional model, SCHA.DIF.3K, can be used for comparing lava flows and regional model predictions to obtain new archaeomagnetic dates (archaeomagnetic dating). This work is being carried out in collaboration with Drs. R. Lanza and E. Tema (University of Torino, Italy).

Referencias

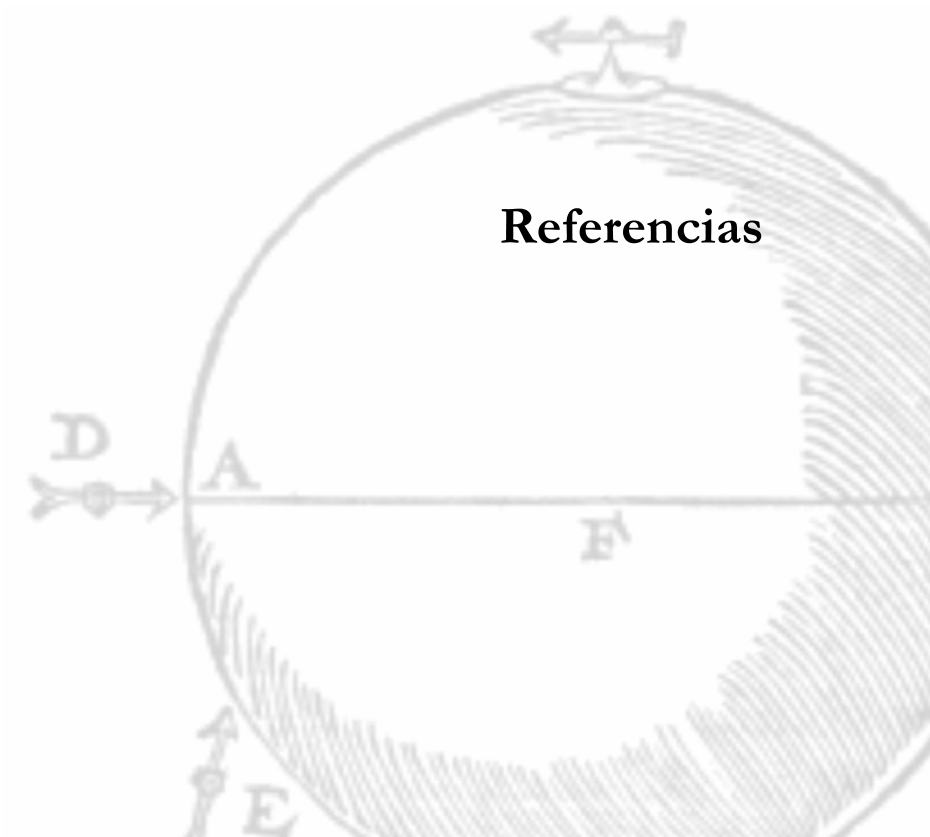

Alldredge, L.R. **1981** Rectangular Harmonic Analysis Applied to the Geomagnetic Field. J. Geophys. Res. 86 No.B4 3021-3026.

An, Z.C., S.Z. Ma, D.H. Tan, D.R. Barraclough, and D.J. Kerridge. **1992**. A Spherical Cap Harmonic Model of the Satellite Magnetic Anomaly Field over China and Adjacent Areas. J. Geomag. Geoelectr. 44 243-252.

Ardizone, J., and M. Herraiz. **2000** Application of the polynomial adjustment to the aeromagnetic survey of the Spanish Mainland; Requirements and shortcoming. Earth Planets Space, 52, 183–196, 2000.

Barraclough, D.R. **1974** Spherical Harmonic analyses of the geomagnetic field for eight epochs between 1600 and 1910. Geophys. J. Int. 36 497-513.

Barraclough, D.R. **1976** Spherical harmonic analysis of the geomagnetic secular vaiation. A review of methods. Phys. Earth Planet. Inter. 12 365-382.

Barraclough, D.R. **1978** Spherical harmonic models of the geomagnetic field. Geomagn. Bull. Inst. Geol. Sci.866 pp.

Barraclough, D.R., and E. Clarke. **1988** Statistical analysis of geomagnetic variations. B.G.S. Tec. Rep. WM/88/15C62 pp.

Bucur, I. **1994** The direction of the terrestrial magnetic field in France during the last 21 Centuries. Phys. Earth Planet. Inter. 87 95-109.

Bullard, E.C. **1967** The removal of trend from magnetic surveys. Earth Planet Sci. Lett.2 293-300.

Butler, R.F. **1992** Paleomagnetism. Blackwell Scientific Publications Cambridge 315pp.

Cain, J.C., D.R. Schmitz, and L. Muth. **1984** Small-scale features in the Earth's magnetic field observed by MAGSAT. J. Geophys. Res.89 No.B2 1070-1076.

Carlut, J., and V. Courtillot. **1998** How complex is the time-averaged geomagnetic field over the last 5 million years. Geohpys. J. Int. 134 527-544.

Casas, Ll., and A. Incoronato. **2007** Distribution analysis of errors due to relocation of geomagnetic data using the 'Conversion via Pole' (CVP) method: implications on archaeomagnetic data. Geophys. J. Int.169 (2)448 - 454.

Chapman, S., and J. Bartels. **1940** Geomagnetism. 2 vols. Oxford: Clarendon Press. 1049 pp.

Chauvin, A., Y. Garcia, Ph. Lanos, and F. Laubenheimer. **2000** Paleointensity of the geomagnetic field recovered on archaeomagnetic sites from France. Phys. Earth Planet. Inter.120 111-136.

Chiappini, M., A. De Santis, G. Dominici, and J.M. Torta. **1999** A normal reference field for the Ionian Sea Area. Phys. Chem. Earth (A) Vol. 24 No. 5 pp. 433-438.

Constable, C.G., C.L. Johnson, and S.P. Lund. **2000** Global geomagnetic field models for the past 3000 years: transientor permanent flux lobes. Phil. Trans. R. Soc. Lond. A 358 991-1008.

Courtillot, V., Y. Gallet, J-L. Le Mouël, F. Fluteau, and A. Genevey. **2007** Are there connections between the Earth's magnetic field and climate?. Earth Planet. Sci. Lett. 253, 328–339.

Curto, J.J., E. Also, E. Pallé, and J.G. Solé. **2009** Sunshine and synoptic cloud observations at Ebro Observatory, 1910-2006, International Journal of Climatology, 29, 2183-2190. DOI: 10.1002/joc.1841.

Daly, L., and M. Le Goff. **1996** An updated and homogeneous world secular variation data base. 1. smoothing of the archaeomagnetic results. Phys. Earth Planet. Inter.93 159-190.

De Marco, E., V. Spatharas, M. Gómez-Paccard, A. Chauvin, and D. Kondopoulou. **2008a** New archaeointensity results from archaeological sites and variation. Phys. Chem. Earth, 33, 578 – 595.

De Marco, E., S. Spassov, D. Kondopoulou, I. Zananiri, and E. Gerofoka. **2008b** Arcaheomagnetic study and dating of a Hellenistic site in Katerini (N. Greece). Phys. Chem. Earth, 33, 481 – 495.

De Santis, A. **1991** Translated origin spherical cap harmonic analysis. Geophys. J. lnt. 106 253-263.

De Santis, A. **1992** Conventional spherical harmonic analysis for regional modelling of the geomagnetic field. Geophys. Res. Lett. 19 N. 10 1065-1067.

De Santis, A., and D.J. Kerridge. **1989** Programmi in Fortran per la determinazione di un modello del campo geomagnetico in armoniche sferiche sviluppate su calotta sferica. Proceedings of the Workshop "Informatics & Earth's Sciences" Sarnano Italy.

De Santis, A., and J.M. Torta. **1997** Spherical cap harmonic analysis: a comment on its proper use for local gravity field representation. Journal of Geodesy 71 526-532.

De Santis, A., D.J. Kerridge, and D.R. Barraclough. **1989** A Spherical Cap Harmonic Model of the Crustal Magnetic Anomaly Field in Europe by Magsat. In Geomagnetism and Paleomagnetism ed. F.J. Lowes et al. pp. 1-17 Kluwer Dordrecht.

De Santis, A., O. Battelli, and D.J. Kerridge. **1990** Spherical cap harmonic analysis applied to regional field modelling for Italy. J. Geomag. Geoelect. 42 1019-1036.

De Santis, A., J.M. Torta, and L.R. Gaya-Piqué. **2002** The first Antarctic geomagnetic Reference Model (ARM). Geophys. Res. Lett. 29 N. 833.1-33.4.

Donadini, F., M. Korte, and C. G. Constable. **2009** Geomagnetic field for 0-3 ka: 1. New data sets for global modeling Geochem. Geophys. Geosyst.10 Q06007 doi:10.1029/2008GC002295.

Evans, M.E. **2006** Archaeomagnetic investigations in Greece and their bearing on geomagnetic secular variation. Phys. Earth Planet. Int., 159, 90–95

Finlay, C.C. **2008** Historical variation of the geomagnetic axial dipole, Phys. Earth Planet. Inter. 170, pp. 1–14

Freeden, W., and M. Schreiner. **2009** Spherical Functions of Mathematical Geosciences. Springer, XVI, 602 p., ISBN: 978-3-540-85111-0

Gallet, Y., A. Genevey, and M. Le Goff. **2002** Three millennia of directional variations of the Earth's magnetic field in western Europe as revealed by archaeological artefacts. Phys. Earth Planet. Inter.131 81-89.

Gallet, Y., A. Genevey, and V. Courtillot. **2003** On the possible occurrence of archeomagnetic jerks in the geomagnetic field over the past three millennia, Earth Planet. Sci. Lett. 214, 237– 242.

Gallet, Y., A. Genevey, and F. Fluteau. **2005** Does Earth's magnetic field secular variation control centennial climate change?. Earth Planet. Sci. Lett. 236, 339–347.

Gallet, Y., A. Genevey, M. Le Goff, F. Fluteau, and S.A. Eshraghi. **2006** Possible impact of the Earh's magnetic field on the history of ancient civilizations. Earth Planet. Sci. Lett. 266, 17–26.

Gallet, Y., A. Genevey, M. Le Goff, J.G-A. Warmé, and A. Lefèvre. **2009** On the use of archaeology in geomagnetism, and vice-versa: Recent developments in archaeomagnetism. C.R. Physique 10, 630 – 648.

García, A., J.M. Torta, J.J. Curto, and E. Sanclement. **1991** Geomagnetic Secular Variation oves Spain 1970 - 1988 by jeans of Spherical Cap Harmonic Análisis. Phys. Earth Plnet. Inter.68 65-75.

Gaya-Piqué, L.R. **2004** Analysis of the geomagnetic field in Antartica from near-surface and satellite data. PhD Thesis Observatori de l'Ebre URL162 pp.

Gaya-Pique, L.R., A. De Santis, and J.M. Torta. **2004** Use of Champ Magnetic Data to Improve the Antarctic Geomagnetic Reference Model. In: Earth Observation with CHAMP. Results from three years in orbit. Reigber C. Luhr H. Schwintzer P. Wickert J. eds Springer-Verlag Heidelberg 317-3222004

Genevey, A., Y. Gallet, C.G. Constable, M. Korte, and G. Hulot. **2008** ArcheoInt: An upgraded compilation of geomagnetic field intensity data for the past ten millennia and its application to the recovery of the past dipole moment. Geochem. Geophys. Geosyst Vol. 9 Number 4.

Gómez-Paccard, M. **2006** Étude de la variation de la direction et de l'intensité du champ géomagnétique en Espagne durant les deux derniers millénaires. Tesis doctoral Universidad Rennes 1 y Universidad Complutense de Madrid.

Gómez-Paccard, M., G. Catanzariti, V.C. Ruiz-Martínez, G. McInstosh, J.I. Núñez, M.L. Osete, Ph. Lanos, A. Chauvin, D.H. Tarling, D. Bernal-Casasola, J. Tiritó, and archeological working group (A. Sáez-Espligares, I. García-Villanueva, J.A. Gisbert-Santona, M.A. Hervás, P. Jiménez-Castillo, M. Mesquida-García, I. García-Ramírez González, M. Retuerce, D. Urbina, and C. Urquijo) **2006a** A cathalogue of Spanish archaeomagnetic data. Geophys. J. Int., 166, 1125–1143.

Gómez-Paccard, M., Ph. Lanos, A. Chauvin, G. McInstosh, M.L. Osete, G. Catanzariti, V.C. Ruiz-Martínez, and J.I. Núñez. **2006b** The first Archaeomagnetic secular variation curve for the Iberian Peninsula. Comparison with other data from Western Europe and with global geomagnetic field models. Geochem. Geophys. Geosyst. 7, Q12001. doi:10.1029/2006GC001476.

Gómez-Paccard, M., A. Chauvin, Ph. Lanos, and J. Thiriot. **2008** New archeointensity data from Spain and the geomagnetic dipole moment in western Europe over the past 2000 years. J. Geophys. Res113 B09103 doi:10.1029/2008JB005582.

Gubbins, D. **1975** Can the Earth's magnetic field be sustained by core oscillations?, Geophys. Res. Lett. 2, pp. 409–512.

Gubbins, D., A.L. Jones, and C.C. Finlay. **2006** Fall in Earth's Magnetic Field is erratic. Science. Vol. 312. no. 5775 pp. 900 - 902.

Haines, G.V. **1968** Polynomial estimation of certain geomagnetic quantities applied to a survey of Scandinavia. Pub. Dom. Obs.37 No.4 79-112.

Haines, G.V. **1985a**. Spherical Cap Harmonic Analysis. J. Geophys. Res. 90 (B3) 2583-2591.

Haines, G.V. **1985b** Magsat Vertical Field Anomalies above 40ºN from Spherical Cap Harmonic Analysis. J. Geophys. Res. 90 (B3) 2593-2598.

Haines, G.V. **1985c** Spherical Cap Harmonic Analysis of Geomagnetic Secular Variation over Canada 1960-1983. J. Geophys. Res. 90 (B14) 12563-12574.

Haines, G.V. **1988** Computer programs for spherical cap harmonic analysis of potential and general fields. Computers & Geosciences.14 No.4 413-447.

Haines, G.V. **1990a** Regional magnetic field modelling: a review. J. Geomag. Geoelect. 42 1001-1018.

Haines, G.V. **1990b** Modelling by series expansions: a discussion. J. Geomagn. Geoelectr.42 No.9 1001-1018.

Haines, G.V., and L.R. Newitt. **1986** Canadian geomagnetic reference field 1985. J. Geomag. Geoelectr. 38 895-921.

Haines, G.V., and L.R. Newitt. **1997** The Canadian geomagnetic reference field 1995. J. Geomag. Geoelectr. 49 317-336.

Haines, G.V., and J.M. Torta. **1994** Determination of Equivalent Currents Sources from Spherical Cap Harmonic Models of Geomagnetic Field Variations. Geophys. J. Int. 118499-514.

Hatakeyama, T., and M. Kono. **2002** Geomagnetic field model for the last 5 Myr: time averaged field and secular variation. Phys. Earth Planet. Interiors 133 181-215.

Hongre, L., G. Hulot, and A. Khokhlov. **1998** An analysis of the geomagnetic field over the past 2000 years. Phys. Earth Planet. Interiors 106 311-335.

Hulot, G., A. Khokhlov, and J-L. Le Mouël. **1997** Uniqueness of mainly dipolar magnetic fields recovered from directional data. Geophys. j. int., vol. 129, pp. 347-354, 1997.

IAGA. **2009** 11th generation of the International Geomagnetic Reference Field. http://www.ngdc.noaa.gov/IAGA/vmod/igrf.html

Irurzun, M., C. Gogorza, M. Chaparro, J. Lirio, H. Nuñez, J. Vilas, and A. Sinito. **2006** Paleosecular variations recorded by Holocene-Pleistocene sediments from Lake El Trébol (Patagonia, Argentina), Phys. Earth Planet. Inter., 154, 1–17.

Jackson, A., A.R.T. Jonkers, and M.R. Walker. **2000** Four centuries of geomagnetic secular variation from historical records. Phil. Trans. R. Soc. Lond. A 358957 - 990.

Jacobs, J.A. (editor). **1987** Geomagnetism. Ed. Academic Press.

Johnson, C.L., and C.G. Constable. **1997** The time-averaged geomagnetic field: global and regional biases for 0-5 Ma. Geohpys. J. Int. 131 643-666.

Johnson, C.L., and C.G. Constable. **1998** Persistently anomalous Pacific geomagnetic fields. Geohpys. Res. Lett. 25 1011-1014.

Kelly, P., and D. Gubbins. **1997** The geomagnetic field over the past 5Myr. Geophys. J. Int. 128 315-330.

Korte, M., and V. Haak. **2000** Modelling European Magnetic Repeat Station and Survey Data by SCHA in search ofTime-Varying Anomalies. Phys. Earth Planet. Int. 122 205-220.

Korte, M., and R. Holme. **2003** Regularization of spherical cap harmonics. Geophys. J. Int. 153 253-262.

Korte, M., and C. G. Constable. **2003** Continuous global geomagnetic field models for the past 3000 years. Phys. Earth Planet. Inter.140 73-89.

Korte, M., and C.G. Constable. **2005** Continuous geomagnetic field models for the past 7 millenia: 2. CALS7K. Geochem. Geophys. Geosyst6 Q02H16 doi:10.1029/2004GC000801.

Korte, M., and E. Thébault. **2007** Geomagnetic repeat station crustal biases and vectorial anomaly maps for Germany, Geophys. J. Int., doi: 10.1111/j.1365-246X.2007.03387.x.

Korte, M., A. Genevey, C.G. Constable, U. Frank, and E. Schnepp. **2005** Continuous geomagnetic field models for the past 7 millennia: 1. A new global data compilation. Geochem. Geophys. Geosyst.6 Q02H15 doi:10.1029/2004GC000800.

Korte, M., F. Donadini, and C. G. Constable. **2009** Geomagnetic field for 0-3 ka: 2. A new series of time-varying global models Geochem. Geophys. Geosyst.10 Q06008 doi:10.1029/2008GC002297.

Kovacheva, M., Y. Boyadziev, M. Kostadinova, N. Jordanova, and F. Donadini. **2009** Updated archeomagnetic data set of the past 8 millennia from the Sofia laboratory Bulgaria Geochem. Geophys. Geosyst.10 Q05002 doi:10.1029/2008GC002347.

Langel, RA, and R.H. Estes. **1982** A geomagnetic field spectrum. Geophys. Res. Lett. 9 250-253.

Lanos, Ph. **2004** Bayesian inference of calibration curves: application to archaeomagnetism in Tools for constructing chronologies: crossing disciplinary boundaries. Vol. 177 edited by C. Buck and A. Millard pp. 43 - 82 Springer-Verlag London.

Lanos, Ph., M. Le Goff, M. Kovacheva, and E. Schnepp. **2005** Hierarchical modelling of archaeomagnetic data and curve estimation by moving average technique Geophys. J. Int.160 440-476.

Lanza, R., and E. Zanella. **2006** Comments on "Chronology of Vesuvius' activity from A.D. 79 to 1631 based on archeomagnetism of lavas and historical sources" by C. Principe et al., Bull Volcanol. Bull Volcanol, 68, 394–396

Le Goff, M., Y. Gallet, A. Genevey, and N. Warmé. **2002** On archaeomagnetic secular variation curves and archaeomagnetic dating. Physics of the Earth and Planetary Interiors 134: 203-211.

Mandea, M., and N. Olsen. **2009** Geomagnetic and Archeomagnetic Jerks: Where Do We Stand?. - Eos, Transactions, American Geophysical Union, 90, 24, 208-208

Marín, V.M., and F.J. Pavón Carrasco. **2006** Modelización Isopórica del campo geomagnético para la época 2005.0. Península e Islas Baleares. Proceedings de la V Asamblea Hispano-Portuguesa de Geodesia y Geofísica. ISBN: 84-8320-373-1. Sevilla (Spain).

Márton, P. **2003** Recent achievements in archaeomagnetism in Hungary. Geophys. J. Int.153 675-690.

Marton, P. **2009** Prehistorical archaeomagnetic directions from Hungary in comparison with those from south-eastern Europe. Earth Planets Space, 61, 1351–1356.

Marton, P., and E. Ferencz. **2006** Hierarchical versus stratification statistical analysis of archaeomagnetic directions: the secular variation curve for Hungary. Geophys. J. Int.164 484-489.

McElhinny, M.W., and J. Lock. **1996** IAGA paleomagnético databases with Access. Surv. Geophys.17 575-591.

McFadden, P.L., and F.J. Lowes. **1981** The discrimination of mean directions drawn from Fisher distributions. Geophys. J. Roy. Astron. Soc. 67, 19–33.

Merrill, R.T., M.W McElhinny, and P.L. McFadden. **1996** The magnetic field of the Earth Ed. Academic Press.

Noël, M., and C.M. Batt. **1990** A method for correcting geographically separated remanence directions for the purpose of archaeomagnetic dating. Geophys. J. Int.102753 - 756.

Núñez, J.I. **2005** Estudio arqueomagnético de la Península Ibérica: Primera curva de variación secular de los últimos tres milenios. Tesis doctoral Universidad Complutense de Madrid.

Olver, F.W.J., and J.M. Smith. **1983** Associated Legendre Functions on the cut. J. Computat. Phys. 51 502-518.

Parkinson, W.D. **1983** Introduction to Geomagnetism. Scottish Academic Press Edinburgh.

Pavón-Carrasco, F.J., M.L. Osete, J.M. Torta, L.R. Gaya-Piqué, and Ph. Lanos. **2008** Initial SCHA.DI.00 regional archaeomagnetic model for Europe for the last 2000 years. Phys. Chem. Earth. Vol. 33 Issues 6-7596 - 608.

Quidelleur, X., J.-P. Valet, V. Courtillot, and G. Hulot. **1994** Long-term geometry of the geomagnetic field for the last five million years: An updated secular variation database. Geophys. Res. Lett.21 1639-1642.

Rotanova, N.M., and S.D. Odintsov. **1999** Model of the Magsat Magnetic Anomaly Field over Europe using SphericaI Cap Harmonic Analysis. Phys. Chem. Earth (A) 24 N. 5455-459.

Rotanova, N.M., S.D. Odintsov, A. Sas-Uhrynowski, and E. Welker. **2000** The Magnetic Anomaly Field over Poland and Adjacent Regions by using Magsat Satellite Data. Acta Geophysica Polonica 48 N. 2 223-240.

Sabaka, T.J., N. Olsen, and R.A. Langel. **2002** A comprehensive model of the quiet-time near-earth magnetic field: phase 3. Geohpys. J. Int. 151 32-68.

Sabaka, T.J., N. Olsen, and M. Purucker. **2004** Extending comprehensive models of the Earth's magnetic field with Ørsted and CHAMP data. Geophys. J. Int. 159, 521—547, doi:10.1111/j.1365—246X.2004.02421.x.

Schnepp, E., R. Pucher, C. Goedicke, A. Manzano, U. Müller, and Ph. Lanos. **2003** Paleomagnetic directions and TL dating from a bread oven-floor sequence in Lübeck (Germany): a record of 450 yr of geomagnetic secular variation. J. geophys. Res. 108(B2)2078 doi:10.1029/2002JB001975.

Schnepp, E., R. Pucher, J. Reinders, U. Hambach, H.C. Soffel, and I. Hedley. **2004** A German catalogue of archaeomagnetic data. Geophys. J. Int.157 64-78.

Schnepp, E., and Ph. Lanos. **2005** Archaeomagnetic secular variation in Germany during the past 2500 years. Geophys. J. Int.163479 - 490.

Schott, J.J., and E. Thébault. **2010** Modelling the earth's magnetic field from global to regional scales, in: Geomagnetic Observations and Models, IAGA, Special Sopron Book Series, planned for 2010.

Sternberg, R., and R. McGuire. **1990** Techniques for constructing secular variation curves and for interpreting archaeomagnetic dates. In: Eighmy, J., Sternberg, R., eds, Archeomagnetic Dating. University Arizona, Tucson: 450pp.

Tarling, D.H. **1983** Palaeomagnetism: Principles and applications in geology geophysics and archaeology. pp 279 Chapman and Hall London.

Tarling, D.H., and M.J. Dobson. **1995** Archaeomagnetism: An error assessment of fired material observations in the British directional database. J. Geomagn. Geoelectr.47 5-18.

Tauxe, L. **1993** Sedimentary records of relative paleointensity of the geomagnetic field: theory and practice. Reviews of Geophys. 31, 3, 319 – 354.

Tauxe, L. **2005** Lectures in Paleomagnetism http://earthref.org/MAGIC/books/Tauxe/2005/

Tema, E., I. Hedley, and Ph. Lanos. **2006** Archaeomagnetism in Italy: a compilation of data including new results and a preliminary Italian secular variation curve. Geophys. J. Int. 1671160 - 1171.

Thébault, E. **2006** Global lithospheric magnetic field modeling by successive regional analysis, Earth Planets and Space, 58, 485–495

Thébault, E. **2008** A proposal for regional modelling at the Earth's surface R-SCHA2D Geophys. J. Int.174 118-134.

Thébault, E. and L.R. Gaya-Piqué. **2008** Applied comparisons between SCHA and R-SCHA regional modeling techniques. Geochem. Geophys. Geosyst. Vol. 9 Number 7.

Thébault, E., J.J. Schott, and M. Mandea. **2002** Geomagnetic field modelling on small spherical caps. EGS XXVII General Assembly EGS02-A-04673 SE6.07 -1 WE2A-003 Nice France2002

Thébault, E., J.J. Schott, M. Mandea, and J.P. Hoffbeck. **2004** A new proposal for Spherical Cap Harmonic Analysis, Geophys. J. Int., 159, p83-105.

Thébault, E., J.J. Schott, and M. Mandea. **2006a** Revised spherical cap harmonic analysis (R-SCHA): Validation and properties. J. Geophys. Res. Vol. 111 B01102 doi: 10.1029/2005JB003836.

Thébault, E., M. Mandea, and J.J. Schott. **2006b** Modeling the lithospheric magnetic field over France by means of revised spherical cap harmonic analysis (R-SCHA), J. Geophys. Res., 111, B05102, doi:10.1029/2005JB004110.

Thellier, E. **1937** Sur l'aimantation dite permanente des basaltes. C.R. Acad. Sci. Paris t.204: 876-879.

Thellier, E. **1938** Sur l'aimantation des terres cuites et ses applications géophysiques Ann. Inst. Phys. Globe Univ. Paris16 157-302.

Thellier, E. **1981** Sur la direction du champ magnétique terrestre en France durant les deux derniers millénaires. Phys. Earth Planet. Inter.24 89-132.

Thellier, E., and O. Thellier. **1952** Sur Ia direction du champ magnétique terrestre dans Ia region de Trèves vers 380 aprés J.C. C.R.Acad Sci. Paris 234: 1464-1466.

Thellier, E., and O. Thellier. **1959** Sur l'intensité du champ magnétique terrestre dans le passé historique et géologique. Ann. Goephys. 15: 285-376.

Torta, J.M. **1992** Modelización regional del campo geomagnético seobre España: campo anómalo variación secular y campo de referencia. Publicaciones del Observatorio del Ebro Memoria 15 Roquetes-Tarragona.

Torta, J.M., A. García, and A. De Santis. **1992** New representation of geomagnetic secular variation over restricted regions by means of SCHA: application to the case of Spain. Phys. Earth Planet. Inter. 74209-217.

Torta, J.M., A. García, and A. De Santis. **1993** A geomagnetic reference field for Spain at 1990. J. Geomag. Geoelect. 45573-588.

Torta, J.M., J.J. Curto, and P. Bencze. **1997** Behavior of the Quiet Day Ionospheric Current System in the European Region. J. Geophys. Res. 102 (A2) 2483-2494.

Torta, J.M., L.R. Gaya-Piqué, J.I. Núñez, and M.L. Osete López. **2000**. Modelización regional del campo geomagnético en Europa a partir de direcciones paleomagnéticas en yacimientos arqueológico. 2ª Asamblea Hispano Portuguesa de Geodesia y Geofísica. S08-06. 307-308.

Torta, J.M., A. De Santis, M. Chiappini,. and RRB. von Frese. **2002** A model of the Secular Change of the Geomagnetic Field for Antarctica. Tectonophysics 347 179-187.

Torta, J.M., L.R. Gaya-Piqué, and A. de Santis. **2006** Spherical cap harmonic analysis of the Geomagnetic Field with application for aeronautical mapping. In Rasson, J.L. and Delipetrov, T., EDS., Geomagnetics for Aeronautical Safety: A case study in and around the Balkans. NATO Security through science series.

Turner, G. M., and R. Thomson. **1981** Lake sediment record of the geomagnetic secular variation in Britain during Holocene times Geophys. J. R. Astron. Soc.65 703-725.

Usui, Y., J.H. Tarduno, M. Watkeys, A. Hofmann, A., and R. Cottrell. **2009** Evidence for a 3.45-billion–year-old magnetic remanence: hints of an ancient geodynamo from comglomerates of South Africa. Geochemistry, Geophysics, Geosystems 10, Q09207. doi:10.1029/2009GC002496.

Zananiri, I., C.M. Batt, Ph. Lanos, D.H. Tarling, and P. Linford. **2007** Archaeomagnetic secular variation in the UK during the past 4000 years and its application to archaeomagnetic dating. Phys. Earth Planet. Int. Volume 160 Issue 2 p. 97 - 107.

Anexos

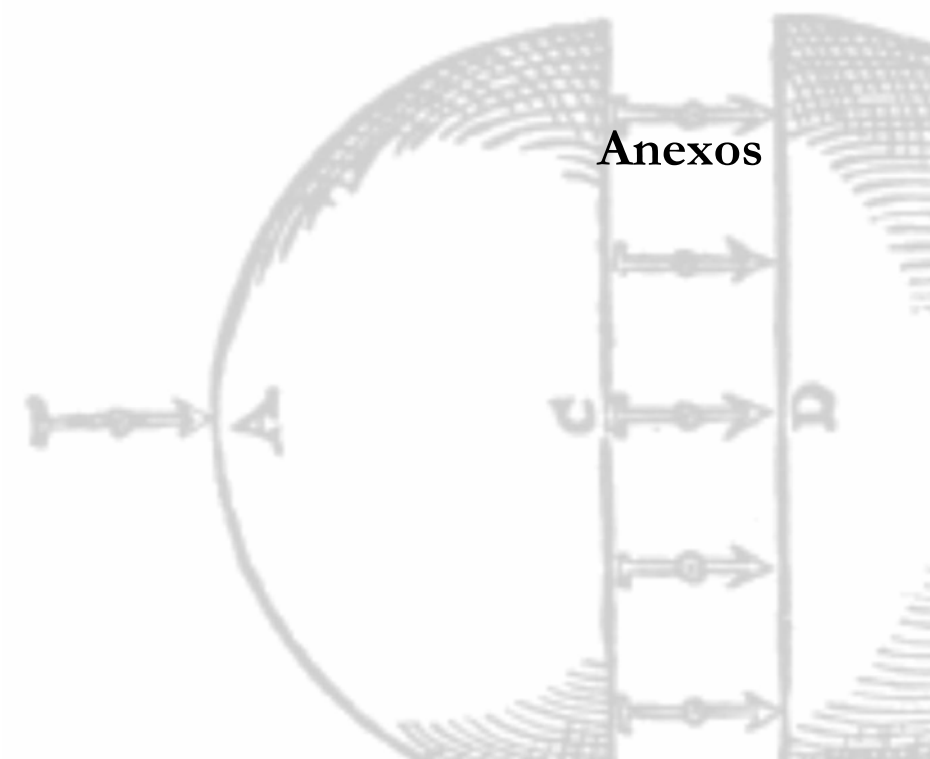

Anexo 1. El método SCHA.DI.

En este anexo se desarrollan las expresiones del Caso 2 (Capítulo 3: sección 3.4.2. Métodos de inversión), para aplicar la técnica de modelado regional SCHA (sólo para el potencial interno) al par de elementos declinación e inclinación. En este caso, la técnica regional descrita por Haines (1988) requiere ser modificada. Aquí proponemos una modificación basada en el método de Bauer (Barraclough, 1974), que consiste en relacionar las componentes del campo X, Y y Z con los elementos declinación e inclinación (D e I, respectivamente).

Teniendo en cuenta las ecuaciones 2.7 – 2.10, las componentes del campo geomagnético pueden ser expresadas en función de la intensidad del campo, F, la declinación, D y la inclinación I. A partir de ellas, podemos establecer tres nuevas ecuaciones en función de la declinación y la inclinación, donde la intensidad aparece de forma implícita:

$$X \sin D = Y \cos D \tag{A1}$$
$$X \sin I = Z \cos D \cos I \tag{A2}$$
$$Y \sin I = Z \sin D \cos I \tag{A3}$$

De las tres ecuaciones anteriores solo dos son independientes, pero serán usadas las tres para que el sistema a resolver esté sobredeterminado. Si sustituimos los valores de las componentes magnéticas por sus desarrollos en función del potencial en el casquete esférico (ec. 3.13, 3.14 y 3.15), tenemos:

$$X = \sum_{j=0}^{J} \alpha_j \cdot g_j \tag{A4}$$

$$Y = \sum_{j=0}^{J} \beta_j \cdot g_j \tag{A5}$$

$$Z = \sum_{j=0}^{J} \gamma_j \cdot g_j \tag{A6}$$

Donde α_j, β_j y γ_j agrupa las funciones asociadas de Legendre, las series de senos y cosenos y las funciones radiales. g_j son los coeficientes SCH (se ha simplificado las expresiones asumiendo un solo índice j que engloba a los índices k y m). Si sustituimos estas expresiones en las ec. A1, A2 y A3, obtenemos:

$$\sum_{j=0}^{J} \alpha_j \cdot g_j \sin D = \sum_{j=0}^{J} \beta_j \cdot g_j \cos D \tag{A7}$$

$$\sum_{j=0}^{J} \alpha_j \cdot g_j \sin I = \sum_{j=0}^{J} \gamma_j \cdot g_j \cos D \cos I \tag{A8}$$

$$\sum_{j=0}^{J} \beta_j \cdot g_j \sin I = \sum_{j=0}^{J} \gamma_j \cdot g_j \sin D \cos I \tag{A9}$$

Si extraemos de los sumandos el primer coeficiente g_0 (que sería el correspondiente a $k = 0$ y $m = 0$) y dividimos todas las expresiones por el mismo, obtenemos:

$$\alpha_0 \sin D + \sum_{j=1}^{J} \alpha_j \cdot \frac{g_j}{g_0} \sin D = \beta_0 \cos D + \sum_{j=1}^{J} \beta_j \cdot \frac{g_j}{g_0} \cos D \tag{A10}$$

$$\alpha_0 \sin I + \sum_{j=1}^{J} \alpha_j \cdot \frac{g_j}{g_0} \sin I = \gamma_0 \cos D \cos I + \sum_{j=1}^{J} \gamma_j \cdot \frac{g_j}{g_0} \cos D \cos I \tag{A11}$$

$$\beta_0 \sin I + \sum_{j=1}^{J} \beta_j \cdot \frac{g_j}{g_0} \sin I = \gamma_0 \sin D \cos I + \sum_{j=1}^{J} \gamma_j \cdot \frac{g_j}{g_0} \sin D \cos I \tag{A12}$$

Pero el primer término del desarrollo en armónicos esféricos de las componentes X e Y es nulo, ello implica que: $\alpha_0 = \beta_0 = 0$. Y si denotamos $G_j = g_j / g_0$, podemos rescribir las ecuaciones anteriores como:

$$\sum_{j=1}^{J} G_j (\alpha_j \cdot \sin D - \beta_j \cdot \cos D) = 0 \tag{A13}$$

$$\sum_{j=1}^{J} G_j (\alpha_j \cdot \sin I - \gamma_j \cdot \cos D \cos I) = \gamma_0 \cos D \cos I \tag{A14}$$

$$\sum_{j=1}^{J} G_j (\beta_j \cdot \sin I - \gamma_j \cdot \sin D \cos I) = \gamma_0 \sin D \cos I \tag{A15}$$

Obtenemos de nuevo un sistema de ecuaciones donde, tanto las funciones base como los observables, dependen de los valores de la declinación e inclinación. En este nuevo sistema los datos de entrada: declinación e inclinación, tienen que sufrir las mismas modificaciones que las establecidas para las componentes *XYZ*, es decir, que hay que transformarlas de geodésicas a geocéntricas y después girarlas hasta referirlas al sistema de referencia del casquete esférico (ver Capítulo 3, sección 3.4.1). Ambos elementos, declinación e inclinación, cambian ligeramente con la transformación de geodésicas a geocéntricas. En el giro al nuevo sistema de referencia, la inclinación es invariante y la declinación se transforma según la siguiente ecuación:

$$D_{SCH} = D_{geocéntrica} - \alpha \tag{A16}$$

donde α es el ángulo de giro dado en la ec. 3.86.

Hay que tener en cuenta algunas consideraciones al aplicar este método:
(i) No estamos considerando el primer término del desarrollo del potencial interno geomagnético en un casquete esférico ($g_0 = g_0^{0,i}$). Sin embargo, se pueden obtener los valores de la declinación e inclinación, ya que ambos valores no dependen del valor numérico de dicho coeficiente.
(ii) No es posible obtener una visión completa del campo geomagnético, pues para ello sería necesario conocer tres componentes/elementos independientes, y

en este caso solo conocemos la declinación y la inclinación, por lo que se obtiene un modelo direccional.
(iii) Si se conoce el valor de $g_0^{0,i}$ por otros medios se puede generalizar el modelo direccional obtenido a uno completo, incluyendo la intensidad (Hulot et al., 1997).

Anexo 2. Desarrollo de Taylor de los elementos geomagnéticos.

En este anexo se dan las expresiones del desarrollo de Taylor de los elementos geomagnéticos: declinación, inclinación e intensidad. Estas expresiones son usadas en el proceso de inversión detallado en el Capítulo 3, sección 3.4.2. Si denotamos al elemento del campo geomagnético como D (pudiendo éste ser declinación, inclinación o intensidad), su desarrollo entorno a un valor inicial (D_0) viene determinado por:

$$D(g) = D_0(g_0) + \frac{1}{1!}\frac{\partial D}{\partial g}\bigg|_0 (g - g_0) + \frac{1}{2!}\frac{\partial^2 D}{\partial g^2}\bigg|_0 (g - g_0)^2 + \ldots \tag{A17}$$

donde g corresponde a los coeficientes SCH.

Si queremos que el elemento geomagnético tenga una expresión lineal con los coeficientes SCH, debemos truncar la serie en el orden primero:

$$D(g) = D_0(g_0) + \frac{1}{1!}\frac{\partial D}{\partial g}\bigg|_0 (g - g_0) \tag{A18}$$

La derivada parcial del elemento geomagnético respecto a los coeficientes SCH es la matriz de Frechet (A_D), que será diferente para cada uno de los elementos geomagnéticos. Ésta puede ser expresada en términos de las componentes cartesianas (X, Y y Z) de la forma:

$$A_D = \frac{\partial D}{\partial g} = \frac{\partial D}{\partial X}\frac{dX}{dg} + \frac{\partial D}{\partial Y}\frac{dY}{dg} + \frac{\partial D}{\partial Z}\frac{dZ}{dg} \tag{A19}$$

Caso 1. Matriz de Frechet para la declinación.

Teniendo en cuenta la relación entre la declinación y las componentes XYZ (ec. 2.10) y las expresiones simplificadas para el potencial SCHA (de forma análoga para los potenciales R-SCHA y R-SCHA2D) dada por A4, A5 y A6 para X, Y y Z respectivamente, obtenemos para cada uno de los sumandos de A19:

$$\frac{\partial D}{\partial X}\frac{dX}{dg} = \sum_{i=1}^{i\max} \frac{-Y_0}{X_0^2 + Y_0^2}\cdot\alpha_i = -\sum_{i=1}^{i\max} \frac{Y_0}{H_0^2}\cdot\alpha_i \tag{A20}$$

$$\frac{\partial D}{\partial Y}\frac{dY}{dg} = \sum_{i=1}^{i\max} \frac{X_0}{X_0^2 + Y_0^2} \cdot \beta_i = \sum_{i=1}^{i\max} \frac{X_0}{H_0^2} \cdot \beta_i \tag{A21}$$

$$\frac{\partial D}{\partial Z}\frac{dZ}{dg} = 0 \tag{A22}$$

La última expresión (A22) es nula, pues la declinación no depende de la componente vertical Z. La expresión final para la matriz de Frechet para la declinación vendrá dada por:

$$A_D = \frac{1}{H_0^2} \sum_{i=1}^{i\max} (-Y_0 \cdot \alpha_i + X_0 \beta_i) \tag{A23}$$

Nota: hay que tener en cuenta que las componentes del campo de referencia (X_0, Y_0, Z_0) deben de estar referidas al sistema de referencia del casquete esférico.

Caso 2. Matriz de Frechet para la inclinación.

Partiendo de la relación de la inclinación y las componentes *XYZ* (ec. 2.9) obtenemos los siguientes sumandos:

$$\frac{\partial I}{\partial X}\frac{dX}{dg} = \sum_{i=1}^{i\max} \frac{-Z_0 \cdot X_0}{(X_0^2 + Y_0^2)^{1/2}(X_0^2 + Y_0^2 + Z_0^2)} \cdot \alpha_i = -\sum_{i=1}^{i\max} \frac{Z_0 \cdot X_0}{H_0 F_0^2} \cdot \alpha_i \tag{A24}$$

$$\frac{\partial I}{\partial Y}\frac{dY}{dg} = \sum_{i=1}^{i\max} \frac{-Z_0 \cdot Y_0}{(X_0^2 + Y_0^2)^{1/2}(X_0^2 + Y_0^2 + Z_0^2)} \cdot \beta_i = -\sum_{i=1}^{i\max} \frac{Z_0 \cdot Y_0}{H_0 F_0^2} \cdot \beta_i \tag{A25}$$

$$\frac{\partial I}{\partial Z}\frac{dZ}{dg} = \sum_{i=1}^{i\max} \frac{(X_0^2 + Y_0^2)^{1/2}}{X_0^2 + Y_0^2 + Z_0^2} \cdot \gamma_i = \sum_{i=1}^{i\max} \frac{H_0}{F_0^2} \cdot \gamma_i \tag{A26}$$

La matriz A_I viene determinada por la suma de A24 a A26:

$$A_I = \frac{1}{H_0 \cdot F_0^2} \sum_{i=1}^{i\max} (-Z_0 \cdot X_0 \cdot \alpha_i - Z_0 \cdot Y_0 \cdot \beta_i - H_0^2 \cdot \gamma_i) \tag{A27}$$

Caso 3. Matriz de Frechet para la intensidad.

Finalmente, a partir de la relación entre la intensidad y las componentes *XYZ* (ec. 2.7), podemos obtener los diferentes sumandos de la matriz A_F:

$$\frac{\partial F}{\partial X}\frac{dX}{dg} = \sum_{i=1}^{i\max} \frac{X_0}{(X_0^2 + Y_0^2 + Z_0^2)^{1/2}} \cdot \alpha_i = \sum_{i=1}^{i\max} \frac{X_0}{F_0} \cdot \alpha_i \tag{A28}$$

$$\frac{\partial F}{\partial Y}\frac{dY}{dg} = \sum_{i=1}^{i\max} \frac{Y_0}{(X_0^2 + Y_0^2 + Z_0^2)^{1/2}} \cdot \beta_i = \sum_{i=1}^{i\max} \frac{Y_0}{F_0} \cdot \beta_i \tag{A29}$$

$$\frac{\partial F}{\partial Z}\frac{dZ}{dg} = \sum_{i=1}^{i\max} \frac{Z_0}{(X_0^2 + Y_0^2 + Z_0^2)^{1/2}} \cdot \gamma_i = \sum_{i=1}^{i\max} \frac{Z_0}{F_0} \cdot \gamma_i \tag{A30}$$

Y sumando los tres términos se tiene:

$$A_F = \frac{1}{F_0} \sum_{i=1}^{i\max} (X_0 \cdot \alpha_i + Y_0 \cdot \beta_i + Z_0 \cdot \gamma_i) \qquad \text{(A31)}$$

Anexo 3. Modelo Arqueomagnético para Asia para los últimos 2000 años mediante la técnica R-SCHA2D.

En este trabajo proponemos un primer modelo regional del campo geomagnético para la región sur y central de Asia. El modelo ha sido desarrollado usando la metodología descrita en el capítulo 7, mediante el uso de datos paleomagnéticos que cubren los últimos 2000 años en dicha región. Dada la distribución espaciotemporal de la base de datos disponible (Donadini et al., 2009) se han considerado como datos de entrada para genera el modelo los datos arqueomagnéticos y los provenientes de estructuras volcánicas bien datadas. La distribución espaciotemporal de los datos usados (Donadini et al., 2009) se muestra en la figura A3.1.

La distribución espacial es muy inhomogénea para la declinación, sin embargo están mejor distribuidos los datos de inclinación e intensidad. Un análisis temporal indica que la densidad de datos de declinación es muy baja y una distribución muy regular para la intensidad. La mayor densidad de datos se obtiene para el parámetro de la inclinación y para los últimos 300 años. El número total de datos considerado es de 102 para la declinación, 368 datos de inclinación y 324 de intensidad.

Teniendo en cuenta la distribución espacial de los datos hemos seleccionado un casquete de 35º centrado en 35ºN de latitud y 102ºE de longitud (ver figura A3.1). La distribución temporal indica que debemos usar ventanas móviles con tamaño mínimo de 80 años. Una vez seleccionado los parámetros del casquete, hemos aplicado la técnica R-SCHA2D (Thébault, 2008) a los datos de entrada usando ventanas móviles de 80 años movidas cada 40 años. Debido a la escasez de datos hemos tenido que reducir el grado y orden del desarrollo del potencial geomagnético a grado y orden 1.

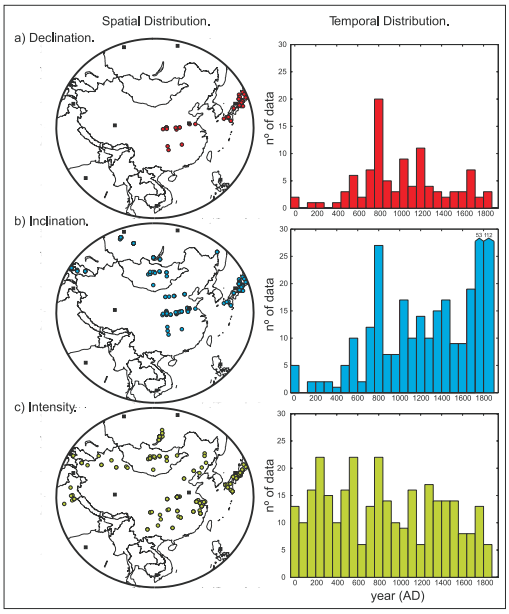

Figura A3.1. Distribución espaciotemporal de la (a) declinación, (b) inclinación e (c) intensidad en la región asiática para los últimos 2000 años. Datos de Donadini et al. (2009).

La figura A3.2, muestra la comparación del modelo obtenido con los datos de entrada, así como con el modelo global de CALS7K.2 (Korte y Constable, 2005). Vemos que el nuevo modelo regional mejora en la zona de estudio las previsiones del modelo global, sobre todo para la declinación.

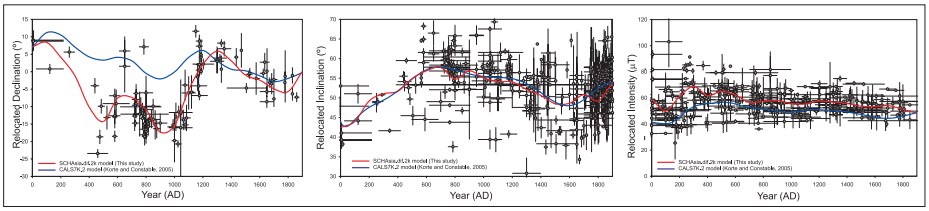

Figura A3.2. Curva de variación secular del modelo obtenido (roja) y datos de entrada (puntos grises) con su respectivos errores. Por comparación se ha incluido el modelo CALS7K.2 (curva azul).

Finalmente, hemos representado los mapas de campo geomagnético para la región Asiática en intervalos temporales de 100 años (Figura A3.3). El número de datos disponible es muy bajo, por lo que el modelo propuesto es un modelo de bajo grado y preliminar, pero se ha obtenido un modelo regional que claramente mejora el modelo global CALS7K.2 (Korte y Constable, 2005). Por tanto, se ha probado la validez del método incluso en regiones menos favorables que Europa. En un futuro pretendemos aplicar la técnica en otras zonas como Norte y Centro América.

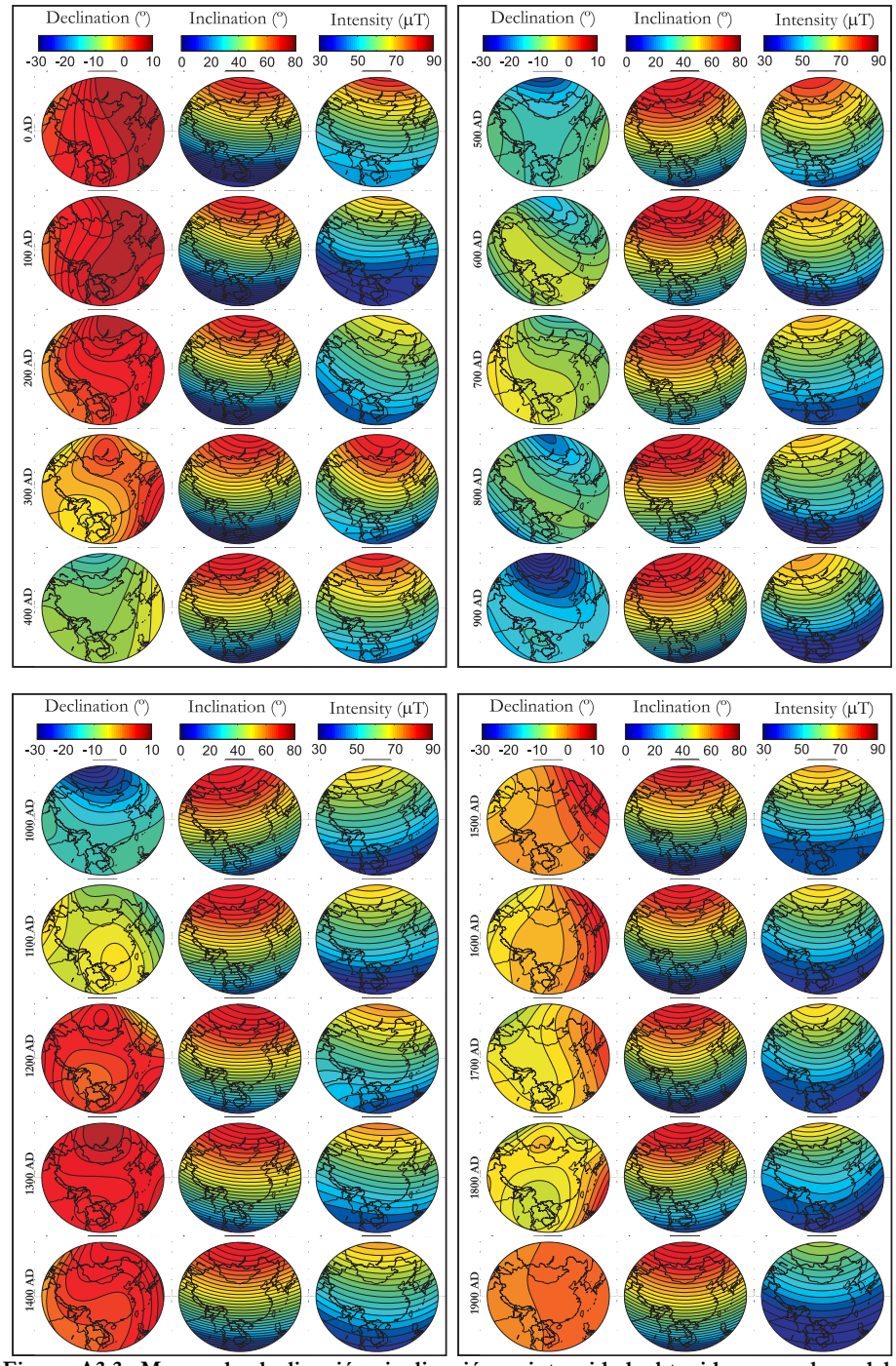

Figura A3.3. Mapas de declinación, inclinación e intensidad obtenidos con el modelo regional. Mapas cada 100 años.

UNIVERSIDAD COMPLUTENSE DE MADRID
FACULTAD DE CIENCIAS FÍSICAS

Departamento de Física de la Tierra, Astronomía y Astrofísica I
(Geofísica y Meteorología)

Modelización regional del Campo Geomagnético en Europa para los últimos 8000 años y desarrollo de aplicaciones.

Madrid 2010

Doctorando

Fco. Javier Pavón-Carrasco

Directores

M. Luisa Osete

J. Miquel Torta

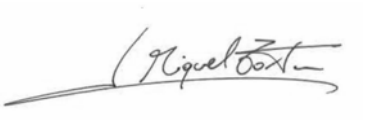

La presente Memoria de Tesis Doctoral
y el material suplementario se encuentra en:

http://pc213fis.fis.ucm.es/tesis_fjpc/index.html

En esta tesis doctoral se proponen los primeros modelos regionales del campo geomagnético en la región europea basados en datos paleomagnéticos (datos arqueomagnéticos y datos de sedimentos lacustres). En conjunto, los modelos regionales obtenidos permiten analizar la variación paleosecular del campo geomagnético en los últimos 8000 años: desde el año 6000 a.C. hasta el 1900 d.C., conectando así con los modelos instrumentales, como el IGRF. Se han analizado numerosas estrategias para la inversión espacial de los datos paleomagnéticos mediante el uso de la técnica de modelado regional con armónicos en un casquete esférico SCHA y de su revisión R-SCHA2D. En el dominio temporal, todos los modelos se han obtenido mediante el uso de ventanas móviles solapadas dependientes de las características del dato paleomagnético.

El primer modelo, SCHA.DI.00, se ha obtenido mediante el uso de las curvas de variación paleosecular bayesianas de Europa. Se trata de un modelo direccional (declinación e inclinación) y proporciona los valores de los elementos del campo geomagnético para los últimos dos milenios. El segundo es una versión actualizada del primero, reescalándolo con los valores de intensidad de los últimos 2000 años. Este nuevo modelo, llamado SCHA.DI.00-F, permite analizar de forma completa los elementos de declinación, inclinación e intensidad de los últimos 2000 años y muestra que el campo geomagnético ha registrado 8 máximos de intensidad en la región europea entorno a 160, 320, 590, 820, 1070, 1310-1400, 1570 y 1770-1850 d.C. Con estos dos modelos iniciales se analiza la aplicación de la técnica SCHA en datos paleomagnéticos, obteniéndose resultados satisfactorios.

En un tercer paso, se ha desarrollado un nuevo modelo regional para Europa, norte de África y oeste de Asia. El modelo SCHA.DIF.3K ha sido desarrollado, también, mediante la aplicación de la técnica SCHA conjuntamente a los tres elementos del campo geomagnético y su período de validez cubre desde el año 1000 a.C. hasta el 1900 d.C. Los datos de entrada de este nuevo modelo son los datos paleomagnéticos in situ, por lo que se elimina el error de relocalización inherente en la creación de las Curvas de Variación Paleosecular, por lo que es más robusto y coherente que el previo SCHA.DI.00-F, aunque son estadísticamente indistinguibles. El modelo permite identificar al menos 5 jerks arqueomagnéticos o variaciones bruscas en los últimos 3000 años (AMJ-300, AMJ300, AMJ800, AMJ1350, AMJ1600) y un supuesto jerk entorno a 1800 d.C. (AMJ1800). Finalmente, el período de validez temporal del modelo anterior ha sido ampliado 5000 años más (desde el 6000 a.C. hasta el 1000 a.C) mediante la inclusión de datos sedimentarios y el uso de la versión revisada de la técnica SCHA (R-SCHA2D): el modelo SCHA.DIF.8K.

Finalmente, se ha visto cómo ambos modelos, SCHA.DIF.3K y .8K, pueden ser usados para analizar la variación paleosecular del campo geomagnético en Europa en los últimos 8000 años y sus características: aparición de jerks arqueomagnéticos, la posible (o causal) relación entre campo magnético de la Tierra y cambio climático, o la hipótesis del Dipolo Geocéntrico Axial (GAD). Además se ha demostrado con casos prácticos cómo pueden ser usados como herramienta de datación arqueológica.